A genome-scale gain-of-function screening platform nominates genetic modulators for CAR T cell therapy enhancement

Benjamin Christopher Curtis

A dissertation

submitted in partial fulfillment of the

requirements for the degree of

Doctor of Philosophy

University of Washington

2023

Reading Committee:

Michael Jensen, Co-Chair

Shannon Oda, Co-Chair

Jesse Zalatan

Program Authorized to Offer Degree:

Laboratory Medicine and Pathology

©Copyright 2023

Benjamin Christopher Curtis

University of Washington

Abstract

A genome-scale gain-of-function screening platform
nominates genetic modulators for CAR T cell therapy enhancement

Benjamin Christopher Curtis

Chairs of the Supervisory Committee:
Michael Jensen
Department of Bioengineering

Shannon Oda
Department of Pediatrics

Chimeric antigen receptor (CAR) T cell therapy has revolutionized cancer care through genetic reprogramming, and next-generation cell engineering aims to encode increasingly complex genetic programs to further modulate T cell behavior, and ultimately potentiate anti-tumor activity. Effective selection of coding sequences for subsequent clinical development requires one or multiple prioritization regimens, but scalable gene nomination platforms for T cell therapy are currently lacking. In this work, I describe the creation of a novel genome-scale, gain-of-function screening platform, powered by CRISPR activation (CRISPRa) technology, and designed for pooled screening in primary human CAR T cells. To achieve this, established

CRISPRa designs were first optimized for fidelity, potency, and durability in T cell lines. Second, restrictive primary T cell requirements were overcome through cell manufacturing featuring transposon-based gene delivery coupled to CAR-restricted expansion (EP-TICLE). To overcome abbreviated CRISPRa activity, CRISPRa expression was reinforced through construct optimization that included dual divergent hybrid promoters (EF1α-HTLV)$_2$ and intronization of the dCas9 coding cassette. Finally, to prevent library distortion, gRNAs were delivered *in trans* via lentivirus immediately prior to landscape initiation. This manufacturing schema was trialed at genome-scale and nominated modulators of CAR T cell homeostatic persistence (MYC, STAT5A, STAT5B) and cytokine-free survival (CSF2RB, TNFRSF1A, TNFRSF1B). Follow-up studies suggested that this platform would tolerate a druggable-ON switch (ERT2) to regulate landscape initiation. In sum, this work demonstrates the utility of a novel cell manufacturing and gain-of-function screening system for next-generation therapy development. Insights into achieving sustained dCas9 expression may also offer a blueprint for orthogonal CRISPR-based screening systems or for *in vivo* CRISPR applications.

Acknowledgements

This work would not have been possible without the support of numerous people. For that, I would like to extend my deepest gratitude to several key individuals in Michael Jensen's lab. First, this project would have never gotten off the ground without the unwavering enthusiasm of James Rosser, who supervised me during my lab rotation and acted as an available sounding board throughout my graduate work. James and his early team also conceived of and tested early iterations of the manufacturing process that would eventually become "TICLE," and without, I perhaps never would have been able to manufacture T cells at the scale required. Along with James, I would like to extend my deep thanks to Chris Saxby, another graduate student in the lab, for his constant willingness to provide material and emotional support, and for serving as a frequent team-player across a multiple of coordinated experiments (#SkunkworksForever). More broadly, I would like to thank the intellectual "brain trust" that consisted of James, Chris, Michael Fitzgerald, Jacob Appelbaum, and Cailyn Spurrell. These five individuals enjoyed hashing out ideas, and were supportive, creative, clinically-minded, and fun.

I would like to also thank the people and teams who labored on parts of this project to bring it to fruition. First, I would like to thank the undergraduate interns in the lab who I mentored during my tenure, which include Marlena Urvater, Natalie Murren, Pittra Jaengprajak, and Jasmin Martinez-Reyes. These four contributed to molecular cloning, cell culture, and (in one instance) NGS development. I thank Joshua Gustafson for allowing me to take on this leadership and advising role, despite the required expenses in lab resources and his own time. I would like to thank the lab's bioproduction core, with a special thanks to Lindsay Flint, Aalton Lande, and Marissa Leonardi. My studies never could have taken place absent the infostructure

that this team had laid for large-scale lentiviral manufacturing, which manifested (in-part) through the production of two batches of 6 liters of viral supernatant to generate genome-scale virus. I especially appreciated this team's enthusiasm and willingness to assist, despite my snowballing series of incremental asks. I would like to thank the lab's molecular core, with a special thanks to Cailyn Spurrell, Ardizon Valdez, and Natalie Murren (alum). This team helped develop CRISPR gRNA processing pipelines and performed the computational processing of NGS sequencing results. Thank you, Cailyn, for pushing through this analysis on a tight deadline so that my defense offered up biological insights rather than ending on a puzzling cliffhanger. I would like to thank Tiffanie Chai for developing our droplet-digital PCR and western blot assays.

I would like to thank all members of my supervisory committee, including Michael Jensen, Shannon Oda, Jesse Zalatan, Rosana Risques, Patrick Paddison, and Raphael Gottardo. I would like to thank Michael Jensen and Shannon Oda for serving as my co-mentors, and for providing invaluable advice. I would like to thank Michael Jensen for permitting me to undertake a high-risk, high-reward project as a graduate student, despite his initial reservations. I would like to thank Michael Jensen for providing funding support and granting me the privileges of undertaking my graduate studies in his lab.

Finally, I would like to thank my partner, Simone Gabara. Graduate and wet-bench research generally demands aligning your calendar with the needs of cells. I am grateful for your understanding, patience, encouragement, and for serving as the conscripted one-person study group for a long line of practice talks. I appreciate you and Abby.

Table of Contents

List of Figures

Chapter 1 | Introduction: CAR T Cell Therapy Challenges and Opportunities

1.1 | Background

1.1.1 | Reducing the impact of cancer through adoptive T cell therapy

Cancer is a leading global health issue and the second most common cause of death worldwide (~10 million/yr).[1] Within the United States, cancer mortality has slowly retreated over the last several decades, but has nevertheless consistently ranked as the second leading cause of death (~600,000/yr) behind heart disease.[1] Recent trends in cancer incidence vary by disease subtype, with observed reductions in cases of lung and colorectal cancer, increases in breast and pancreatic cancer cases, and stability in prostate cancer diagnoses. Four of these five cancers are the most common form among men and women, and together comprise a majority of annual cancer deaths (50 - 52%).[1]

While disease prevention through the cessation or avoidance of high-risk behaviors (particularly tobacco use) likely represents the most significant contributor to the overall decline in cancer mortality, directed efforts at early detection and treatment have also made considerable impacts.[1,2] Today, as during decades prior, standard treatment options largely consist of forms of chemotherapy, radiotherapy, and surgery.[3] Despite their evident value, these treatments can be toxic or disabling, and often fail to completely eliminate or adequately control disease.[4–6] To improve the tolerability of therapy and improve patient outcomes, researchers have hence looked toward other treatment modalities, including targeted therapy options.

Long before the advent of modern molecular medicine, researchers suspected that the immune system may provide some degree of natural anti-cancer surveillance.[7,8] Based on the body's ability to precisely and completely eradicate local as well as systemic pathogens, scientists postulated that this organ system might be an ideal vehicle to target patients' tumors. Early efforts based on this premise built on the success of vaccines, to break the body's tolerance to tumor-associated self-antigens, and drive an immunological response favoring cancer elimination.[7] While particular cancer immunization strategies have seen glimmers of success,[9–11] researchers soon discovered that inducing reliable immunity against truly tumor-specific antigens to be immensely challenging given (1) the paucity of reliable cancer neoantigens and (2) demonstrated hurdles of overcoming central and peripheral tolerance to self-proteins.[12] Researchers however had improved success with a different form of immunotherapy known as adoptive cell transfer (ACT). In this approach, most often T lymphocytes (T cells), especially those residing within tumors (tumor-infiltrating lymphocytes (TILs)) are isolated, grown, and returned via infusion to the cancer patient. For patients with cancers of high mutational burdens such as metastatic melanoma, this form of therapy occasionally led to dramatic results,[13] and was enabled mechanistically by the expansion of rare cancer-specific T cell clones. Importantly, this success definitively demonstrated that certain cancers were highly susceptible to an arm of the adaptive immune system, namely T cells, provided that these cells were expanded to sufficient numbers and possessed specificity for a patient's tumor.

As a result, rather than pursuing an immunization strategy dependent on individual patients' heavily edited T cell repertoires, other researchers sought to impart non-native specificity through other means. Incidentally, success with adoptive TIL therapy provided scientists with a

source of potential tumor-specific T cell clones. When sequenced, researchers were able to identify specific T cell receptors (TCRs) specific to tumor antigen.[14] These DNA sequences could be combined with a strong promoter and then delivered as transgenes via viral vectors *ex vivo* to the T cell isolates of patients from defined genetic backgrounds.[15]

Therapies utilizing transgenic TCRs are powerful in that they can overcome self-tolerance, and also can target both extra- and intra-cellular epitopes provided that their cognate antigen is capable of proteasomal processing and subsequent loading onto class I or II major histocompatibility complexes (MHC). However, human MHC (also known as human leukocyte antigen, HLA) genes comprise a class of polymorphic alleles that diversified throughout the human population, likely in response to a multitude of evolving microbial threats.[16] As a result, transgenic TCRs obtained via sequencing can only be effectively paired with patient cells possessing an identical HLA gene allele group; this greatly limits the pool of potential patients that can benefit from a specific TCR, which is often already restricted to a very narrow molecular subtype of tumor.

To expand the pool of potential patients eligible for T cell therapy, while also preserving tumor specificity, researchers devised other targeting strategies. Inspired by antibodies and their non-secreted form, the B cell receptor, researchers designed a variety of chimeric antigen receptors (CAR) with specificity to a cell-surface protein and incorporating intracellular protein domains known to operate within the native TCR complex.[2–4] After extensive trialing spanning decades, researchers began to advance CAR designs capable of meaningful T cell responses. Today, conventional “second generation” CARs consist of (1) a single-chain variable fragment (scFv) from an antibody binding domain or fragment antigen-binding region (Fab), (2) spacer and

transmembrane sequences, (3) intracellular CD3 ζ chain to drive T cell activation, and (4) co-stimulatory signaling domains (originating most frequently from CD28 or CD137/4-1BB). So-called “first-generation” CARs lacked co-stimulatory peptide sequences, and thus, gave responses of (1) low magnitude, (2) short duration, or (3) highly dependent on exogenous cytokine support.[17]

1.1.2 | CAR T cells: clinically approved and on the move

In 2017, the first chimeric antigen receptor (CAR) T cell therapy, tisagenlecleucel (Kymriah), received FDA approval for the treatment of relapsed B cell acute lymphoblastic leukemia (ALL).[18,19] As of March 2023, the FDA has approved five additional CAR T cell therapies in the United States for the treatment of B-ALL and other B cell malignancies (e.g. multiple myeloma, B cell non-Hodgkin lymphoma, mantle cell lymphoma, and follicular lymphoma). While the first four approved therapies uniformly targeted CD19 (axicabtagene ciloleucel, Yescarta; brexucabtagene autoleucel, Tecartus; lisocabtagene maraleucel, Breyanzi), recently-approved drugs have also included an alternative B cell target, B-cell maturation antigen (BMCA) (idecabtagene vicleucel, Abecma; ciltacabtagene autoleucel, Carvykti).[20] Currently, all authorized CAR T cell therapies are limited to second- or (more often) third-line treatment or later.[21,22] Given the direction of research and pace of steady FDA approvals, market projections have suggested that CAR T and other gene-modified cell product approvals will likely number above 50 by 2030, with annual revenue forecasts for the same time period exceeding $30 billion USD.[23–25]

1.1.3 | Efficacy of CAR T in the clinic

For patients with B cell malignancies, CAR T cells can produce complete or partial responses (up to 70 - 94%),[26,27] many of which are durable (~60%).[28,29] These remarkable response rates for refractory disease have encouraged clinical researchers to trial CAR T cell therapy for the treatment of other cancers of the blood, or for solid tumors.[30–32] However, despite this optimism, the current treatment outcomes of CAR T-treated patients with non-B cell malignancies has ranged from modest to poor.[30,33–37] Among immunotherapy recipients who experience tumor progression, causes of treatment failure are broad and frequent. Common mechanisms currently under investigation include T cell hypofunction,[34] unestablished immunological memory,[38] the emergence of antigen loss variants,[39,40] or insufficient persistence[41] due in part to cell-extrinsic barriers imposed by the hostile tumor microenvironment.[42,43]

1.1.4 | CAR T potency enhancement

Given the range of obstacles, current cell enhancement strategies now routinely venture beyond optimization of the CAR transgene to include gene payloads that modify many different facets of cell behavior.[44–48] Common areas of focus include (1) amelioration of T cell exhaustion or hypofunction, (2) preservation of stem cell-like memory states, (3) resistance to hypoxia or nutrient deprivation, (4) improved T cell persistence, and (5) sustained T cell killing of tumor cells. I will now explore several of these topics in further detail here.

Observed both in cancer and chronic viral infections, T cell "exhaustion" is driven both by persistent antigen stimulation and cell-extrinsic inhibitory signaling that impedes T cells' ability to fully eliminate cellular targets. T cell exhaustion is generally defined as both a functional and epigenetic state of dysfunction characterized by reduced proliferative capacity, poor effector function (low cytokine secretion or target-cell killing), and often the fixed upregulation of multiple inhibitory receptors.[49–51] It has been suggested that solid tumors with a high antigen burden and often upregulated immunoinhibitory ligands are high-risk settings for inducing exhaustion in therapeutic T cells.[52] Indeed, numerous studies have evidenced immune-evasion strategies employed by conditioned tumors, whereby these immortalized cells hasten T cell dysfunction via negative signaling through well-identified inhibitory receptors (e.g. PD1, CTLA-4, Lag-3, Tim-3, TIGIT).[53–55] It is perhaps worth clarifying that T cell exhaustion is in fact a naturally programmed process, presumably aimed at preventing damage from unchecked inflammation, that is co-opted by patients' tumors in the setting of malignancy.[56,57] Given the disagreement around formal definitions of exhaustion, researchers sometimes more broadly refer to this as T cell hypo- or dysfunction, to describe the general dwindling of activity that culminates in T cell death.

To date, multiple strategies have attempted to reverse or prevent T cell dysfunction. One approach includes forced intermittent T cell "resting" whereby the cell is temporarily barred from engaging in T cell activation by removal of cognate antigen[58,59] or disruption of one or multiple components of its respective CAR or TCR signaling cascade.[60–64] Pharmacological interventions also take the form of blocking antibodies targeting immunoinhibitory receptors on the modified T cells, broadly referred to as "checkpoint blockade." Often this mode of

therapy can increase the potency and durability of modified T cells and improve clinical outcomes.[65,66] Perhaps unsurprisingly then, these treatments exist already today as potent stand-alone options for select cancers with high mutational burdens (e.g. melanoma, small cell lung cancer), despite their high-incidence of observed off-tumor toxicity.[67,68]

One favored strategy to thwart T cell hypofunction relies on genetic programming of therapeutic cells. Here, in addition to a CAR transgene, cells are endowed with synthetic receptors that are insensitive to negative signaling (e.g. dominant negative transforming growth factor beta receptor ii, TGFBR2); alternatively, chimeric "switch receptors" are fusion proteins composed of an inhibitory receptor ectodomain paired with an intracellular signaling domain derived from a potent positive or co-stimulatory domain (e.g. PD1-CD28). Deployed to an immunosuppressive microenvironment, antigen-specific T cells armed with this dual defense-offense weapon respond to tumors' failed inhibitory signaling with enhanced effector activity. Given the elegance of this approach and breadth of potential customization, numerous switch receptor species have been created and characterized in recent years.[44,69–73]

Overlapping with T cell exhaustion, but non-identical, is the biological process of T cell differentiation. Indeed, there exists considerable debate surrounding the precise hierarchy and plasticity of T cell fates,[74–76] as well as the ideal composition in order to engineer the most potent, durable cell product.[77] Nevertheless, generally-accepted principles have emerged, bolstered by studies suggesting that less-differentiated CAR T cell populations such as naïve (T_N), central memory (T_{CM}), and stem cell memory (T_{SCM}), may possess heightened capacity for future cell expansion and thus sustained persistence.[38,78–82] Unsurprisingly as a result, numerous T cell enhancement strategies aim to deliver native or synthetic genes to prevent T

cell differentiation to shorter-lived cell subsets, and thus enhance cell renewal and ultimately prolong persistence (e.g. c-Jun, IL-7).[46,83] As T cell exhaustion lies near the terminus of a differentiation pathway, it is common for interventions that preserve T cell "stemness" to likewise resist or outright prevent exhaustion.

Sustained T cell killing, as with other phenotypes such as persistence, are heavily influenced by T cell differentiation status. As such, efforts to maintain naïve or stem-like cell populations often lead to functional outcomes that include a heightening capacity for long-term tumor target killing. Nevertheless, some groups have opted to pursue this behavioral output in a more targeted way. Advances in live cell imagining have provided platforms for high-throughput cytotoxicity assays,[84] while molecular proxies of T cell-mediated killing such as of LAMP-1 (CD137),[85] IFNg,[86] or cytolytic granules (e.g. GZMB, PRF1)[87] provide other potential avenues of evaluation.

Lastly, as alluded to earlier, microenvironments deficient in nutrients, growth signals, or molecular oxygen limit the growth and effector functions of trafficked T cells. To overcome specific metabolic vulnerabilities, researchers have deployed transgene payloads to bolster oxidative phosphorylation and ultimately improve tumor killing *in vivo*.[88,89] Likewise, the overexpression of modified hypoxia-responsive genes have produced more durable CAR T cells in xenograft models.[90] Interestingly, particular groups have managed to exploit this hurdle by engineering hypoxia-responsive CAR devices that restrict tumor targeting to low oxygen environments.[91,92]

1.1.5 | Picking the best of the best: embracing gene-nominating platforms

Given the plethora of cell features partly summarized here, over the last decade the list of potential genetic enhancements has swelled. In response, increasingly deliberate efforts have been made to streamline candidate evaluation across a variety of screening platforms to advance only the most-promising leads. Most of these platforms take the form of a pooled format, where a collection or library of diverse candidate molecules are distributed across a population of cells. This mixture of cells is put through a selection landscape of interest intended to expand, prune, or otherwise modify the cells – which are then recovered in bulk ("survival screen") or sorted into separate population bins based on a defined phenotypic proxy (e.g. marker^{high} vs. marker^{low}, "phenotypic screen"). After collection, genomic (g)DNA – or in some instances, RNA – is extracted, and the frequency of each candidate is determined by next-generation sequencing (NGS) based on candidate barcoding. Compared to more traditional arrayed screening methods, pooled screening substantially reduces the experimental footprint required to perform head-to-head comparisons and incurs markedly lower marginal costs as a function of increasing library size. Given the obvious utility of this approach, numerous research programs have pivoted towards this general framework, with several reporting successful nomination of candidates exhibiting (1) superior CAR signaling scaffolds,[87,93] (2) resistance to immunosuppressive ligands, [94] and (3) enhanced proliferation.[95] For pooled libraries to operate efficiently, they depend on the relatively even delivery of candidate molecules to provide sufficient predictive power. Given the sequence diversity of synthetic and native genes that inevitably populate most large libraries, molecular size heterogeneity imposes a formidable

obstacle by incurring a significant loss of screening sensitivity as pooled libraries accumulate sequence-diverse candidates.[96]

1.1.6 | Toward reliable genome-scale screening methods via CRISPR

In the last decade, massively parallel screening platforms based on CRISPR/Cas9 technology have emerged, operating at low cost and high scalability, primarily afforded by its programmable, modular unit of standardized size, the guide (g)RNA. This species can be readily packaged via lentiviral (LV) delivery platforms and delivered to primary T cells to re-program expression patterns of specific genomic loci.[97,98] While traditional CRISPR-based screens concentrate on irreversible gene deactivation ("loss of function"), this platform has been re-tooled to engage in broader gene modification, which today includes gene activation (CRISPRa), inhibition (CRISPRi), and various forms of epigenetic modulation.[99,100]

Among these, CRISPRa is most similar to therapies delivering native or synthetic transgenes in that it functions by overexpressing genes of interest, with the aim of modifying cell behavior – or "gain of function" (GoF). By directing dCas9 and transcriptional activators to a gene's promoter, subsequent transcription can be dialed up to very high levels, and sometimes far in excess of endogenous gene expression.[101] When executed as a pooled system, with different cells across a population each receiving unique gene-specific gRNAs, this technology can test the effect of many genes among a population of cells and context of interest. When properly scaled, this system can ultimately interrogate the entire protein-coding genome (i.e. the

exome) as it hunts for genes that modify select cell behavior or states. As a technical, matter, such a system may also be capable of modulating non-coding genes as well.

1.1.7 | Envisioning CRISPRa-CAR T cells

If applied successfully to CAR T cell or related adoptive T cell therapy paradigms, CRISPRa technology holds tremendous promise as a gene-nomination platform to better inform the next generation of potent cells products for immunotherapy. Here, I describe my efforts to adapt and deploy this tool to populations of primary human CAR T cells, and simultaneously establish broad GoF screening pipelines for cell-based immunotherapy enhancement.

1.1.8 | Overview of thesis research

This document details my efforts building a durable GoF screening platform for primary human CAR T cells. Chapter two focuses on early efforts to profile and adjust established CRISPRa coding sequences (CDSs) for optimal behavior and high potency in an immortalized T cell line. Chapter three follows my transition into primary CAR T cell manufacturing, detailing vector and molecular optimization. Chapter three also seeks to describe key design features identified during serial optimization and associated molecular mechanisms. Also outlined is the partial characterization of my final cell manufacturing process and the long-term potency and durability of my optimized CRISPRa-CAR T cells. Chapter four deploys this system at-scale through the execution of a genome-wide CAR T cell *in vitro* persistence. Finally, chapter five aims to increase the flexibility and screening power of my system by examining potential

alternative modes of regulation (e.g. druggable, cell-autologous) – first using immortalized T cells then with primary CAR T cells.

Chapter 2 | Optimization of CRISPRa Platform in T cells

2.1 | Abstract

CRISPR activation (CRISPRa) can potently overexpress target genes as programmed by specific gRNA, but reliable implementation within particular human cell subsets, particularly T lymphocytes, has been challenging. Here I profile serial improvements to a CRISPRa second generation synergistic activation mediator system as evaluated within the Jurkat immortalized T cell line. Among them, I identified: the (1) replacement of dCas9-tethered VP64 with a fluorescent reporter, (2) substitution of PP7 for MS2-based aptamer designs, and (3) exchange of a viral N-terminal nuclear localization signal for a peptide sequence derived from human c-Myc. These alterations increased the positive identification of CRISPRa-competent cells while maintaining or increasing CRISPRa potency. In contrast, I identified no observable benefit from increased gRNA valency, activator substitutions/complexing, or CRISPRa effector multimerization. My studies recommend new CRISPRa species for optimal T cell programmed gene overexpression, while suggesting a focused investigation of transcriptional sterics for future optimization efforts.

2.2 | Background

2.2.1 | CRISPRa technological iterations

Since the recognition of CRISPR-Cas9 as a programmable endonuclease,[102] rapid and concerted efforts have been made to expand its scope and application.[103] Early derivatives were formed by first mutating core residues (D10A, H841A) in Cas9 and thereby generating a "dead" (d)Cas9 with abolished endonuclease but retained DNA-homing function.[103] This Cas9 variant now could be used as a programmable trafficking scaffold upon which effector proteins could be affixed, selected based on the specific form of modulation desired – without the risk of causing DNA double-stranded breaks. To enable transcriptional activation, researchers first tested tethering activation modules directly to dCas9 in the form of VP16 concatamers (e.g. VP64), a transcriptional activator derived from the Herpes Simplex Virus.[104] When also supplied a gRNA addressed to a narrow region of a gene's respective promoter,[99,105–108] this constellation of proteins was shown capable of upregulating target genes with high specificity.[109–112] This programmable gene overexpression system was termed "CRISPR activation" (CRISPRa). An alternative activation strategy omitted the dCas9 tether and instead appended to the gRNA 3' end aptamer hairpins (MS2) which bind with extremely high affinity to their cognate receptor, the MS2 bacteriophage coat protein (MCP).[113] By then also supplying a soluble MCP-VP64 fusion protein, this synthetic CRISPRa effector can likewise increase gene expression as programmed by specific gRNAs.[104]

As a result of promising early demonstrations, CRISPRa derivatives have proliferated rapidly. Many subsequent iterations expanded on established designs, with candidates intended for mammalian cellular systems exchanging VP64 for activators of greater valency (e.g. VP192)[114], power (e.g. p65, HSF1),[115] and/or complexity (e.g. VP64-p65-Rta or VPR).[116] Likewise, other research groups iterated on designs dependent on activator recruitment to the gRNA.[117] One of the most broadly adopted and potent designs known as the synergistic activation mediator (SAM) system blended these strategies, with dCas9 bearing a tethered VP64 and introducing an MCP-p65-HSF1 soluble fusion protein that binds to an optimized gRNA with aptamer sequences installed internally within the molecule's tetraloop and secondary stem loop.[115] Interestingly, optimal placement of these aptamers appears to be particular to both species and cell type.[117] Lastly, while CRISPRa has been shown to induce very high levels of overexpression of select genes, it is not always able to do so reliably or uniformly across cell lines or timescales.[118] This is likely the result of gene-specific overexpression inefficiencies dictated both by epigenetic and related biophysical features. Given that CRISPRa depends on the molecular localization, attachment, and often the recruitment of effectors (that themselves recruit higher-order effectors or even RNA polymerase II directly), it is inherently sensitive to (1) gene and chromatin accessibility, (2) specificity and strength of gRNA binding, (3) competition from trafficked transcription factors, (4) and other locus-specific molecular sterics.[108,119] As such, no large, multi-locus targeting system might adequately address all possible causes of transcriptional interference, which vary even within the same cell as a function of time and environmental perturbations. Nevertheless, efforts to maximize potency will ensure that gene-specific differences in CRISPRa induction potential are minimized.

2.2.2 | Challenges in CRISPR expression

As mentioned previously, researchers have reported challenges in reliable, sustained expression of CRISPRa and other Cas9-derivative systems.[97] Given the high potency of various transactivators, many delivered in an unregulated, soluble form, scientists have suggested that CRISPRa effectors may trigger cell death through non-specific genotoxicity.[120,121] Other lines of research have indicated that dCas9 itself has the capacity to impose toxicity in certain environments, which may be driven by its DNA-homing function with or without a targeting gRNA.[122,123] Indeed, early forms of CRISPRi operated merely by targeting the dCas9 at or immediately downstream of a gene's transcription start site (TSS) – indicating that even in the absence of effector modules, dCas9 has the inherent capacity to modulate gene expression.[103] Ultimately, regardless of the precise mechanism or mechanisms, the forced expression of a toxic payload would inevitably select against high-expressers, and unintentionally impose a ceiling on tolerable CRISPRa activity.

2.2.3 | CRISPRa content and versatility

Early CRISPRa screens, like other pooled screens, initially generated simple readouts of candidate enrichment over time as a consequence of bulk cell survival or within the context of a specific, predetermined phenotype.[115] This information is regularly extracted from CRISPR-based screens through the targeted PCR-amplification of gRNA cassettes that have integrated into host cell genomes, spread across the library of candidate cells. As NGS platforms and associated bioinformatics tools have matured in the last decade, library-based screens have begun to successfully capture increasingly larger degrees of bioinformatic content on a per-cell

basis. Leveraging single-cell RNA sequencing (scRNA-seq) pipelines which most often operate via droplet-based cell compartmentalization, researchers can now capture single cell informatics on mRNA ("transcriptome"),[124] TCR clonotype,[125,126] limited protein expression,[127] and a seemingly ever-expanding set of modalities or "omics." Often included in these scRNA-seq pipelines is a modality to also capture cells' expressed CRISPR gRNAs.[128] This additional capacity however is non-trivial, as unlike protein-coding mRNAs, gRNAs are preferentially transcribed by RNA polymerase III (RNAPIII). RNAPIII products are unique in that they lack a 5' 7-methylguanosine (m7G) cap and a polyadenylated [poly(A)] tail; as such, they are not efficiently exported from the cell's nucleus, nor are they copied *ex vivo* into complementary (c)DNA by reverse transcription that prime on mRNA poly(A) tails using deoxythymidine oligonucleotides (oligo(dT)).

To circumvent this problem researchers have devised several potential workarounds. One simple solution is to spike a gRNA-specific primer into the emulsion-based systems to enable targeted reverse transcription of gRNA.[129] Often this is performed by introducing a 'capture' sequence directly into the gRNA backbone,[130] and extreme care must be taken not to negatively impact CRISPRa potency through changes to gRNA structure. One research group employed a slight alteration to this general method by directly installing a poly(A) mimic directly into one of the gRNA hairpins.[131] In contrast, a very different strategy utilizes a feature of lentiviral replication, whereby a gRNA expression cassette is inserted within the 3' long terminal repeat (LTR) of a lentiviral transfer vector.[132] As part of lentivirus's integration into host cell genomes, it obligatorily copies its 3' LTR to the 5' end in order to reconstitute its full genome – a feature that is routinely exploited by self-inactivating (SIN) lentiviral vectors. As a result, cells

successfully transduced with this special gRNA-containing SIN lentivirus now possess two gRNA copies: one upstream that generates functional gRNA, and a secondary copy present still within the 3' LTR that is caught up in RNAPII-transcription originating from the vector's protein-coding promotor. It is this latter transcript that is then detected by oligo(dT) processing.

2.2.4 | Efficient CRISPRa use in T cells

Given the varied CRISPRa efficiencies reported as a function of cell line, I first sought to profile and refine borrowed CRISPRa CDS in a model cell line, prior to implementation in primary T cells. The Jurkat cell line was derived in the 1970s from a child with T cell leukemia.[133,134] This line has been used across hundreds of studies to model T cell behavior.

2.3 | Results

2.3.1 | Getting started

To initiate my studies, I first acquired publicly-available plasmids with CRISPRa sequences originating from the lab of Feng Zhang and built on the potent SAM system design.[115,135] To simplify my initial evaluation and enable the ability to quickly iterate my designs, I chose to transiently express candidate vectors as naked plasmid, facilitated by electroporation (i.e. nucleofection). Prior to implementation I transferred the CRISPRa CDSs to a dual-promoter parent vector containing the strong gammaretroviral *MPSV LTR, NCR deleted, and d/587 PBS* (MND)[136] promoter driving expression of the CRISPRa transgene, and the *Elongation Factor 1 alpha / human T-lymphotropic virus* (EF1α-HTLV) hybrid promoter driving expression of a

putative selectable marker (PuroR or DHFR^{FS}).[137,138] The selectable marker was intended to be later replaced or supplemented with CAR transgene. Both promoters have supported very high levels of transgene expression in primary T cells when paired with a variety of diverse payloads.[139–143] Lastly, I flanked coding CDS with two well-described insulator core sequences derived from the chicken hypersensitive site-4 (cHS4); these insulators have been shown to dramatically improve sustained transgene expression when integrated into host cell genomes.[144,145] In addition to standard SAM design elements of a tethered dCas9 and soluble MCP-p65-HSF1 (MPH) effector, this polycistronic CDS also included a c-terminal mCherry fluorescent reporter to monitor protein expression.

To simplify efforts, I chose to test CRISPRa activity by targeting genes coding for proteins that traffic to the cell membrane, and thus, would be quickly and easily measured by flow cytometry. I began by profiling representatives from three distinct expression classes: CD25 (low basal), C-X-C chemokine receptor type 4 (CXCR4) (high basal), and CD22 (no basal). In line with expectations, CD25-targeting gRNAs potently overexpressed their cognate protein, while CXCR4 gRNAs exhibited a variable, very modest increase in already very high CXCR4 expression (**Fig 2.1**). Of some excitement, the CRISPRa system modestly activated CD22, a lectin molecule absent in T cells.[146] CD25 is the high-affinity IL-2 receptor alpha chain and is rapidly and potently upregulated in T cells in response to TCR stimulation; as a result, this behavior potentially restricted its utility as a CRISPRa reporter in certain contexts. To avoid this limitation, I also profiled a set of chemokine receptor genes that prior studies had suggested were not upregulated in response to T cell activation, nor had high basal T cell expression. Among these genes was C-C Motif Chemokine Receptor 2 (CCR2).[147,148] When targeted, this

gene exhibited ideal behavior for my intended purpose as a CRISPRa target reporter: (1) low basal expression, (2) stable expression upon T cell activation, (3) and non-trivial upregulation in response to CRISPRa targeting (**Fig 2.1**). CXCR4 insensitivity to T cell activation was later exploited in **Chapter 5**.

Of note, despite achieving marked on-target gene overexpression throughout the aforementioned experiments, I observed only very low levels of expressed CRISPRa translation marker (mCherry), that was dwarfed by the CRISPRa target^{+} cell population across multiple attempts. I suspected that the mCherry marker may be operating on a different kinetic timetable, having matured and then vanished prior to data acquisition while the CRISPRa protein target had not yet peaked. To evaluate this, I engaged in repeated efforts to purify Jurkat T cells, relying on low-frequency, random integration. This process produced very few viable clones, even after extensive culturing and selection. When evaluated, the vast majority of these clones still evidenced extremely low levels of mCherry expression – a puzzling result, that would not be fully elucidated for some time. However, this did suggest to us that the low levels of observable transfection marker were unlikely to be merely a problem of kinetic profiling. Furthermore, recognizing that gRNA target expression did not offer a reliable general means to assess the true population of CRISPRa-competent cells, I sought to first improve the strength and fidelity of the fluorescent reporter.

2.3.2 | Marking CRISPRa-competent cells

I recognized that the CRISPRa polycistronic coding cassette containing ribosomal skip sequences, while a ubiquitous and invaluable device for multiprotein expression, likely conferred preferential expression to early, n-terminal cistron products.[149,150] Given that multiple groups have successfully produced numerous Cas9-based fusion proteins, I chose to relocate mCherry to the dCas9 c-terminus (CTD), replacing the tethered VP64. As assessed by total CCR2 positivity, I saw no apparent reduction in gene activation (**Fig 2.2**) despite losing VP64 – a result that is both consistent with observations made elsewhere[151] and may also be an alternative interpretation of data presented characterizing the original SAM design.[115] In fact, dCas9 CTD-mCherry not only better 'captured' the population of CCR2-induced cells (48%), it may have modestly increased potency. Desiring even greater improvements, I iterated on this design by testing other bright red fluorescent proteins (RFPs), including mRuby3[152] and mScarlet.[153] Both candidate RFPs dramatically improved upon the tethered mCherry design, exhibiting similar CRISPRa 'capture' or reporting efficiencies; mScarlet behaved similarly at both termini of dCas9, and I did not test an n-terminal (NTD) tether of mRuby3 based on prior reporting that its family of RFPs disfavored this positioning.[153] As before, the new class of RFPs did not reduce CCR2 activation, and may have even increased it (**Fig 2.2**). Moving forward, the vast majority of subsequent studies employed the dCas9 NTD-mScarlet with a flexible $(GGGS)_3$ linker ("SAM.10"), in part due to its very high capture efficiency and observed CRISPRa potency; I also considered mScarlet, having a slightly more red-shifted emission spectra than mRuby3 ("SAM.7"), to be more compatible with future multiplexing with green fluorescent protein (GFP) derivatives.

2.3.3 | Optimization of CRISPRa expression, potency, and versatility

In addition to establishing a more trackable CRISPRa system, I also sought to maximize expression and ultimately gene activation potency to the extent reasonably achievable. As alluded to earlier, CRISPRa implementation, while highly programmable, can suffer gene-specific overexpression inefficiencies, and often has reduced power compared to pooled GoF screens that employ collections of open reading frames (ORFs).[154,155] To address this, I first examined nuclear localization signals (NLSs) flanking dCas9. Within an anuclear prokaryote, native Cas9 resides in the cell's cytoplasm; when transferred to a eukaryotic cell, Cas9 will (perhaps surprisingly) take up part-time residence in the cell's nucleus.[156] Nevertheless, others have shown that NLS fusions can improve Cas9 intracellular trafficking, and therefore performance.[157,158] My parent vector included two copies of the simian virus 40 (SV40) large T antigen NLS [PKKKRKV],[159] which I choose to replace with a bipartite NLS extracted from c-Myc [PAAKRVKLD].[160] Studies have suggested $NLS_{c\text{-}Myc}$ may permit more efficient nuclear trafficking and retention in human cells.[161,162] Using the new set of improved CRISPRa transfection reporters, I next tested various alterations of NLS species (e.g. replacement, deletion), NLS concatemerization, and linker substitution as informed by recent studies.[162,163] Interestingly in my model system, a single CTD $NLS_{c\text{-}Myc}$ was able to reproduce the effect of two flanking $NLSs_{SV40}$, while the vast majority of additional candidate implementations failed to improve and often appeared to impede effective CCR2 overexpression. An exception to this trend was a design that included a dCas9-CTD $NLS_{c\text{-}Myc}$ +NTD NLS_{SV40} that appeared to modestly improve upon parent vector (**Fig 2.3**). Overall, this exploration appeared to yield only a minor benefit to CRISPRa potency enhancement in my system.

Next, I turned my attention to the other components of within my CRISPRa system: the gRNA and CRISPRa effector. While the inherited design included a CRISPRa effector based on MCP, other groups have also examined an analogous aptamer-binding coat protein derived from the PP7 bacteriophage (PCP).[164] Relative performance of MCP or PCP fusions may be particular to specific model systems, with studies producing discordant results.[117,151] Some have indicated that lentiviral vectors that include MCP often produce substantially low-titer virus, which may suggest a generalized problem in efficient expression or incidental toxicity.[154] Thus, I tested a vector series that included MS2/MCP replacement with PP7/PCP. Indeed, in my hands, I observed higher levels of both RFP and CCR2 expression using a PP7/PCP implementation relative to MS2/MCP, concurring with the explanation that PP7/PCP may exhibit improved expression or lower toxicity in the immortalized T cell line (**Fig 2.4a, b**). Additionally, I tested a variety of gRNA variants with reshuffled RNA aptamers.[117] Beyond CRISPRa potency enhancement, my secondary goal here was to test if baseline designs would tolerate two additional features: (1) an internal gRNA 'capture' or pseudo-poly(A) sequence to enable downstream capability with scRNA-seq processing pipelines and (2) a cell-specific barcode (iBAR)[165] to increase the power of the screening platform and limit the impact of renegade T cell clones that might expand due to factors independent of CRISPRa target contribution. Tests indicated that these gRNAs tolerate displacement of PP7 and MS2 aptamers to the 3' end, although this appeared to negatively impact the PP7 design uniquely. Additionally, efforts to further boost activity through the installation of additional aptamers impeded activity in either system (PP7/MS2), which may reflect unfavorable aptamer-coat protein sterics (**Fig 2.4a, b**). Finally, I also tested substitutions to CRISPRa activator fusion protein. The original SAM design

includes the NF-κB p65 subunit (RelA) transactivation domain, and incidentally, the version selected is of mouse origin; it is unclear if this is of intentional design as it is not explicitly stated in the original study.[115] Nevertheless, I unexpectedly observed a modest loss in potency when I replaced mp65 with the humanized equivalent that also contained amino acid substitutions known to reduce hp65 negative signaling (K310Q, S536E).[166–168] In a similar vein, iterative attempts aimed at increasing potency through the addition of other common CRISPRa activators (e.g. VP64, Rta) also reduced potency relative to parent vector – in this case, substantially (**Fig 2.4c ,d**). Going forward, I chose to implement a CRISPRa effector composed of PCP-mp65-HSF1 (PPH). Somewhat fortuitously for alignment purposes, this corresponds to more prevalent modern designs.[154,86]

Having observed increases in CRISPRa expression and potency as a function of aptamer-binder substitution, I considered whether similar gains in performance might exist with unconventional ligand-receptor pairs beyond MCP and PCP. Scouring various lists, I came across two CRISPR RNA (class III and I-F) endonucleases derived from *Thermus thermophilus* (Cas6a) and *Pseudomonas aeruginosa* (Cas6f or Csyf). Like MCP and PCP, Cas6a and Cas6f proteins recognize their cognate RNA aptamer sequences with very high affinity (≈10^{-10} and 5×10^{-11} M, respectively), surpassing MCP/MS2 and PCP/PP7 (≈4×10^{-9} and 10^{-9} M).[169] Conveniently, as with Cas9, mutant forms of both Cas6 enzymes have been created; although notably the abolishment of endonuclease activity in Cas6a (H37A) incurs a reduction in binding affinity (to ≈4×10^{-8} M).[170] Similarly, while the Cas6f mutant (H29A) does not have reduced affinity relative to its native form, it naturally binds as a monomer[171]; in contrast, all the other three receptors operate as dimers. When evaluated, remarkably all dCas6-aptamer pairs generated observable

CRISPRa activity of some degree as measured by CCR2 expression (**Fig 2.5a, b**). As with PP7 equivalents, the installation of aptamer sequences within the gRNA proper (i.e. tetraloop and secondary stem loop) were preferred. Interestingly, Cas6a and Cas6f mutants achieved CCR2 positivity at equivalent or increased levels relative to PCP, but decreased CCR2 geometric mean intensity (gMFI). A concurrent attempt to correct for the lower valency of the Cas6f mutant binding by increasing aptamer number did not lead to higher CCR2 levels (**Fig 2.5a, b**). In conclusion, while the profiles of the Cas6 mutants suggested having compatibility with my approach, because they did not offer a clear advantage over the established PCP CRISPRa effector, they were not advanced further.

Failing to meaningfully improve the activity of my system through activator substitution, I undertook a final, concerted approach aimed at increasing the activator density. Alternative CRISPRa designs for instance, have shown modest benefits beyond SAM though other forms or types of effector recruitment (P300Core[172–174] or SPH[175] designs). However, given the ultimate purpose, which included stably delivering CRISPRa and CAR payloads to primary T cells, I intentionally excluded designs likely to afford only modest CRISPRa potency improvements with substantial increases in CDS length. To potentially stretch the impact of current CDSs, I turned to self-assembling protein sequences intended to spur CRISPR activator multimerization. To that end, I examined the effect of tethering various GCN4 leucine zippers with self-affinity to the PPH CTD (e.g. PCP-p65-HSF1-GCN4). These sequences have been shown to spontaneously engage in dimerization or tetramerization, in parallel, anti-parallel, or circular patterns.[176–179] To ensure an adequate dynamic range and thereby guarantee that I was not operating at a potential biological limit of maximum CCR2 expression, I chose to test these iterations using a

PP7 gRNA design with reduced potency. Disappointingly, regardless of valency or alignment, all multimer candidates performed at or below the baseline PPH potency level (PP7.14) (**Fig 2.6a, b**). I noticed that on average, the parallel-oriented GCN4 variants performed slightly better than their anti-parallel equivalents of the same valency (despite still being reduced relative to baseline). Thinking that perhaps this might suggest that higher local concentrations of activators were preferred, I re-engineered several new parallel-assembly or a circular version with the GCN4 domains wedged between the PCP and co-activator domains (e.g. PCP-GCN4-p65-HSF1). Again disappointingly, these alterations fared no better (**Fig 2a, c**). Finally, employing a highly divergent approach, I also considered maximizing the spread of activators, based on a recently published, thoroughly-characterized self-assembling toroid structure shown capable of interacting with human primary T cells.[180] Designs of this nature also fared poorly (**Fig 2.6a, c**). In conclusion, none of my attempts to engage in multimerization increased CRISPRa potency above baseline.

2.4 | Discussion

2.4.1 | CRISPRa expression: a general problem?

In this chapter I identified substitutions to CRISPRa reporters and second-generation SAM systems that increase apparent CRISPRa transgene expression while also improving or maintaining CRISPRa potency (**Fig 2.2, Fig 2.4a, b**). As mentioned within the chapter, my designs included secondary transgene cassettes that encoded Puro or $DHFR^{FS}$ resistance genes. Despite my repeated attempts, I was not able to reliably isolate clones via conventional purification

methods following stable transfection that relies on unmediated random integration. Therefore, and as a consequence of using PiggyBac-compatible donor vectors, I repeated these experiments with supplemented transient PiggyBac mRNA. While these successive attempts did more reliably generate clones following selection, I was surprised to again witness very low levels of mScarlet-dCas9 expression. Further literature review indicated this to be a commonplace result when deploying dCas9-based gene payloads.[181] Given my ability to extract useful insights from transient experiments with unpurified cells, I tabled this limitation for the time being (**see Chapter 3**).

2.4.2 | Fluorescent reporter boosts CRISPRa ID, but hidden costs may be lurking

While I was pleased to observe increases in reporter fidelity, achieved through serial optimization, I confess to shortcomings in my approach. First, fluorescent reporter proteins possess intrinsic maturation and decay properties. Given the nature of my studies, I unintentionally biased screens for recombinant proteins reaching maximum fluorescence intensity at approximately 24 hours post-transfection. A more preferrable assay would have first generated stable cell lines, selecting on an invariant downstream secondary cassette. Second, I uncovered evidence during my studies that fusions to dCas9 may introduce unwanted steric constraints on downstream CRISPRa activity. As an example, I profiled two leading dCas9 fusions: dCas9-mRuby3 (SAM.7) and mScarlet-dCas9 (SAM.10). I observed that SAM.10 demonstrated lower on-target gene activation (CCR2) relative to SAM.7 when supplied gRNA designs with 3' 2xPP7 aptamer placements; in contrast, I saw no difference in activity with 2xPP7 aptamers situated within the tetraloop and secondary stem loop (***data not shown***).

While the overall evidence is scant, I suspect that these difference arise from interactions of mScarlet with the gRNAs as they protrude from dCas9.[182] Lastly, the introduction of a constitutive red fluorescent tag to my system precludes the use of flow cytometry detection reagents occupying similar emission spectra – particularly the bright fluorochrome, phycoerythrin (PE). Admittedly, tracking dCas9, a nuclear protein, would have required time-intensive permeabilization steps that would have reduced iteration speed, and may also have reduced detection ability of other antigens of interest, particularly cell surface proteins.

2.4.3 | Challenges in CRISPRa potency enhancement

While I was able to achieve increases in potency with select gRNA modifications and pivoting to a second-generation SAM system (PP7/PCP) (**Fig 2a, b**), it should be noted that most implementation attempts yielded little to no benefit. Namely, the attempted optimization of N- and C-terminal NLSs only boosted potency slightly at best, with reported C-terminal linkers underperforming relative to prior reports.[161,162] These differences may be a function of species or cell type or perhaps could indicate that dCas9 is well in excess of the limiting reagent in my system, which I suspect to be PCP. Indeed, I imagine the inversion of mScarlet-dCas9 and PPH within the current bicistron to be a worthy future experiment, and aligning with some recent contemporary designs.[181]

I was excited to observe measurable CRISPRa activity utilizing the dCas6 designs. To my knowledge, this is the first demonstration of dCas6 operating within the framework of a soluble CRISPRa effector. Given the known tradeoffs in valency or reduced affinity outlined earlier, I

was not surprised to observe that these dCas6 forms evidenced inferiority relative to PCP/PP7 baseline formats. I suspect that there may exist theoretical forms of nuclease-deficient (d)Cas6a not yet identified that retain the high affinity of native Cas6a.

Perhaps most surprising was the detrimental addition of known self-oligomerizing peptides to the CRISPRa effector. It remains elusive why diverse forms of multivalent recruitment are consistently disfavored. Generally, I suspect that the recruitment of multiple CRISPRa effectors to a narrow biophysical space could initiate a kind of molecular 'traffic jam,' that leads to ultimately lower levels of gene transcription. My strategy was based on the partial success of the CRISPRa SunTag system,[183] which derives potency from a tethered scaffold and subsequent signal amplification via VP64. Indeed, adapted versions of this design replace VP64 with the p65 and HSF1 activators ("SPH"), and may be more potent than SAM designs generally.[175] It is unclear how this strategy may succeed where mine appears to have failed, although I note that the potent SunTag and SPH designs likely form flexible linear effector concatamers, whereas my designs prioritized three-dimensional density – a molecular arrangement that may restrict the recruitment of higher order effectors. Notably, I am not the first researcher who has failed to advance combinatory CRISPRa homing and multiplexing strategies despite executing design principles that appear sound; in fact, one such unfruitful attempt characterized their results as "particularly unexpected given the dramatically different ways in which the systems generate a functional activator."[118] I strategically avoided designs that would substantially increase molecular footprint. As a result, I did not pursue implementations with SPH, nor alternative CRISPRa forms that seek to exchange or supplement CRISPRa activators with epigenetic modulators such as demethylases,[100,184,185]

2.5 | Materials and Methods

2.5.1 | General cloning workflow

SAM.1 (PB-UniSAM) was a provided by Lesley Forrester (Addgene 99866), derived originally from Feng Zhang's CRISPRa dual vector system (Addgene 61422, Addgene 73797). Subsequent constructs were generated via simple ligation cloning or isothermal (Gibson) assembly using double-stranded (ds)DNA templates: annealed oligonucleotides (Integrated DNA Technologies, IDT), gBlocks (IDT), DNA strings (GeneArt), or PCR-amplification sourced (in-house).

For protospacer cloning, 2 µg of CRISPRa parent vector was digested with BsmBI/BsmBI-v2 (NEB) or Esp3I (Thermo Scientific) at 50 °C overnight in supplied 1X buffer. The next day, plasmid digests were run on a 1% agarose gel with SYBR Safe (Thermo Scientific) at 100 mA for 45 - 60 minutes. Cut backbones were gel extracted and purified using the PCR Cleanup and Gel Extraction Kit (Takara) per the manufacturer's instructions. 100 µM complementary, reverse ssDNA fragments (IDT) were annealed by warming to 98 °C for 5 minutes in 1X Tris-EDTA (TE) buffer and allowed to passively cool to RT. For ligation cloning, duplexed oligonucleotides were combined with T4 ligase (Thermo Scientific) and appropriate buffer and together incubated at RT for 10 minutes or at 4 °C overnight. 2 µL of this reaction product was used directly for transformation. Alternatively, protospacer addition also proceeded via Gibson assembly due to its generally superior efficiency. Here, dsDNA templates included ~ +10 5' basepairs (bp) derived from the parent vector. Upon combining, insert and digested backbone were incubated with NEBuilder® HiFi DNA assembly (New England Biolabs, NEB) mix for 15 minutes to 1 hour at

50 °C. General insert:backbone molar ratios were 5:1 and 1:1 for ligation and Gibson assembly cloning, respectively.

DNA products were propagated through bacterial transformation using NEB Stable high efficiency chemically-competent *E. coli* cells (NEB) following the manufacturer's protocol. Transformed cells were plated on LB-agar Kanamycin (50 μg/mL) plates (Teknova) overnight at 37 °C. The next day, single colonies were picked and placed in 5 mL starter cultures in LB-Kan50 (Corning, Teknova) and shaken (250 rpm) at 37 °C overnight. The next day, plasmid DNA was extracted using the PureLink™ Quick Plasmid Miniprep Kit (Thermo Scientific) per the manufacturer's instructions. Successful cloning was verified via Sanger sequencing (Genewiz).

Dependent on the level of estimated transformation efficiency (as judged by a transformation plate made from reaction mix lacking an insert), colony PCR was also at times employed to prioritize clones for subsequent sequencing. In brief, prior to initiating starter cultures, clones were picked with a sterile micropipette tip and wiped in both a clean PCR tube and parallel culture vessel. Primers were chosen that specifically amplified a portion of the target insert, or that amplified just outside the intended cloning region (but would be expected to generate a PCR amplicon of unique size). Suitable forward and reverse primers (0.5 uM), 2X Sapphire Amp Fast master mix (Takara), and water were added to the PCR vessel wiped with culture cells. Colony PCR thermocycling conditions were dictated by both the master mix manufacturer and melting temperature of the particular DNA primers. PCR products were run on a 1% agarose gel as previously described. Bands of the expected size confirmed the putative positivity of specific clones and prioritized them for subsequent sequencing.

2.5.2 | Cell line maintenance and electroporation

Jurkat Clone E6-1 (ATCC) cells were cultured in RPMI-1640 (Gibco) supplemented with 10% fetal bovine serum (Hyclone) and 1% 200 mM L-glutamate (Gibco), 5% CO_2, 37 °C. Cells were passaged 1 or 2 times a week, split 1:5 or 1:10, respectively. Cells were not allowed to grow denser than 1.5 x 10^6/mL. For electroporation (EP), cells were split the day before manipulation to ensure high viability and cell turnover, thus maximizing EP efficiency.

For EP, 1 - 2.5 × 10^6 cells were centrifuged at 90 × g for 10 minutes. Upon completion, media was aspirated and cells were resuspended in 100 µL Nucleofector Kit V buffer (with supplement) and 1 µg (1 µg/uL) of experimental plasmid. Cells and DNA were carefully pipetted into cuvettes provided by the Nucleofector Kit V (Lonza). Air bubbles were then assessed to be absent or were carefully removed through gentle tapping. These loaded cuvettes were placed in the Nucleofector carousel and the X-005 (high efficiency) program was selected and run. Immediately afterwards, the cuvettes were returned to the biosafety cabinet (BSC) and topped-off with 1 mL of warm fresh culture media. After 10 minutes, the entirety of each cuvette's contents was individually moved via a transfer pipette to the well of a 24-well plate. When all EPs were finished, these plates were returned to the incubator overnight for up to 24 hours.

2.5.3 | Flow cytometry

Transfected cells were collected the day after EP and centrifuged for 7 min at 300 × g to pellet cells. Spent media was aspirated and cells were washed with 1 mL of 1X phosphate buffered saline (PBS) (Gibco). Cells were spun down again and had wash buffer removed. The samples

were then incubated for 30 minutes at RT with viability stain and antibodies specific to the CRISPRa targets listed in the section below. After staining, the cells were spun down again and had staining mix replaced with fresh wash. This was then followed by a secondary, identical wash, and then finally cells were spun down and resuspended in 1X PBS with 0.5% paraformaldehyde (PFA). Cell samples were stored at 4 °C in fixative for up to 72 hours prior to sample acquisition. To acquire relative antigen density data, these cells were run on an LRSFortessa (BD Biosciences) using FACSDiva software (BD Biosciences). Cells were isolated by first gating on bulk cell input (no FSC-A^{low}/SCS^{low} events) and live (IR-dead^{neg}) singlets (proportional FSC-A/FSC-H). Additional gating occurred in some instances on TurboGFP^{+} or RFP^{+} fluorophore equivalent (e.g. mCherry, mScarlet, MRuby3) cells as indicated. Live cells were chosen as the acquisition stopping gate at 10,000 - 50,000 specific events. Collected data was compiled and analyzed on FlowJo v10; select graphics were plotted and exported (see figures). Quantitative data was visualized using GraphPad Prism 8. Marker positivity, median fluorescence intensity (MFI), and geometric mean fluorescence intensity (gMFI) were calculated by FlowJo software.

2.5.4 | Table: Sequence origins

DNA CDS	Source	PMID
dCas9	Fidanza et al, 2017	28743878
MCP	Fidanza et al, 2017	28743878
PCP	Martella et al, 2019	31398008
dCas6a	Niewoehner et al, 2014	24150936
dCas6f	Haurwitz et al, 2010	20829488
(Mult.2/2b)	Harbury et al, 1993	8248779
(Multi.3)	Gurnon et al, 2003	12812483
(Mult.4/4b)	Harbury et al, 1993	8248779
(Multi.5)	Deng et al, 2006	16472744
(Multi.6/6b)	Boyle et al, 2012	22917063
(Multi.7/8)	Correnti et al, 2020	32203491

DNA CDS	Source	PMID
2xMS2 (SAM)	Konerman et al, 2015	25494202
2xMS2-PP7 (Calabrese SAM)	Sanson et al, 2018	30575746
2xPP7	Martella et al, 2019	31398008
3' 2xPP7	Zalatan et al, 2015	25533786
iBAR	Zhu et al, 2019	30678704
10XGenomics_Capture	Choo et al, 2021	33625849
pseudoPoly(A) L2-ext-8A8G	Song et al, 2020	32513233
pseudoPoly(A) 8A6G	Song et al, 2020	32513233
2xMS2 (SAM)	Konerman et al, 2015	25494202
2xMS2-PP7 (Calabrese SAM)	Sanson et al, 2018	30575746
PuroR	Vara et al, 1986	3714487
$DHFR^{FS}$	Jonnalagadda et al, 2013	23755242

2.5.5 |Table: Protospacer sequences

gRNA ID	Protospacer sequence	Source	PMID
CD25.1	TTATGGGCGTAGCTGAAGAA	Simeonov et al, 2017	28854172
CD25.2	TCTTCTCTCATCTCAAATAT	Simeonov et al, 2017	28854172
CXCR4.1	GCAGACGCGAGGAAGGAGGGCGC	Chavez et al, 2016	27214048
CXCR4.2	CCGACCACCCGCAAACAGCA	Chavez et al, 2016	27214048
CD22.1	CCAAGCAGCACCGTGATCTG	Sanson et al, 2018	30575746
CD22.2	GCACCGTGATCTGGGGAGTG	Sanson et al, 2018	30575746
CCR2.1	AAAGTGAAGGCGGAGATACA	Sanson et al, 2018	30575746
CCR2.2	CGGAGATACAGGGCAACTAA	Sanson et al, 2018	30575746
NT (LacZ)	TGCGAATACGCCCACGCGAT	Platt et at, 2014	25263330

2.5.6 | Table: Antibodies and reporter proteins

Antigen	Fluorochrome (laser-bandpass filter)	Vendor	Product No	PMID
(Dead)	IR Dye	Invitrogen	L10119	*NA*
mCherry	*NA* (YG-610)	*NA*	*NA*	28743878
mRuby3	*NA* (YG-610)	*NA*	*NA*	26879144
mScarlet	*NA* (YG-610)	*NA*	*NA*	27869816
TurboGFP	*NA* (Blue-530)	Lonza	VCA-1003	*NA*
CD25	BV421 (v-450)	Biolegend	356113	*NA*
CXCR4	BV605 (V-450)	Biolegend	306522	*NA*
CD22	BV421 (V-450)	Biolegend	363512	*NA*
CCR2	BV421 (V-450)	Biolegend	357210	*NA*

2.5.7 | Table: Reagents

Reagent or Equipment	Vendor	Product No.
RPMI 1640 with L-Glutamine and HEPES	Gibco	22400-089
L-Glutamine 200mM (100X)	Gibco	25030081
FBS	Hyclone	SH30070.03
Cell Line Nucleofector™ Kit V	Lonza	VCA-1003
Puromycin	Invivogen	ANT-PR-1
Methotrexate 25mg/mL	Medline	16729-277-30
1X PBS	Gibco	10010023
Molecular-grade Water	Ambion	AM9937
NucleoSpin® Gel and PCR Clean-up	Takara	740609.25
Nucleobond Xtra Maxi EF	Takara	740424.5
SapphireAmp Fast PCR—Hot-Start Master Mix	Takara	RR350B
Q5® Hot Start High-Fidelity 2X Master Mix	NEB	M0494S

BsmBI-v2	NEB	R0739L
NEBuilder® HiFi DNA Assembly Master Mix	NEB	E2621L
NEB® Stable Competent E. coli (High Efficiency)	NEB	C3040H
Miller's LB Broth	Fisher	MT46050CM
LB Agar plates with 30 µg/mL Kanamycin, 100 mm	Teknova	L1024
LB Agar plates with 100µg/mL Carbenicillin, 100 mm	Teknova	L1010
Kanamycin solution, 50mg/mL	Teknova	K2125
Carbenicillin solution, 100mg/mL	Teknova	C2130

2.6 | Acknowledgements

The author thanks Marlena Urvater and Natalie Murren – two undergraduate students attending the University of Washington – for their assistance with molecular cloning and Jurkat T cell electroporation. Also enabling this work were useful suggestions and feedback provided by other members of the Jensen lab including Adam Johnson, James Rosser, Jacob Appelbaum, and Christopher Saxby. Michael Jensen supervised the project and provided funding.

All studies were conceived of by Benjamin Curtis.

2.7 | Figures

Figure 2.1

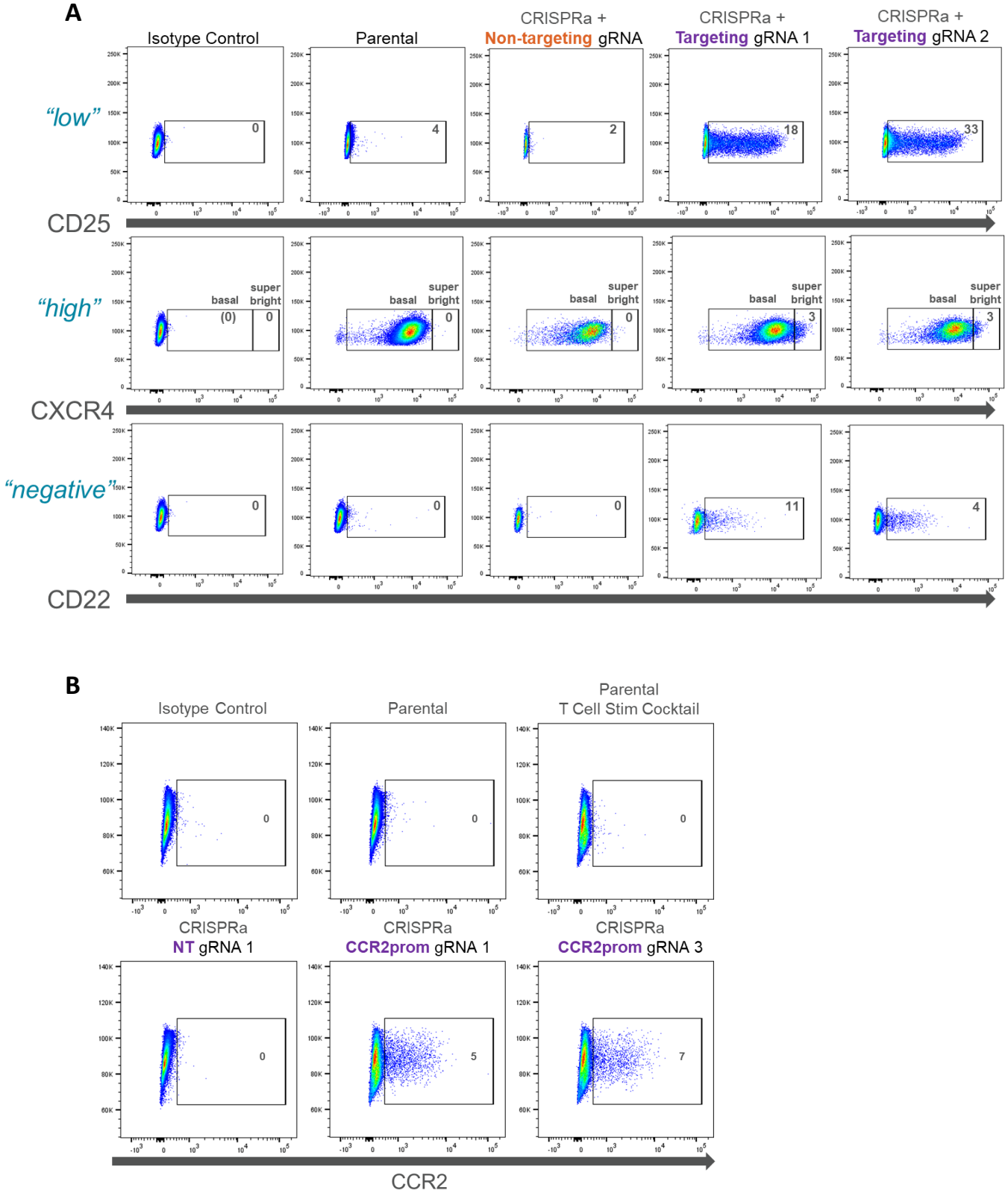

Figure 2.1: Profiling of select CRISPRa gene activation. (**A**) Representative flow cytometry plots of Jurkat T cells transiently transfected (EP) with designated variant donor plasmid (*right three columns*) or mock EP (left two columns) and assessed for antigen positivity for CD25 (IL-2Rα) (*top*), CXCR4 (*middle*), or CD22 (*bottom*). (**B)** Representative flow cytometry plots of Jurkat T cells transiently transfected (EP) with designated variant donor (*bottom*) or mock EP (*top*) and assessed for antigen positivity for CCR2 (CD192). Each class of CRISPRa target/antigen are classified as "low," "high," or "negative," relative to their basal left of expression in resting Jurkat T cells.

Figure 2.2

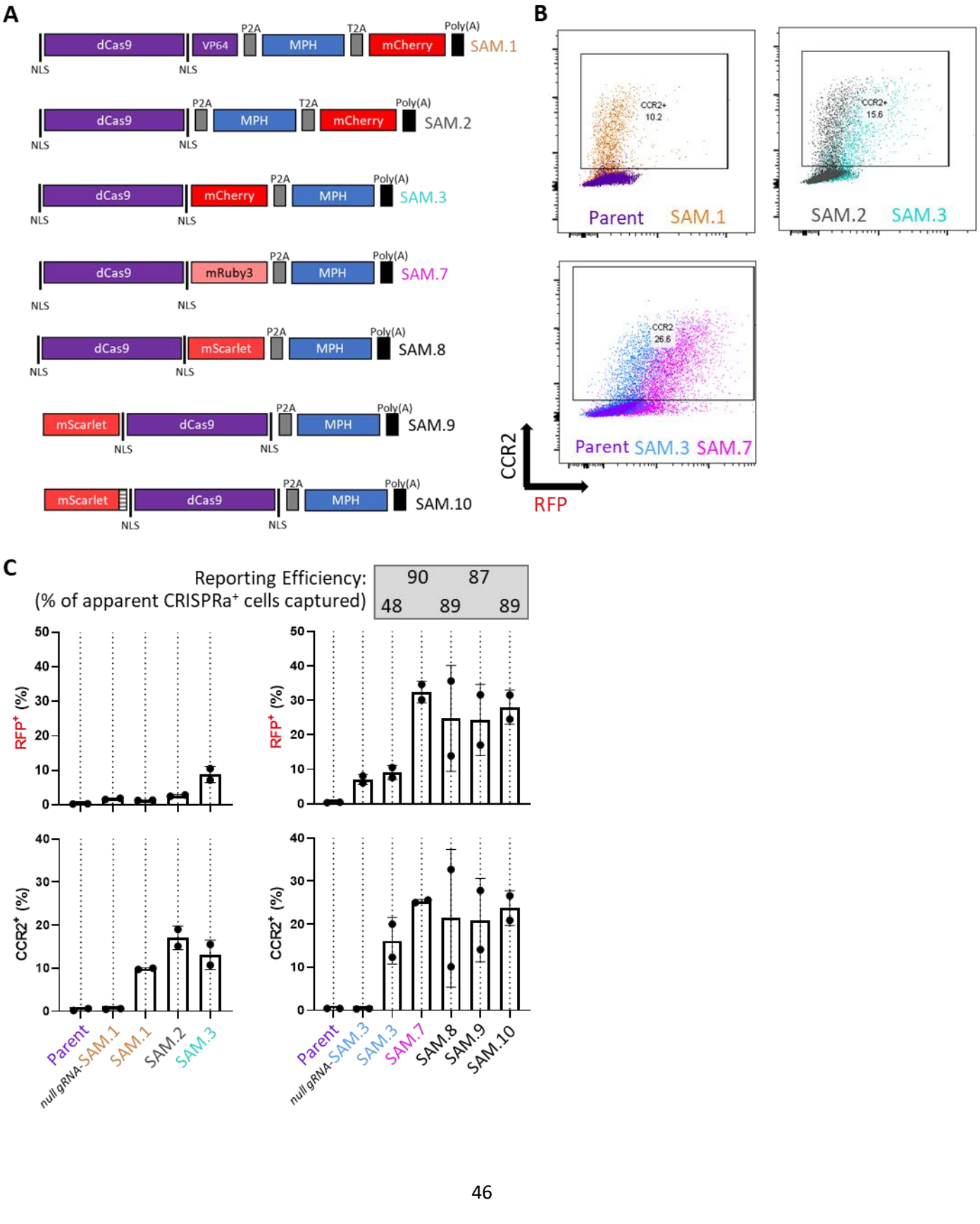
A
dCas9
VP64
P2A
MPH
T2A
mCherry
Poly(A)
SAM.1
NLS
SAM.2
SAM.3
mRuby3
SAM.7
mScarlet
SAM.8
SAM.9
SAM.10
B
CCR2+ 10.2
Parent
SAM.1
CCR2+ 15.6
SAM.2
SAM.3
CCR2 26.6
Parent SAM.3 SAM.7
CCR2
RFP
C
Reporting Efficiency:
(% of apparent CRISPRa+ cells captured)
90
87
48
89
89
RFP+ (%)
CCR2+ (%)
Parent
null gRNA-SAM.1
SAM.1
SAM.2
SAM.3
null gRNA-SAM.3
SAM.3
SAM.7
SAM.8
SAM.9
SAM.10

Figure 2.2: Evaluation of CRISPRa fluorescent reporters. (**A**) Curated graphics of CRISPRa reporter variants. (**B**) Representative flow cytometry plots of Jurkat T cells transiently transfected (EP) with designated variant donor plasmid and analyzed after overnight incubation. (**C**) Quantified, normalized geometric mean fluorescent intensities from flow analysis of all cultures. Samples are gated on live, RFP (CRISPRa transgene)$^{+}$ singlets (C, upper) or live singlets only (C, lower). Quantitative data in (C) depicts mean and standard deviation of two EP replicates.

Figure 2.3

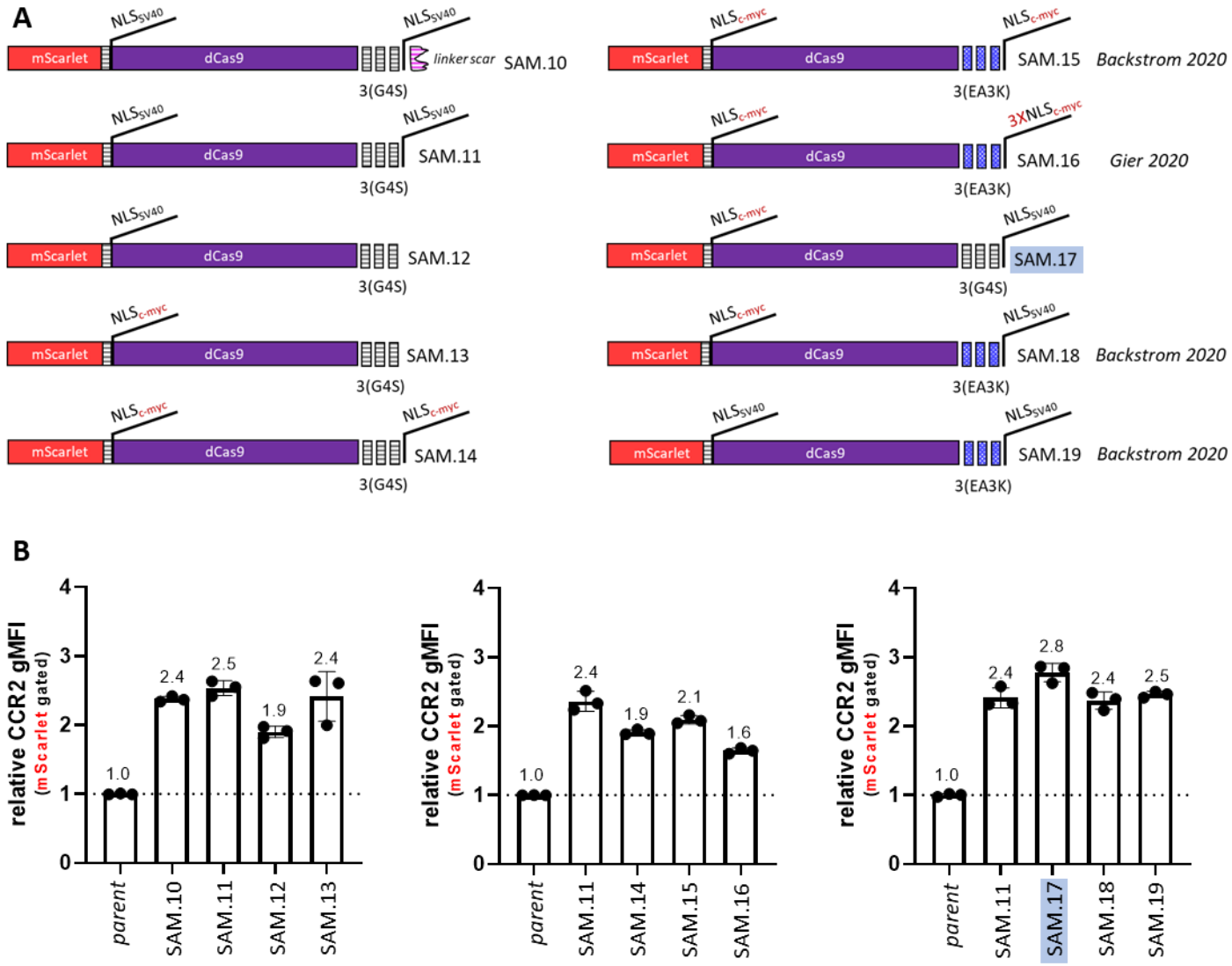
A
mScarlet
dCas9
NLSSV40
NLSc-myc
linker scar
3(G4S)
3(EA3K)
3XNLSc-myc
SAM.10
SAM.11
SAM.12
SAM.13
SAM.14
SAM.15
SAM.16
SAM.17
SAM.18
SAM.19
Backstrom 2020
Gier 2020
B
relative CCR2 gMFI
(mScarlet gated)
parent
1.0
2.4
2.5
1.9
2.4
1.6
2.1
2.8
2.5

Figure 2.3: Evaluation of impact of NLS variation in number, species, and proximal tether on CRISPRa activity. (**A**) Curated graphics of CRISPRa NLS variants. (B) Quantified, normalized geometric mean fluorescent intensities from flow analysis of all cultures. Samples are gated on live mScarlet-dCas9^{+} singlets or live singlets only (parent cultures only). Quantitative data in (B) depicts mean and standard deviation of three EP replicates.

Figure 2.4

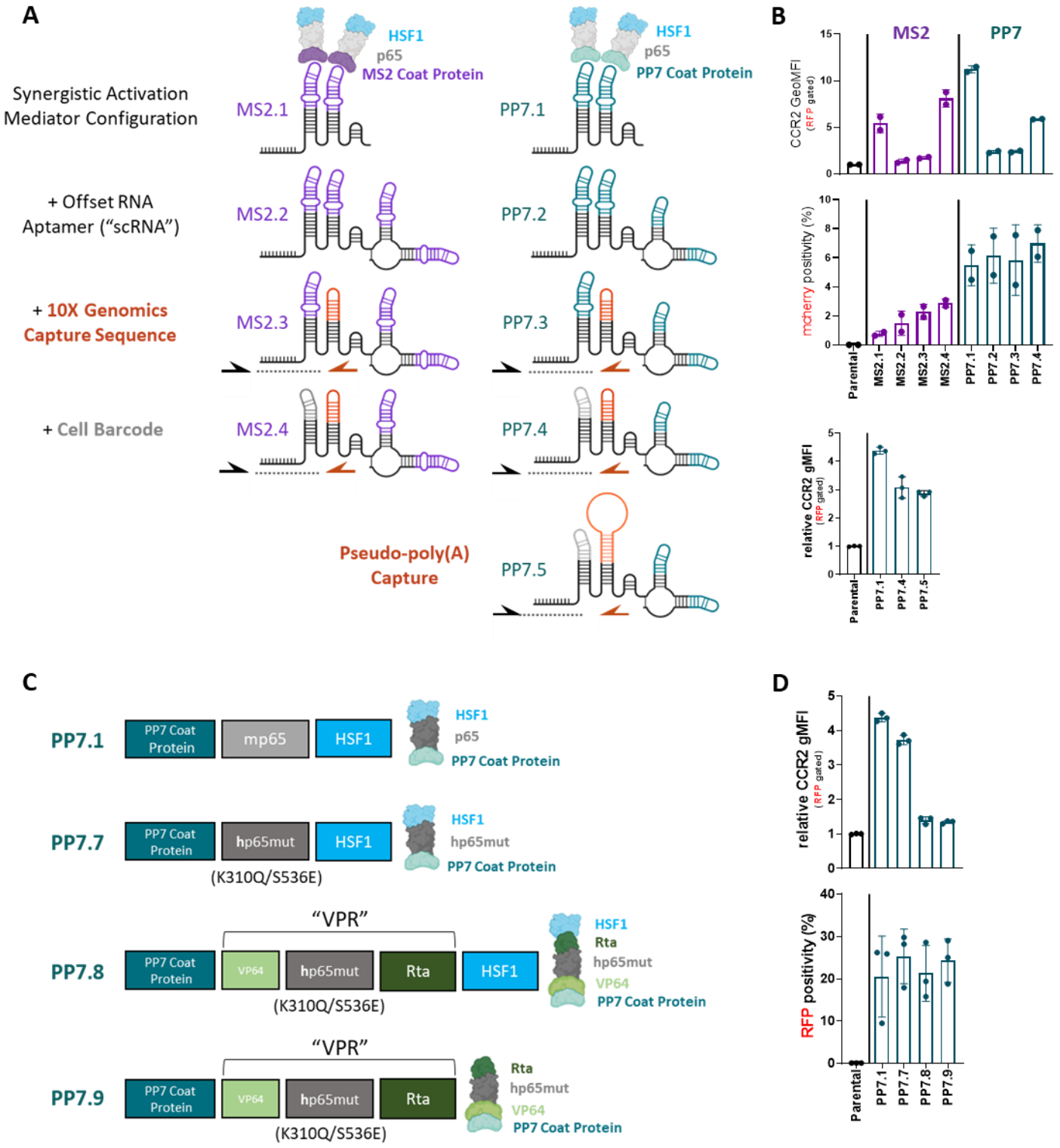
A
Synergistic Activation Mediator Configuration
+ Offset RNA Aptamer ("scRNA")
+ 10X Genomics Capture Sequence
+ Cell Barcode
HSF1
p65
MS2 Coat Protein
PP7 Coat Protein
MS2.1
MS2.2
MS2.3
MS2.4
PP7.1
PP7.2
PP7.3
PP7.4
Pseudo-poly(A) Capture
PP7.5
B
MS2
PP7
CCR2 GeoMFI (RFP gated)
mCherry positivity (%)
relative CCR2 gMFI (RFP gated)
Parental
C
PP7.1
PP7 Coat Protein
mp65
HSF1
PP7.7
hp65mut
(K310Q/S536E)
PP7.8
"VPR"
VP64
Rta
PP7.9
D
RFP positivity (%)

Figure 2.4: Optimization of CRISPRa aptamer-activator and gRNA variants. (**A**) gRNA variant designs. (**B**) Quantification of CRISPRa endogenous target (CCR2) (*top and bottom graphs*) and fluorescent reporter (mCherry) (*middle graph*) positivity across gRNA designs transiently delivered via EP using plasmid to Jurkat T cells and assessed the next day. (**C**) PP7 coat protein CRISPRa effector variants designs. (**D**) Quantification of CRISPRa endogenous target (CCR2) (*top graph*) and fluorescent reporter (*middle graph*) positivity across gRNA designs transiently delivered via plasmid to Jurkat T cells via electroporation and assessed the next day. All quantified data was obtained via flow cytometry gated on live singlets. Quantitative data in (B) and (D) depict mean and standard deviation of two or three EP replicates.

Figure 2.5

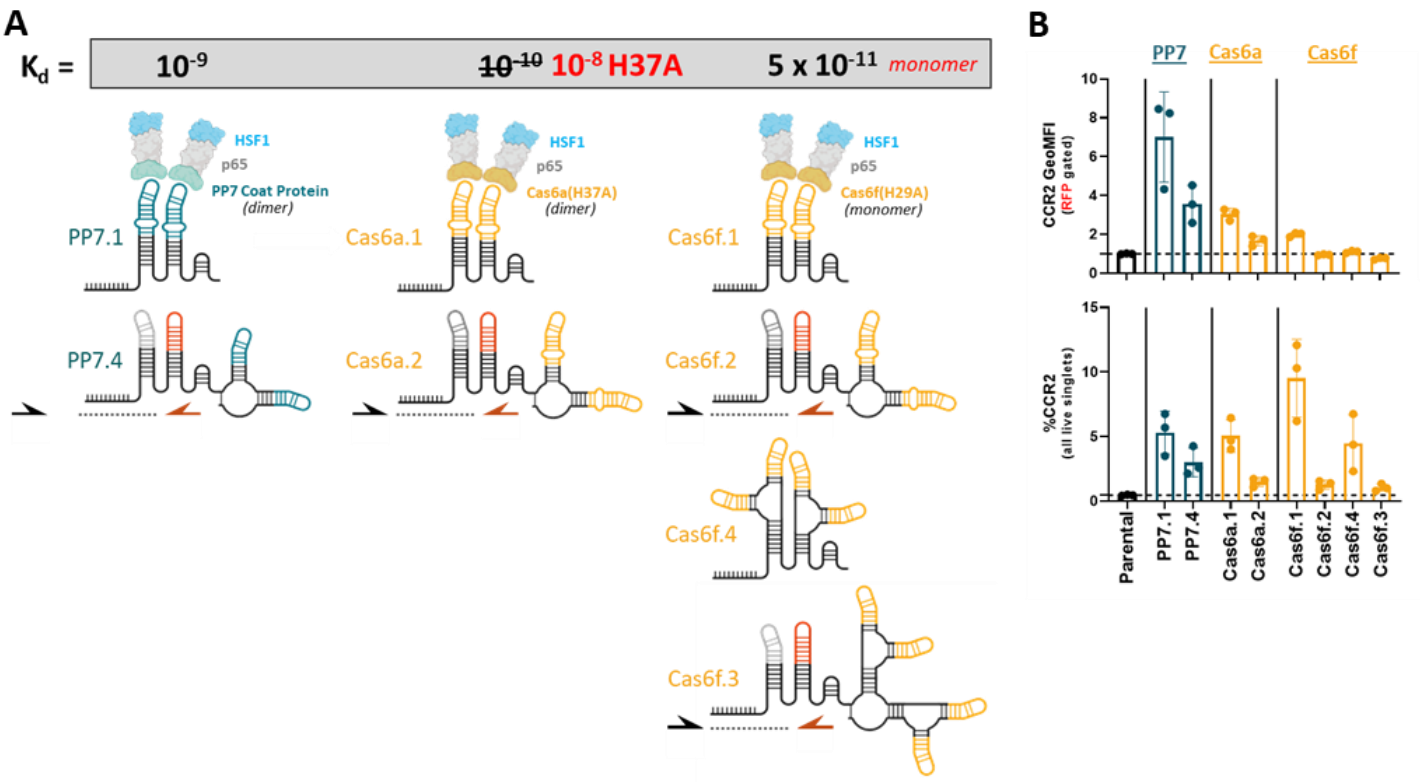
A
K_d =
10^{-9}
~~10^{-10}~~ 10^{-8} H37A
5 x 10^{-11} monomer
HSF1
p65
PP7 Coat Protein
(dimer)
PP7.1
PP7.4
Cas6a(H37A)
(dimer)
Cas6a.1
Cas6a.2
Cas6f(H29A)
(monomer)
Cas6f.1
Cas6f.2
Cas6f.4
Cas6f.3
B
PP7
Cas6a
Cas6f
CCR2 GeoMFI
(RFP gated)
%CCR2
(all live singlets)
Parental
PP7.1
PP7.4
Cas6a.1
Cas6a.2
Cas6f.1
Cas6f.2
Cas6f.4
Cas6f.3

Figure 2.5: dCas6f (dCsy4) CRISPRa effector performance across gRNA designs. (**A**) Graphics of depicted dissociation constant (*upper*) and CRISPRa effector variant design (*lower*). (**B**) Quantification of CRISPRa endogenous target (CCR2) geometric mean intensity (*top*) and positivity (*lower*) across gRNA designs transiently delivered via electroporation using plasmid to Jurkat T cells and assessed the next day. All quantified data was obtained via flow cytometry gated on live singlets. Where indicated, data has also been gated on RFP (mCherry)$^{+}$ cells. Quantitative data in (B) depicts mean and standard deviation of three EP replicates.

Figure 2.6

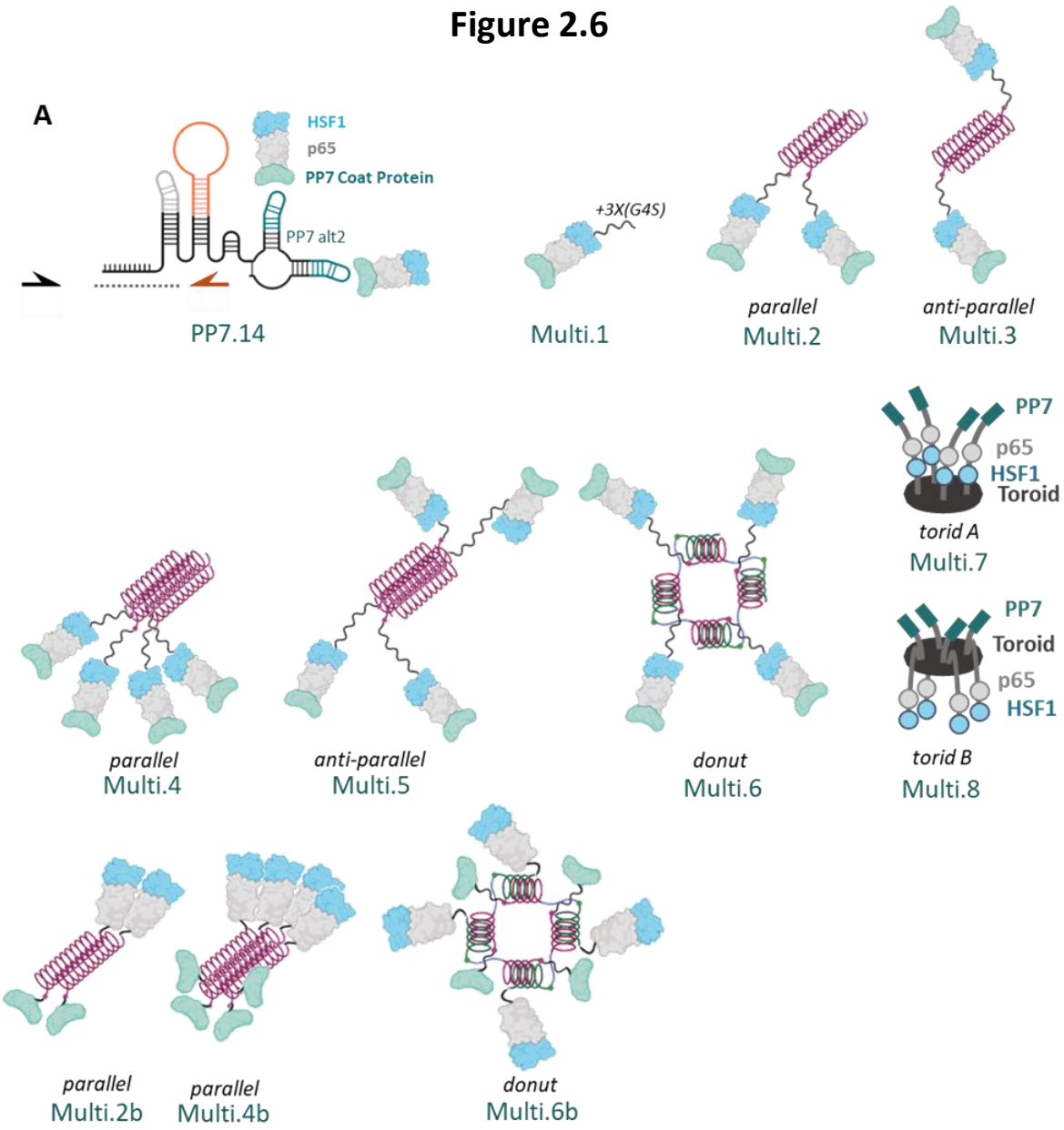
A
HSF1
p65
PP7 Coat Protein
PP7 alt2
PP7.14
+3X(G4S)
Multi.1
parallel
Multi.2
anti-parallel
Multi.3
PP7
p65
HSF1
Toroid
torid A
Multi.7
parallel
Multi.4
anti-parallel
Multi.5
donut
Multi.6
PP7
Toroid
p65
HSF1
torid B
Multi.8
parallel
Multi.2b
parallel
Multi.4b
donut
Multi.6b

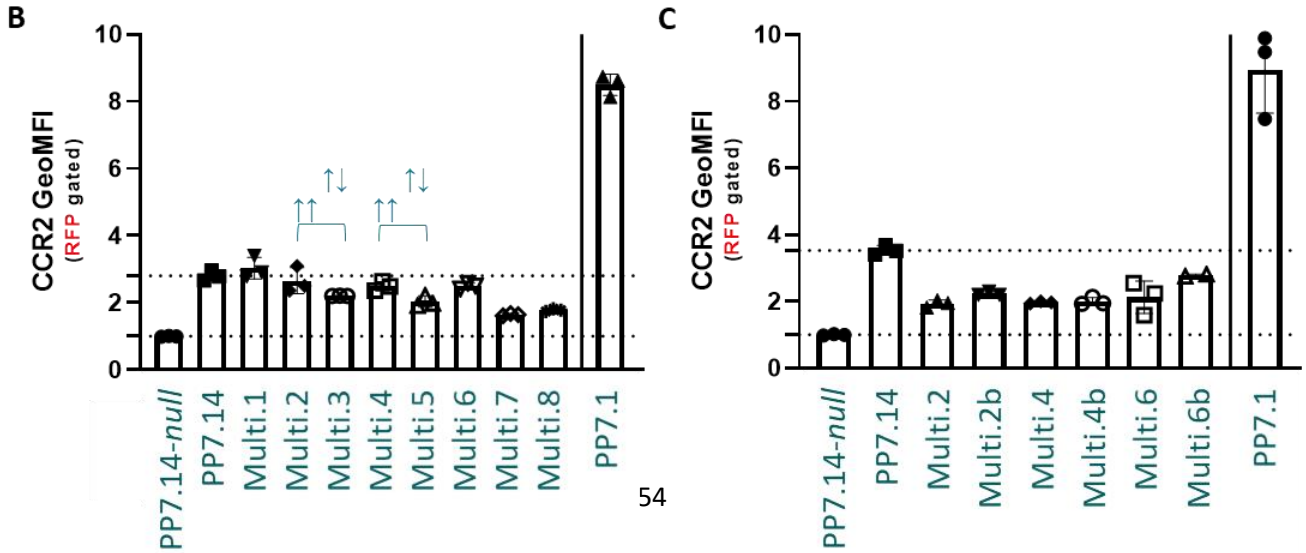
B
CCR2 GeoMFI
(RFP gated)
0
2
4
6
8
10
PP7.14-null
PP7.14
Multi.1
Multi.2
Multi.3
Multi.4
Multi.5
Multi.6
Multi.7
Multi.8
PP7.1
C
CCR2 GeoMFI
(RFP gated)
0
2
4
6
8
10
PP7.14-null
PP7.14
Multi.2
Multi.2b
Multi.4
Multi.4b
Multi.6
Multi.6b
PP7.1

Figure 2.6: Assessment of CRISPRa effector multimerization. (**A**) Graphics of base gRNA and CRISPRa effector design (*upper left*) and multimerizing CRISPRa effector variants (*right and lower*). (**B**) Quantification of CRISPRa endogenous target (CCR2) geometric mean intensity across the CRISPR effector designs depicted above, transiently delivered via EP using plasmid to Jurkat T cells and assessed the next day. All quantified data was obtained via flow cytometry gated on live singlets, and RFP (mRuby3)$^{+}$ cells. PP7.1 gRNA design is depicted in figures 2.3 and 2.4. Quantitative data in (B) and (C) depict mean and standard deviation of three EP replicates.

Chapter 3 | CRISPRa-CAR Primary T Cell Manufacturing

3.1 | Abstract

Chimeric Antigen Receptor (CAR) T cell therapy has revolutionized the treatment of B cell malignancies and translating this success to other cancers remains an ongoing clinical objective. Next-generation T cell products in development today aim to genetically modulate many facets of cell behavior, and gene-nominating platforms have provided a useful framework for prioritization. Among competing screening approaches, CRISPR activation (CRISPRa) technology permits gain-of-function (GoF) gene surveys at genome-wide scale, but routine implementation in primary T cells has been stymied by high cell requirements (~10^7 - 10^8) and lackluster activity. Here, I describe a novel cell manufacturing schema using an all-in-one transposon-based gene delivery system coupled with CAR-restricted cell expansion to generate yields of primary T cells bearing CAR and CRISPRa transgenes, well above the threshold needed for genome-scale screening (>10^9). Long-term GoF potency is achieved via vector optimization to prevent CRISPRa gene silencing (>90%$^+$); library representation is preserved by delaying guide RNA transfer until late in primary manufacturing, thus preventing bottlenecking and premature candidate pruning. CRISPRa-CAR T cells manufactured via this pipeline retain potent on-target gene-overexpression (>85% target$^+$) across varied cell subsets (e.g. Tim-3$^+$/Lag3$^+$) and timescales (>14 days). When deployed to survival-based genome-wide selection landscapes, CRISPRa-CAR pools can successfully nominate endogenous genes capable of enhancing CAR T persistence. This system will have broad utility for therapy-enhancing gene discovery.

3.2 | Background

Since 2017, chimeric antigen receptor (CAR) T cell therapy has been an approved treatment for relapsed B cell acute lymphoblastic leukemia.[19] In patients with this disease, CAR T cells can produce incredibly rates of response (70 - 94%).[26,27] This clinical success has encouraged researchers to consider CAR T cell therapy as a potential treatment option for other cancers of the blood and for solid tumors. Clinical outcomes of these recent attempts have ranged from modest to poor.[35,34]

Consequently, emerging strategies for next generation therapy development often look beyond refinement of the CAR transgene to include prospective gene payloads that modify many different facets of cell behavior – with the ultimate aim of enhancing T cell potency.[45–48,71] As the list of contenders has swelled, efforts have been made to streamline their evaluation using pooled molecular libraries, enabling researchers to test many candidate molecules simultaneously.[94] CRISPR Activation (CRISPRa) is a CRISPR/Cas9-derivative empowering pooled gene overexpression, as directed by a collection of modular gRNAs.

Applying this and other updated CRISPR technologies to primary human cells however, particularly lymphocytes, has been hampered due to presumptive inefficient gene delivery of the core homing component, the endonuclease-dead (d)Cas9.[97] Despite this challenge, a recent study demonstrated that CRISPRa^{+} antigen-agnostic primary T cells could be manufactured using high-quality lentivirus; when deployed to adaptive landscapes of limited duration, they could successfully nominate endogenous genes capable of modulation towards cell phenotypes of therapeutic relevance.[86] Translated to CAR or related adoptive T cell therapy paradigms,

CRISPRa holds tremendous promise as a gene-nomination platform to steer cell product development. Here, I describe the development of a CRISPRa-enabling novel CAR T cell manufacturing method and subsequent first demonstration of a genome-scale GoF CAR T cell screen for therapy enhancement.

3.3 | Results

3.3.1 | Lentiviral gene delivery yields few CRISPRa^{+}CAR^{+} T cells

To deploy my refashioned CRISPRa tools (**see chapter 2**) to primary T cells, I evaluated the feasibility of lentiviral delivery. CRISPRa and CAR transgenes are large DNA payloads, together spanning more than 10 kilobases in total length. For this reason, they cannot be efficiently packaged into a single viral transfer vector.[186,187] Similar to previous studies,[86] I distributed transgenes across lentiviral pairs (**Fig 3.1a**). Remarkably, my lab's clinic-tested CD19CAR vector[188] tolerated additional gRNA and CRISPRa effector (PCP-p65-HSF1, PPH) sequences, generating quantities of functional virus similar to its parent. In contrast, despite minimizing the overall DNA footprint, the stand-alone mScarlet-dCas9 vector achieved significantly lower viral titers (**Fig 3.1b**). To manufacture CRISPRa-CAR$_{gRNA}$ or reference populations, primary T cells were purified and activated with α-CD3/α-CD28-coated beads, followed by lentiviral transduction the following day (**Fig 3.1c**). Three days later, cells began methotrexate (Mtx) selection, which enriches for cells expressing the double mutant dihydrofolate reductase (DHFR^{FS}) transgene contained within the CAR expression cassette. As a consequence of selection, both cultures achieved high levels of CAR purification (87 - 98%) (**Fig 3.1d**), and as

expected, cells receiving an mScarlet control lentiviral vector achieved moderate levels of positivity (55 - 62%); however, in line with most prior reports, mScarlet-dCas9 positivity registered at very low levels (3 - 6%), despite being transduced at an identical multiplicity of infection (= 1) (**Fig 3.1e**).

3.3.2 | EP-TICLE can generate CRISPRa-CAR T cells of high yield and purity but limited CRISPRa expression dampens potency

To increase the proportion of cells receiving the full complement of transgenes, I pivoted to an all-in-one PiggyBac transposon-based delivery system (**Fig 3.2a**), which uses electroporation to shuttle donor plasmid acting as DNA template along with mRNA coding for transient transposase. While electroporation with donor plasmid is largely known to exhibit diminishing efficiencies with increasing size (similar to LV),[189] recent studies have suggested that native, antigen-specific stimulation of re-programmed T cells coupled with peripheral blood mononuclear cell (PBMC) feeders can support incredible rates of cell-specific T cell expansion from rare founding populations.[190,191]

After electroporation, gene-modified T cells were returned to a bed of autologous PBMCs bathed in a cytokine-rich media that includes IL-4, with Mtx selection initiated on Day 0 or 3 (**Fig 3.2a).** I term this cell manufacturing method electroporation-mediated T-cell Interface for CAR-limited Expansion (EP-TICLE), and via this process, were able to generate approximately 100- and 10-fold expansion rates of CAR_{gRNA} and CRISPRa-CAR_{gRNA} T cells, respectively, relative to

bulk cell input (**Fig 3.2b, c**). I assume the true CAR-restricted expansion rates to be considerably higher.

Intriguingly, despite achieving high CD19CAR purity in CRISPRa-CAR.v1$_{gRNA}$ T cells (**Fig 3.2d**), expression of the CRISPRa transgene and its target gene (Epidermal Growth Factor Receptor, EGFR) remained persistently low (**Fig 3.2e, f, Fig 3.3b**). Subsequent relative transgene copy number analyses indicated that CRISPRa$_{gDNA}$ was in fact modestly reduced (18 - 29%) in 2 out of 3 donor cell products by endpoint, although these frequencies could not appreciably account for the observed incidence of CRISPRa-negative cells (73 - 94%) (**Fig 3.2f, Fig 3.3c**). Careful inspection of the donor plasmids uncovered no gross impurities or abnormalities (**Fig 3.3f - h**), suggesting that CRISPR$_{gDNA-}$ cells did not necessarily arise from contaminating single-transgene donor templates, but instead emerged *de novo* over the course of cell manufacturing. Consistently, cells from a single T cell donor exhibited a progressively declining CRISPRa$_{gDNA}$:CAR$_{gDNA}$ ratio over the course of manufacturing (**Fig 3.3c**).

Having now twice observed poor dCas9 activity across orthogonal gene delivery systems, I considered if features within our CDS may be hindering ideal expression. For instance, foreign genes, regardless of their mechanism of delivery (e.g. LV, transposon-based) often suffer from varying degrees of epigenetic silencing.[192,193] By subjecting CRISPRa-CAR.v1$_{gRNA}$ cells to chemical species including IL-15; decitabine, a hypomethylating agent; butyrate, a histone deacetylase inhibitor; and TransAct™ (Miltenyi Biotec), a soluble T cell activation reagent, I observed additive increases in gene re-activation (**Fig 3.2g, h, Fig 3.4a, b**). Indeed, prolonged exposure (168 hours) of cells to anti-silencing drug cocktails led to near total restoration of CRISPRa positivity in CRISPRa-CAR.v1$_{gRNA}$ donor cells (**Fig 3.2h**). Together, these results suggest that

dampened or absent CRISPRa activity is primarily driven by severe DNA silencing of the CRISPRa transgene.

In my view however, continuous supplementation of epigenetically modifying drugs did not represent a viable path to rescue CRISPRa activity. For while short-term exposures at the end of cell manufacturing led to transient increases in total CRISPRa^{+} cells, specific yields turned net-negative by one week, while combination treatment maintained throughout manufacturing completely prevented cell expansion (**Fig 3.2h, Fig 3.4a - d**). Furthermore, since large doses of these drugs are not routinely prescribed in adoptive T cell patient care settings, they would risk substantially confounding screening results if introduced into subsequent selection landscapes.

Given the dominant CRISPRa transgene deactivation observed across multiple donor samples, resulting from both gene silencing and recombination, I worried that CRISPRa loss might arise as the product of inadvertent selection imposed by a toxic payload. Prior studies for example have indicated that high doses of either dCas9 or endogenous trans-activators have the potential in various model systems to impose genotoxicity, limiting cell viability.[120,122,194]

To probe for this suspect toxicity, I engineered a set of CRISPRa-deficient vectors to determine if CRISPRa transcription or subsequent translation lowered the yield of CRISPRa-CAR T cells. Surprisingly, I observed no gross differences in relative cell counts (**Fig 3.5a, b**), suggesting that CRISPRa transgenes were neither causing apparent toxicity nor contributing to overt silencing that had spread to the neighboring CAR transgene (i.e. position effect variegation). As a potential means to shield against premature transgene deactivation, I profiled a Tet-Off regulated CRISPRa system in Jurkat T cells and then transferred this design to CAR-containing

constructs (**Fig 3.5a, c,** see also **chapter 5**).[195] Primary T cells produced in this manner could theoretically have their CRISPRa cassettes reversibly silenced when in presence of doxycycline (Dox), which could thereafter be relieved prior to selection landscape initiation.

I tested manufacturing $^{Tet\text{-}Off}$CRISPRa-CAR T cells, with and without concomitant Dox supplementation. Untreated, cell yields using these constructs were very poor – a finding consistent with toxicity and/or silencing that had spread to the CAR transgene, possibly via a Tet transactivator-mediated positive feedback loop (**Fig 3.5d**). Dox-treated $^{Tet\text{-}Off}$CRISPRa-CAR T cells in contrast had much higher cell yields, approaching those of CRISPRa-CAR.v1, although disappointingly these cells did not display improved CRISPRa expression after late repressor removal. As a separate experimental condition, I also examined the impact of omitting PPH, the CRISPRa effector, but ultimately saw no increase in CRISPRa positivity, suggesting that dCas9 alone is sufficient to drive CRISPRa transgene silencing.

In total, these findings suggest that while gene silencing poses a significant barrier to achieving robust CRISPRa expression in CAR T cells, it is not likely to be primarily driven by CRISPRa-imposed toxicity, at least at the expression levels afforded by the MND promoter – a finding that aligns with other recent results.[196]

3.3.3 | Optimized architecture resists CRISPRa deactivation

Encouraged by this finding, I reversed my approach, and now sought to reinforce CRISPRa expression rather than curb it. To improve upon baseline molecular architecture, I began by screening various candidate promoters for enhanced CRISPRa durability (**Fig 3.6a**). Among

those examined, MND re-emerged as a top performer along with hPGK and EF1α-HTLV (**Fig 3.6b**). The Elongation Factor 1α core/human T-cell leukemia virus (EF1α-HTLV) promoter is a well-documented hybrid promoter shown to drive robust, sustained expression of transgenes,[140] including CAR[141–143] and consequently was already occupying a downstream position in my original dual promoter vector designs. With identical tandem promoters at presumptive heightened risk for deletion of the flanked CRISPRa transgene, I hedged against this vulnerability by also cloning a recombination-insensitive, divergent promoter form of the same. Ultimately this experimental choice was of high consequence, as CRISPRa driven by divergent EF1α-HTLV promoters yielded significantly higher CRISPR positivity and intensity than previous designs (**Fig 3.6b**). Follow-up analyses directly comparing unidirectional and divergent EF1α-HTLV promoter orientations detected equimolar transgenes ratios in divergent EF1α-HTLV cells, with only modest CRISPRa transgene loss (20 - 36%) in the unidirectional equivalent – far too low a recombination frequency to serve as a robust explanation for the observed differences in transgene expression (**Fig 3.7c**). Additional testing across a variety of promoter combinations and orientations confirmed superiority of the divergent dual EF1α-HTLV design (**Fig 3.7a, b, d, e**). To further increase CRISPRa positivity and MFI, I then transferred the selectable marker from the CD19CAR-containing coding cassette to the N- or C-terminus of the CRISPRa ORF, with the C-terminal DHFRFS positioning yielding slightly higher CRISPRa positivity and intensity without sacrificing yield (**Fig 3.6b**). In total, these findings suggest that the silencing-resistance of the divergent dual EF1α-HTLV promoter design is an emergent property arising from the combination of promoter selection and molecular arrangement, rather than due to either feature in isolation.

To further increase CRISPRa transgene level – and ultimately activity – I also trialed additional vector variations. Recent reports have highlighted the success of including scattered introns throughout the dCas9 transgene to boost or sustain expression levels,[192,197,198] and so similarly, I tested installing within the mScarlet-dCas9 cassette 11 short human introns drawn from essential housekeeping, cell cycle, tumor suppressor, or T cell-enriched genes. Rewardingly, cells manufactured using this candidate vector expressed greater CRISPRa levels with a slight drop in overall positivity. Lastly, I also tested the deployment of two 'enhancer' elements: either a novel ubiquitous chromatin opening element (SRF-UCOE6.3) or a synthetic collection of tiled endogenous transcription factor binding motifs ("S1-61"), shown to potently engage *in cis* genes following T cell activation (**Fig 3.6b**).[199,200]

Ultimately, I selected two final candidates for further study: C-terminal-selected CRISPRa driven by divergent EF1α-HTLV promoters ("CRISPRa-CAR.v2") and the intronized version of the same ("CRISPRa.CAR.v2i"). In contrast to CRISPRa-CAR.v1, cells generated from these optimized candidate vectors expressed much higher levels of on-target gene activation (EGFR) when supplied an *in cis* targeting gRNA, with the non-intronized form achieving slightly higher levels of on-target positivity and MFI (**Fig 3.6f, g, Fig 3.8a - c**). CRISPRa-CAR.v2i cells maintained high levels of CRISPRa expression throughout EP-TICLE manufacturing without transgene loss or indication of gross improper intron processing (**Fig 3.6c - e**). CRISPRa-CAR.v2i cells were also successfully generated using CD4 or CD8 monoculture input and achieved both similar cell yields and CRISPRa target expression levels compared to EP-TICLE cultures seeded with 50:50 mixtures of CD4/CD8 T cells (**Fig 3.8d**). In sum, using low cellular input, my second-generation

EP-TICLE vectors were capable of producing potent CD4 or CD8 CRISPRa-CAR T cells at quantities (>10^9) well in excess of the requirements for genome-scale screening.

3.3.4 | gRNA-LV can be delivered to CRISPRa-CAR T cells near the end of primary cell manufacturing and direct cells to activate endogenous genes

Given the lengthy duration of cell manufacturing (~ 3 weeks) and cell-specific expansion estimated to be >100-fold, I was concerned about the potential for significant and unpredictable distortion of gRNA representation. Specifically, culture bottlenecking and subsequent drift might skew the distribution of $gRNA^+$ clones, while premature CRISPRa activity would inadvertently shape and prune gRNAs prior to landscape initiation. To address both concerns, I contemplated delaying the introduction of gRNAs until late in primary culture. To execute this strategy, I once again turned to LV.

I hypothesized that T cells rapidly proliferating at least through Day 14 of day EP-TICLE retain sensitivity to lentiviral transduction, despite their chronological distance from frank T cell activation. Prior work for instance, has indicated that resting T cells can be successfully transduced using LV, albeit at reduced efficiencies compared to their activated counterparts.[201–203] Other labs have taken the approach of engineered lentivirus pseudotyped with unconventional, envelopes that possess high affinity for cell receptors decorating the surface of quiescent T cells.[204] In contrast, to increase viral tropism, conventional LV is generated using envelope borrowed from the Vesicular stomatitis virus (VSV-G).[201]

Faced with biological uncertainties, I chose to evaluate four species of viral envelope proteins for compatibility with my production method: VSV-G, α-CD3scFv, combination H and F envelope glycoproteins derived from Measles virus, and the Baboon envelope R-less glycoprotein (BaEVRless) (**Fig 3.9a**). CRISPRa-CAR T cells on Day 17 of EP-TICLE manufacturing are distal from T cell activation, and to my surprise, transduced most efficiently on a per volume basis with conventional VSV-G packaged LV, although virus pseudotyped with BaEVRless approached this result (**Fig 3.9b, Fig 3.10g, h**). Further optimization of plating conditions increased late transduction efficiencies of EP-TICLE cells further still (**Fig 3.11b - f**).

Additionally, having generated cells expressing a functional CRISPRa transgene prior to subsequent gRNA transfer, this obviated the need for components of existing public CRISPRa gRNA libraries, which routinely bundle together the CRISPRa activator (e.g. PPH) at a substantial cost to lentiviral titer. Accordingly, I set about building a simplified and efficient gRNA transfer vector. Along with removing PPH, I tested modifications to gRNA-LV format based on early iterations. After evaluating a variety of designs, I ultimately selected the PP7 gRNA variant present in the all-in-one CRISPRa-CAR.v1$_{gRNA}$ donor plasmid. Of interest, I also developed alternate gRNA-LV formats capable of oligo(dT) capture and downstream scRNA-seq processing that are distinct from previous reports,[86] although I observed that these high content gRNA forms evidence tradeoffs in CRISPRa potency (Libr.3) or viral titer (Libr.7) (**Fig 3.10a-f**). To evaluate these new tools, CRISPRa-CAR T cells were generated via EP-TICLE, then transduced with gRNA-LV, and thereafter selected with Puromycin for 2 or 3 days. Cell produced in this fashion were shown to exhibit similar levels of target gene activation compared to cells made via EP-TICLE alone using all-in-one CRISPRa-CAR$_{gRNA}$ donor plasmids (**Fig 3.9c**). Leveraging this

novel manufacturing schema of combination EP and distal transduction, I generated CRISPRa-CAR_{gRNA} cells, and demonstrated marked, highly specific overexpression of a variety of target gene products normally absent on conventional T cells (**Fig 3.9d, Fig 3.11a**).

3.3.5 | CRISPRa-CARgRNA T cells are functional and can be applied to selection landscapes to identify genes that improve cellular fitness

To determine the constellation of selection landscapes compatible with CRISPRa-CAR_{gRNA} GoF T cells, I examined the frequency and duration of CRISPRa activity within various T cell subsets of clinical interest (**Fig 3.9e**). Following EP-TICLE and distal gRNA-LV cell manufacturing, both CRISPRa-CAR.$v2_{gRNA}$ and CRISPRa-CAR.$v2i_{gRNA}$ T cells evidenced robust and stable on-target gene expression (EGFR) over an additional two weeks of culture, with only minor loss of potency upon Mtx removal (**Fig 3.9f, Fig 3.12a**). While all forms of commonly defined T cell differentiation subsets exhibited significant CRISPRa target overexpression, it appeared that central ($CD45RO^+CD62L^+$) and effector memory ($CD45RO^+CD62L^-$) subsets displayed modestly higher CRISPRa target activity than naïve ($CD45RO^-CD62L^+$) or terminal effector cells ($CD45RO^-CD62L^-$) (**Fig 3.9g, Fig 3.12b**). In contrast, T cells serially challenged with CAR targets or bearing high levels of inhibitory receptors ($Lag3^+$, $Tim\text{-}3^+$) exhibited no differences in CRISPRa activity compared to cells challenged less frequently or free of these markers ($Lag3^-$, $Tim\text{-}3^-$) (**Fig 3.9h, i, Fig 3.12c, d**). These results broadly indicate that $gRNA^+$ CRISPRa-CAR.v2 and CRISPRa-CAR.v2i are likely to efficiently drive gene overexpression across a diverse set of cell subsets and timescales.

3.4 | Discussion

3.4.1 | A new tool to guide therapy enhancement

In the last decade, CAR T cell therapy has advanced considerably from its underperforming first-generation aspirants[205] to today comprising multiple clinical treatment options.[206] And yet, T cell therapies require further development if they are to provide predictable, durable cancer remissions. Among therapy recipients who experience tumor progression, causes of treatment failure include T cell hypofunction,[34] unestablished immunological memory,[38] the emergence of antigen loss variants,[39,40] or insufficient persistence.[41] For experimental therapies aimed at solid tumors, modified cells must also contend with varied cell-extrinsic threats imposed by the hostile tumor microenvironment.[42,43] These challenges are multifaceted, involve the interplay of complex biological circuitry, and may be met via therapy candidates prioritized by genuinely agnostic, pooled screening platforms.

3.4.2 | Vector optimization sustains CRISPRa activity

One of my key findings was the observation that divergent dual EF1α-HTLV promoters markedly protected their transgene dependents from silencing. This result aligns with research demonstrating that native divergent promoters may better resist heterochromatin formation[207,208] During exploration of further divergent promoter pairings, only EF1α-HTLV/MND ("Div-MNDrvs") with EF1α-HTLV aimed at the CRISPRa transgene behaved similarly (**Fig 3.7d**). However, this also suggests that both promoters need not be identical in future

designs to extract the same benefit, so long as EF1α-HTLV drives transcription of the susceptible CDS.

While I did not observe evidence of gross template impurities, because of the high incidence of sporadic recombination observed within the nanoplasmid-component cell line, I cannot exclude the possibility that trace amounts of contaminating CRISPRa-negative donor plasmid may be a significant contributor to the emergence of $CRISPRa_{gDNA-}$ cells beyond *de novo* recombination within human T cells. Indeed, as these truncation products would preferably integrate into host cell genomes, they would be overrepresented in early culture. CRISPRa-negative cells may also preferentially accumulate throughout the course of culture as a function elevated $DHFR^{FS}$ gene dosage protecting against persistent Mtx.

I was also pleased to observe that intronization of dCas9 was tolerated and produced protein products of correct size (**Fig 3.6c**), and observable CRISPRa activity (**Fig 3.6d, e**). To my knowledge, this is the first implementation of Cas9 intronization in primary human T cells, and perhaps human primary cells more broadly.

3.4.3 | dCas9 transgene silencing: a generalized problem?

While I do not assert that the epigenetic phenomena observed here necessarily apply to all manner of CRISPR requiring sustained dCas9 expression, I find it noteworthy that the dual-transduced (dCas9 LV + CAR-PPH_{gRNA} LV) T cells, upon treatment with de-silencing and T cell activation drug cocktails, had mScarlet-dCas9 levels surge to as high as 67% positivity (**Fig 3.4e**), while subsequent copy number analysis uncovered a mean CRISPRa-to-CAR transgene ratio of

1.2 (**Fig 3.4f**). Together, these results hint that poor dCas9 expression observed in numerous prior published studies, having been attributed to mediocre lentiviral delivery, may instead be driven by more general transgene silencing. Given that HUSH templates include episomal as well as integrated DNA,[192] this phenomenon may also constrain viral producer cells and reduce dCas9 LV yield in a time-dependent manner. For these reasons, GoF adaptive landscapes that minimize the duration of necessary CRISPRa expression and/or activate T cells as a screening component may mask underlying challenges in long-term dCas9 expression. The implementations demonstrated here may enable more complex, longitudinal screening regimens with durable overexpression systems that more closely mirror the intended expression kinetics of next-generation cell therapies.

More generally, I suspect that the challenge of reinforcing dCas9 expression likely represents a specific instance of broad vulnerability in transgene therapy. Specifically, DNA silencing of foreign genetic material is a well-recognized, non-trivial problem, occurring in primary T cells at high frequency.[209] And yet, arrayed and pooled screening systems routinely deploy CDSs with uncharacterized long-term durability.[95] For this reason, pooled ORF screens are expected to spur many false negatives, especially as a function of increasing CDS size – a candidate type already likely to be underrepresented, and therefore underpowered, in most ORF pools.

3.4.4 | VSV-G: the reigning champion of lentiviral envelopes

In my studies, I observed consistent superiority of VSG-G LV packaging for downstream EP-TICLE transduction on a per volume basis (**Fig 3.9b**). The low-density lipoprotein receptor (LDL-

R) is VSV-G's major port of viral entry.[210] While LDL-R is known to be rapidly upregulated in response to T cell activation,[211] its off-kinetics are not well defined. More generally, lentiviral infection greatly favors post-G0 cells, a preference that likely corresponds with higher transduction efficiencies seen with cells sourced from early EP-TICLE cell manufacturing (**Fig 3.9b, Fig 3.10h**). However, I was particularly surprised not to witness an inversion in these relative efficiencies late in culture as proliferation slowed. These results contrast with reports suggesting a BaEVRless advantage in transducing non-proliferating T cells. I concede that my studies did not adjust viral input to reflect differences in physical or functional titer; in my view, while this normalization may have provided a clearer indication of envelope infectivity, it did not support my aim of maximizing $gRNA^+$ cell yield as a function of material input. Alternatively, interstudy differences in LV production or T cell culturing methods may explain these discordant outcomes.

3.4.5 | CRISPRa-CAR T cell… therapy?

To reiterate, my research here is driven by a primary desire to discover novel endogenous regulators of therapeutic relevance, and then translate these genes to common ORFs for CAR or other forms of adoptive T cell therapy. Still, it does not escape my notice that $CRISPRa^+$ T cells could conceivably be offered, either as an off-the-shelf or personalized GoF treatment option in its own right in due course; however, several prominent barriers likely preclude imminent direct implementation. Firstly, prior studies have described evidence of preexisting anti-Cas9 humoral and cellular immunity within the human population, although the reported prevalence has varied widely.[212–214] Such findings suggest that cell therapies requiring sustained expression

of dCas9 may exhibit restricted efficacy across diverse patient populations, while also posing an undefined immunological safety hazard. Recognizing these concerns, others have begun to explore possible workarounds, with strategies ranging from expanding Cas9-specific T regulatory cells[215] to engineering "immunosilenced" forms of Cas9.[216]

Secondly, CAR T cells generated using piggyBac-mediated donor plasmids recently resulted in two instances of CD19CAR$^+$ T cell lymphoma and the death of a trial patient.[217] Currently the biological mechanism underlying these malignant transformations remains uncertain, although high CAR transgene copy number may play a role. It is therefore worth noting that CRISPRa-CAR.v2i cells averaged a transgene copy of number of 1.1 (SD = 0.08) (**Fig 3.3d**), whereas the deceased patient received malignant CAR T cells with a mean copy number of ~ 24.[217] In any event, these very serious adverse events have placed subsequent clinical use of cell products relying on piggyBac-mediated gene delivery in serious doubt.

3.4.6 | Future CRISPR screening in T cells and beyond

Durable, potent CRISPRa activity was enabled through sustained expression of dCas9. With many emerging CRISPR-dependent effector systems operating via interactions with dCas9 derivatives, I believe that design principles identified here may form the basis of broad future interventions – for T cell therapy iterations or other cell types.

3.5 | Materials and Methods

3.5.1 | Plasmids and vectors

The SAM.1 (PB-UniSAM) parent vector was a gift from Lesley Forrester (Addgene 99866), that itself was a polycistronic derivative of Feng Zhang's dual vector system (Addgene 61422, Addgene, 73797). Successive daughter plasmids were generated via simple ligation or Gibson assembly using annealed complementary oligonucleotides (Integrated DNA Technologies) or premade dsDNA templates (e.g. Integrated DNA Technologies, GeneArt, PCR-amplification sourced) using routine molecular biology methods. Constructs containing second-generation SAM (PP7) components were cloned utilizing synthesized templates derived from previously published sequences.[151,154]

For intronization studies, candidate introns were positioned within dCas9 using Intronserter[218] and evaluated *in silico* for high splicing fidelity using NetGen2.[219] Ultimately eleven native human introns were chosen based on their:
(1) small size (<250 bp), (2) status within documented housekeeping, cyclin, tumor suppressor, or T cell-rich genes, (3) invariant splicing removal in every known mature RNA isoform, and (4) high splice donor and acceptor scores (≥ 0.94) when positioned within dCas9. Intron sequences can be found in **table 3.5.12**.

To generate lentiviral transfer vectors, I deposited CRISPRa, CAR, and reference components within a third-generation version of pHIV7.[188] To minimize construct size for T cell implementation, CRISPR-CAR CDSs were cloned into PiggyBac donor Nanoplasmid™ that features an RNA-OUT[220] counterselection system (Aldevron). These donor plasmids were

further modified with transposon-flanking HS-A insulator sequences[145] and a miniaturized insulator sequence inserted between coding cassettes.[221] The origin of additional CDSs is indicated in **table 3.5.11**. All cloned constructs were sequence-verified via end-to-end Sanger sequencing (Genewiz) and/or long-read Nanopore sequencing (Plasmidsaurus).

BaEVRless and Measles H/F plasmids were the kind gifts of Els Verhoeyen (CIRI, Université Côte d'Azur). All arrayed gRNA sequences used in my studies are listed in **table 3.5.13**.

3.5.2 | LV production

HEK293T/17SF cells between passage 3 and 20 were grown in FreeStyle™ 293 Expression Medium (Gibco) to a density of 1.5×10^6 to 2×10^6 cells/mL in a shaking incubator at 85 - 120 RPM, 37 °C, 5% CO2. Transfer plasmid mixture was prepared in Opti-MEM™ Reduced-Serum Medium (Gibco) at 50 µL/mL culture. Plasmids were added to the Opti-MEM™ at a concentration of 6.25 µg/mL transfer plasmid, 6.25 µg/mL Gag-Pol, 2.5 µg/mL Rev, and 5 µg/mL VSV-G. For the envelope series screen, VSV-G was replaced with alternative envelope plasmids at an equivalent mass, alone or in combination. Separately, the transfection reagent mixture was prepared in Opti-MEM™ at 50 µL/mL culture by adding PEIpro® transfection reagent to the Opti-MEM™ at a concentration of 40 µL/mL. Both mixtures were individually vortexed, then combined and incubated undisturbed at RT for 15 - 30 minutes before being added to the HEK293T/17SF cell culture and incubated overnight. After 24 hours, sodium butyrate was added at a concentration of 1 µL/mL culture, then incubated for an additional 48 hours. To harvest LV, the transfected cell culture was centrifuged at 1000 × g for 15 minutes to remove cells. The

supernatant was then filtered through a Stericup 0.45 µm Sterile Vacuum Filter to remove cell debris and centrifuged in a Fiberlite™ F14-6 x 250LE Fixed Angle Rotor at 10,000 × g for 4 hours at 4 °C with 30% brake. The supernatant was discarded and the resulting cell pellet resuspended in OptiMEM™ at 1 - 1.5 µL/mL initial culture volume.

For functional titering, Jurkat or Raji cell lines between passage 3 and 20 were harvested, centrifuged and resuspended at concentration of 4×10^5 cells/mL in RPMI-1640 (Gibco) supplemented with 10% FBS and 5% L-glutamine. Protamine sulfate was added to the cell suspension at 8 µL/mL. LV aliquots were thawed at RT and mixed thoroughly before 4 µL was added to the first column of a 96 well plate. Using an Integra Assist Plus platform fitted with 1250 µL Voyager pipette, 50 µL of compounded (c)RPMI was added to columns 2 - 11 of the plate, while 96 µL was added to the first column. Starting from column 1, the samples were mixed and serially diluted two-fold over the remaining wells. The prepared cell suspension was added at 50 µL per well for a final concentration of 4×10^5 cells/mL, then the plates incubated at 37 °C, 5% CO_2 for 24 hours. The following day, 100 µL cRPMI was added to each well and the plates were incubated for an additional 4 days. After incubation the samples were centrifuged at 500 × g for 3 minutes, the media was removed and samples were washed once in a PBS staining buffer containing 2% FBS and 250 mg/L sodium azide before being fixed in PBS containing 0.5% formaldehyde. Data was collected using a BD LRS Fortessa Flow Cytometer with the 488 nm laser and a 530/30 bandpass filter set. Data was analyzed using BD FlowJo software. Sample populations were gated on SSC-A × FSC-A for lymphocytes then FSC-H × FSC-A for single cells. Transfected single cell populations were compared to a non-transfected mock to

determine positivity by the Overton method. Producer cell transfection reagents can be found in **table 3.5.14**.

3.5.3 | Primary T cell isolation

Fresh peripheral blood Leukopaks enriched for leukocytes (StemExpress) were processed within 24 hours of collection. Donor pool was limited to non-smokers between the ages of 18 - 35 and with a BMI <29.9. PMBCs were incubated with 3 - 5 mL CD8-specific StraightFrom® or CliniMACS® magnetic beads (Miltenyi) for 30 minutes at 4 °C with gentle agitation, then sorted on a Miltenyi MultiMACS™ Cell24 Separator with a Multi-24 Column Block and washed with autoMACS® Running Buffer. The $CD8^+$ fraction was counted, centrifuged to remove the running buffer, then resuspended in CryoStor CS5 (StemCell) and aliquoted into vials for cryopreservation. The CD8-depleted PBMCs were incubated with 3 - 5 mL CD4-specific StraightFrom® or CliniMACS® magnetic beads (Miltenyi) for 30 minutes at 4 °C with gentle agitation, then sorted on a Miltenyi MultiMACS™ Cell24 Separator with a Multi-24 Column Block and washed with autoMACS® Running Buffer. The $CD4^+$ fraction was counted, centrifuged to remove the running buffer, then resuspended in CryoStor CS5 and aliquoted into vials for cryopreservation. The CD4- and CD8-depleted PBMCs were washed three times in running buffer to deplete platelets, then resuspended in CryoStor CS5 and aliquoted into vials for cryopreservation.

For isolation and use of fresh, unfrozen T cells, leukocytes were recovered from spent leukocyte reduction system chambers (LRSCs), a byproduct of donor platelet collection (Puget Sound Blood Center). $CD8^+$ and $CD4^+$ T cells were isolated via sequential positive selection using the RoboSep™ cell separation system (StemCell). Live CD4- and CD8-depleted peripheral blood mononuclear cells of the retained negative fraction were further purified by Lymphoprep™ (StemCell) and thoroughly washed. All recovered cell fractions were rested overnight in EP-TICLE culture media consisting of X-Vivo-15 (Lonza) supplemented with 2% KnockOut serum replacement, 4.6 ng/mL (~83 IU/mL) IL-2 (StemCell), 20 ng/mL IL-4 (Miltenyi), 10 ng/mL IL-7 (Miltenyi) and 20 ng/mL IL-21 (Miltenyi) at 37 °C, 5% CO_2 prior to use.

3.5.4 | Classic lentiviral transduction

CD4+ and CD8+ T cells were combined 1:1 and stimulated with CTS™ Dynabeads™ CD3/CD28 (Invitrogen) at a 1:1 ratio overnight in X-Vivo-15 (Lonza) supplemented with 2% KnockOut serum replacement (ThermoFisher), 4.6 ng/mL (~83 IU/mL) IL-2 (StemCell). The next day, the culture volume was reduced and fresh media containing protamine sulfate (40 µg/mL final) (Medline) was added. Viruses were thawed, vortexed and added to each corresponding well, calibrated to a multiplicity of infection (MOI) of 1 (0.5 - 11% v/v). Cells were returned to the incubator, and fresh media was added six hours later, doubling the culture volume. Four days later, Mtx was added to a final concentration of 100 nM and maintained throughout culture. Seven days following activation, Dynabeads™ were removed with DynaMag columns (Invitrogen). On Day 10, cells were counted and assessed via flow cytometry. Cells were maintained in their selective media formulations throughout the duration of culture.

3.5.5 | Primary T cell EP and EP-TICLE

T cells were resuspended in supplemented P3 buffer with 1.5 µL (~10 - 20 nM) PiggyBac donor plasmid and 40 nM RNA encoding PiggyBac transposase, generated via in vitro transcription (Aldevron). Cells were nucleofected using the Lonza 4D system with pulse program EO-115. For EP-TICLE experiments, electroporated cells were transferred to a G-REX culture vessel (Wilson Wolf) seeded with CD4- and CD8-depleted PBMCs and fresh EP-TICLE media. Mtx (Medline) was added to cultures to a final concentration of 100 nM on Day 0 (fresh-sourced cells) or Day 3 (cryopreserved cells) and maintained throughout manufacturing. Media was replaced twice weekly, and cells were expanded for up to 21 days. For conventional EP experiments, nucleofected primary T cells were transferred to G-REX wells with culture media alone. A list of both culture and general reagents can be found within **table 3.5.15**.

3.5.6 | Distal lentiviral transduction

Day 17 EP-TICLE CAR T cells were counted, spun down, and resuspended in complete TICLE media with 40 µg/mL protamine sulfate at a density of approximately 5×10^6/mL. For gRNA-LV tiling, 10^7 cells were transduced using 2.5% v/v concentrated gRNA-LV, resuspended in a final volume of 2 mL; spinoculation consisted of a 30 min centrifugation at 800 × g with low brake applied, maintained at 32 °C. Immediately thereafter, cells were returned to the incubator. Approximately 6 hours later, cultures were volumed up to 4 mL using fresh TICLE media. For medium-scale culture experiments cells and virus were scaled proportionally.

3.5.7 | Flow cytometry

For relative antigen quantification, cells were collected and washed with 1X PBS. Cells were stained with antibodies or reactive dyes resuspended in 1X PBS for 30 minutes at RT. This was followed by two additional washes. For methods including a biotinylated primary antibody, the cells underwent a 20-minute subsequent stain at RT with Streptavidin-PE (Biolegend), followed by two additional washes. Following the last wash, the cells were fixed in 0.5% paraformaldehyde / 1X PBS. Cells were stored at 4 °C while awaiting data acquisition. Data was collected using a BD LRSFortessa Flow Cytometer. Data was analyzed using BD FlowJo software. Sample populations were routinely gated on SSC-A × FSC-A for lymphocytes and FSC-H × FSC-A for single cells. Cell positivity and intensity calculations were performed by FlowJo software. All antibodies and staining reagents used for flow cytometric analysis can be found in **table 3.5.15**.

3.5.8 | Cell killing assay

For T cell cytotoxicity assays, CRISPRa-CAR T cells generated from EP-TICLE and transduced with gRNA-LV were plated 1:1 with mCherry^{+} Raji targets in Nunc™ Edge™ flat-bottom microplates. Whole wells were imagined using the Incucyte® Live-Cell Analysis System (Sartorius) every four hours up until 30 hours had passed. Total target cell counts were obtained for each timepoint using the Incucyte® Basic Analyzer tool and normalized to time zero in the absence of T cell effectors.

3.5.9| Immortalized cell culture EP and maintenance

Jurkat, Clone E6-1 (ATCC) and Raji (ATCC) were cultured in RPMI-1640 (Gibco) supplemented with 10% fetal bovine serum (Hyclone) and 1% 200 mM L-glutamate (Gibco). Cells were passaged 1 or 2 times a week, split 1:5 or 1:10, respectively. Cells were not allowed to grow denser than 1.5×10^6/mL. For electroporation, cells were split the day before manipulation to ensure high viability and maximize EP efficiency.

For transient transfection experiments, $1 - 2.5 \times 10^6$ Jurkat T cells were resuspended in supplemented buffer from the Nucleofector® Kit V (Lonza). Cells were combined with 1.5 µg of donor plasmid in a reaction volume of 100 µL and electroporated on the Amaxa® Nucleofector® II using pulse code X-005.

3.5.10 | Duplex-droplet digital PCR

Genomic (g)DNA of CRISPRa-CAR T cells from multiple donors was extracted at various timepoints throughout EP-TICLE manufacturing using the PureLink gDNA Mini Kit (Invitrogen). gDNA yield and purity were evaluated with the NanoDrop One spectrophotometer (Thermo Scientific). Prior to each experiment, fresh working stocks of gDNA were prepared by diluting with nuclease-free water to a concentration of 25 ng/µL. For each 20 µL ddPCR reaction, 100 ng of gDNA was directly digested with 5 U of EcoRI-HF (New England Biolabs) in the ddPCR Supermix for Probes (no dUTPs) (Bio-Rad), with FAM/HEX primers and probes at final concentrations of 900 nM and 250 nM, respectively. Following droplet generation with the Automated Droplet Generator (Bio-Rad), PCR was performed in a C1000 Touch Thermal Cycler

equipped with a 96-deep well reaction module (Bio-Rad). The PCR cycling program was optimized for the specific primer/probe sets and is as follows: 95 °C for 10 minutes (ramp rate of 2 °C/second), 40 denaturation/annealing cycles of 94 °C for 30 seconds (ramp rate of 2 °C/second) and 59.4 °C for 2 minutes (ramp rate of 1 °C/second), and a final extension at 98 °C for 10 minutes (ramp rate of 2 °C/second). Droplet plates were subsequently loaded into the QX200 Droplet Reader (Bio-Rad) for fluorescence analysis. Amplitude thresholds used to define positive and negative droplets were manually adjusted in the complementary QuantaSoft Analysis Pro software (Bio-Rad).

All primers and FAM/HEX-labeled probes were designed with PrimerQuest (Integrated DNA Technologies) and are listed in **table 3.5.17**. Primer/probe sets specific to either the mScarlet or dCas9 region and the FMC63scFv were used to assess relative copy number of the CRISPRa transgene in relation to the CD19CAR transgene. Albumin served as the reference gene for absolute copy number determination.

3.5.11 | Table: Sequence origins

Sequence	Source	PMID
dCas9	Fidanza et al, Sci Rep 2017	28743878
mScarlet	Bindels et al, Nature Methods 2017	27869816
mScarlet-I	Bindels et al, Nature Methods 2017	27869816
mRuby3	Bajar et al, Scientific Report 2017	26879144
PP7 Coat Protein	Martella et al, ACS Synth. Biol 2019	31398008
TurboGFP	*Lonza*	*NA*
2xMS2 (SAM)	Konerman et al, Nature 2015	25494202
2xMS2-PP7 (Calabrese SAM)	Sanson et al, Nature Com 2018	30575746
2xPP7	Martella et al, ACS Synth. Biol 2019	31398008
3'2xPP7	Zalatan et al, Cell 2015	25533786
iBAR	Zhu et al, Genome Biol 2019	30678704
10XGenomics_Capture	Choo et al, ACS Synth. Biol 2021	33625849
pseudoPoly(A) L2-ext-8A8G	Song et al, Genome Biol 2020	32513233

pseudoPoly(A) 8A6G	Song et al, Genome Biol 2020	32513233
U6mini	Preece et al, Gene Ther 2020	32203198
H1	Gao et al, Mol Ther Nucleic Acids 2019	30530211
SRF-UCOE 6.3	Rudina et al, BioRxiv 2021	*NA*
S1-61	Wei et al, 2018 WIPO	*NA*
EF1	Uetsuki et al, Biol Chem 1989	2564392
EF1-HTLV	Stavrou et al, Sci Rep 2017	28106085
MND	Astrakhan et al, Blood 2012	22431569
MSCV	Choi et al, Stem Cells 2001	11359949
hPGK	Naldini et al, Science 1996	8602510
UbC	Qin et al, PLoS One 2010	20485554
CMV	Qin et al, PLoS One 2010	20485554

3.5.12 | Table: introns

Parent Gene	Sequence	sD Score	sA Score
TFRC	gtaagttgagaaaaAtgaatgaacaaactaatagaaaagcagagattctacctactacattaggtagaatctaaatctgtccttgcattgaacttacttacacctaaagatattcagctaaagaatttattttggatgggggg actagcacgatagaacagtctattctttaaaacactttctaaagacacattctttgtctttgcag	**1.00**	**1.00**
BCL2	gtaagttctctgcacaggaaattggtttaatgtaactttcaatggaaacctttgagatttttttacttaaagtgcattcgagtaaatttaatttccaggcagcttaatacattctttttagccgtgttacttgtagtgtgtatgccctgctttcactcagtgtgtacagggaaacgcacctgatttttttacttattagtttgttttttctttaacctttcag	**1.00**	**1.00**
TP53	gtaagcaagcaggacaagaagcggtggaggagaccaagggtgcagttatgcctcagattcacttttatcaccttttccttgcctctttcctag	**0.99**	**1.00**
CDC25C	gtaaaggCtggggcatgcggggagccaaactttaacaactcaactcccagggcctgcaaagccttcagagaagaaactgctgctcctccttagccactgccagcagcagcatctctattatccttcatTggtagagttcaggagtctagagaatcccttactctgttccttacctttcag	**0.94**	**1.00**
EF1	gtaaggatgactacttaaatgtaaaaaagttgtgttaaagatgaaaaatacaactgaacagtactttgggtaataattaacttttttttttaatag	**1.00**	**0.96**
ACTB	gtaggggagctggctgggtggggcagccccgggagcgggcgggaggcaagggcgctttctctgcacaCgagcctcccggtttccggggtgggggctgcgcccgtgctcagggcttcttgtcctttccttcccag	**0.97**	**1.00**
ACTB	gtgagtggagactgtctcccggctctgcctgacatgagggttacccctcggggctgtgctgtggaagctaagtcctgccctcatttccctctcag	**1.00**	**0.97**
ACTB	gtgggtgtctttcctgcctgagctgacctgggcaggtcggctgtggggtcctgtggtgtgtggggagctgtcacatccagggtcctcactgcctgtccccttccctcctcag	**0.94**	**1.00**
HMBS	gtaagtggggcctggataggcagcttggtgggatgtgcccagaagatgcagggatgggaggaggaggaaaggaacagtgactgcctagtgttaaaatctcattgtaacttctctctgggcag	**1.00**	**0.96**
PGK1	gtaagtgccaggctctggtgctggtagactttgtggcgggggaagttgtcaagcacgttgttactggttttaactttcatactgctcaagtgtcttcatctcttcctcttctcag	**1.00**	**1.00**
GAPDH	gtgagtggaagacagaatggaagaaatgtgctttggggaggcaactaggatggtgtggctcccttgggtatatggtaaccttgtgtccctcaatatggtcctgtccccatctccccccccacccccatag	**0.97**	**1.00**

3.5.13 | Table: gRNA and shRNA sequences

Form	Target	Protospacer/Sequence	Source	PMID
gRNA	CCR2	CGGAGATACAGGGCAACTAA	Sanson et al, Nature Com 2018	30575746
gRNA	EGFR	GGAGGGAGGAGAACCAGCAG	Konerman et al, Nature 2015	25494202
gRNA	EGFR	CCACCGCTGTCCACCGCCTC	Konerman et al, Nature 2015	25494202
gRNA	HER2	TTGTTGGAATGCAGTTGGAG	Sanson et al, Nature Com 2018	30575746
gRNA	HER2	TGTTGGAATGCAGTTGGAGG	Sanson et al, Nature Com 2018	30575746
gRNA	GARP	TCCGGATAAACCGAGGCACG	Chen et al, JI 2018	30021769
gRNA	GARP	AAATTGCAGCCGGAGCGCGG	Chen et al, JI 2018	30021769
gRNA	CD22	CCAAGCAGCACCGTGATCTG	Sanson et al, Nature Com 2018	30575746
gRNA	CD22	GCACCGTGATCTGGGGAGTG	Sanson et al, Nature Com 2018	30575746
gRNA	NT	TGCGAATACGCCCACGCGAT	Platt et al, Cell 2014	25263330
gRNA	NT	CTGAAAAAGGAAGGAGTTGA	Konerman et al, Nature 2015	25494202
gRNA	*Null*	GAGACGGACGTCTCT	*this study*	*NA*

3.5.14 | Table: LV production recipe

Component	Amount	Unit
Cell culture	1	mL
mixture 1		
Tranfer plasmid	0.3125	µg
VSV-G	0.25	µg
GagPol	0.3125	µg
Rev	0.125	µg
OptiMEM	50	µL
mixture 2		
PEIPro	2	µL
OptiMEM	50	µL

3.5.15 | Table: Flow antibodies

Antigen Name	Target Species	Fluorochrome	Clone	Vendor	Product No
(Dead)	Human	Near-IR		Invitrogen	L10119
CD3	Human	BV421	UCHT1	Biolegend	300434
CD4	Human	BUV737	SK3	BD Biosciences	612748
CD8a	Human	BUV395	RPA-T8	BD Biosciences	563795
FMC63scFv	Human	(Biotin)		Acro Bio	FM3-BY54
Biotin	Human	SA-APC		Biolegend	405207
CCR2	Human	BV421	K036C2	Biolegend	357210
EGFR	Human	BV421	AY13	Biolegend	352911
HER2	Human	BV421	24D2	Biolegend	324420
GARP	Human	BV421	7B11	Biolegend	352509
CD22	Human	BV421	S-HCL-1	Biolegend	363512
CD45RO	Human	BV750	UCHL1	Biolegend	304262
CD62L	Human	PE/Cy5	DREG-56	Biolegend	304808
Lag3	Human	PE/Cy5	11C3C65	Biolegend	369346
Tim-3	Human	BV750	F38-2E2	Biolegend	345056
CD69	Human	PE/Cy5	FN50	Biolegend	310907
CD25	Human	BV785	M-A251	Biolegend	356139

3.5.16 | Table: General reagents

Reagent	Vendor	Product No.
EasySep HLA Chimerism Whole Blood CD4 Positive Selection Kit	StemCell	17888A
EasySep HLA Chimerism Whole Blood CD8 Positive Selection Kit	StemCell	17889
Anti-Human CD32 Antibody, Clone IV.3	StemCell	60012
RoboSep Filter Tips	StemCell	20125
RoboSep™ Buffer	StemCell	20104
1000mL CliniMACS PBS/EDTA Buffer	Miltenyi	130-070-525
Lymphoprep™	StemCell	7861
autoMACS® Running Buffer – MACS® Separation Buffer	Miltenyi	130-091-221
StraightFrom® Leukopak® CD4 MicroBead Kit, human	Miltenyi	130-117-022
StraightFrom® Leukopak® CD8 MicroBead Kit, human	Miltenyi	130-117-019
CliniMACS® CD4 GMP MicroBeads	Miltenyi	170-076-702
CliniMACS® CD8 GMP MicroBeads	Miltenyi	170-076-703

CryoStor® CS5	StemCell	7933
Opti-MEM™ Reduced-Serum Medium	Gibco	31985088
FreeStyle™ 293 Expression Medium	Gibco	12338018
X-VIVO 15 w/o gentamicin or phenol red, with L-glutamine	Lonza	04-744Q
KO Serum Replacement	Gibco	10828028
Human IL-2	StemCell	78220.3
Human IL-2	Miltenyi	130-097-746
Human IL-7	Miltenyi	130-095-364
Human IL-4	Miltenyi	130-093-924
Human IL-21	Miltenyi	130-095-784
25% Human Albumin (Plasbumin-25)	Grifols	68516-5216-1
RPMI 1640 with L-Glutamine and HEPES	Gibco	22400-089
L-Glutamine 200mM (100X)	Gibco	25030081
FBS	Hyclone	SH30070.03
FBS (Tetracycline-Free)	Takara Bio	631101
Protamine Sulfate	Medline	63323-229-30
1X PBS	Gibco	10010023
UltraPure™ DNase/RNase-Free Distilled Water	Thermo Scientific	10977015
EDTA (0.5 M), pH 8.0, RNase-free	Invitrogen	AM9260G
Brilliant Staining Buffer Plus	BD Biosciences	566385
Molecular-grade Water	Ambion	AM9937
Cell Line Nucleofector™ Kit V	Lonza	VCA-1003
P3 Primary Cell 4D-Nucleofector® X Kit L	Lonza	V4XP-3024
P3 Primary Cell 4D-Nucleofector® X Kit S	Lonza	V4XP-3032
Puromycin	Invivogen	ANT-PR-1
Methotrexate 25mg/mL	Medline	16729-277-30
Doxycycline Hyclate, USP grade	Sigma	1226003200MG
Sodium Butyrate Solution, 1M, 10ml	Sigma	19-137
5-Azacytidine Hybri-Max™	Sigma	A1287-1VL
5-Aza-2'-deoxycytidine	Sigma	A3656-5MG
T Cell TransAct™, human	Miltenyi	130-111-160
EmbryoMax® Nucleosides (100X)	Sigma	ES-008-D
Ex Taq DNA Polymerase	Takara	RR001C
NucleoSpin® Blood XL	Takara	740950.5
NucleoSpin® Gel and PCR Clean-up	Takara	740609.25
Nucleobond Xtra Maxi EF	Takara	740424.5

SapphireAmp fast PCR—hot-start master mix	Takara	RR350B
CloneAmp™ HiFi PCR Premix	Takara	639298
Q5® Hot Start High-Fidelity 2X Master Mix	NEB	M0494S
NEBNext® Ultra™ II Q5® Master Mix	NEB	M0544S
BsmBI-v2	NEB	R0739L
NEB® Golden Gate Assembly Kit (BsmBI-v2)	NEB	E1602S
NEBridge® Ligase Master Mix	NEB	M1100S
NEBuilder® HiFi DNA Assembly Master Mix	NEB	E2621L
NEB® Stable Competent E. coli (High Efficiency)	NEB	C3040H
NEB 10-beta Electrocompetent E. coli	NEB	C3020K
Miller's LB Broth	Fisher	MT46050CM
LB Broth, No Salt, Sucrose 6%	Teknova	L8610
LB Agar plates with 30 µg/mL Kanamycin, 100 mm	Teknova	L1024
LB Agar plates with 100µg/mL Carbenicillin, 100 mm	Teknova	L1010
LB Agar plates with 6% sucrose, without salt, 100 mm	Teknova	L1143
LB Agar plates with 100µg/mL Spectinomycin, 100 mm	Teknova	L1028
Spectinomycin dihydrochloride pentahydrate	Sigma	S9007-5G
Kanamycin solution, 50mg/mL	Teknova	K2125
Carbenicillin solution, 100mg/mL	Teknova	C2130

3.5.17 | Table: ddPCR reagents

Oligonucleotide	Sequence
mScarlet Fwd	5’-CACCCTGATCTACAAGGTGAAG-3’
mScarlet Rvs	5’-CCCAGCCCATTGTCTTCTT-3’
mScarlet Probe	5’–/56-FAM/TGGCACCAA/ZEN/CTTCCCTCCTGAC/3IABkFQ/-3'
dCas9 Fwd	5’-TCAGCAACGAGATGGCCAAG-3'
dCas9 Rvs	5'-TCCACGATGTTGCCGAAGATG-3'
dCas9 Probe	5'-/56-FAM/TGGAAGAGG/ZEN/ATAAGAAGCACGAGCG/3IABkFQ/-3'
FMC63scFv Fwd	5’–TGACCATCATCAAGGACAACTC–3’
FMC63scFv Rvs	5’–CTACTATTGCGCCAAGCACTA–3’
FMC63scFv Probe	5’–/5HEX/TCGGTCTGC/ZEN/AGGCTGTTCATCTTC/3IABkFQ/–5’
Albumin Fwd	5’–GCTGTCATCTCTTGTGGGCTGT–3’
Albumin Rvs	5’–ACTCATGGGAGCTGCTGGTTC–3’
Albumin Probe	5’–/5HEX/CCTGTCATG/ZEN/CCCACACAAATCTCTCC/3IABkFQ/–3’

3.6 | Author Contributions

The author would like to thank Natalie Murren, Pittra Jaengprajak, and Jasmin Martinez-Reyes – three undergraduate students attending the University of Washington – for their assistance with molecular cloning, Jurkat T cell nucleofection, T cell culture maintenance, and select EP-TICLE experiments. James Rosser, Christopher Saxby, and Taylor Ishida assisted with T cell isolation and provided sporadic cell maintenance. James Rosser, Jeremy Bjelajac, Mariliis Ott, and Ricardo Miranda were instrumental in co-conceiving the EP-TICLE manufacturing process and piloted numerous early process development experiments not shown here.

Lentivirus used within the course of these studies was manufactured by the Seattle Children's Therapeutics Bioproduction Core consisting of Marissa Leonardi, Lindsay Flint, Aalton Lande, Samantha Steuer, and Sakinah Abdul-Khaliq; this team also generated lentiviral functional titer results using Jurkat or Raji cell lines.

ddPCR studies were carried out by Tiffanie Chai. dCas9 immunoblot was performed by Rachael Logan. ChIP-seq and ChIP-qPCR experiments were performed by Ryan McCarthy. Long-read sequencing fastq analysis was performed by Ardizon Valdez.

Also enabling this work were useful suggestions and feedback provided by other members of the Jensen lab including Jacob Appelbaum and Michael Fitzgerald. Michael Jensen supervised the project and provided funding.

All studies were conceived of by Benjamin Curtis.

3.7 | Figures

Figure 3.1

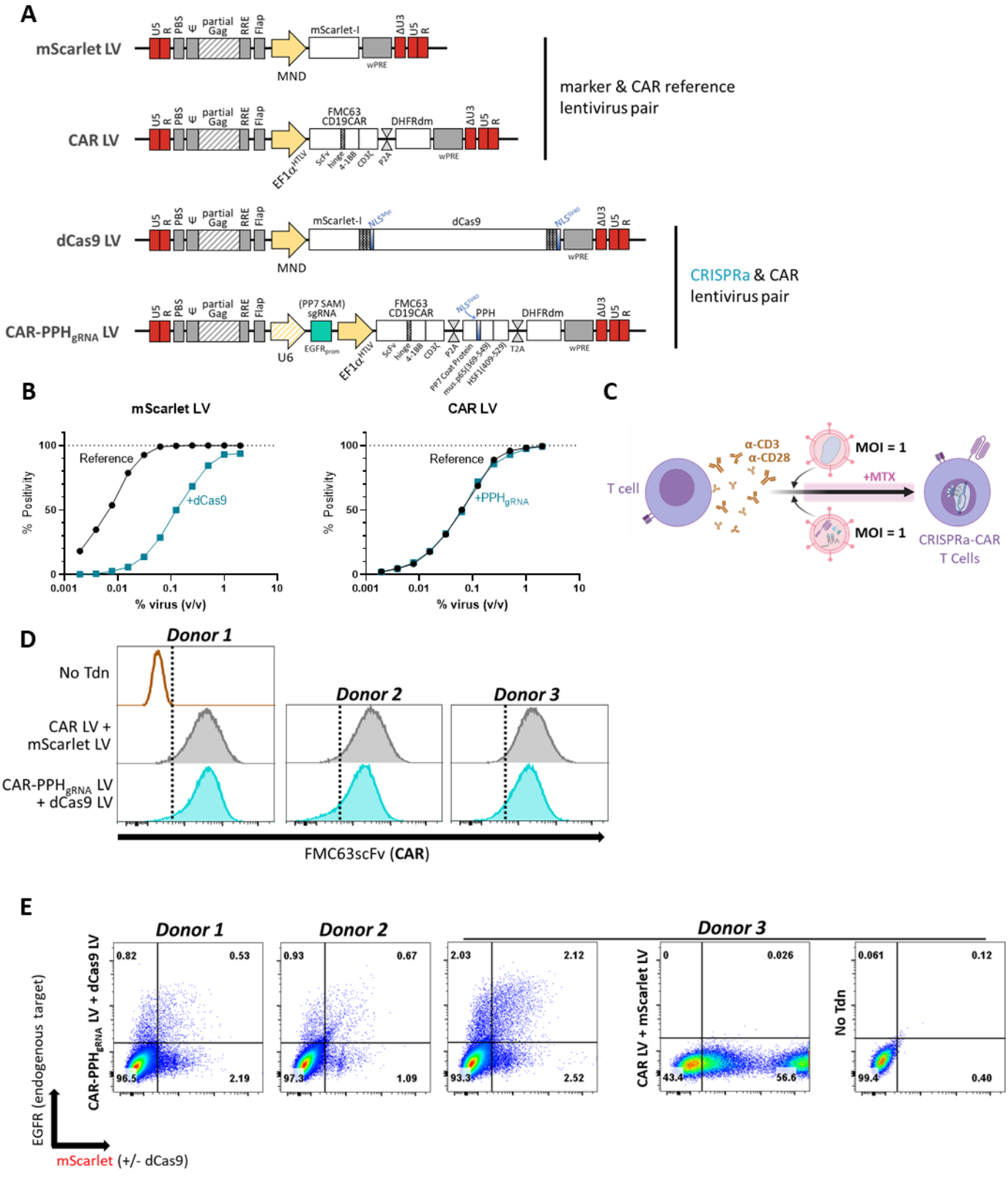

Figure 3.1: CRISPRa-CAR T cell production via lentiviral transduction. (**A**) Lentiviral RNA payload maps of CRISPRa/CAR pair and reference pair. (**B**) Plots depicting titration of CRISPRa lentiviruses and reference lentiviruses in Jurkat T cell line. (**C**) Cell production schema of α-CD3/α-CD28 bead-activated (Day 0) CD8 and CD4 T cells transduced (Day 1) with CRISPRa/CAR or reference lentivirus pairs at an MOI = 1 per each virus, then MTX selection initiated (Day 4) and maintained throughout. (**D**) Lentiviral cell manufacturing Day 7 flow cytometry histograms of FMC63scFv (CAR) expression from T cell populations generated via mScarlet-LV/CAR-LV or dCas9-LV/CAR-PPH$_{gRNA}$ lentivirus pairs. (**E**) Flow cytometry plots of mScarlet(+/- dCas9) and EGFR expression from cells described in (D). Cells in (D) and (E) are gated on $CD8^+$ or $CD4^+$ live singlets.

Figure 3.2

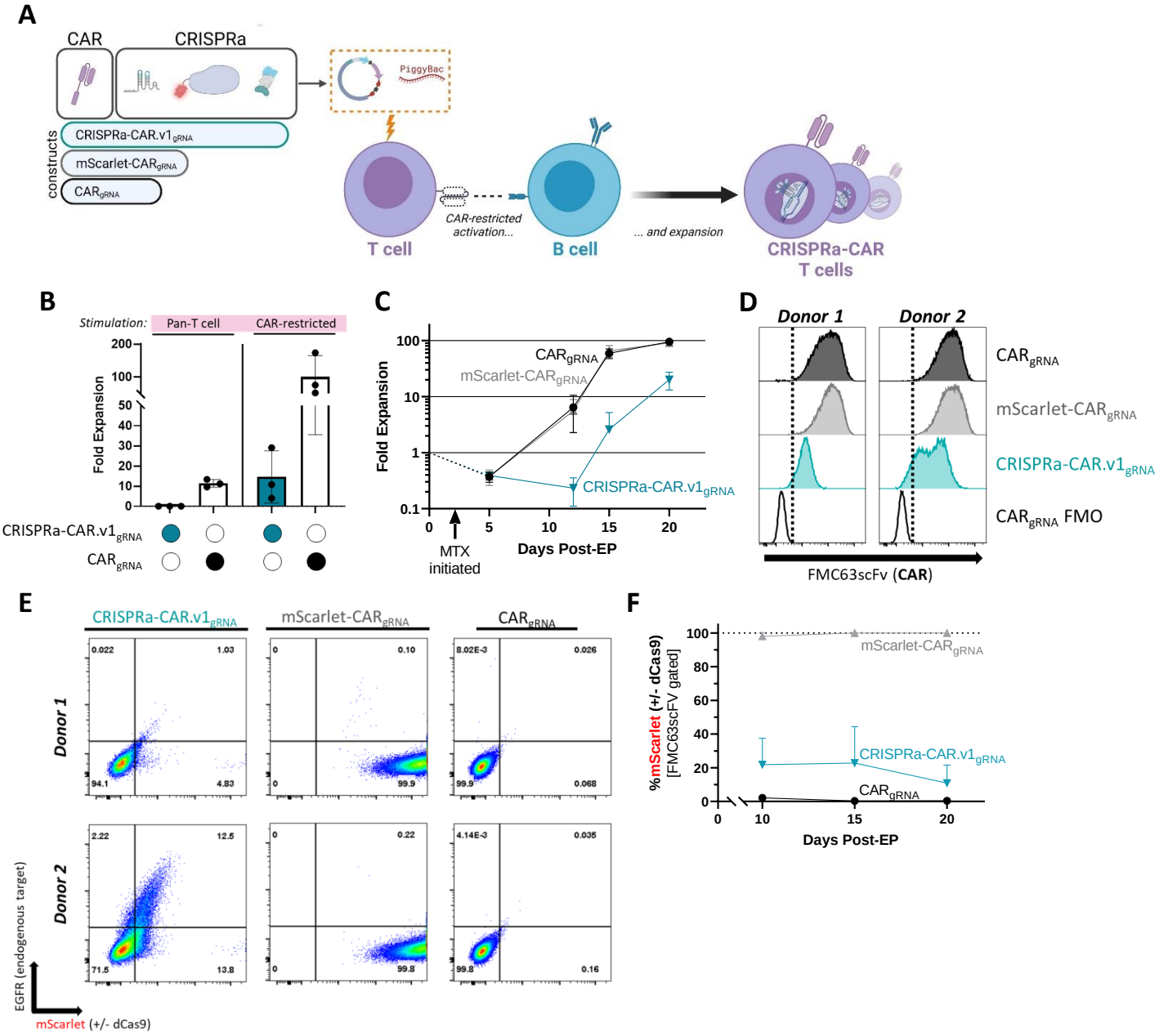
A
CAR
CRISPRa
PiggyBac
constructs
CRISPRa-CAR.v1gRNA
mScarlet-CARgRNA
CARgRNA
T cell
CAR-restricted activation...
B cell
... and expansion
CRISPRa-CAR T cells
B
Stimulation:
Pan-T cell
CAR-restricted
Fold Expansion
CRISPRa-CAR.v1gRNA
CARgRNA
C
Fold Expansion
CARgRNA
mScarlet-CARgRNA
CRISPRa-CAR.v1gRNA
MTX initiated
Days Post-EP
D
Donor 1
Donor 2
CARgRNA
mScarlet-CARgRNA
CRISPRa-CAR.v1gRNA
CARgRNA FMO
FMC63scFv (CAR)
E
CRISPRa-CAR.v1gRNA
mScarlet-CARgRNA
CARgRNA
Donor 1
Donor 2
EGFR (endogenous target)
mScarlet (+/- dCas9)
F
%mScarlet (+/- dCas9)
[FMC63scFV gated]
mScarlet-CARgRNA
CRISPRa-CAR.v1gRNA
CARgRNA
Days Post-EP

Figure 3.2, cont'd

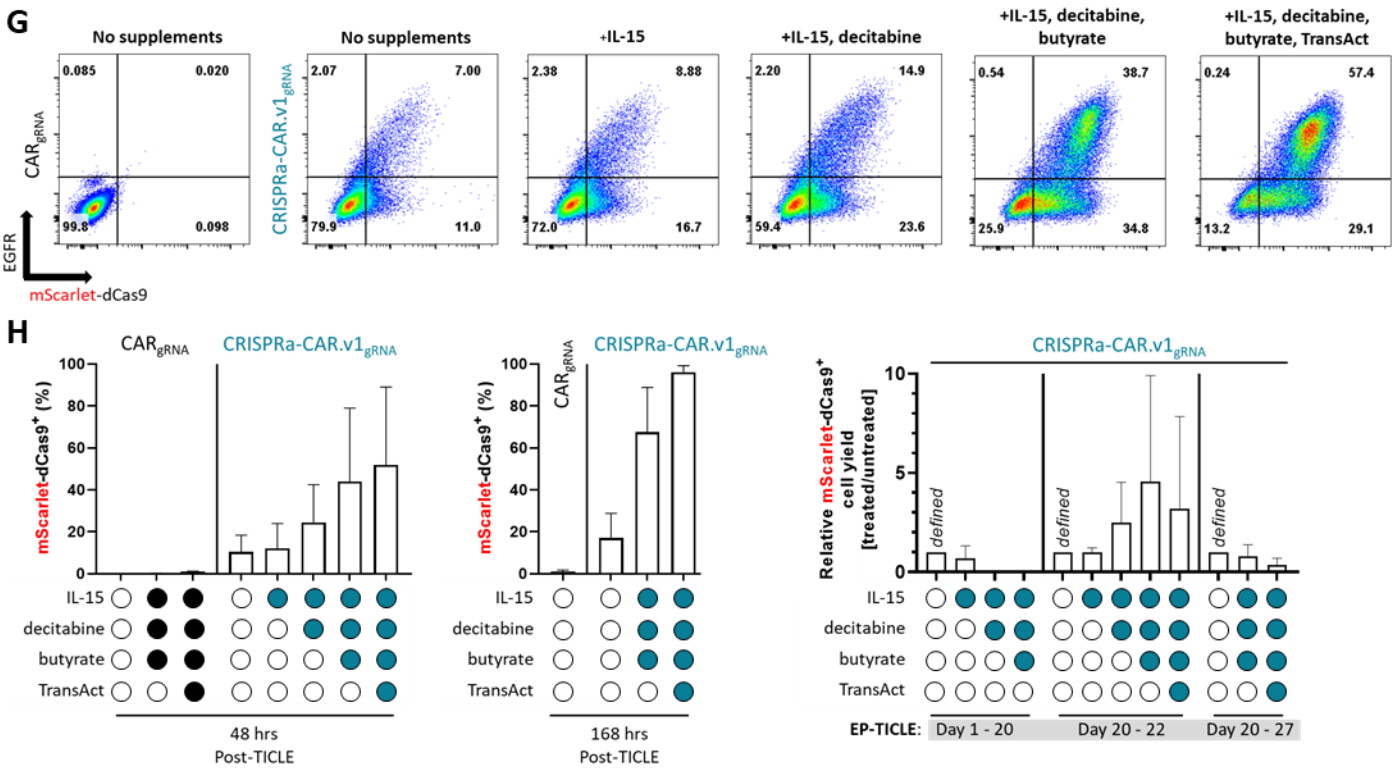

Figure 3.2: CRISPRa-CAR T cell EP-TICLE manufacturing and product analysis. (**A**) EP-TICLE manufacturing schema graphic. (**B**) Total live cell fold-expansion as a function donor plasmid and T cell stimulation method. (**C**) EP-TICLE live cell fold-expansion as function of time and donor plasmid. (**D**) Flow cytometry histograms depicting FMC63scFv (CAR) expression at Day 20 of EP-TICLE cell manufacturing as function of blood donor and donor plasmid. (**E**) Flow cytometry plots of EGFR (CRISPRa target gene) and mScarlet (+/-dCas9) expression in CAR_{gRNA}, mScarlet-CAR_{gRNA}, and CRISPRa-CAR.v1$_{gRNA}$ $CD8^+$ or $CD4^+$ cells. (**F**) mScarlet positivity of EP-TICLE cells as a function of time and donor plasmid. (**G**) Flow cytometry plots of EGFR and mScarlet-dCas9 expression in CAR_{gRNA} or CRISPRa-CAR.v1$_{gRNA}$ mixed $CD8^+$ and $CD4^+$ T cells as a function of donor plasmid and 48-hour treatment with anti-silencing drug cocktails (e.g. IL-15, decitabine, butyrate, TransAct). (**H**) Quantification of mScarlet-dCas9 positivity or mScarlet-$dCas9^+$ cell yield in CAR_{gRNA} or CRISPRa-CAR.v1$_{gRNA}$ as a function of donor plasmid, anti-silencing drug cocktail, and treatment time horizon indicated below each dataset. Data in (B), (C), (F), and (H) display the mean +/-SD of indicated measurement of cells generated from three human blood donors. Cells in (F) are gated on $FMC63scFv^+$, $CD8^+$ or $CD4^+$ live singlets. Cell plots or quantified data in (D), (E), and (H) are gated on $CD8^+$ or $CD4^+$ live singlets only. All experiments depicted here used 1:1 mixtures of $CD8^+$ and $CD4^+$ T cells as EP-TICLE input.

Figure 3.3

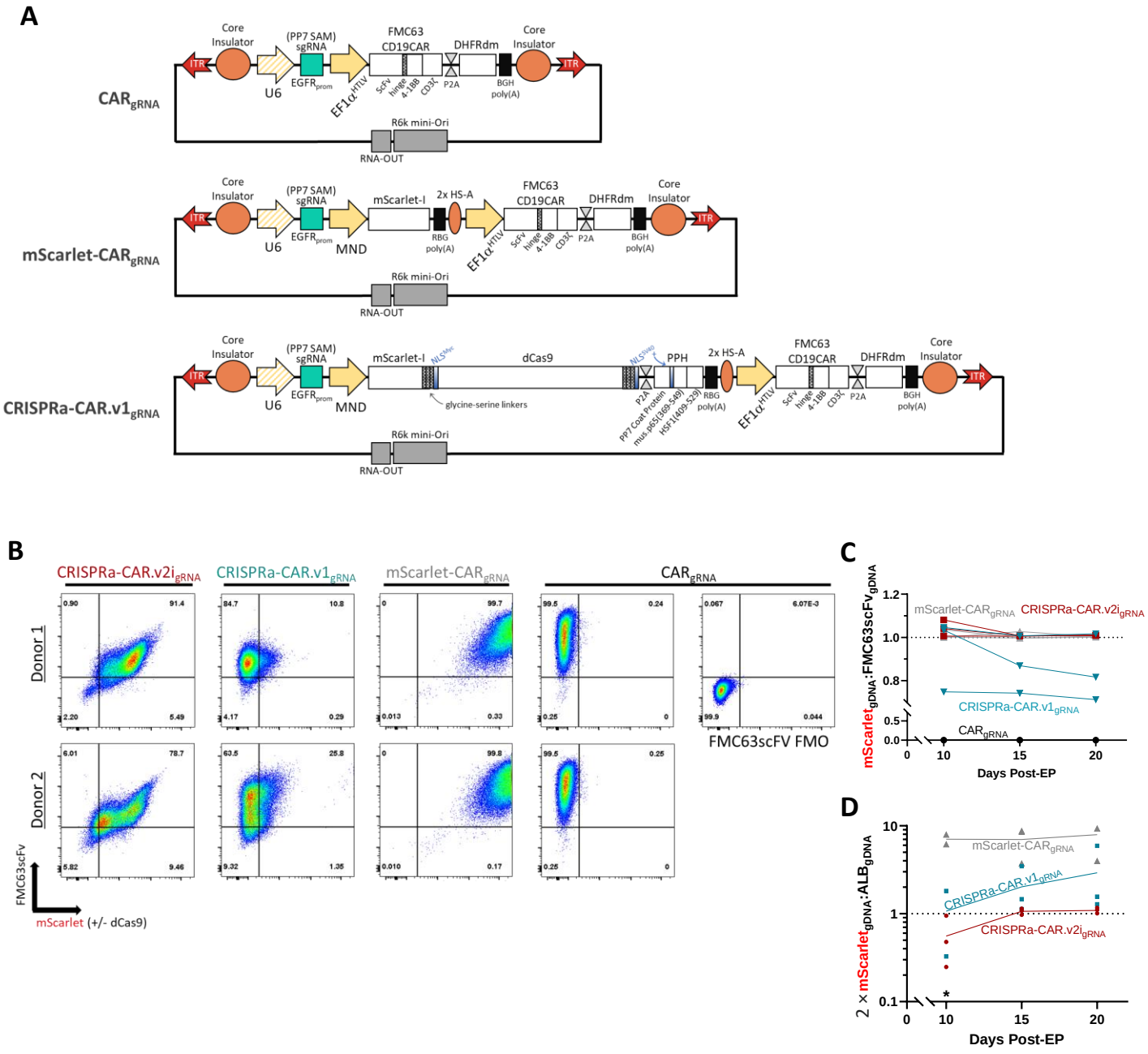
A
CAR gRNA
mScarlet-CAR gRNA
CRISPRa-CAR.v1 gRNA
Core Insulator
(PP7 SAM) sgRNA
U6
EGFR prom
MND
EF1α HTLV
FMC63 CD19CAR
ScFv
hinge
4-1BB
CD3ζ
P2A
DHFRdm
BGH poly(A)
RBG poly(A)
ITR
R6k mini-Ori
RNA-OUT
mScarlet-I
2x HS-A
dCas9
PPH
glycine-serine linkers
PP7 Coat Protein
mus p65(369-549)
HSF1(409-529)
B
CRISPRa-CAR.v2i gRNA
CRISPRa-CAR.v1 gRNA
mScarlet-CAR gRNA
CAR gRNA
Donor 1
Donor 2
FMC63scFv
mScarlet (+/- dCas9)
FMC63scFV FMO
C
mScarlet-CAR gRNA
CRISPRa-CAR.v2i gRNA
CRISPRa-CAR.v1 gRNA
CAR gRNA
mScarlet gDNA:FMC63scFv gDNA
Days Post-EP
D
mScarlet-CAR gRNA
CRISPRa-CAR.v1 gRNA
CRISPRa-CAR.v2i gRNA
2 × mScarlet gDNA:ALB gDNA
Days Post-EP

Figure 3.3, cont'd

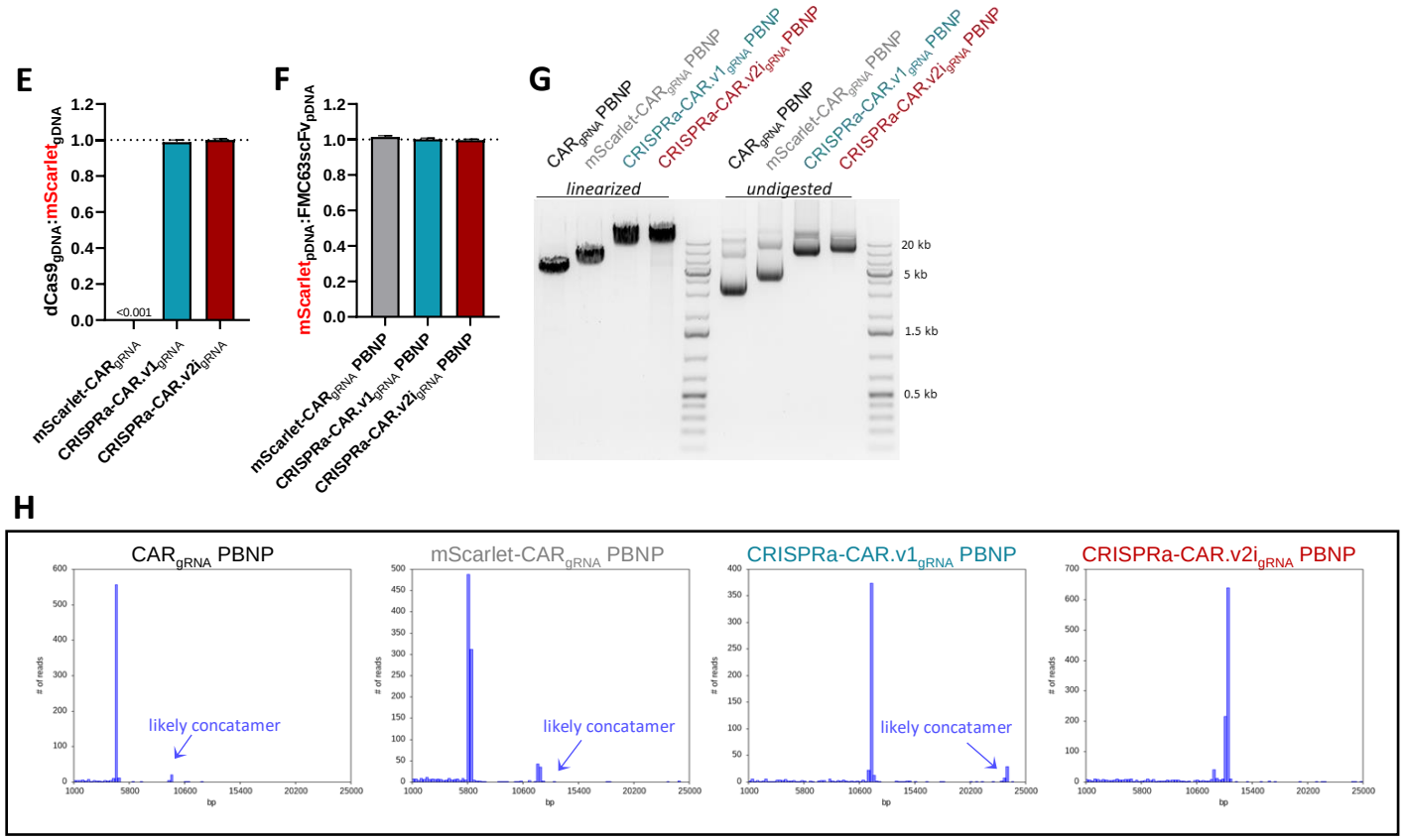

Figure 3.3: Extended flow cytometry of CRISPRa-CAR T cells, donor plasmid maps and analysis. (**A**) PiggyBac nanoplasmid donor maps. (**B**) Extended flow cytometry plots of FMC63scFV (CAR) and mScarlet (+/-dCas9) expression in CRISPRa-CAR.v1$_{gRNA}$, mScarlet-CAR$_{gRNA}$, and CAR$_{gRNA}$ mixed CD8^{+} and CD4^{+} cells. (**C**) Droplet-digital (dd)PCR relative quantification of mScarlet$_{gDNA}$ to FMC63scFv$_{gDNA}$ during EP-TICLE manufacturing in cells generated using CAR$_{gRNA}$, mScarlet-CAR$_{gRNA}$, CRISPRa-CAR.v1$_{gRNA}$, or CRISPRa-CAR.v2i$_{gRNA}$ donor plasmid. (**D**) ddPCR absolute quantification of mScarlet$_{gDNA}$ to Albumin (ALB)$_{gDNA}$ during EP-TICLE manufacturing in cells generated using mScarlet-CAR$_{gRNA}$, CRISPRa-CAR.v1$_{gRNA}$, or CRISPRa-CAR.v2i$_{gRNA}$ donor plasmid. To report copy number, ratio has been adjusted to account for diploid genome. (**E**) ddPCR relative quantification of dCas9$_{gDNA}$ to mScarlet$_{gDNA}$ in EP-TICLE cells at Day 20 as a function of indicated donor plasmid. (**F**) ddPCR relative quantification of mScarlet$_{gDNA}$ to FMC63scFv$_{gDNA}$ detection in mScarlet-CAR$_{gRNA}$, CRISPRa-CAR.v1$_{gRNA}$, and CRISPRa-CAR.v2i$_{gRNA}$ donor plasmid pools. (**G**) Visual agarose gel electrophoresis of CAR$_{gRNA}$ (4.8 kb), mScarlet-CAR$_{gRNA}$ (6.0 kb), CRISPRa-CAR.v1$_{gRNA}$ (11.8 kb), and CRISPRa-CAR.v2i$_{gRNA}$ (13.0 kb) donor plasmids with (*left*) or without (*right*) linearization via NruI restriction enzyme. (**H**) Nanopore sequencing DNA string read frequency of mScarlet$_{gDNA}$ and FMC63scFv$_{gDNA}$ ddPCR amplicons for CRISPRa-CAR.v1$_{gRNA}$ donor plasmid. Each curve in (C) and (D) is generated from cells sourced for a distinct blood donor. Asterisk in (D) indicates that banked cells were limited at this timepoint, and so copy number was not assessed for several samples.

Figure 3.4

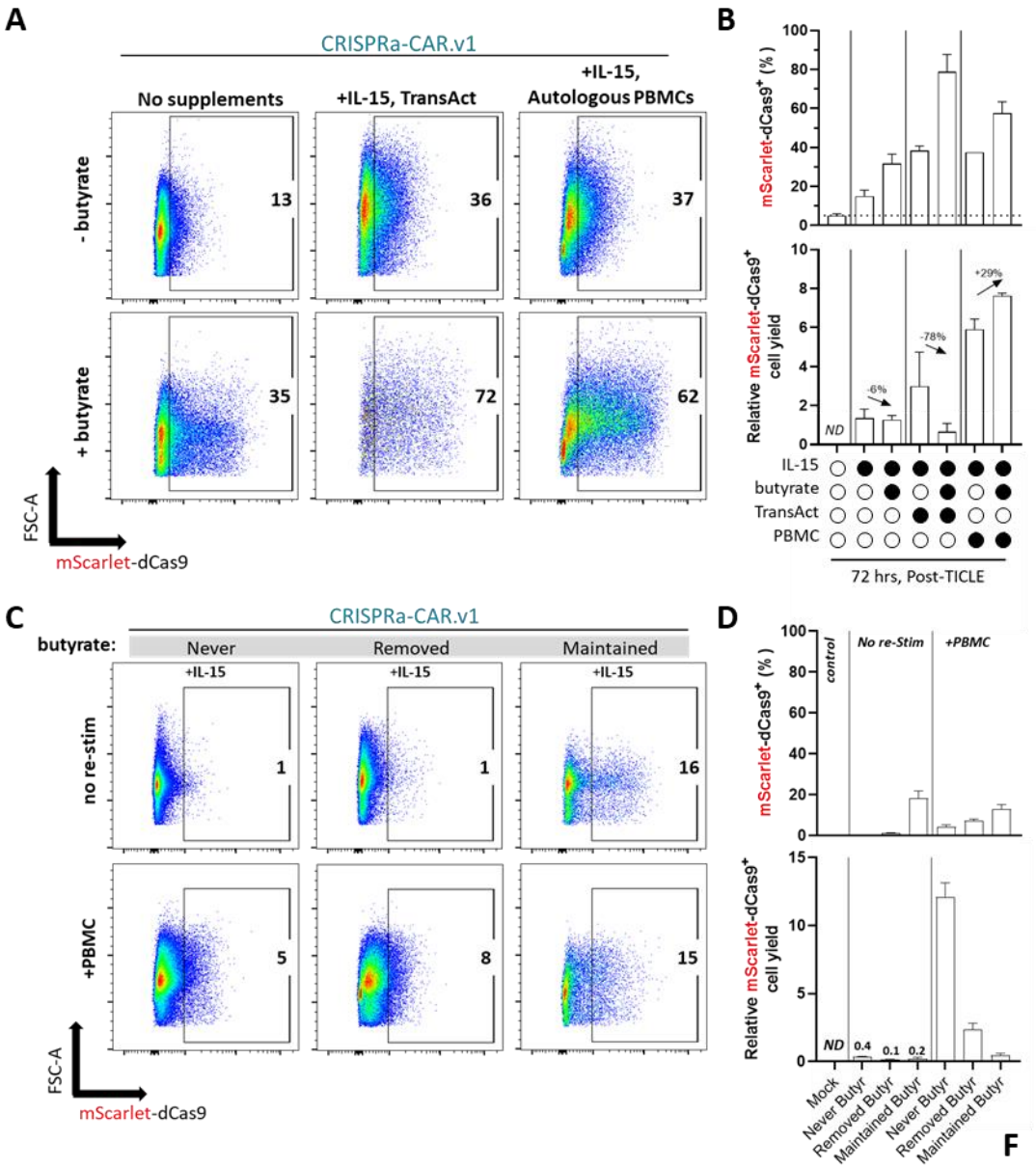
A
CRISPRa-CAR.v1
No supplements
+IL-15, TransAct
+IL-15, Autologous PBMCs
- butyrate
+ butyrate
13
36
37
35
72
62
FSC-A
mScarlet-dCas9
B
mScarlet-dCas9+ (%)
Relative mScarlet-dCas9+ cell yield
ND
-6%
-78%
+29%
IL-15
butyrate
TransAct
PBMC
72 hrs, Post-TICLE
C
CRISPRa-CAR.v1
butyrate:
Never
Removed
Maintained
+IL-15
no re-stim
+PBMC
1
1
16
5
8
15
FSC-A
mScarlet-dCas9
D
control
No re-Stim
+PBMC
mScarlet-dCas9+ (%)
Relative mScarlet-dCas9+ cell yield
ND
0.4
0.1
0.2
Mock
Never Butyr
Removed Butyr
Maintained Butyr
Never Butyr
Removed Butyr
Maintained Butyr
F

Figure 3.4, cont'd

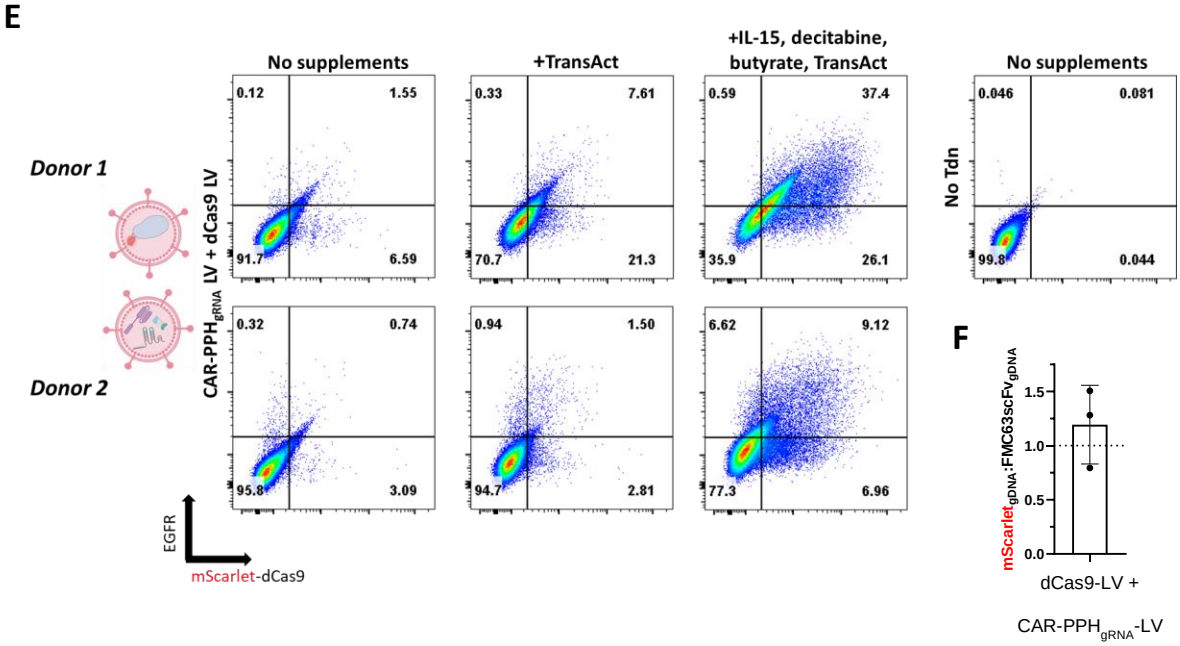

Figure 3.4: Extended de-silencing of CRISPRa-CAR T cells generated via transposon-based or lentiviral integration methods. (**A**) Flow cytometry plots and (**B**) accompanying quantification of mScarlet-dCas9 cell positivity in CRISPRa-CAR.v1 $CD8^+$ T cells generated via EP-TICLE and treated with various de-silencing compounds for 72 upon completion of cell manufacturing. (**C**) Flow cytometry plots and (**D**) accompanying quantification of mScarlet-dCas9 cell positivity in CRISPRa-CAR.v1 $CD8^+$ T cells generated via EP-TICLE and treated thereafter with or without autologous PBMCs and variable butyrate exposure to include 10 days off ("never"), 4 days on/ 6 days off ("removed"), or continuous exposure for 10 days ("maintained"). (**E**) Flow cytometry plots of mScarlet (+/-dCas9) and EGFR expression in mixed $CD4^+$ and $CD8^+$ T cells transduced with CRISPRa and CAR lentiviral pairs (vector maps shown in Fig 3.1a) and treated with various de-silencing compounds for 48 hours upon completion of cell manufacturing after 11 days. (**F**) ddPCR relative quantification of $mScarlet_{gDNA}$ to $FMC63scFv_{gDNA}$ in cells generated via transduction with dCas9-LV/CAR-PPH_{gRNA} lentivirus pairs. Cells for (A thru D) were sourced from a single blood donor but (B and D) represent independent EP-TICLE cultures (n = 2) per condition shown. Cells in (A) thru (E) are gated on live singlets.

Figure 3.5

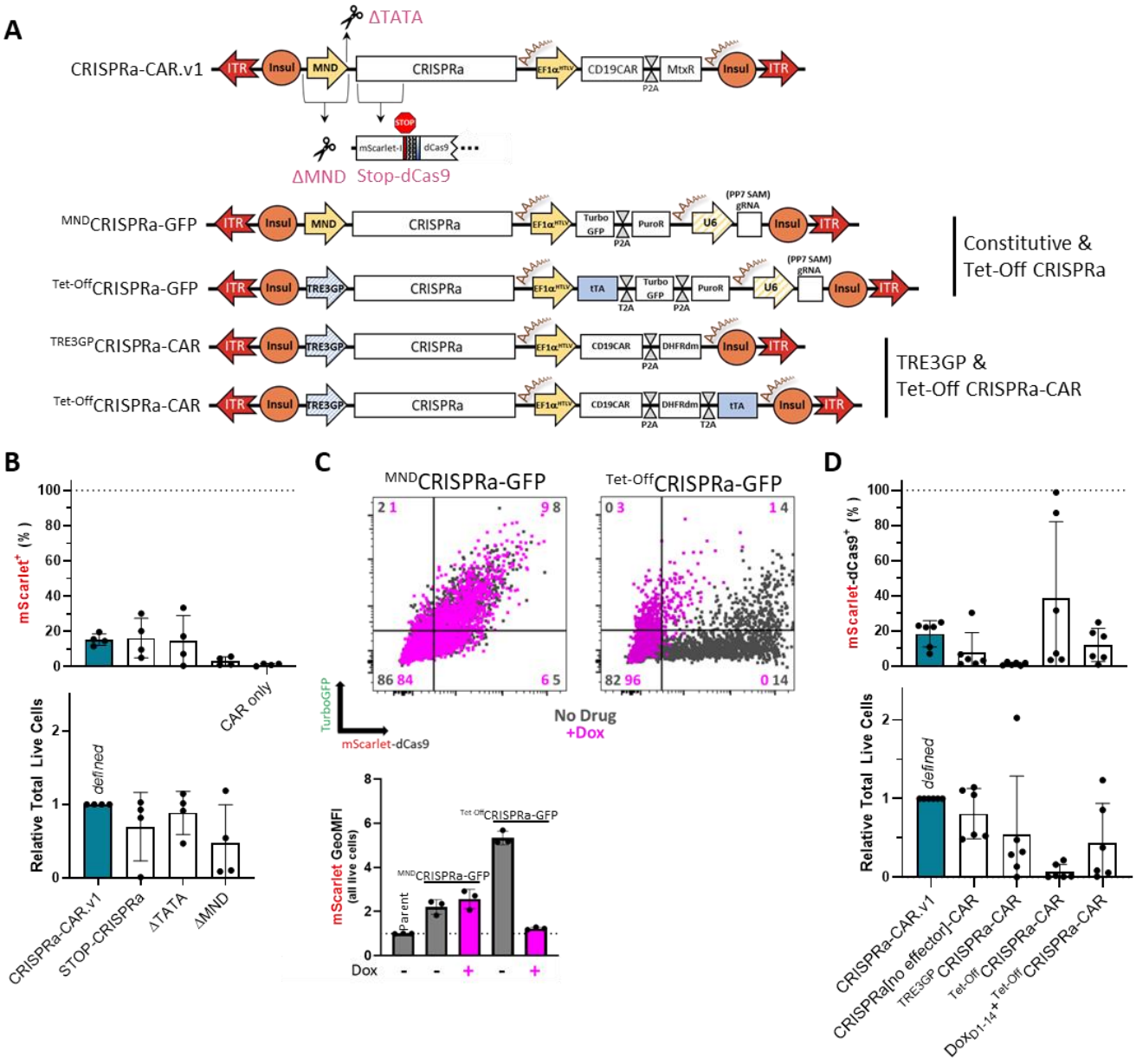
A
ΔTATA
CRISPRa-CAR.v1
ITR
Insul
MND
CRISPRa
EF1α
CD19CAR
MtxR
P2A
STOP
mScarlet-i
dCas9
ΔMND
Stop-dCas9
MNDCRISPRa-GFP
Turbo GFP
PuroR
U6
(PP7 SAM) gRNA
Tet-OffCRISPRa-GFP
TRE3GP
tTA
T2A
TRE3GPCRISPRa-CAR
DHFRdm
Tet-OffCRISPRa-CAR
Constitutive & Tet-Off CRISPRa
TRE3GP & Tet-Off CRISPRa-CAR
B
mScarlet+ (%)
Relative Total Live Cells
defined
CAR only
CRISPRa-CAR.v1
STOP-CRISPRa
ΔTATA
ΔMND
C
MNDCRISPRa-GFP
Tet-OffCRISPRa-GFP
2 1
9 8
86 84
6 5
0 3
1 4
82 96
0 14
TurboGFP
mScarlet-dCas9
No Drug
+Dox
mScarlet GeoMFI (all live cells)
Parent
Dox
D
mScarlet-dCas9+ (%)
Relative Total Live Cells
defined
CRISPRa-CAR.v1
CRISPRa[no effector]-CAR
TRE3GP CRISPRa-CAR
Tet-Off CRISPRa-CAR
DoxD1-14 + Tet-Off CRISPRa-CAR

Figure 3.5: Restrained and modified CRISPRa expression attempts. (**A**) CRISPRa and CRISPRa-CAR plasmid donor maps. (**B** and **D**) Quantification of mScarlet(+/- dCas9) positivity (*top graph*) and relative total live cells (*bottom graph*) of 1:1 CD4 and CD8 bulk EP-TICLE cultures made from indicated donor plasmids. (**C**) Flow cytometry plots of TurboGFP and mScarlet-dCas9 expression (*upper*) and geometric mean fluorescent intensity (*lower*) in Jurkat T cells transiently electroporated with donor plasmids depicted in (A) with or without doxycycline (dox) treatment. All cells are gated on live singlets. Calculated values in (B) and (D) are generated from data additionally gated on $CD4^+$ or $CD8^+$ cells, generated from 4 or 3 (where cells limiting) human blood donors.

Figure 3.6

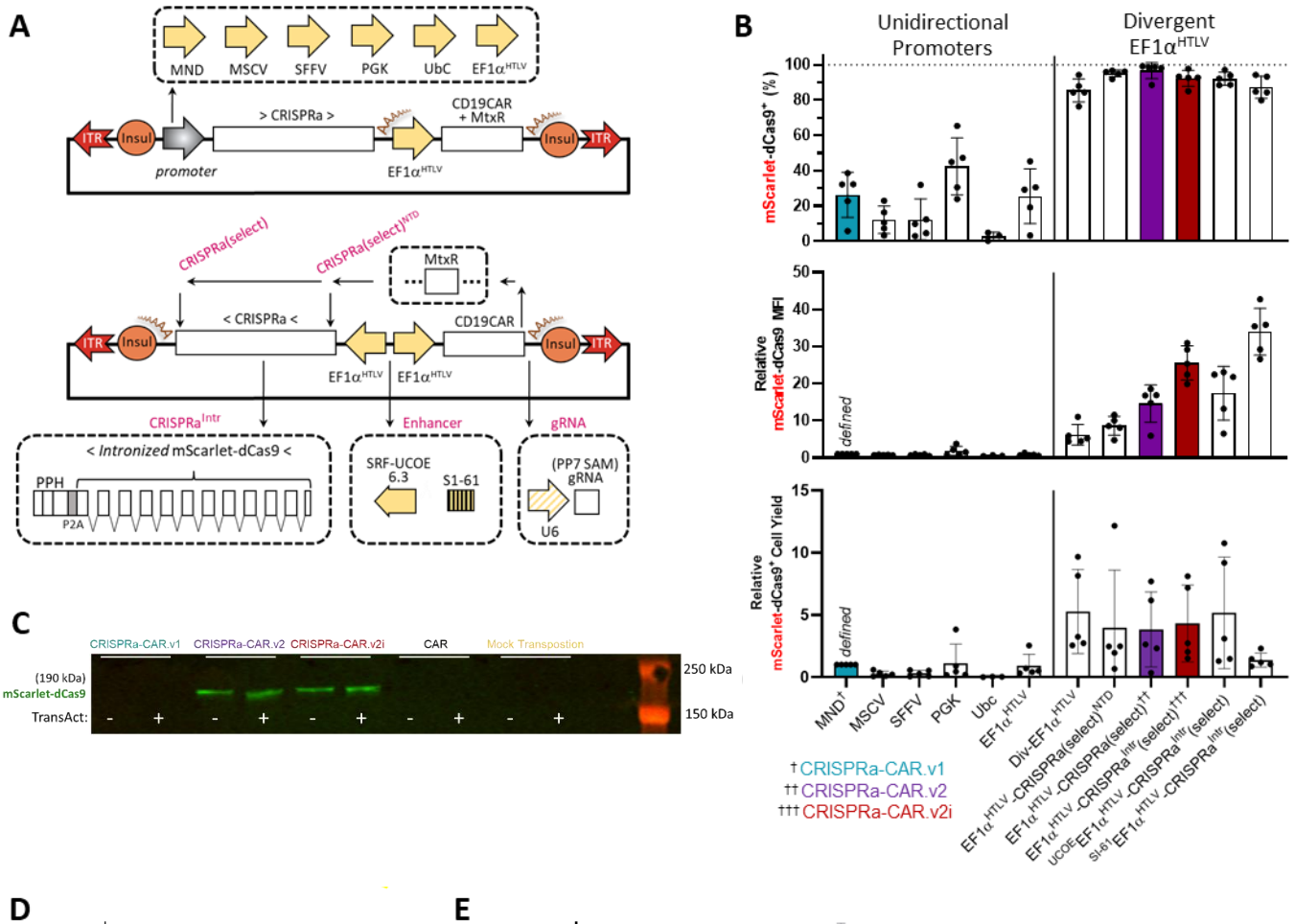
A
MND
MSCV
SFFV
PGK
UbC
EF1α HTLV
> CRISPRa >
CD19CAR + MtxR
ITR
Insul
promoter
EF1α HTLV
CRISPRa(select)
CRISPRa(select) MTD
MtxR
< CRISPRa <
CD19CAR
EF1α HTLV
EF1α HTLV
CRISPRa Intr
Enhancer
gRNA
< Intronized mScarlet-dCas9 <
PPH
P2A
SRF-UCOE 6.3
S1-61
(PP7 SAM) gRNA
U6
B
Unidirectional Promoters
Divergent EF1α HTLV
mScarlet-dCas9+ (%)
Relative mScarlet-dCas9 MFI
defined
Relative mScarlet-dCas9+ Cell Yield
defined
MND†
MSCV
SFFV
PGK
Ubc
EF1α HTLV
Div-EF1α HTLV
EF1α HTLV_CRISPRa(select) MTD
EF1α HTLV_CRISPRa(select)††
EF1α HTLV_CRISPRa Intr (select)†††
UCOE-EF1α HTLV_CRISPRa Intr (select)
S/-61EF1α HTLV_CRISPRa Intr (select)
† CRISPRa-CAR.v1
†† CRISPRa-CAR.v2
††† CRISPRa-CAR.v2i
C
CRISPRa-CAR.v1
CRISPRa-CAR.v2
CRISPRa-CAR.v2i
CAR
Mock Transposition
(190 kDa) mScarlet-dCas9
TransAct:
250 kDa
150 kDa
D
% mScarlet-dCas9 [FMC63scFV gated]
CRISPRa-CAR.v2i gRNA
CRISPRa-CAR.v1 gRNA
CAR gRNA
Days Post-EP
E
Relative mScarlet (+/-dCas9) MFI [FMC63scFV gated]
mScarlet-CAR gRNA
CRISPRa-CAR.v2i gRNA
CRISPRa-CAR.v1 gRNA
CAR gRNA
Days Post-EP

Figure 3.6, cont'd

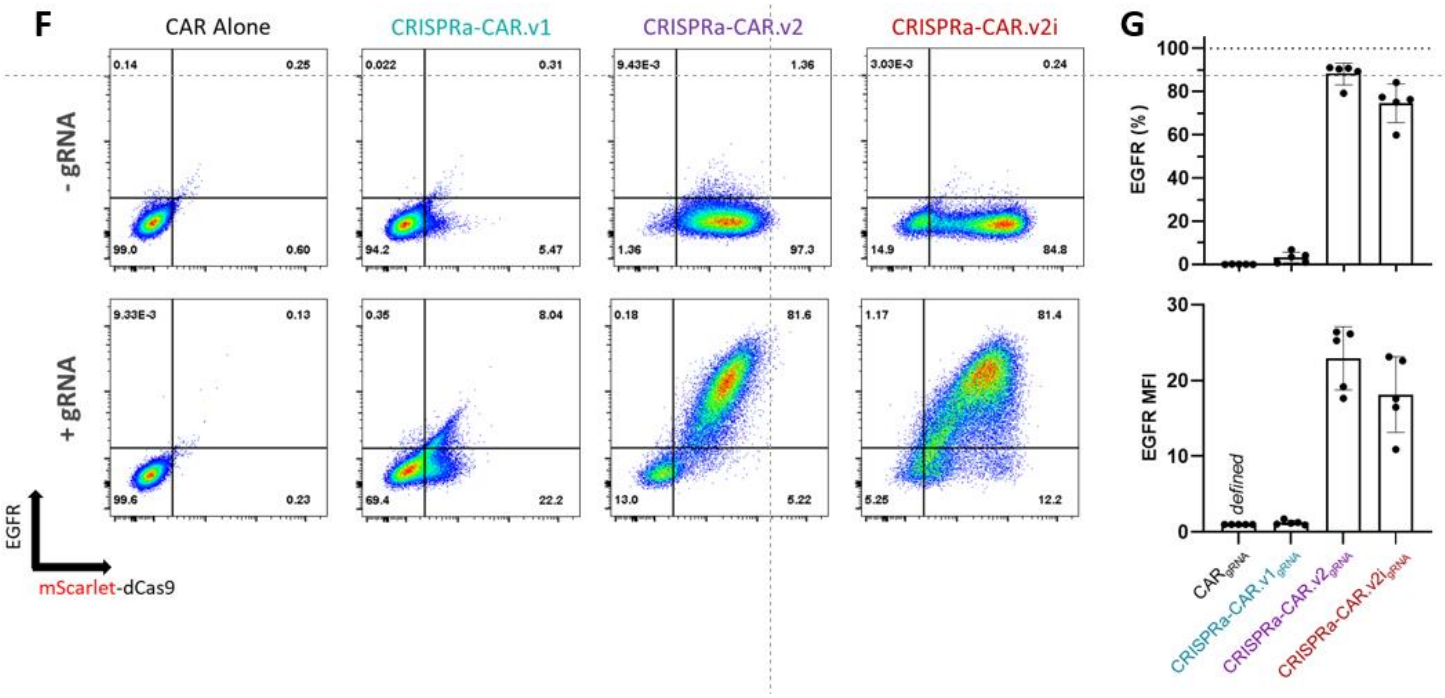

Figure 3.6: Optimization of CRISPRa-CAR vectors. (**A**) Abridged donor plasmid maps of select CRISPRa-CAR variants. (**B**) Quantification of Day 20/21 mScarlet-dCas9 positivity (*top graph*), relative mScarlet-dCas9 mean fluorescence intensity (*middle graph*), and relative mScarlet-dCas9$^+$ T cell yield (*bottom graph*) of indicated CAR T cells generated via EP-TICLE. (**C**) Combined CRISPRa and CAR immunoblot of untransposed mock, CAR, CRISPRa-CAR.v1, CRISPRa.v2, and CRISPRa-CAR.v2i EP-TICLE cells at Day 20/21. (**D**) mScarlet-dCas9 positivity and (**E**) relative mScarlet(+/- dCas9)$^+$ cell yield of CAR_{gRNA}, mScarlet-CAR_{gRNA}, CRISPRa-CAR.$v1_{gRNA}$, and CRISPRa-CAR.$v2i_{gRNA}$ T cells as a function of time and donor plasmid. (**F**) Day 20 flow cytometry plots of EGFR and mScarlet-dCas9 expression in cells generated via EP-TICLE from indicated donor plasmid with or without accompanying all-in-one U6-gRNA(EGFRprom) expression cassette. (**G**) Day 20/21 quantitative EGFR positivity (*top graph*) and EGFR mean fluorescence intensity (*bottom graph*) of cells generated via EP-TICLE from indicated donor plasmid. Cells in (D) and (E) are gated on FMC63scFv$^+$, CD8$^+$ or CD4$^+$ live singlets. Cells in (B), (F) and (G) are gated on CD8$^+$ or CD4$^+$ live singlets only. All experiments depicted here used 1:1 mixtures of CD8$^+$ and CD4$^+$ T cells as EP-TICLE input. Quantified data in (B) and (G) are compiled from cells generated from five human blood donors. Time course data in (D) and (E) display the mean +/-SD of indicated measurement of cells generated from three human blood donors.

Figure 3.7

A

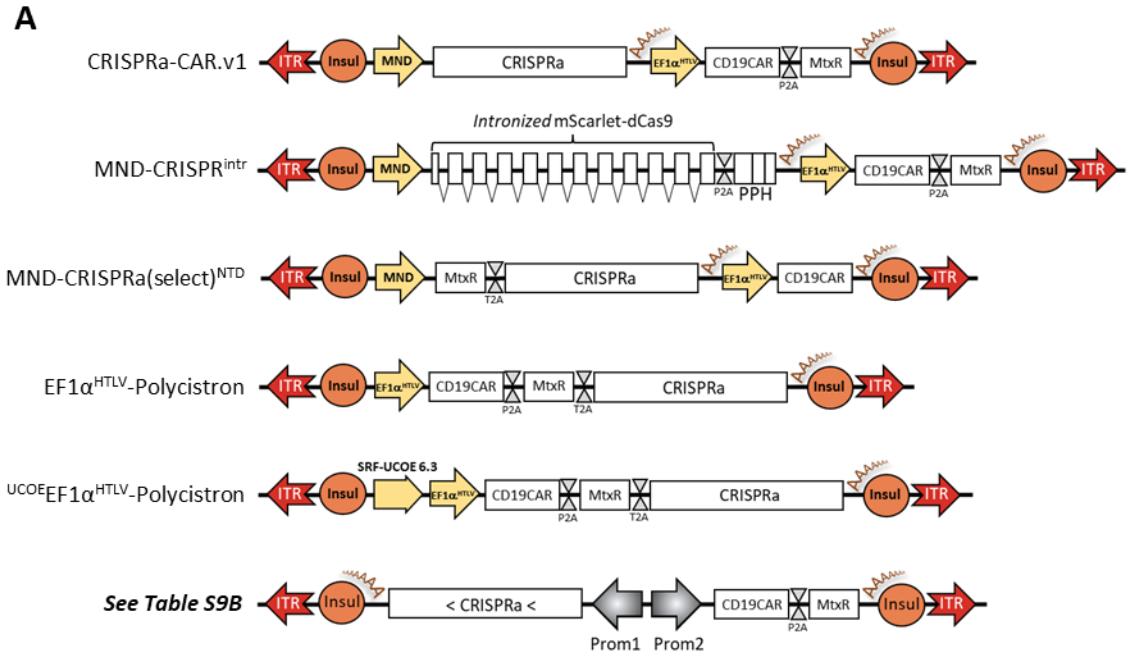

B

Plasmid ID	Prom1	Prom2
Div-EF1α^{HTLV}	EF1α^{HTLV}	EF1α^{HTLV}
Div-MND	MND	EF1α^{HTLV}
Div-2xMND	MND	MND
Div-MNDrvs	EF1α^{HTLV}	MND
Div-PGK	PGK	EF1α^{HTLV}
Div-2xPGK	PGK	PGK
Div-EF1α^{Core}	EF1α^{Core}	EF1α^{HTLV}
Div-2xEF1α^{Core}	EF1α^{Core}	EF1α^{Core}

C

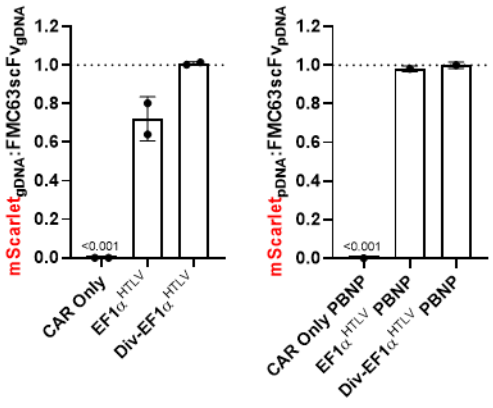

Figure 3.7, cont'd

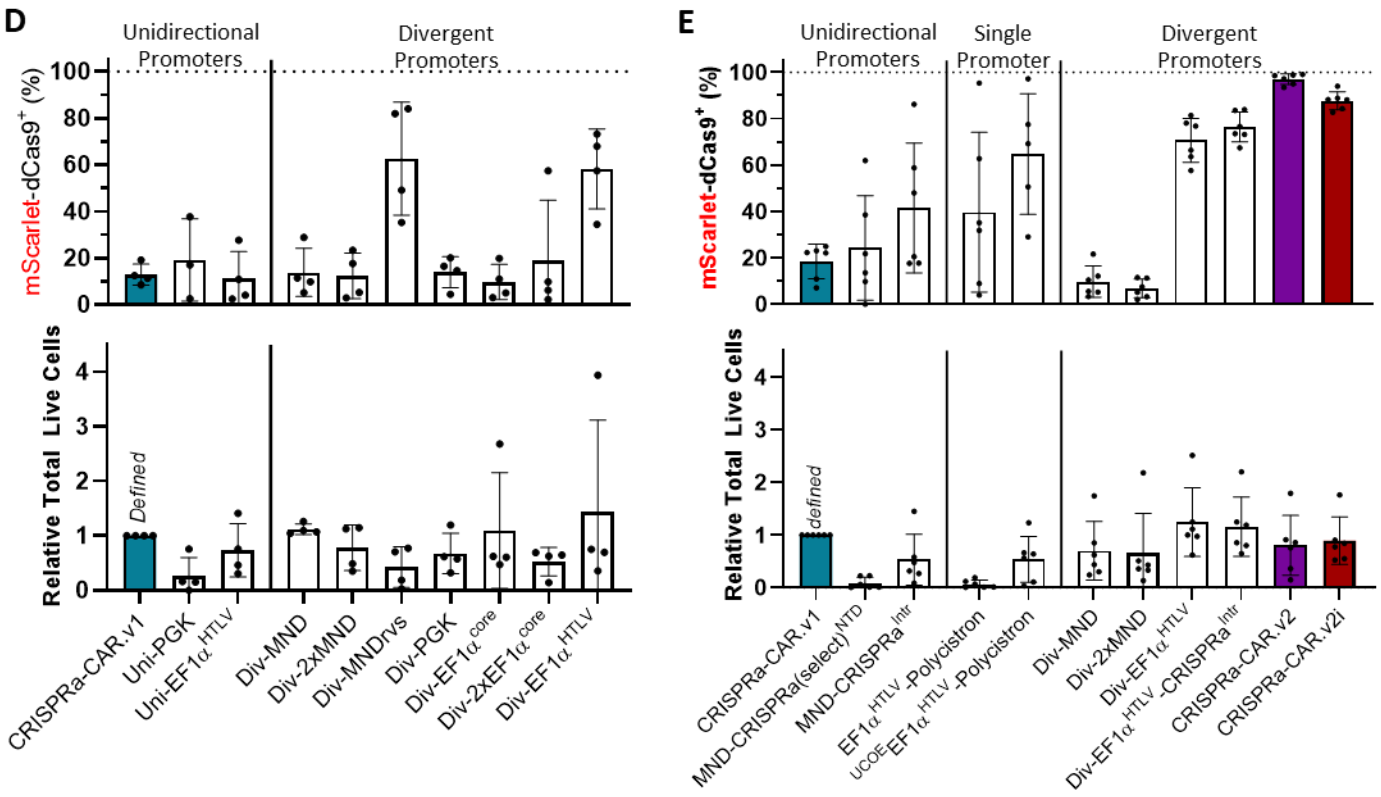

Figure 3.7: Partial or variant route CRISPRa-CAR vector optimization. (**A**) Abridged donor plasmid maps of select CRISPRa-CAR variants and (**B**) Accompanying table outlining indicated divergent promoter pairs. (**C**) Ratio of T cell $mScarlet_{gDNA}$ / CAR_{gDNA} as a function of time and EP-TICLE donor plasmid indicated in plot (*left*) and ratio of $mScarlet_{pDNA}$ / CAR_{pDNA} measured in donor plasmid prep (*right*). (**D** and **E**) mScarlet-dCas9 positivity (*top graph*) and relative total live cell yield (*bottom graph*) as a function of EP-TICLE donor plasmid. mScarlet-dCas9 positivity is measured by flow cytometry, gated on $CD4^+$ or $CD8^+$ live singlets. Cells in (D) and (E) are gated on $CD8^+$ or $CD4^+$ live singlets only. All experiments depicted here used 1:1 mixtures of $CD8^+$ and $CD4^+$ T cells as EP-TICLE input. Quantified data in (D and E) and compiled from cells generated from 3 (where cells limiting) to 6 human blood donors.

Figure 3.8

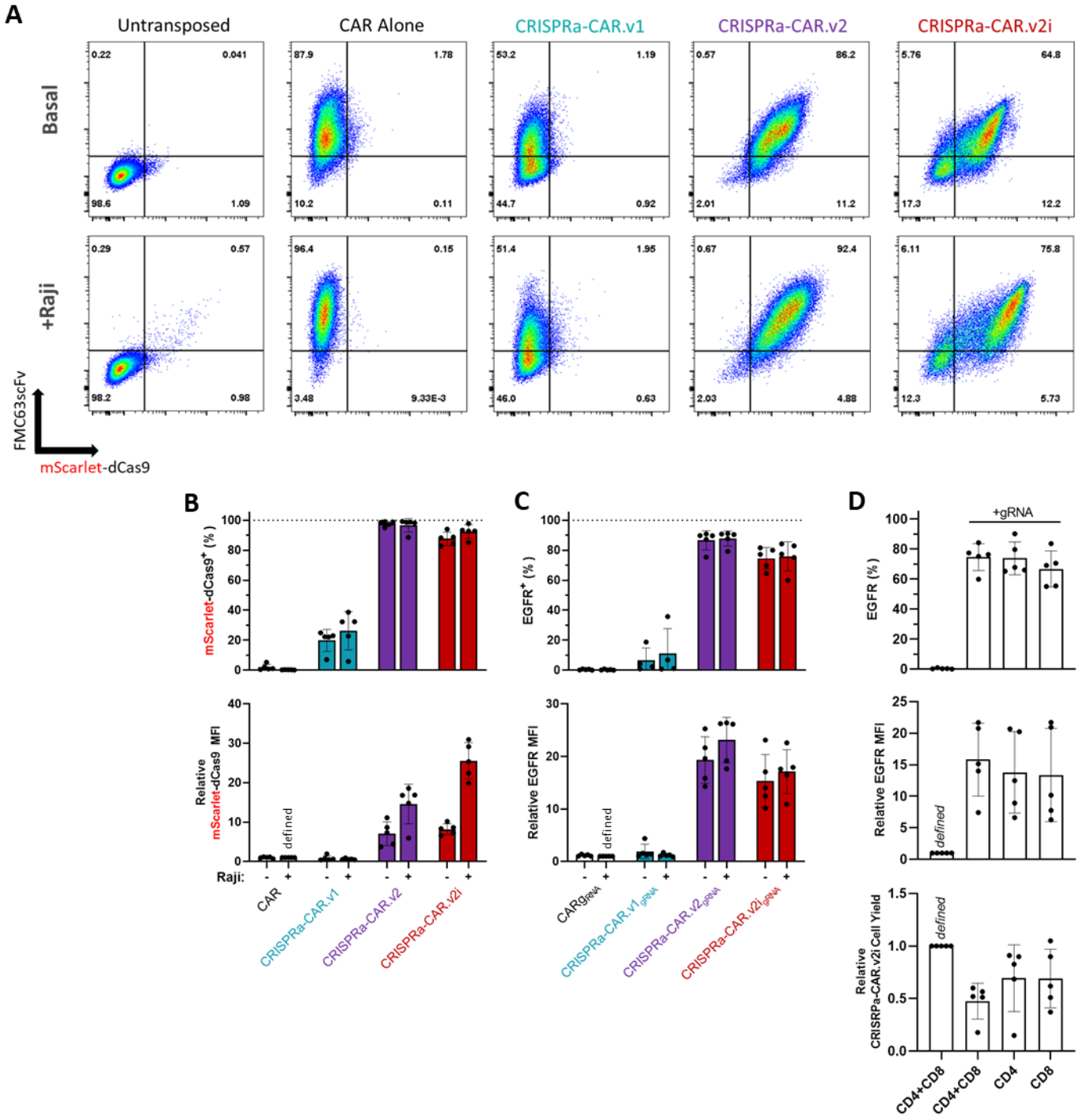
A
Untransposed
CAR Alone
CRISPRa-CAR.v1
CRISPRa-CAR.v2
CRISPRa-CAR.v2i
Basal
+Raji
FMC63scFv
mScarlet-dCas9
B
mScarlet-dCas9+ (%)
Relative mScarlet-dCas9 MFI
defined
Raji:
CAR
CRISPRa-CAR.v1
CRISPRa-CAR.v2
CRISPRa-CAR.v2i
C
EGFR+ (%)
Relative EGFR MFI
CARgRNA
CRISPRa-CAR.v1gRNA
CRISPRa-CAR.v2gRNA
CRISPRa-CAR.v2igRNA
D
+gRNA
EGFR (%)
Relative EGFR MFI
Relative CRISRPa-CAR.v2i Cell Yield
CD4+CD8
CD4+CD8
CD4
CD8

Figure 3.8: Additional analyses of top candidate CRISPRa-CAR T cells produced via EP-TICLE. (**A**) Day 20 flow cytometry plots of FMC63scFv mScarlet-dCas9 expression in cells generated via EP-TICLE from indicated donor plasmid (or mock transposition, TransAct-stimulated control cells), with or without 48-hr Raji cell line culture at a 1:2 effector-to-target ratio. (**B**) Quantification of Day 20 or 21 mScarlet-dCas9 positivity (*top graph*) and relative mScarlet-dCas9 median fluorescence intensity (*bottom graph*) of indicated CAR T cells generated via EP-TICLE. (**C**) Quantification of Day 20/21 EGFR positivity (*top graph*) and relative EGFR median fluorescence intensity (*bottom graph*) of indicated CAR T cells generated via EP-TICLE. (**D**) Quantification of Day 20 or 21 EGFR positivity (*top graph*), relative EGFR median fluorescence intensity (*middle graph*), and relative mScarlet-dCas9^{+} cell yield *(bottom graph)* of CRISPRa-CAR.v2i T cells generated from indicated starting cell T cell population via EP-TICLE. Labeled CD4 and CD8 cultures (D) were combined 1:1. Cells in (A) thru (D) are gated on CD8^{+} or CD4^{+} live singlets. Quantified data in (B) thru (D) depicted mean and standard deviation and are compiled from cells generated from five human blood donors.

Figure 3.9

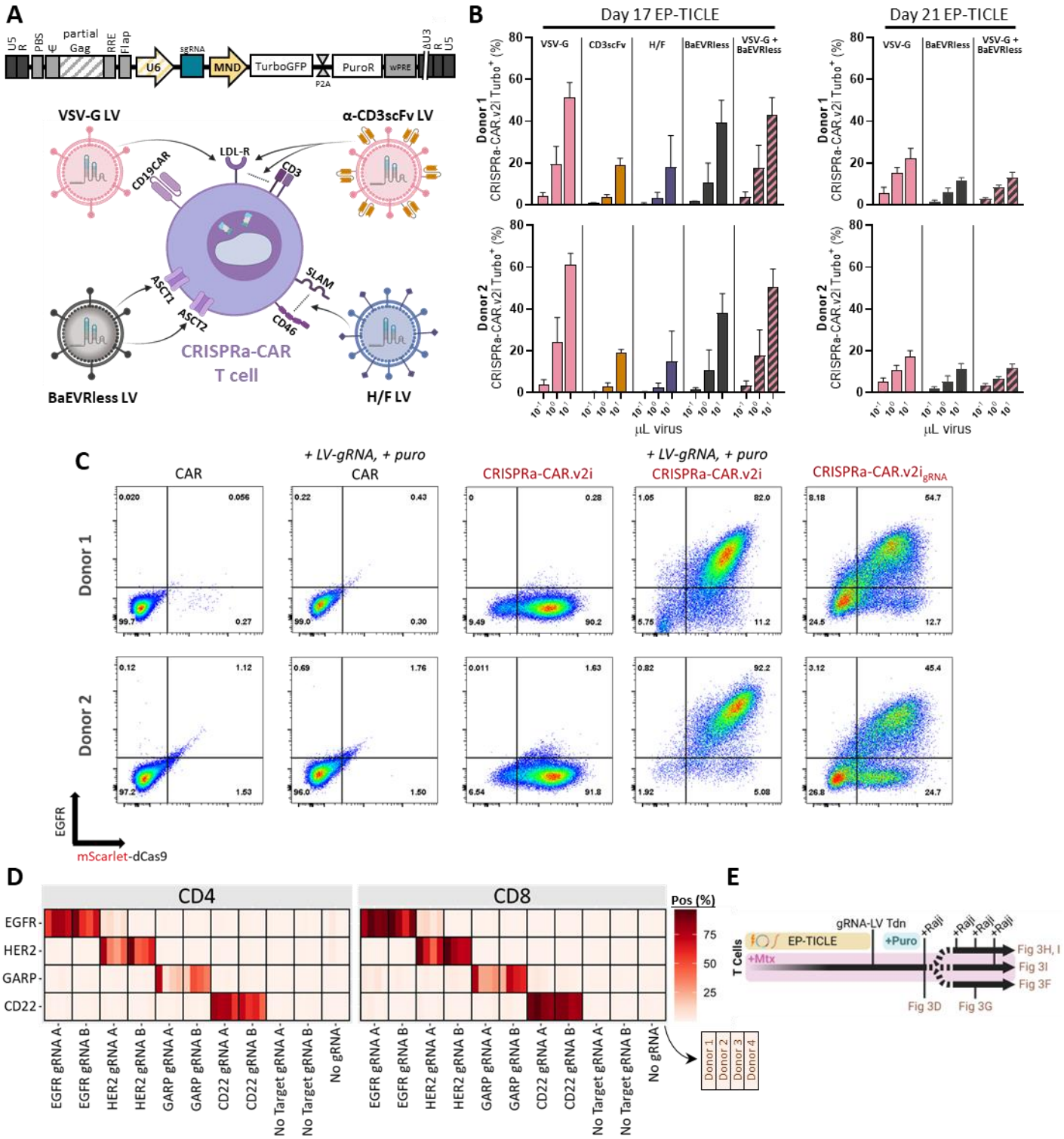
A
U5 R
PBS
Ψ
partial Gag
RRE
Flap
U6
sgRNA
MND
TurboGFP
P2A
PuroR
WPRE
ΔU3 R U5
VSV-G LV
α-CD3scFv LV
CD19CAR
LDL-R
CD3
SLAM
ASCT1
ASCT2
CD46
CRISPRa-CAR T cell
BaEVRless LV
H/F LV
B
Day 17 EP-TICLE
Day 21 EP-TICLE
VSV-G
CD3scFv
H/F
BaEVRless
VSV-G + BaEVRless
Donor 1
Donor 2
CRISPRa-CAR.v2i Turbo+ (%)
μL virus
C
CAR
+ LV-gRNA, + puro
CRISPRa-CAR.v2i
CRISPRa-CAR.v2i gRNA
Donor 1
Donor 2
EGFR
mScarlet-dCas9
D
CD4
CD8
EGFR
HER2
GARP
CD22
Pos (%)
EGFR gRNA A
EGFR gRNA B
HER2 gRNA A
HER2 gRNA B
GARP gRNA A
GARP gRNA B
CD22 gRNA A
CD22 gRNA B
No Target gRNA A
No Target gRNA B
No gRNA
Donor 1
Donor 2
Donor 3
Donor 4
E
T Cells
gRNA-LV Tdn
EP-TICLE
+Puro
+Mtx
+Raji
Fig 3H, I
Fig 3I
Fig 3F
Fig 3D
Fig 3G

Figure 3.9, cont'd

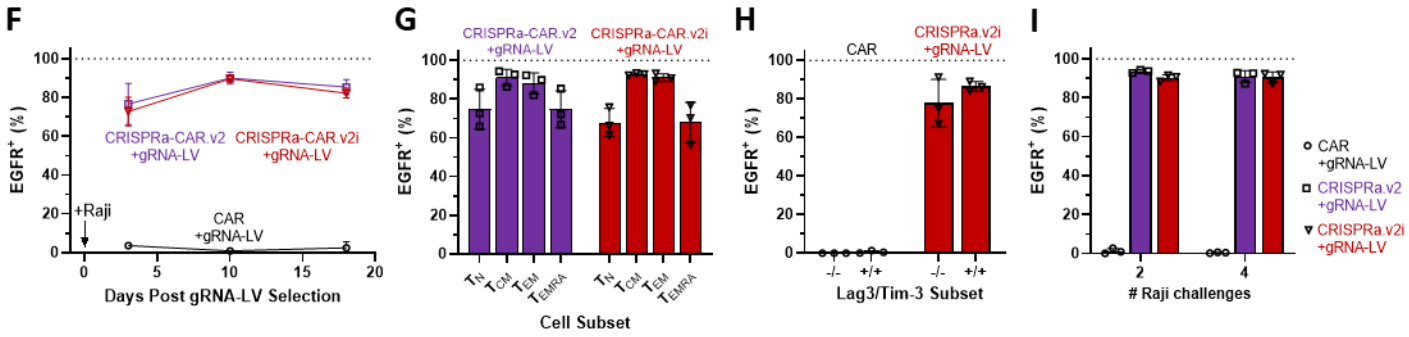

Figure 3.9: gRNA-LV transduction of CRISPRa-CAR T cells. (**A**) Abridged map of ssRNA lentiviral genome (*top*) and graphic depicting pseudotyped lentiviral virions and envelope cognate receptor on CRISPRa-CAR T cells (*bottom*). (**B**) TurboGFP (gRNA) positivity of CRISPRa-CAR.v2i T cells post-transduction as a function of designated viral envelope variant (*top*) and volume of concentrated lentivirus. Transductions were performed on Day 17 or 21 of EP-TICLE (indicated) using cells manufactured from two donors. (**C**) Flow cytometry plots of EGFR and Scarlet-dCas9 expression in cells generated via EP-TICLE and where indicated, puromycin-selected after transduction with (U6p-)gRNA-lentivirus. (**D**) Heat map of indicated gRNA target gene protein percent positivity as a function of gRNA-LV across CD4 (left) and CD8 (right) in CRISPRa-CAR.v2i T cell subsets and among four separate human blood donor sourced cells generated via EP-TICLE and distal lentiviral transduction. gRNA "A" and "B" contain distinct protospacer sequences specific to each respective gene's promoter. (**E**) Cell manufacturing and experimental schema for data displayed in figures (F) thru (I). (**F**) Quantification of EGFR positivity in CAR-CRISPRa or CAR T cells after EP-TICLE and subsequent distal transduction. (**G**) Proportion of $EGFR^+$ CRISPRa-CAR T cells in designated differentiation class (T_N, $CD45RO^-CD62L^+$; T_{CM}, $CD45RO^+CD62L^+$; T_{EM}, $CD45RO^+CD62L^-$; T_{EMRA}, $CD45RO^-CD62L^-$) after manufacturing and target cell stimulation. (**H**) Proportion of $EGFR^+$ T cells as a function of inhibitory receptor positivity (Lag3, Tim-3) and donor plasmid after cell manufacturing and serial tumor challenge.) (**I**) Proportion of $EGFR^+$ CRISPRa-CAR or CAR T cells as a function of number of CAR target cell line challenges after EP-TICLE and subsequent distal transduction. Cells in (D) were selected with puromycin (except "no gRNA") for 48 hours and were then co-incubated with Raji cells for 48 hrs at a 1:2 effector-to-target ratio. Cells in (C) are gated on $CD8^+$ or $CD4^+$ live singlets. Cells in (D) are gated on mScarlet-$dCas9^+$, $CD8^+$ or $CD4^+$ live singlets. Cells in (F) and (I) are gated on $TurboGFP^+$, $CD8^+$ or $CD4^+$ live singlets. Cells in (G) are gated on $TurboGFP^+$, mScarlet-$dCas9^+$, $CD8^+$ or $CD4^+$ live singlets. Cells in (H) are gated on $CD8^+$ live singlets. Plotted values in (F) thru (I) are the mean +/-SD of cells from three human blood donors. In plots (F) thru (I) the following cell groups are designated by the indicated shape: CAR (●), CAR + gRNA (○), CRISPRa-CAR.v2 + gRNA (□), CRISPRa-CAR.v2i + gRNA (▽).

Figure 3.10

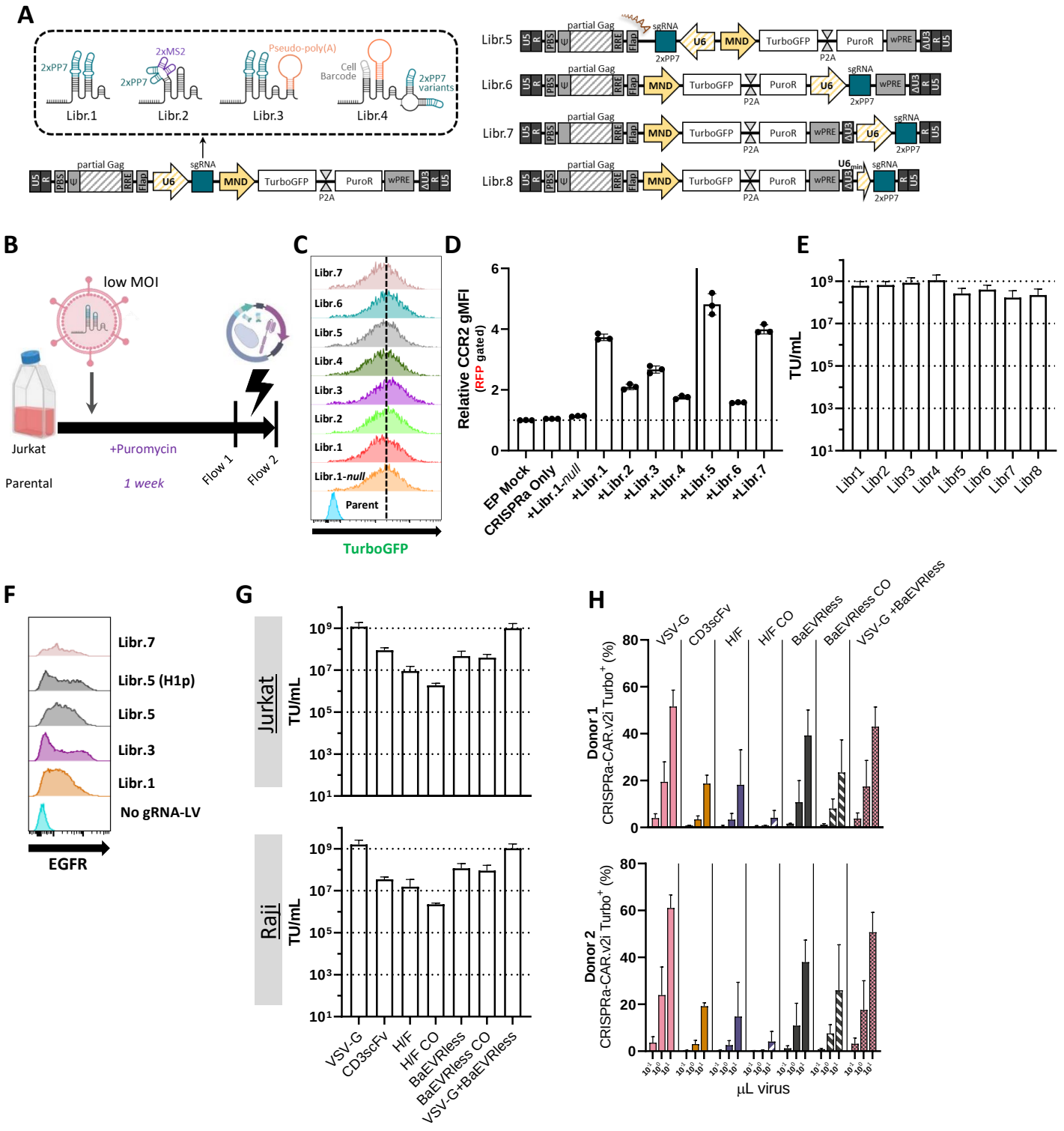
A
2xPP7
2xMS2
Pseudo-poly(A)
Cell Barcode
2xPP7 variants
Libr.1
Libr.2
Libr.3
Libr.4
partial Gag
sgRNA
U6
MND
TurboGFP
PuroR
wPRE
P2A
2xPP7
Libr.5
Libr.6
Libr.7
Libr.8
B
low MOI
Jurkat
Parental
+Puromycin
1 week
Flow 1
Flow 2
C
Libr.7
Libr.6
Libr.5
Libr.4
Libr.3
Libr.2
Libr.1
Libr.1-null
Parent
TurboGFP
D
Relative CCR2 gMFI
(RFP gated)
EP Mock
CRISPRa Only
+Libr.1-null
+Libr.1
+Libr.2
+Libr.3
+Libr.4
+Libr.5
+Libr.6
+Libr.7
E
TU/mL
Libr1
Libr2
Libr3
Libr4
Libr5
Libr6
Libr7
Libr8
F
Libr.7
Libr.5 (H1p)
Libr.5
Libr.3
Libr.1
No gRNA-LV
EGFR
G
Jurkat
Raji
TU/mL
VSV-G
CD3scFv
H/F
H/F CO
BaEVRless
BaEVRless CO
VSV-G+BaEVRless
H
Donor 1
Donor 2
CRISPRa-CAR.v2i Turbo+ (%)
µL virus

Figure 3.10: Additional analyses of gRNA-LV ssRNA genome and packaging envelope. (**A**) Abridged maps of library (libr.) series candidate ssRNA lentiviral genomes. (**B**) Graphic depicting experimental schema to generate and assess stable Jurkat cell lines. (**C**) histograms of TurboGFP expression assessed via flow cytometry of Jurkat T cell lines after puromycin selection at "Flow 1" timepoint. (**D**) Relative CCR2 geometric mean fluorescence intensity of indicated Jurkat parental ("EP mock," "CRISPRa Only") or puromycin-selected cell lines the day after electroporation using CRISPRa-CAR.v1 PiggyBac donor plasmid (except "EP mock"). (**E**) Calculated lentiviral functional titers in Jurkat T cells of library LV series depicted in (A). (**F**) Histograms of EGFR expression in CRISPRa-CAR.v2i $CD8^+$ $Turbo^+$ (except untransduced reference) lines as function of LV-gRNA species indicated. (**G**) Calculated lentiviral functional titers in Jurkat (*top graph*) and Raji (*bottom graph*) cell lines as a function of pseudotyped viral envelope (depicted in Fig 3A). (**H**) Extended figure depicting TurboGFP positivity mean and standard deviation of CRISPRa-CAR.v2i T cells as a function of viral packaging by designated viral envelope variant (*top*) and volume of concentrated lentivirus. Each individual envelope titration series in (H) was calculated using lentivirus generated from three independent productions. Cells in (F) are gated on mScarlet-$dCas9^+$ live singlets. Cells in (H) were transduced on Day 17 of EP-TICLE and assessed for TurboGFP positivity on Day 21 after gating on live singlets.

Figure 3.11

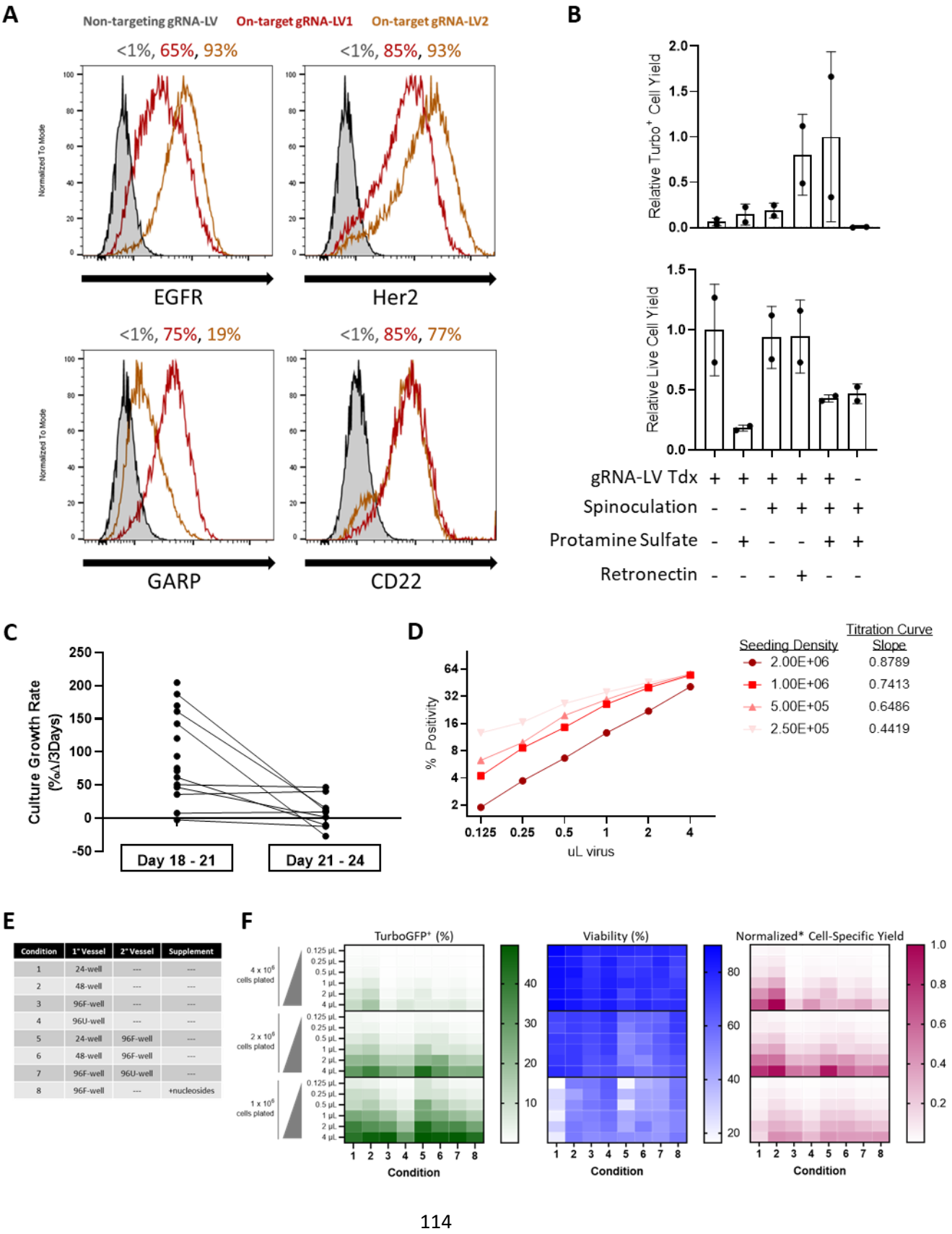
A
Non-targeting gRNA-LV
On-target gRNA-LV1
On-target gRNA-LV2
<1%, 65%, 93%
<1%, 85%, 93%
EGFR
Her2
<1%, 75%, 19%
<1%, 85%, 77%
GARP
CD22
Normalized To Mode
B
Relative Turbo+ Cell Yield
Relative Live Cell Yield
gRNA-LV Tdx + + + + + -
Spinoculation - - + + + +
Protamine Sulfate - + - - + +
Retronectin - - - + - -
C
Culture Growth Rate (%Δ/3Days)
Day 18 - 21
Day 21 - 24
D
% Positivity
uL virus
Titration Curve Slope
Seeding Density
2.00E+06 0.8789
1.00E+06 0.7413
5.00E+05 0.6486
2.50E+05 0.4419
E
Condition | 1° Vessel | 2° Vessel | Supplement
1 | 24-well | --- | ---
2 | 48-well | --- | ---
3 | 96F-well | --- | ---
4 | 96U-well | --- | ---
5 | 24-well | 96F-well | ---
6 | 48-well | 96F-well | ---
7 | 96F-well | 96U-well | ---
8 | 96F-well | --- | +nucleosides
F
TurboGFP+ (%)
Viability (%)
Normalized* Cell-Specific Yield
4 x 10^6 cells plated
2 x 10^6 cells plated
1 x 10^6 cells plated
Condition

Figure 3.11: gRNA target expression and optimization of distal transduction conditions. (**A**) Representative histograms of indicated protein expression as determined by flow cytometry as a function of transduction of indicated gRNA-LV to CRISPRa-CAR.v2i T cells generated from single donor. (**B**) Calculated Turbo$^+$ relative cell yield (*top graph*) and relative total live cell yield (*bottom graph*) relative to each indicated transduction condition in CRISPRa-CAR.v2i T cell generated by EP-TICLE. (**C**) Calculated culture growth rates of CRISPRa-CAR T cell candidate lines between EP-TICLE Day 18 through 21 (*left*) and Day 21 through 24 (*right*) spread across two human blood donors and CD8 only input cells. (**D**) Calculated Turbo positivity of transduced CRISPRa-CAR.v2i T cell transduced at Day 17 of EP-TICLE at four different cell densities and assessed four days later. (**E**) Table of transduction conditions profiled in figure (F). (**F**) Transduction TurboGFP positivity (*left heatmap*), cell viability (*middle heatmap*) and normalized cell-specific yield (*right heatmap*) of CRISPRa-CAR.v2i cells as a function of cell density, virus volume, plating conditions (*see bottom labels*). Cells in (A), (D), and (F) used 1:1 mixtures of CD8$^+$ and CD4$^+$ T cells as EP-TICLE input. Cells in (B) and (C) used CD8$^+$ T cells as EP-TICLE input. All transductions were performed on Day 17 of EP-TICLE manufacturing and assessed four days later via flow cytometry. Cells in (A) are gated on mScarlet-dCas9$^+$ CD8$^+$ or CD4$^+$ live singlets. Cells in (B), (D), and (F) are gated on live singlets only.

Figure 3.12

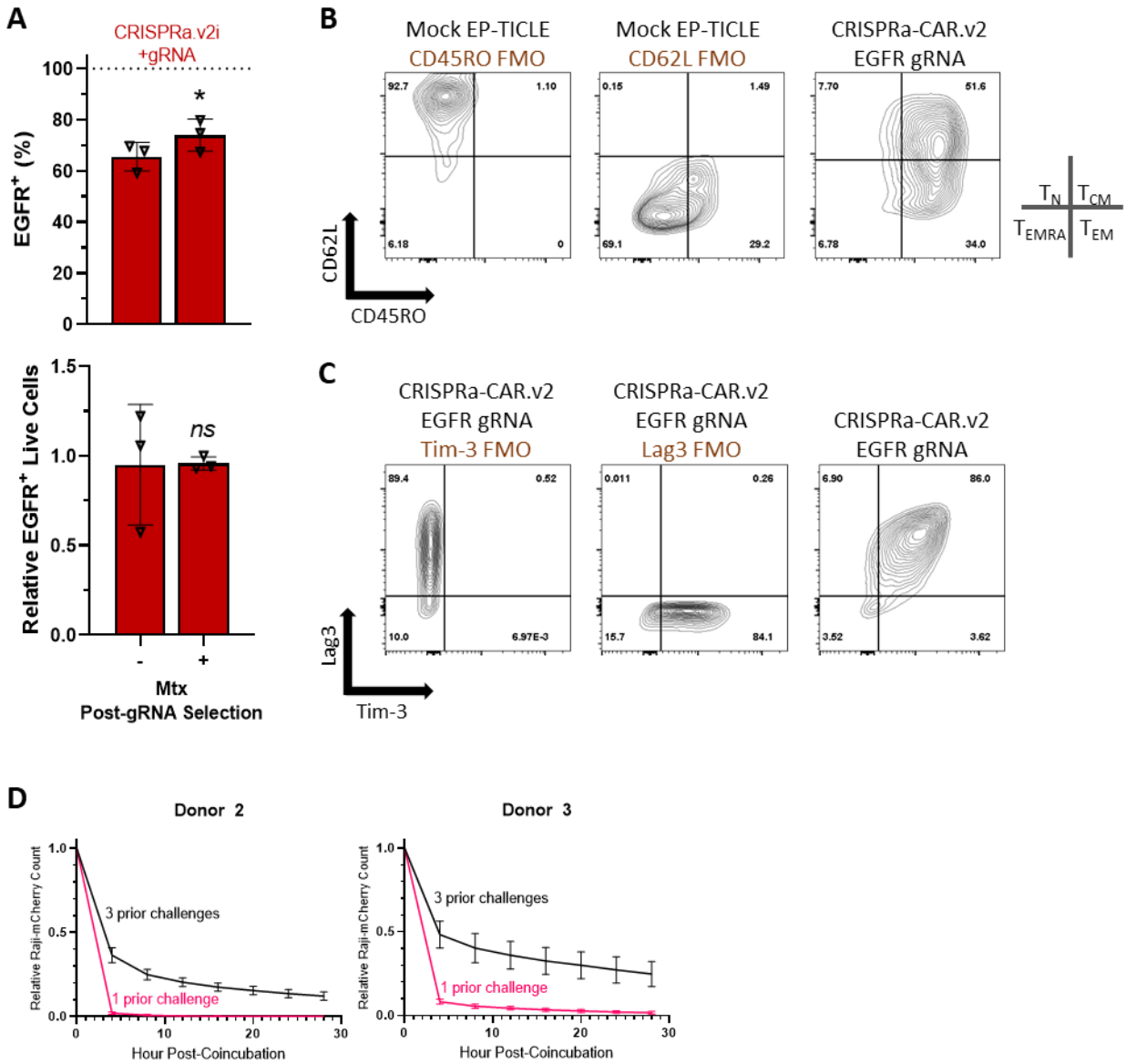
A
CRISPRa.v2i
+gRNA
EGFR+ (%)
100
80
60
40
20
0
*
Relative EGFR+ Live Cells
1.5
1.0
0.5
0.0
ns
-
+
Mtx
Post-gRNA Selection
B
Mock EP-TICLE
CD45RO FMO
Mock EP-TICLE
CD62L FMO
CRISPRa-CAR.v2
EGFR gRNA
92.7
1.10
6.18
0
0.15
1.49
69.1
29.2
7.70
51.6
6.78
34.0
CD62L
CD45RO
TN
TCM
TEMRA
TEM
C
CRISPRa-CAR.v2
EGFR gRNA
Tim-3 FMO
CRISPRa-CAR.v2
EGFR gRNA
Lag3 FMO
CRISPRa-CAR.v2
EGFR gRNA
89.4
0.52
10.0
6.97E-3
0.011
0.26
15.7
84.1
6.90
86.0
3.52
3.62
Lag3
Tim-3
D
Donor 2
Donor 3
Relative Raji-mCherry Count
1.0
0.5
0.0
3 prior challenges
1 prior challenge
0
10
20
30
Hour Post-Coincubation

Figure 3.12: Supporting data for figure 3.9. (**A**) Measured EGFR positivity (*top graph*) and total EGFR+ cell yields (*bottom graph*) of CRISPRa-CAR.v2i + gRNA-LV T cell as a function of subsequent MTX incubation for 14 days. (**B**) and (**C**) Representative two-dimensional flow plots measuring expression of indicated antigens (CD45RO, CD62L, Tim-3, Lag3) on CRISPRa-CAR.v2 + gRNA-LV cells quantified in Figure 3 or FMO control. (**D**) Raji-mCherry CRISPRa-CAR.v2i + gRNA-LV T cell cytotoxicity as a function of prior Raji challenges. Cells in (A) thru (C) used 1:1 mixtures of $CD8^+$ and $CD4^+$ T cells as EP-TICLE input. Cells in (D) used $CD8^+$ T cells as EP-TICLE input. All transductions were performed at Day 17 of EP-TICLE manufacturing and assessed four days later via flow cytometry. Cells in (B) and (C) were gated on mScarlet-$dCas9^+$ $CD8^+$ or $CD4^+$ live singlets.

Chapter 4 | CRISPRa Genome-wide Screens in Primary CAR T Cells

4.1 | Abstract

Efficient coding sequence prioritization for next-generation chimeric antigen receptor (CAR) T cell engineering would benefit from scalable gene-nomination platforms, but such massively-parallel tools have been difficult to implement in primary T cells. Here, we demonstrate the first successful genome-scale, gain-of-function primary human CAR T screen powered by CRISPR activation. Our survival-based screen revealed genetic modulators of homeostatic proliferation, with documented (MYC, STAT5A, STATB, IL7R, IL2RA, MUC) and unknown or weakly characterized (GSE1, SERPINB9, DYM) roles in T cell proliferation or survival. Separately, our screen uncovered modulators of cytokine-free survival (CSF2RB, STAT6, TNFRSF1A, TNFRSF1B, GSE1). Mutant forms of CSF2RB, notably, have been observed in T cell leukemias and shown to exhibit cytokine-independent growth. These hits are awaiting secondary validation, but concurrence with well-documented T cell biology and preliminary identification of uncharacterized phenotypic roles, together suggest that this screening platform will be a highly useful tool for subsequent cell therapy development.

4.2 | Background

4.2.1 | CRISPRa-CAR T cells are ideal for gain-of-function survival screening

Having built a cell manufacturing schema to reliably generate CRISPRa-CAR T cells, I was in the position to now execute genome-scale GoF screens to identify endogenous modulators capable of steering CAR T cells toward therapeutically relevant outcomes. CRISPR-Cas9 screens routinely employ cell sorting to separate populations by molecular phenotypes of interest; for experiments utilizing primary cells, this is likely motivated in part by a desire to simultaneously isolate (d)Cas9^{high} cells and avoid the diluting effect of (d)Cas9^{-} or (d)Cas9^{low} cell populations on screening power. Having largely overcome the challenges of durable CRISPRa transgene expression, I felt that whole, survival-based screens were an attractive, viable selection landscape option. To that end, I conceived of *in vitro* CRISPRa-CAR T cells screens monitoring T cell persistence in response to (1) basal level growth (i.e. homeostatic proliferation), (2) CAR-mediated activation, (3) and CAR-mediated activation without cytokine support.

4.2.2 | CRISPRa-CAR T cells for gain-of-function *in vitro* persistence screening

I selected *in vitro* persistence as a functional readout given (1) the ease of real-time monitoring and sample collection without the need for exhaustive pilot studies, and (2) relevance for therapy. Indeed, within CAR T cell clinical settings, even where complete, durable responses are common, loss of T cell persistence is a frequent feature preceding cancer recurrence.[27] My discovery principles assume that genes conferring resistance to cell death and/or increased proliferation are likely to better equip cell populations to survive long-term *in vivo*.

Also well-recognized is that due to T cells' extreme dependence on proliferation-supporting cytokines (e.g. IL-2, IL-7, IL-15, and/or IL-4),[222–225] CAR T cells penetrating deep into tissues are limited in their access to such critical growth signals. T cells in such settings are also tasked with engaging in repetitive, bulk tumor cell killing that drives cellular differentiation and culminates in exhaustion.[226] As a result, therapeutic strategies that attempt to supplement or mimic cytokine signaling are of high interest as a means to encourage sustained T cell persistence.[227] Recognizing that native and synthetic cytokine receptors integrate cell signals that converge on downstream signaling pathways, I also elected to include within my *in vitro* T cell persistence screen a treatment arm that included tumor co-culture not supplying exogenous cytokine.

4.3 | Results

4.3.1 | CRISPRa-CAR T cells respond to *in vitro* treatment arms in predictable manner

To execute a $CD8^+$ CAR T cell GoF persistence screen, I manufactured $library^+$ CRISPRa-CAR.v2i $CD8^+$ T cells from three healthy donors as described in **Chapter 3**. Briefly, I thawed cryopreserved $CD8^+$ T cells and performed EP-TICLE by pooling multiple EPs, with the final amount of necessary donor-specific starting input determined by a pilot study. At Day 16 of EP-TICLE, cells were transduced separately with Calabrese-Jensen gRNA-LV half-library A and B. Following three days of selection with puromycin, I completely exchanged media and assigned the cells to the following treatment arms: (1) cytokine-rich (EP-TICLE) media only, (2) Raji co-culture in cytokine-rich media, and (3) Raji co-culture in cytokine-free media. Culture media was replaced every 3 - 4 days with media formulations proscribed by each treatment arm.

As expected, T cells in cytokine-rich media demonstrated high persistence, with an acute divergence in growth trajectories relative to Raji-stimulated and cytokine-free treatment arms after Day 4 (**Fig 4.2**). Given rapidly declining cell numbers in the cytokine-free treatment arms, I banked samples at Day 7 across all treatment conditions, generally exhausting most cultures; however, as cell populations receiving Raji targets cell preferentially expanded, I was able to again sample this treatment arm at Day 14 across all donor subsets. Additionally, I noted a treatment-invariant cell contraction occurring among Donor B and C cells between landscape Day 1 and 4. It is unclear if this phenomenon is the result of (1) residual puromycin toxicity, (2) donor-specific biological T cell contraction, (3) or perhaps caused by improper sample handling (e.g. delayed cell transfer to aerated culture plates and return to incubator).

Interestingly, as Donor A had available more cells generally, sample collections at Landscape Day 7 did not completely consume cells from the Raji co-culture arm without cytokines. As a result, I continued to monitor the number and viability of cells from this lingering treatment. I was excited to observe improvements in cell viability and number beginning around Landscape Day 18 (**Fig 4.2f**), despite maintaining these cells in cytokine-free media throughout. Fearing that I might lose these few straggling cells due to culture age or microbial contamination, I performed a rapid amplification protocol (REP) to increase the number of viable T cell clones available for collection. I did not observe a significant increase in viable cells a week after initiating the REP, and thus, elected to recover all remaining cells, terminating the experiment (**Fig 4.2f**)

4.3.2 | CRISPRa-CAR T cell gRNAs are bioinformatically recovered from banked samples

To process collected samples, frozen cell pellets were thawed and processed for gDNA extraction. These samples were then subjected to targeted protospacer PCR amplification that simultaneously introduced sample-specific sequencing indices so that PCR amplicons could then be pooled, subjected to NGS, and thereafter deconvoluted computationally. I first submitted samples for donors B and C from landscape Day 0 (reference) and (1) Day 7 with cytokine supplementation and (2) cytokine-supplemented Raji co-culture. Samples were run through computational pipelines detailed in **4.5.4**. Following processing, I obtained normalized gRNA counts, which indicated very high levels of concordance between established Jensen-Calabrese gRNA transfer vector plasmid pools and donor B and C reference samples from Day 0 (**Fig 4.4a**). Likewise, donor to donor reproducibility was incredibly high at Day 0, with a Pearson correlation coefficient (r) = 0.998, and p-value = 2×10^{-16} (**Fig 4.4b**). Day 7 samples demonstrated lower but visible concordance, with spreading likely occurring as a result of biological and random variation (**Fig 4.4c**). Quality control metrics demonstrated gRNA recoveries >99.95%, with loss of ~ 20 - 40 gRNA relative to the original Calabrese gRNA transfer vector library (**Fig 4.4b *right*, d *left***). Similarly, the Gini index, or evenness of reads was <0.06, within published guidelines suggesting a target below 0.1.[228] The read mapping rate in 2/6 samples, however, was lower than advised proportion (<65%), which may indicate a higher degree of sample/amplicon contamination or sequencing error. Additionally, for reasons not clear, one of the two donor samples in the Raji-stimulated cytokine-supplemented treatments arms mapped closer to the Day 0 sample than the Day 7 cytokine-supplemented controls (**principal component analysis plot not shown**). The technical or biological cause of this

outcome was not immediately clear, but consequently, analysis of this treatment arm was deprioritized as a result.

4.3.3 | CRISPRa screens nominate modulators of CAR T cell homeostatic persistence

Following quality assessments outlined above, Day 0 and Day 7 (cytokine-supplemented, no targets) samples were chosen as initial comparators and processed through the MAGeCKFlute algorithm to determine changes in gRNA library composition (**see 4.5.4**).[229] These results indicated a collection of differentially accumulated ("positive hits") or differentially diminished ("negative hits") gene-specific gRNAs as measured by median log-foldchange (FC) (**Fig 4.5a, b, c**). Tellingly, positive hits included genes known proto-oncogenes / positive-growth regulators (MYC, WT1, MUC1, MDM2). Also represented were two cytokine receptor subunits (IL-2RA, IL-7R) and downstream IL-7 receptor pathway mediators (STAT5B, STAT5B, AKT1); notably, the Day 7 cytokine-supplemented samples were fed media containing exogenous IL-2 and IL-7 (along with IL-21 and IL-4). Perhaps of equal importance, negative hits included known regulators of cell intrinsic death (BID, BIK, BAK1), cell extrinsic death (FAS, TNFRSF10A, CASP8, CASP10), common cell death pathway (CASP3), and cell cycle inhibitors (CDKN1A, CDKN1C, CDKN2A, CDKN2C, TP53). Notably, NR4A3, another positive hit, is a known regulator of T cell effector differentiation, and therefore may be hypothesized to provide a short-lived proliferative benefit when overexpressed.[230] Lastly, CD19 arose as an unpredicted negative hit, but suggests both CRISPRa and CD19CAR functionality, culminating in CRISPRa-mediated "programmed fratricide" or selective CAR T cell killing of CD19-specific gRNA T cells.

4.3.4 | CRISPRa screens nominate modulators of CAR T cell cytokine-free survival

Other technical challenges included an unexpectedly high percentage of cell loss following dead cell depletion prior to pellet collection for the cytokine-free treatment arms. Consequently, Donor B and C lacked sufficient cell numbers in their cytokine-free treatment arms to move forward with NGS. Nevertheless, I successfully prepared Day 0 and Day 7 Raji-stimulated, cytokine-free treatment samples from donor A and submitted them for NGS. While I am unable to entirely disentangle the layered treatment variables of time, Raji-stimulation, and lack of cytokine, I nevertheless observe statistically-significant screening hits that are both overlapping (IRF4, STAT5A, GSE-1) and highly distinct (CSF2RB, STAT6, TNFRSF1A, TNFRSF1B, LDLRAD4) from those found in the previous (i.e. Day 7 cytokine-rich) treatment arm (**Fig 4.6**).

4.4 | Discussion

4.4.1 | Initial CRISPRa-CAR readouts suggest high-quality, biologically-relevant screening hits

Prior to chapter 3, my work has centered on creating, refining, and characterizing a primary CAR T cell gain-of-function screening platform that can be deployed to diverse adaptive landscapes to nominate genetic modulators of clinical relevance. Here, I finally execute my first set of screens. While these early experiments encountered unanticipated (yet addressable) problems of (1) sample loss, (2) and occasional sample quality concerns, I nevertheless am pleased to have obtained sample data containing high-quality recoverable gRNA counts and ultimately statistically-significant gRNA-gene hits. Moreover, this collection of hits aligns closely with documented biology.

For cytokine-supplemented CAR T cell persistence arms, my results recapitulated many components of the IL-7 signaling pathway previously shown to enhance T cell survival or proliferation.[231–236] Analogously MYC, WT1, MUC1, and MDM2 are known proto-oncogenes.[237–240] Along with the negative hits outlined previously, I view these hits as key confirmation that this screening system is functional. Given that the system has also nominated an assortment of more weakly-characterized genes (GSE-1, SERPIN9, DYM, GCNT2), this suggests that it also can uncover unknown biology. Interestingly, SERPINB9 has been suggested to protect T cells from lysosomal damage or granzyme-mediated attack.[241]

In addition to the cytokine-rich treatment arms, I also identified hits using cells sourced from a single donor, screened for cytokine-free survival. One of the strongest positive hits, CSF2RB, is the cytokine receptor common subunit beta, which pairs with other subunits to constitute the GM-CSF receptor, IL-3 receptor, or IL-5 receptor. Interestingly, a CSF2RB mutant form (R461C) has been implicated in driving cytokine-independent growth in a patient with T-ALL, marked by constitutive STAT5, STAT3, ERK, and PI3K signaling.[242] I hypothesize that excessive levels of native CSF2RB may likewise trigger ligand-independent signaling, providing at least partial protection from cytokine-free growth conditions. Another very strong positive hit in this treatment arm is STAT6, which interestingly, appeared at a negative hit in the cytokine-rich media condition. STAT6 has been implicated in both Treg and Th2 differentiation.[243,244] This suggests that it provides a context-specific benefit or harm. Other positive hits include TNFRSF1A (TNF receptor 1) and TNFRSF1B (TNF receptor 2), both of the TNF superfamily, which together form a heterocomplex that recruits anti-apoptotic proteins. Interestingly, TNFRSF1A and TNFRSF1B have both arisen as nominees in the one prior CRISPRa human T cell screen.[86] In

that context, they were shown to enhance IL-2 and IFNg secretion in $CD4^+$ and $CD8^+$ T cells respectively – which perhaps may suggest one mechanism of cytokine-free survival – via upregulation of autocrine cytokine signaling.

Ultimately, to serve as a verifiable screening tool, these genetic nominees will need to be translated to their ORF equivalents, and delivered using conventional CAR T cell manufacturing methods. Still, absent these final confirmatory results, the findings thus far establish strongly suggest that my platform possess the potency, reproducibility, and scale to perform as a valuable genome-scale nomination platform for next-generation CAR T cell development.

4.5 | Materials and Methods

4.5.1 | Subcloning gRNA-LV pooled libraries

The human Calabrese CRISPR activation pooled library was a gift from David Root and John Doench (Addgene 92379, 92380). To subclone this pool I digested protospacer-empty Libr.1-null transfer vector with BsmBI-v2 (New England Biolabs, NEB) overnight at 55 °C. To generate a pool of inserts for Gibson assembly, I performed a series of separate identical PCR reactions to avoid jackpotting. Reaction mix included forward [5'-GGCTTTATATATCTTGTGGAAAGGACGAAACACCG-3'] and reverse [5'-TCCTTTCGGCCCAGCATAGCTCTTAAAC-3'] primers, Calabrese template, in 2X NEBNext® Ultra™ II Q5® Master Mix (NEB) subjected to the following reaction: 98 °C for 30 sec; five cycles of 98 °C for 10 sec, 54 °C for 30 sec, 65 °C for 30 sec; 20 cycles of 98 °C for 10 sec, 60 °C for 30 sec, 65 °C for 30 sec; 65 °C for 2 min; hold at 4 °C. The next day, I ran linearized plasmid backbone and 83

bp PCR products on a 1% agarose gel and recovered each using the Gel and PCR Clean-up Kit (Takara) per the manufacturer's instructions. Insert and vector were combined at a 5:1 ratio and held at 50 °C for 1 hour in NEBuilder® HiFi DNA Assembly Master Mix (NEB). Gibson assembly products were purified using the MinElute® PCR Purification Kit (Qiagen). Purified product was delivered to NEB® 10-beta Electrocompetent E. coli using the Micropulser (BioRad) with pulse setting Ec1. Multiple electroporations were pooled, with reaction number scaled to ensure efficiencies yielding >200 transformants per gRNA on average. Following a 1-hour recovery at 37 °C, 250 rpm, bacteria were directly inoculated into large scale culture vessels containing LB-Kan (30 µg/mL) and grown up overnight. The next day these cultures were pelleted and immediately processed for plasmid extraction using the Nucleospin® Xtra Maxi Plus EF (Takara).

To assess the quality of the new Jensen-Calabrese plasmid pool, gRNA protospacer sequences were amplified using NEB Q5 hot start HiFi master mix (M0515S) and Illumina-compatible primers (**table 4.5.5**). After clean-up with AMPure XP Beads (Beckman Coulter), the sequencing library was quantified by qubit and diluted to 4nM. The library was sequenced using paired end 150bp reads on an Illumina HiSeq with 25% PhiX spike-in. Genome-wide libraries were sequenced to a targeted depth of 1000-fold coverage. All reads were analyzed by PoolQ v3.2.2 (https://github.com/broadinstitute/poolq). Next-generation sequencing indicated gRNA recoveries of 99.997% (AUC = 0.62) and 99.986% (AUC = 0.64) of subcloned Calabrese half-library A and B, respectively (**Fig 4.1**).

4.5.2 | Distal lentiviral transduction for genome-wide screens

For genome-wide screening, Day 16 EP-TICLE CAR T cells were transduced at 0.625% v/v [multiplicity of infection (MOI) ≈ 0.3 – 0.7], plated at 5.2 x 10^6/cm^2; donor-specific gRNA library functional titers were pre-determined via a pilot study with donor apheresis cells. Two days after transduction, cells were selected with puromycin at 2.0 μg/mL for 48 hours and then assessed for gRNA positivity as indicated by TurboGFP. Due to lower-than-expected purification efficacy, puromycin selection was extended for an additional day at reduced cell density (<4 x 10^6/cm^2). Cell positivity was reassessed then and again several times throughout following selective landscape initiation (**Fig 4.3**). Three days after puromycin selection began, cells were assigned to treatment arms and had their media completely replaced.

4.5.3 | Genome-wide CRISPRa-CAR T cell persistence screen

Following cell manufacturing and selection, a culture cell sample was taken (Day 0), washed, and frozen down for later analysis. The next day, CRISPRa-CAR-library$^+$ cells were equally distributed across two treatment arms: (1) a 1:1 (E/T) Raji co-culture or (2) TICLE media alone. Cell numbers and viability were assessed every 3 - 4 days. Cell cultures samples were banked on Day 7 and Day 14 following assignment to treatment arms. Due to relative differences in expansion, cells grown in TICLE media alone did not have sufficient cells for analysis on Day 14. At all timepoints, cells were maintained in sufficient numbers (≈26 x 10^6) to maintain coverage of >400 copies per gRNA on average.

To process gDNA, banked cell pellets were rapidly thawed and processed using the Nucleospin® Blood XL kit (Takara) following the manufacturer's instructions. gDNA quantity and quality was assessed using the NanoDrop® One (Thermo Scientific). For protospacer amplification, gDNA was diluted 1:4 with molecular grade H_2O to reduce the effect of PCR inhibitors. gDNA template was combined with Illumina-compatible (0.5 µM) forward and (0.5 µM) reverse primers, dNTPs, 10X buffer, and *Ex Taq* polymerase (Takara) per the manufacturer's instructions. Combined gDNA template and PCR master mix was divided into multiple 100 uL reactions to reduce the effect of PCR jackpotting. Thermocycling conditions consisted of an initial denaturation of 95 °C; then 28 cycles of 95 °C 30 sec, 53 °C 30 sec, 72 °C 30 sec; a final extension of 72 °C for 10 min; and holding at 4 °C. Following amplification, each 100 uL reaction was re-pooled. Each sample was run on a 4% agarose gel and TapeStation 4150 (Agilent) to verify the presence of PCR products of the appropriate size (383 bp). A fraction of each sample pooled PCR product was cleaned using AMPure XP beads, then quantified by qubit and diluted to 4nM. The library was Illumina-sequenced as previously described.

4.5.4 | CRISPRa-CAR screen analysis

For analysis of recovered libraries, reads were aligned to the combined Calabrese A and B library as a single reference file library using MAGeCK version 0.5.9.4 (REF). Each of the matching samples across library A and B were merged to generate a single normalized read count table. Normalized read counts in high versus low bins were compared using *mageck*

test with *–norm-method none*, *–paired* options, pairing samples by donor. Gene hits were classified as having a median absolute log_2FC >0.5 and a false discovery rate (FDR) <0.05.

4.5.5 | Table: sequencing primers

Purpose	Index	Sequence
Plasmid Pool Seq	P5	aatgatacggcgaccaccgagatctacactctttccctacacgacgctcttccgatctgcttaccgtaacttgaaagtatttcgatttcttggct
Plasmid Pool Seq, CAR T Cell Screen Seq	P7 A01	caagcagaagacggcatacgagatcggttcaagtgactggagttcagacgtgtgctcttccgatcttcaaaaaaagcaccgactcggtgccac
Plasmid Pool Seq, CAR T Cell Screen Seq	P7 A02	caagcagaagacggcatacgagatgctggattgtgactggagttcagacgtgtgctcttccgatcttcaaaaaaagcaccgactcggtgccac
CAR T Cell Screen Seq	P7 A05	caagcagaagacggcatacgagatatactcaagtgactggagttcagacgtgtgctcttccgatcttcaaaaaaagcaccgactcggtgccac
CAR T Cell Screen Seq	P7 A06	caagcagaagacggcatacgagatgctgagaagtgactggagttcagacgtgtgctcttccgatcttcaaaaaaagcaccgactcggtgccac
CAR T Cell Screen Seq	P7 D03	caagcagaagacggcatacgagatcgcagaccgtgactggagttcagacgtgtgctcttccgatcttcaaaaaaagcaccgactcggtgccac
CAR T Cell Screen Seq	P7 F10	caagcagaagacggcatacgagatgccagaccgtgactggagttcagacgtgtgctcttccgatcttcaaaaaaagcaccgactcggtgccac

4.6 | Acknowledgements

The author would like to thank Natalie Murren – an undergraduate student attending the University of Washington – for their assistance with Jensen-Calabrese NGS sequencing. Ardizon Valdez assisted with Illumina library QC and sample pooling prior to sample submission for NGS. Cailyn Spurrell performed NGS data processing and analytics for Illumina sequencing results for the genome-scale screen. Michael Jensen supervised the project and provided funding.

All studies were conceived of by Benjamin Curtis.

4.7 | Figures

Figure 4.1

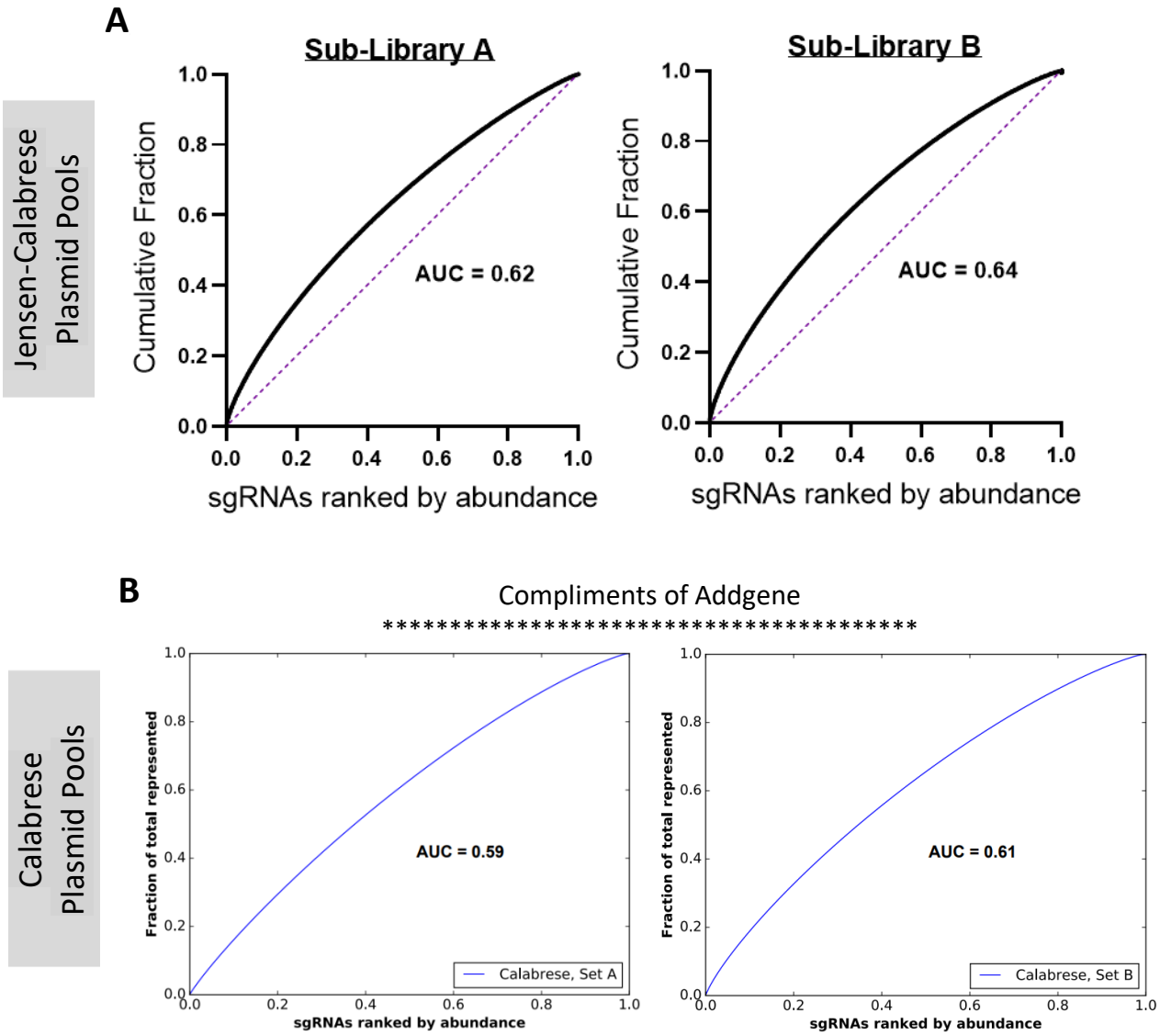

Figure 4.1: Assessment of gRNA Jensen-Calabrese plasmid pool subcloning. (**A**) Jensen-Calabrese plasmid pool half-library A (*left*) and B (*right*) cumulative gRNA frequency as ranked by gRNA abundance. (**B**) Calabrese plasmid pool half-library A (*left*) and B (*right*) cumulative gRNA frequency as ranked by gRNA abundance. Graphics in (B) are compliments of Addgene/Broad Institute (https://www.addgene.org/pooled-library/broadgpp-human-crispra-calabrese-p65hsf/) Area under the curve approximates library distortion (0.5 = perfect representation, 1.0 = perfect skew). Dashed purple lines in (A) indicate hypothetical AUC = 0.5.

Figure 4.2

A

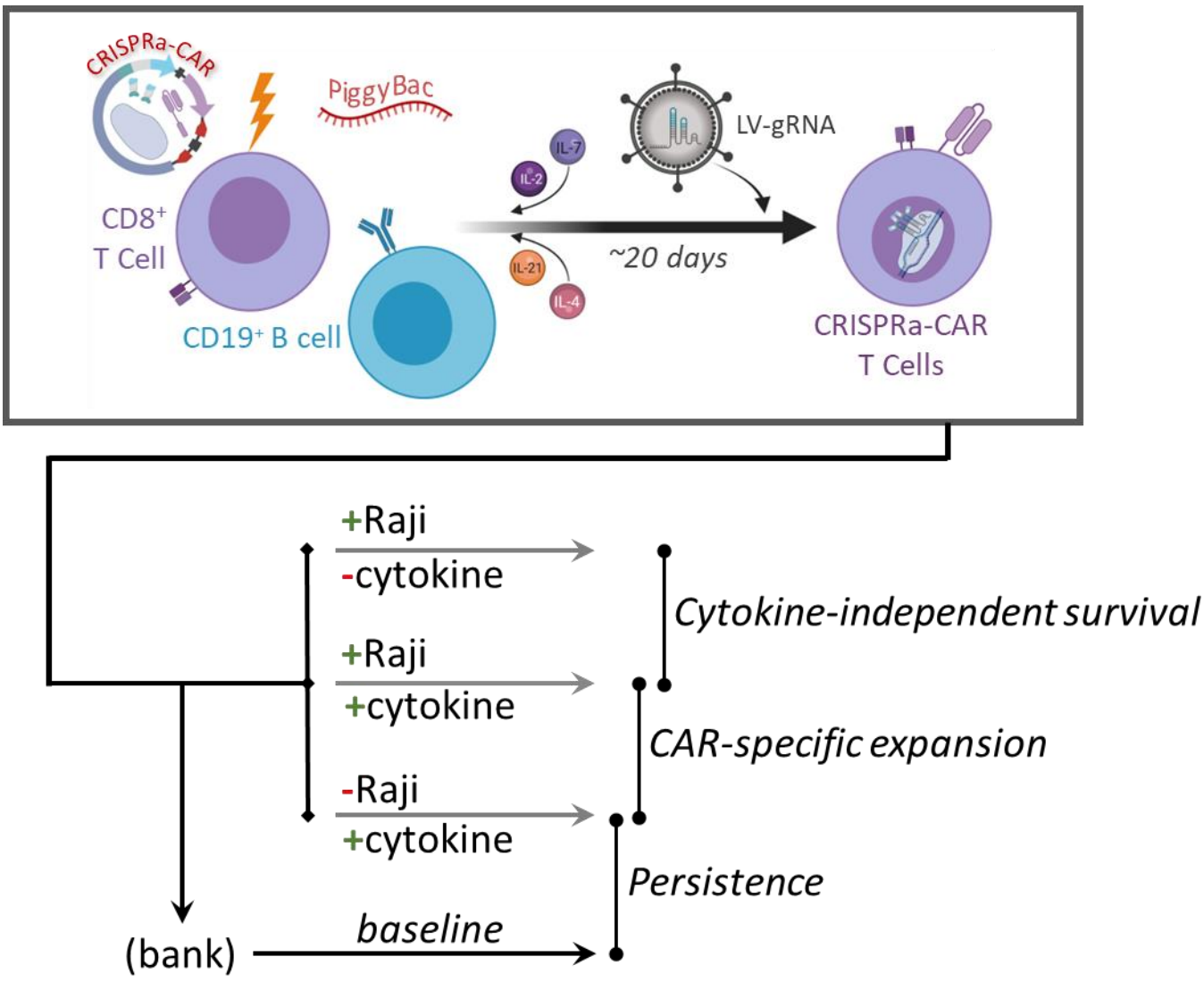
CRISPRa-CAR
PiggyBac
LV-gRNA
IL-7
IL-2
IL-21
IL-4
CD8+
T Cell
CD19+ B cell
~20 days
CRISPRa-CAR
T Cells
+Raji
-cytokine
+Raji
+cytokine
-Raji
+cytokine
(bank)
baseline
Cytokine-independent survival
CAR-specific expansion
Persistence

Figure 4.2, cont'd

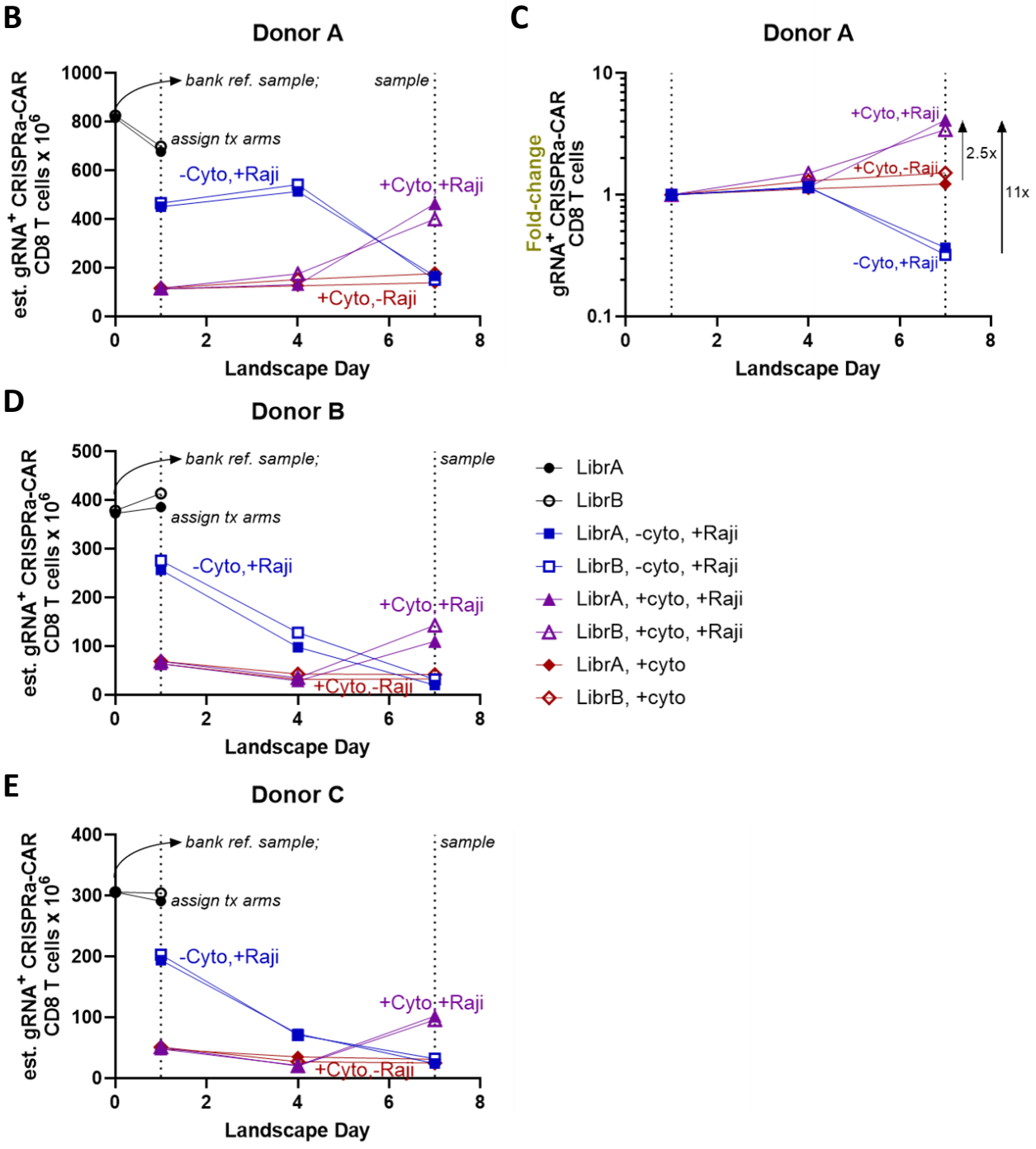

Figure 4.2, Cont'd

F

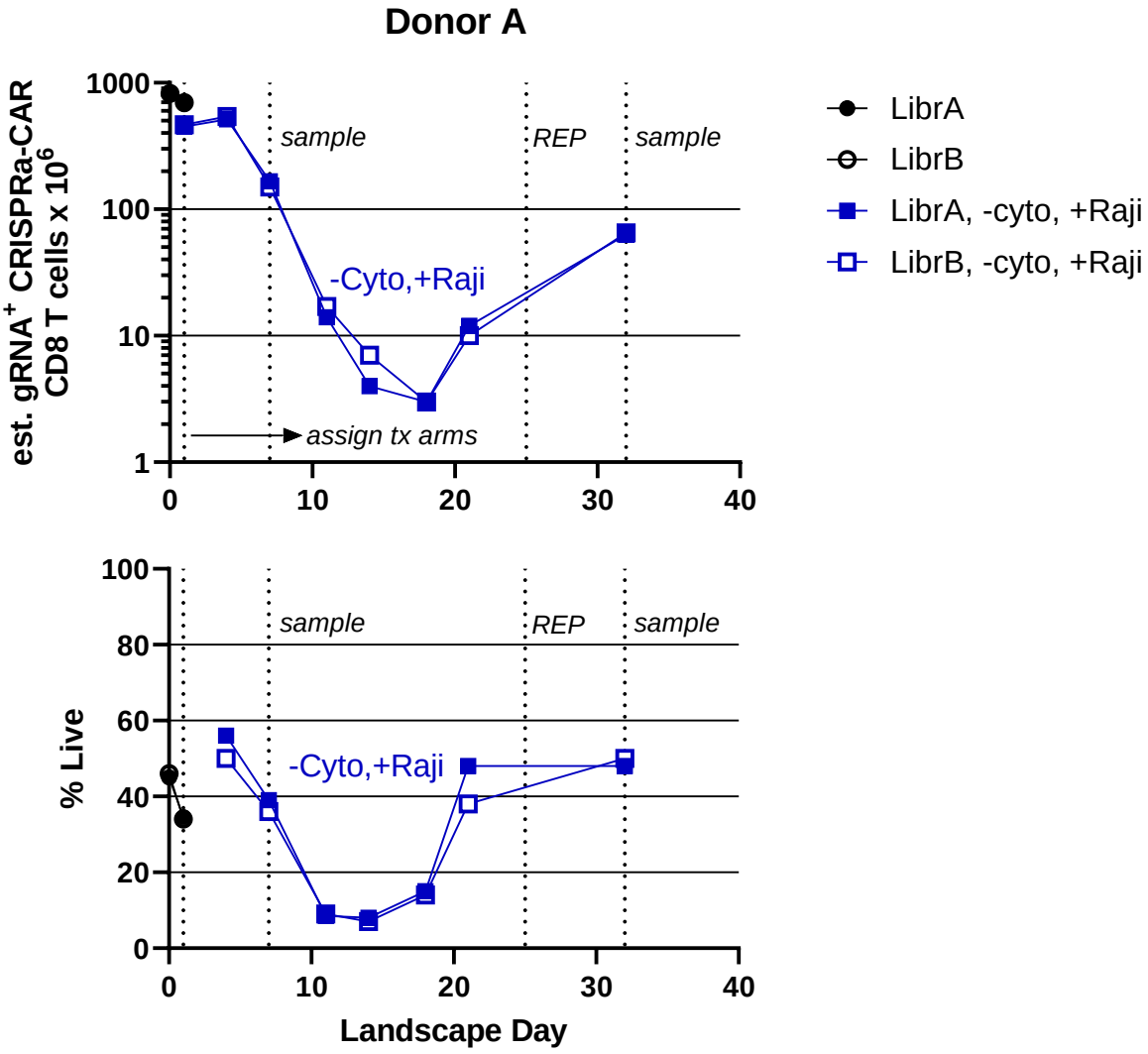

Figure 4.2: CRISPRa-CAR T cell cell numbers and viability during genome-scale screening. (**B, D, E**) CRISPRa-CAR theoretical $CD8^+$ T cell counts at each selective landscape timepoint as a function of treatment arm and gRNA library subgroup (A versus B). (**C**) Treatment arm fold-change relative to Day 1 (= 1, defined). (**F**) CRISPRa-CAR theoretical $CD8^+$ T cell counts (*top*) and viability (*bottom*) at each selective landscape timepoint for cell assigned to -cytokine/Raji treatment arm. Dotted lines indicate manipulation of culture (e.g. treatment initiation, sample collection, REP) outside of biweekly media changes. ◆ (+cytokine, Library A) ◇ (+cytokine, Library B), ▲ (+cytokine/Raji, Library A), △ (+cytokine/Raji, Library B), ■ (-cytokine/Raji, Library A), □ (-cytokine/Raji, Library B), ● (unassigned, Library A), ○ (unassigned, Library B).

Figure 4.3

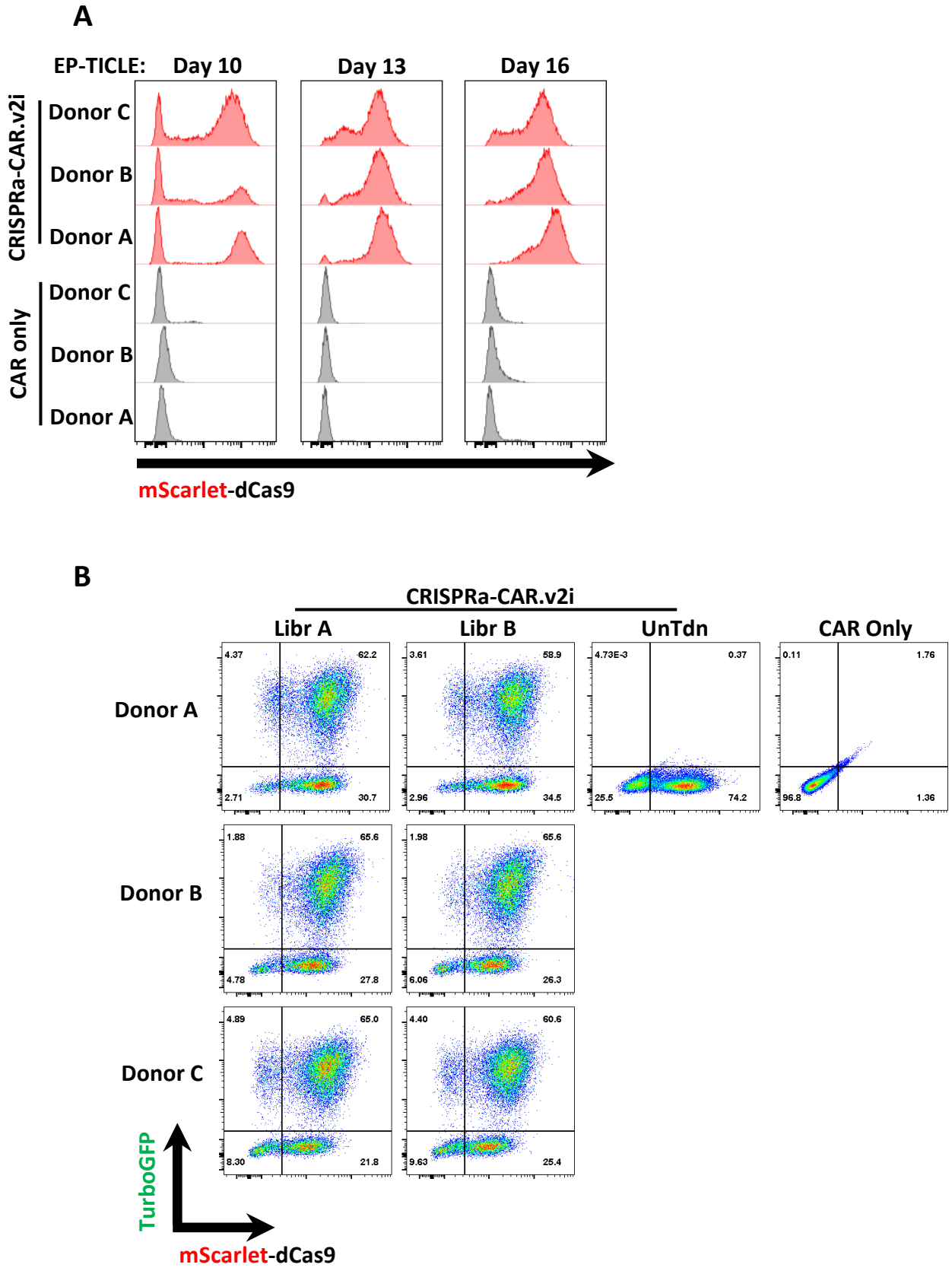
A
EP-TICLE:
Day 10
Day 13
Day 16
CRISPRa-CAR.v2i
Donor C
Donor B
Donor A
CAR only
Donor C
Donor B
Donor A
mScarlet-dCas9
B
CRISPRa-CAR.v2i
Libr A
Libr B
UnTdn
CAR Only
Donor A
4.37
62.2
2.71
30.7
3.61
58.9
2.96
34.5
4.73E-3
0.37
25.5
74.2
0.11
1.76
96.8
1.36
Donor B
1.88
65.6
4.78
27.8
1.98
65.6
6.06
26.3
Donor C
4.89
65.0
8.30
21.8
4.40
60.6
9.63
25.4
TurboGFP
mScarlet-dCas9

Figure 4.3, cont'd

C

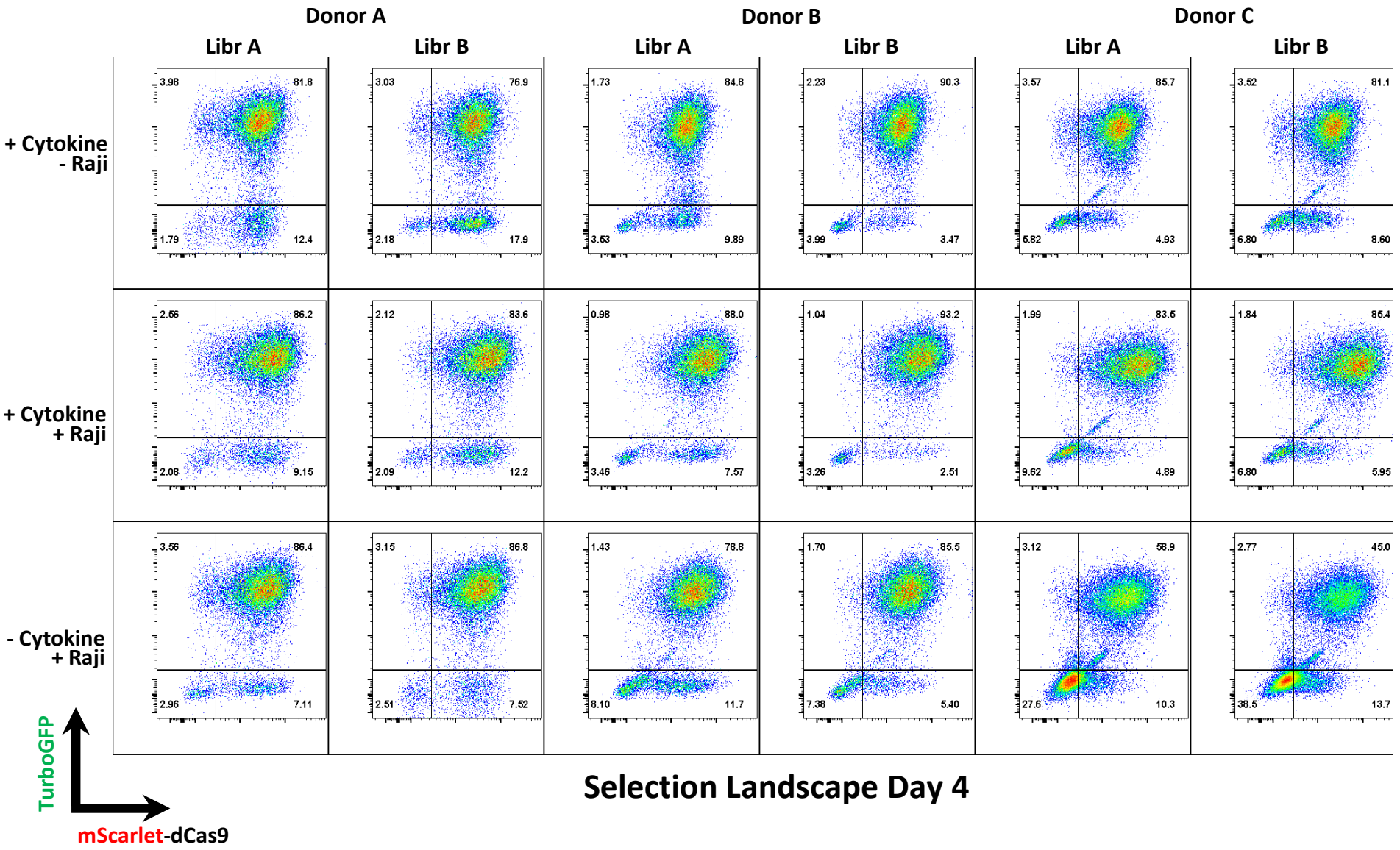

Selection Landscape Day 4

Figure 4.3, cont'd

D

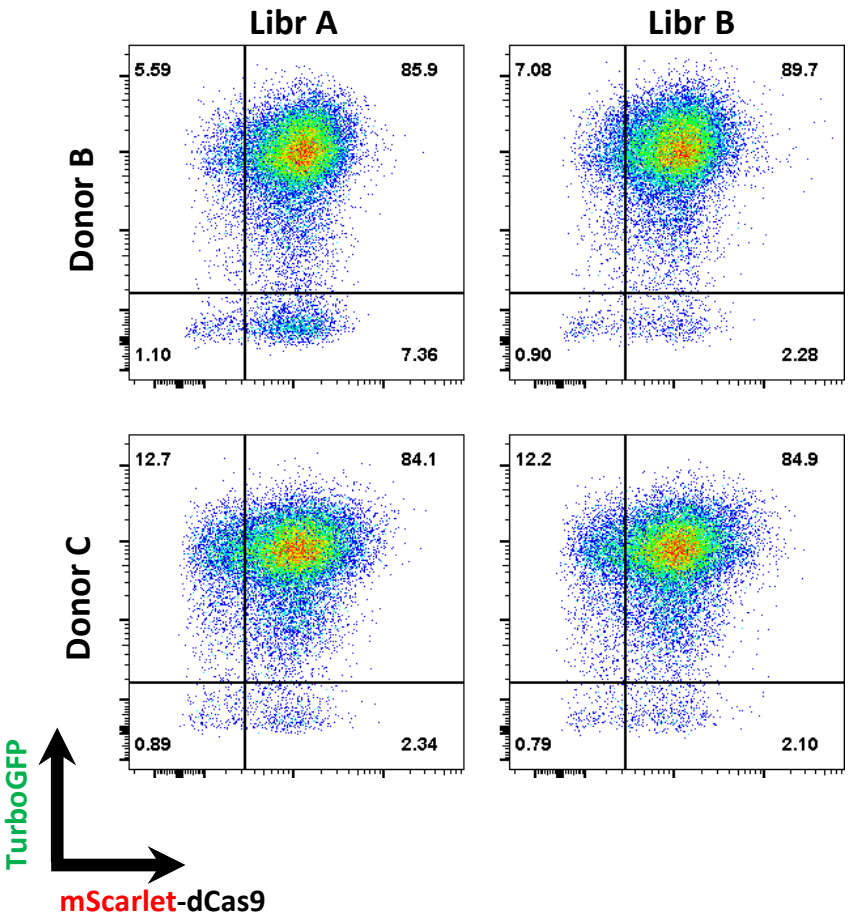

Selection Landscape
Day 14

Figure 4.3: CRISPRa-CAR mScarlet-dCas9 and gRNA-LV expression throughout genome-scale manufacturing and landscape screening. (**A**) Histograms of mScarlet-dCas9 expression of CRISPRa-CAR.v2i $CD8^+$ T cells at each EP-TICLE timepoint indicated. (**B**) Flow cytometry plots of mScarlet-dCas9 and TurboGFP (gRNA) expression in $CD8^+$ T cells at EP-TICLE Day 21 (Selection Landscape Day 1). (**C**) Flow cytometry plots of mScarlet-dCas9 and TurboGFP (gRNA) expression in $CD8^+$ T cells by gRNA-LV half-library, treatment arm, and donor at Selection Landscape Day 4. (**D**) Flow cytometry plots of mScarlet-dCas9 and TurboGFP (gRNA) expression in $CD8^+$ T cells receiving +cytokine/+Raji co-culture, separated by gRNA-LV half-library and indicated donor at Selection Landscape Day 14.

Figure 4.4

A

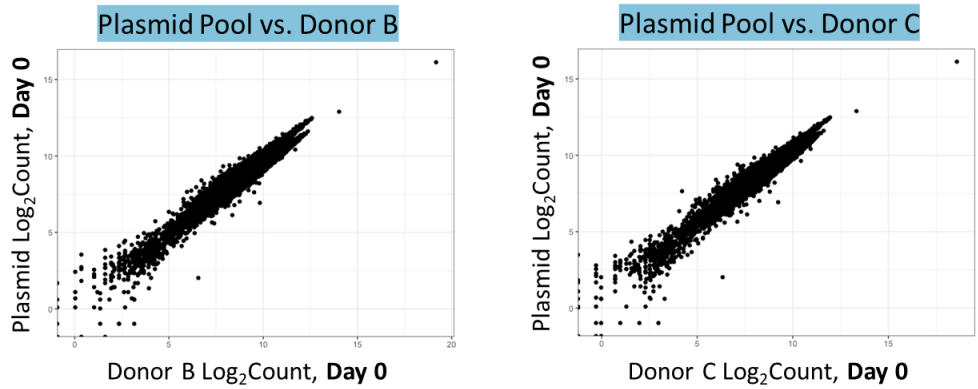

B

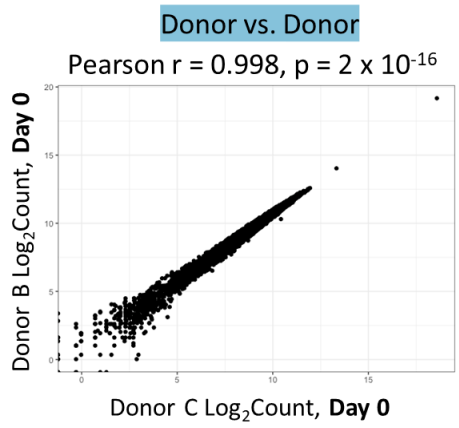

Donor B Day 0 gRNA Recovery: 99.97% (113,205/113,238)
Donor C Day 0 gRNA Recovery: 99.95% (113,184/113,238)

C

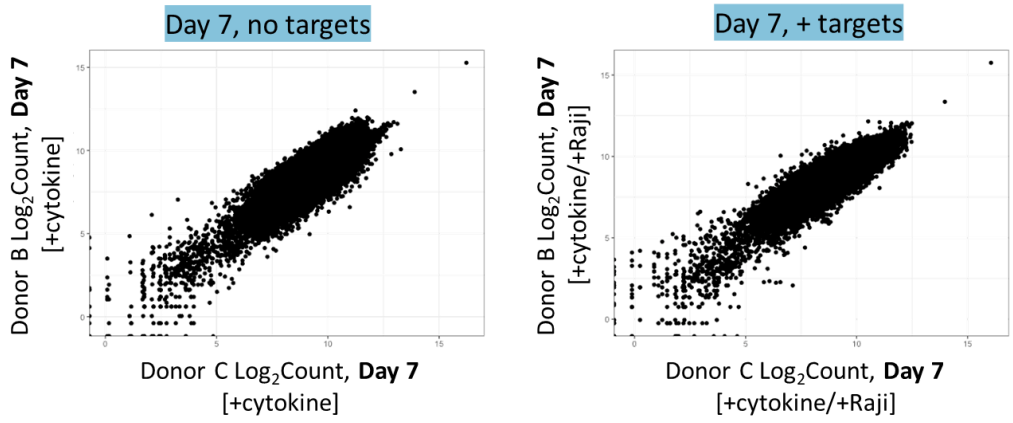

Figure 4.4, cont'd

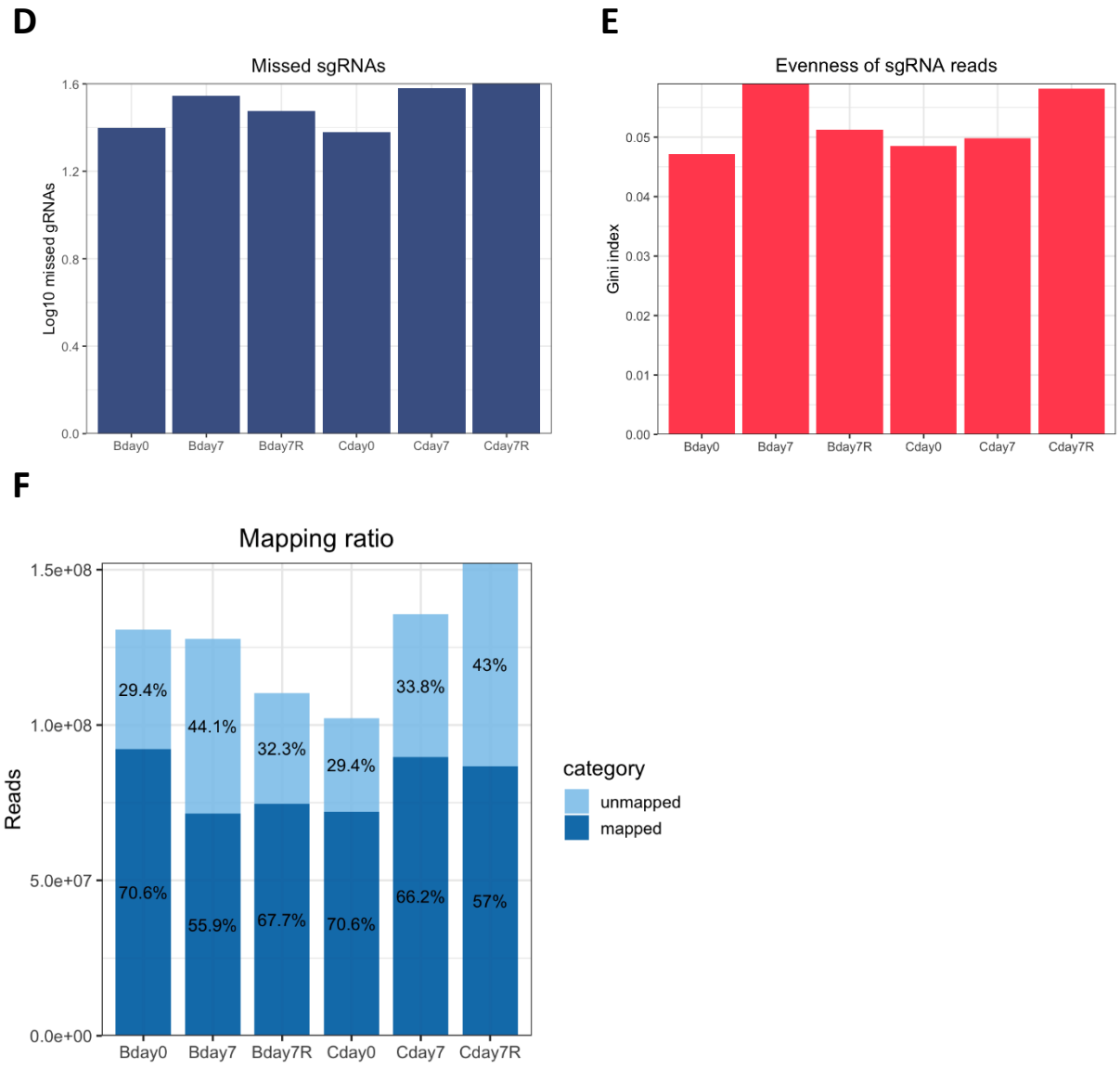

Figure 4.4: CRISPRa genome-scale quality control metrics. (**A**) gRNA read counts of Jensen-Calabrese gRNA-LV transfer vector pools vs. recovered Donor B (*left*) or Donor C (*right*) CRISPRa-CAR CD8$^+$ T cell gRNAs at Landscape Day 0. (**B**) gRNA read counts of recovered Donor B vs. Donor C CRISPRa-CAR CD8$^+$ T cell gRNAs at Landscape Day 0. (**C**) gRNA read counts of recovered Donor B vs. Donor C CRISPRa-CAR CD8$^+$ T cell gRNAs at Landscape Day 7 for +cytokine/-Raji (*left*) or +cytokine/+Raji (*right*) treatment arm. (**D**) Number of unaccounted gRNAs retrieved from indicated Day 0 and Day 7 CRISPRa-CAR CD8$^+$ T cell samples relative to annotated Calabrese donor plasmid pool. (**E**) Gini Index of indicated Day 0 and Day 7 CRISPRa-CAR CD8$^+$ T cell gRNAs. (**F**) Ratio of reads from Day 0 and Day 7 CRISPRa-CAR gRNA mapped to Calabrese donor plasmid pool.

Figure 4.5

A

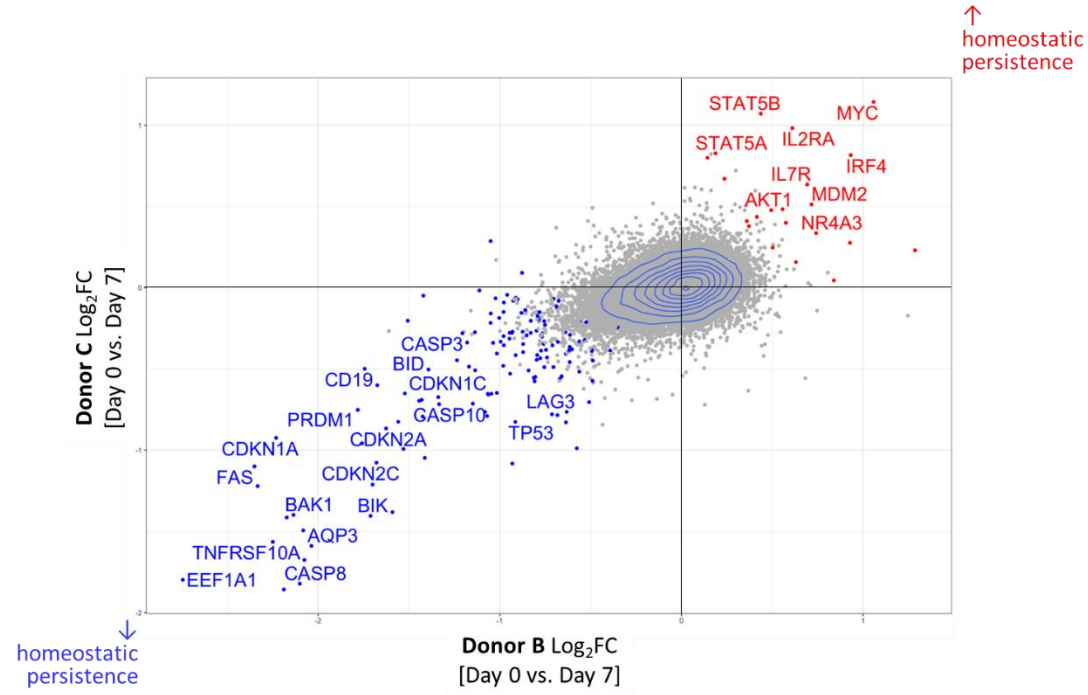
↑ homeostatic persistence
STAT5B
MYC
STAT5A
IL2RA
IRF4
IL7R
AKT1
MDM2
NR4A3
CASP3
BID
CD19
CDKN1C
LAG3
GADD45A
PRDM1
TP53
CDKN2A
CDKN1A
CDKN2C
FAS
BAK1
BIK
AQP3
TNFRSF10A
CASP8
EEF1A1
↓ homeostatic persistence
Donor C Log2FC [Day 0 vs. Day 7]
Donor B Log2FC [Day 0 vs. Day 7]

B

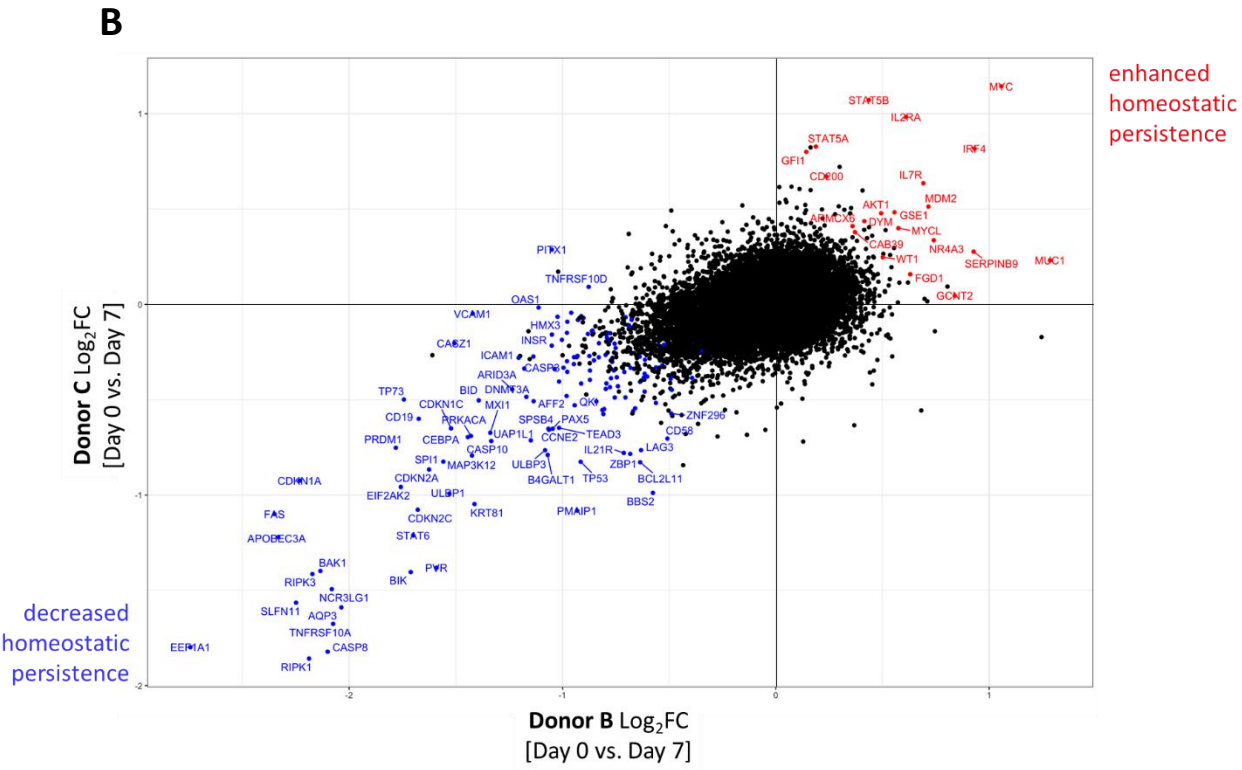
enhanced homeostatic persistence
decreased homeostatic persistence
Donor C Log2FC [Day 0 vs. Day 7]
Donor B Log2FC [Day 0 vs. Day 7]

Figure 4.5, cont'd

C

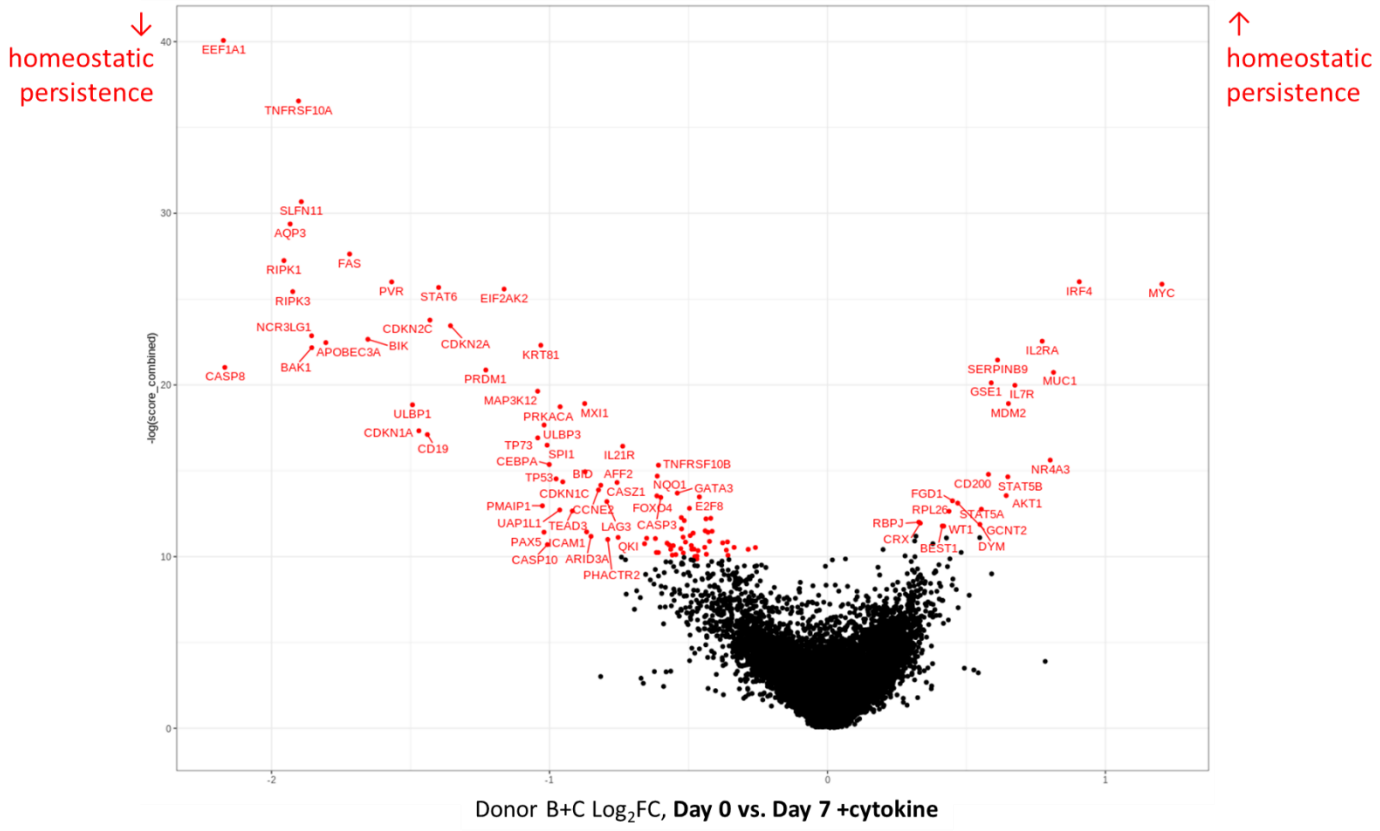

D

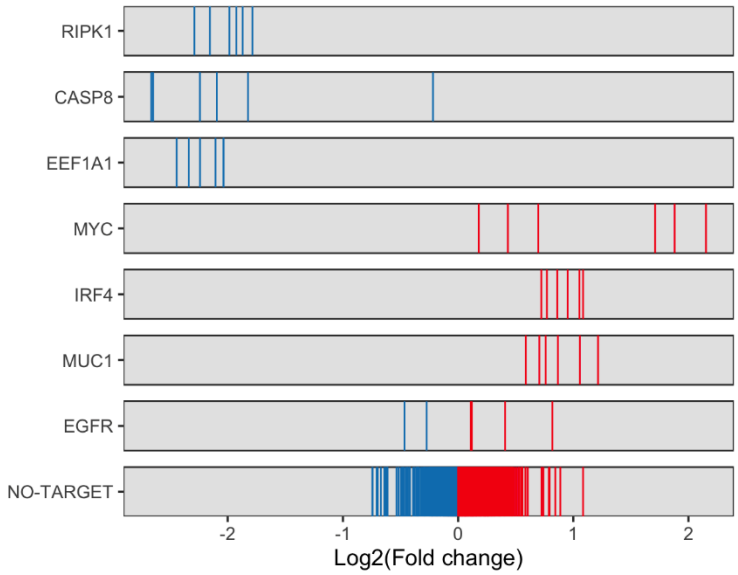

Figure 4.5: CRISPRa genome-scale screen for genetic modifiers of CAR T cell persistance. (**A**) Abridged plot of median Log_2 fold-change (FC) of gene-specific gRNAs from Day 0 to Day 7 (cytokine-rich treatment arm) for Donor B (horizontal) and Donor C (vertical). (**B**) Comprehensive plot of (A). (**C**) Comprehensive gRNA median Log_2FC of combined Donor B and C from Day 0 to Day 7 (cytokine-rich treatment arm) (x-axis) vs. - Log_2Score (y-axis). (**D**) gRNA donor-averaged Log_2FC of select gRNAs from Day 0 to Day 7 (cytokine-rich treatment arm).

Figure 4.6

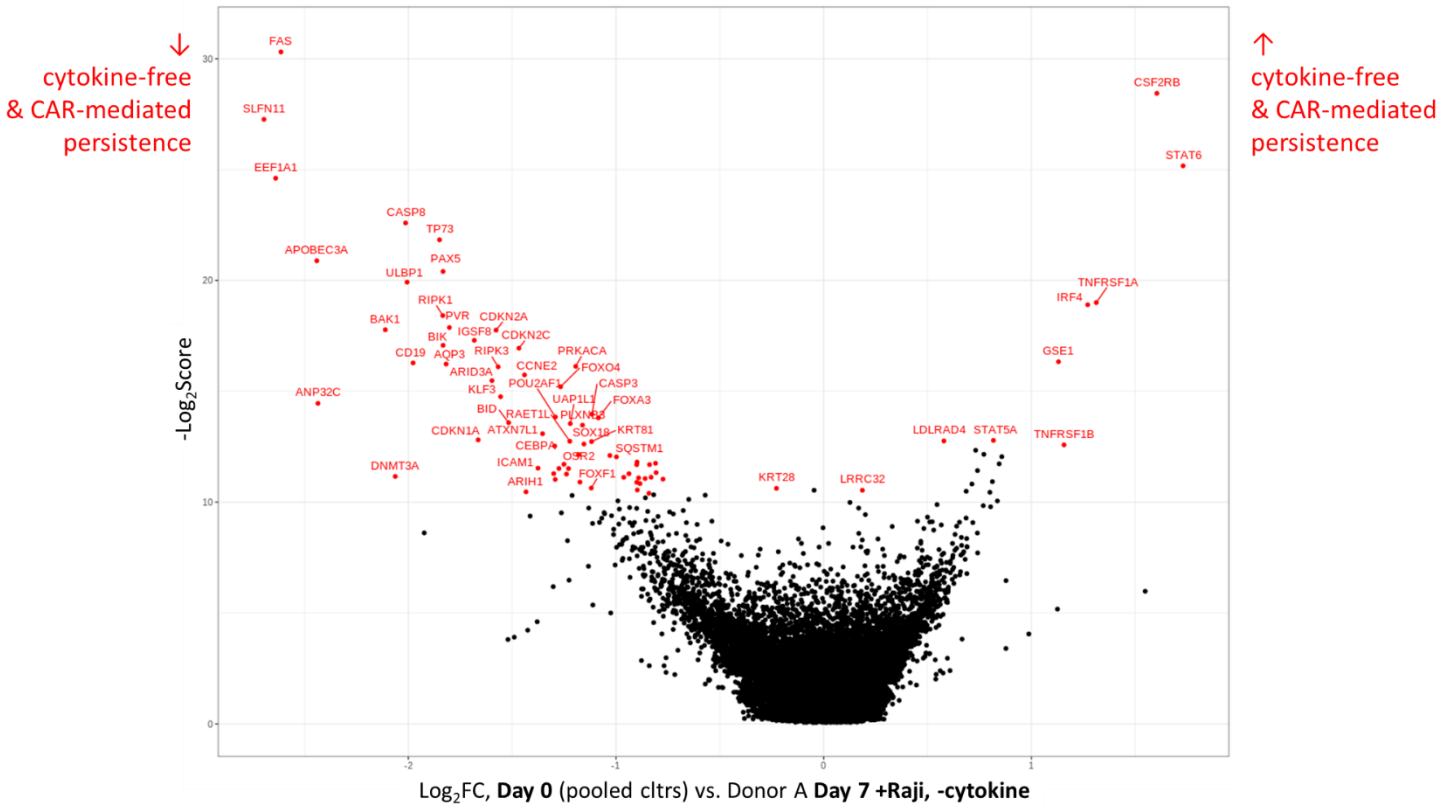
↓
cytokine-free
& CAR-mediated
persistence
↑
cytokine-free
& CAR-mediated
persistence
-Log2Score
Log2FC, Day 0 (pooled cltrs) vs. Donor A Day 7 +Raji, -cytokine
FAS
SLFN11
EEF1A1
CASP8
TP73
APOBEC3A
PAX5
ULBP1
RIPK1
PVR
CDKN2A
BAK1
IGSF8
CDKN2C
BIK
CD19
AQP3
RIPK3
PRKACA
ARID3A
CCNE2
FOXO4
KLF3
POU2AF1
CASP3
ANP32C
UAP1L1
FOXA3
BID
RAET1L
PLXNB3
CDKN1A
ATXN7L1
SOX18
KRT81
CEBPA
SQSTM1
ICAM1
OSR2
DNMT3A
ARIH1
FOXF1
KRT28
LRRC32
CSF2RB
STAT6
TNFRSF1A
IRF4
GSE1
LDLRAD4
STAT5A
TNFRSF1B

Figure 4.6: CRISPRa genome-scale screen for genetic modifiers of CAR T cell cytokine-free survival (**A**) Comprehensive plot of median Log_2FC of gene-specific gRNAs from Day 0 (combined donor pool) to Day 7 (donor A, cytokine-free treatment arm) (x-axis) vs. - Log_2Score (y-axis).

Chapter 5 | CRISPRa-inducible CAR T Cells

5.1 | Abstract

Gene overexpression systems commonly operate by enforcing constitutive transcription programs to maintain steady-state levels of proteins of interest. While such implementations greatly simplify execution, as a platform for pooled candidate screening *en masse* they fail to provide opportunities for customization of gene dose, timing, or periodicity. Here, I explore regulatory devices to restrain CRISPRa-driven gene overexpression systems operating within human T cells. First, I profile attempts ultimately aimed at conferring direct control upon gRNA production or processing, and thus downstream CRISPRa activity. I then engineer and test drug-responsive switches operating post-translationally, and demonstrate highly-sensitive, stringently-regulated ON and OFF devices for CRISPRa function. Next, I couple CRISPRa expression to an inducible promoter system responsive to T cell activation, achieving activation-dependent CRISPRa function in T cells. Lastly, I demonstrate that my CRISPRa druggable-ON system reproduces its model behavior in primary CAR T cells (CRISPRa[ON]-CAR.v2i). These implementations may have broad utility for diverse CRISPR-based T cell screening platforms.

5.2 | Background

5.2.1 | Gene effect is likely dependent on screening context

Gene expression in mammalian cells is a dynamic process, with variation among and within commonly defined populations of cells.[245–248] T cells in particular, have a well-recognized state change upon TCR ligation with its cognate antigen, triggering a host of global transcriptional and post-transcriptional programs.[249–252]

GoF screens are conventionally conducted with transcriptional regulators that enforce constitutive expression reliably across a broad spectrum of cell types.[253,254] The thinking goes, that by enforcing a predictable, uniform expression level, library candidates can be separated into groupings (molecular phenotype) or outcomes (typically survival) based on the cell behavior in question. This dominant strategy has been successfully applied across numerous cell types and selection landscapes to yield crude hits. And yet, foreign, fixed gene expression may not effectively match gene dose with the targeted behavioral output. Direct evidence for this premise, however, is somewhat limited; to date, few large-scale regulated CRISPRa or CRISPRi screens have been undertaken, and none to my knowledge have carefully benchmarked relative to their unregulated/constitutive cognates. Nevertheless, in the absence of concrete evidence, a simple thought experiment may prove useful in bolstering this assertion. For instance, I might imagine segregating screening outcomes into the following possible categories as a function of total gene output or patterning:

(1) Gene is expressed at a level favoring the phenotype (assumed always to be at a sufficient effect size)

(2) Gene is expressed at too low a level to favor the phenotype

(3) Gene is expressed at too high a level to favor the phenotype

(4) Gene is expressed at a level favoring the phenotype, but incurs toxicity (i.e. 'gain of toxic function')[8,9]

(5) Gene is expressed at a level, but not duration and/or interval favoring the phenotype

Outcomes (2) through (5) could broadly be classified as conditional false negatives – meaning that under different gene regulatory conditions but the same screening condition, they would instead steer the host cell towards the behavior of interest. Screening outcome (2) or (3) or a potential blend of the two might mirror biological goldilocks zones, where optimal gene dose is a narrow band hovering between defined local minima.[255–257] Similarly, gain of toxic function (4) resulting from targeted gene overexpression has been described in previous cell populations.[258,259] In such an instance, although a gene may be steering cells towards a particular phenotype when overexpressed, such a high level of expression imposes a cost to cell viability. A phenotypic screen with defined high and low bins may be less affected by toxic gene dropout, permitted the frequency of cell dropout does not dilute the effect size to point of avoiding statistical detection.

And so, despite lacking confirmatory data evidencing these scenarios in published GoF screens, I feel confident that I can reasonably predict their occurrence in genome-scale screening results *a priori*. I further suspect that these theoretical scenarios are likely to be especially prevalent in T cell selection landscapes, given the myriad of ways that overexpressed genes may interplay

with context-specific endogenous gene programs – especially as CAR T cells are activated by cognate antigen and later return to a quiescent state.

5.2.2 | Utility of regulated overexpression: dose

Shortcomings of excessive or insufficient gene dosing may admittedly be resolved through careful evaluation and selection of candidate promoters of varied transcriptional strength. An assortment of fixed calibrators could then conceivably be used to generate arrayed-pooled screening data across a range of crude global gene doses. Such a strategy would be a largely impractical solution for traditional pooled ORF library implementation, given that promoter behavior varies extensively as a function of sequence-specific features that remain poorly defined.[260,261] In contrast, however, ascertaining the output of a defined CRISPRa CDS as a function of promoter species is a relatively straightforward measurement. Notably, care would need to be taken to carefully catalogue potential deviation in long-term potency over time, particularly as a function of transgene silencing – a phenomenon shown in chapter 3 to be exquisitely dependent on promoter selection and other molecular features.

One potential simplification would involve the use of a fixed promoter with tunable 'levers' capable of registering discrete global overexpression as a function of some defined input. Such a system – a regulated system – might largely avoid the complications arising from varied transgene composition, while still providing the opportunity for dose customization.

5.2.3 | Utility of regulated overexpression: timing

Regulated gene overexpression of course could provide benefits beyond only maximizing screening returns. For instance, if the enhancement desired were very particular to a specific cell state, then withholding inducer prior to the onset of this state could maximize ideal gene enrichment. As mentioned earlier in this chapter, gene expression is a dynamic process, and optimal gene dosage consequently depends on a variety of temporal and cell-specific factors. For T cells lineages, whose histories can stretch from initial antigen encounter, to differentiation and expansion, and then to either long-lived persistence or programmed senescence, timing and cellular context are paramount variables. For T cells that take up arms against malignant cell populations, there may arise a particular need to resist inhibitory signals that might, in other environments or times, be welcomed. For instance, T cell differentiation often balances between the aims of generating cytotoxic, short-lived effector and prolonged memory cell populations with heightened capacity for future proliferative expansion. Applied to T cell manufacturing and subsequent screening methods, one might imagine scenarios where an active GoF system might accumulate particular candidates early (e.g. genes favoring preserved T memory cell population with high growth potentials) that later impose costs to late-function cellular fitness (reduced cytotoxicity). Phenotypic-screening methods may guard against the emergence of false hits as they are agnostic to global candidate relative frequency, but they cannot protect against a loss of screening sensitivity from candidate overcrowding (i.e. unintentional library skewing).

Without limits on CRISPRa activity, potential library sculpting would occur immediately once all the components were fully assembled in the host cell. In Chapter 3 I proposed a primary CAR-T cell production schema that withheld library delivery until near the end of cell manufacturing. As such, I believe that my particular implementation is already well-shielded from the presumptive event of extensive candidate bottlenecking and skewing. Nevertheless, I strongly believe that my design could benefit from additional safeguards and control devices to limit activity (and thereby the effective landscape debut or cadence) to a defined period of interest.

5.2.4 | Utility of regulated overexpression: simplified controls

Until now, I have discussed selective landscapes that identify candidate hits by comparing relevant candidate abundancy (1) between cell populations +/- exposure to a defined selection landscape or (2) between defined phenotypic cell populations within a single landscape. A third potential system would segregate candidates into populations on the basis of a supplied effector molecule (inducer or repressor). In this implementation, each parent cell pool might also serve as its own control or reference population, even in the absence of a prescribed molecular phenotype binning. In this way, the selection landscape could be dramatically simplified, which is expected to be an attractive feature as landscapes increase in complexity.

5.2.5 | Utility of regulated overexpression: context-specific output

With each individual gene providing value in a context-specific and temporal fashion, the optimum form of regulation particular to each candidate would ultimately depend on its

identity and the landscape selected. Generally, these conditions cannot be optimally chosen *en masse, a priori*, but instead would require multiple screening iterations under carefully defined regulatory schema.

Looking beyond screening regimen, if it were known that an identified regulatory system was likely to be selected to drive expression of identified CRISPRa hits, it might be most efficient to include this parameter in the primary screening embodiment, as this would better align screening hits with implemented therapy and minimize the risk of subsequent translation. As an example, if one were to desire a gene that enables cytokine-free T cell growth, such a program – when fashioned as a bone fide therapy – would likely need to be coupled to one or several forms of regulation to protect against unintentional, unrestrained cell growth, the hallmark of an immortalized T cell lymphoma.[236,262,263] In this scenario, selecting candidates that also cease to enrich after inducer removal could take the form of coupled positive followed by negative candidate selection. In a similar vein, some gene products are known to cause systemic toxicity, and are usually designed with regulation 'baked-in.'[264,265]

5.2.6 | Druggable-CRISPRa designs

To that end, many research groups have experimented with regulated CRISPRa systems – both for the purposes of enhancing pooled screening methods, as well as to establish versatile tools for generalized programmable gene regulation. Given that CRISPRa is a multicomponent system expressed *in trans* to the gene it modulates, it thus offers many potential control nodes (**Fig**

5.1A). Consequently, strategies for its regulation vary widely. In this chapter I describe my attempts to profile several of the most popular implementations in T cells.

5.2.7 | T cell-autonomous CRISPRa designs

Already, many T cell synthetic potency enhancement designs attempt to respond to context-specific tumor cues (e.g. switch receptors, see **Chapter 1**). More recently, various groups have aimed to design more payload-agnostic logic circuits that primarily function at the transcriptional level, that can direct transgene expression in response to defined cell inputs. To build these modules, research groups generally test genetic response elements in an arrayed or pooled setting and then advance designs with high potency and high ON:OFF kinetics – that is, versions that do not excessively leak by releasing their variable payload in the absence of specific stimulus. Notable examples include circuits driven in response to inflammation/hypoxia,[92,266] cytokine detection,[267] and T cell activation.[200,268,269]

5.2.8 | Implementing regulated CRISPRa in CAR T cells

Here, I outline my efforts to establish regulated CRISPRa expression in T cells. As in **Chapter 1**, I make routine use of the Jurkat T cell line as a starting point to quickly test potential design implementations. I begin my exploration by testing gRNA modifications before pivoting to directed alterations or additions to the RNAPII-driven CRISPRa transgene proper, coding for dCas9 and PPH, the CRISPRa effector. To model a CAR-synchronized overexpression system I profile CRISPRa coupled to an inducible promoter developed previously in my lab, known to be

responsive to T cell activation.[200] Lastly, I examine the performance of the most promising design implementations in primary CAR T cells.

5.3 | Results

5.3.1 | gRNA regulation: a deceptively simple path

To begin my studies on regulated CRISPRa in CAR T cells, I first carefully considered how an ideal regulatory system would function. Attractive features included (1) effector tolerability; (2) graded dosing (i.e. dynamic range); (3) rapid and sustained induction; and (4) minimal DNA footprint. Given that the modified second-generation SAM CRISPRa system relies upon transcriptional modulation mediated by three separate, essential subunits (e.g. dCas9, PPH, gRNA), I recognized that I might attempt to regulate one or more of these potentially tunable inputs to steer global CRISPRa activity (**Fig 5.1A**). Swiftness of induction was valued in part because it would limit gene gradients of unknown benefit, but more so because the final validation of CRISPRa hits is expected to be a gene's reverse-engineered ORF – which would have very different expression kinetics as a consequence of not being dependent on the transcription, accumulation, and emergent activity of the triad of CRISPRa molecules. However, RNAPIII transcription is a rapid process occurring on the order of seconds rather than minutes to hours for significant protein accumulation.[270,271] Because of these kinetics, as well as the potential for a reduced genetic footprint via RNA modification, I first examined regulation strategies based on alterations to the gRNA coding cassette. To complicate matters, as outlined earlier, gRNA is routinely described by RNAPIII-specific (e.g. U6)[272] or preferencing (e.g. H1)[273]

promoters, which recruit a dedicated class of transcription factors and complexes [270]; therefore, they are generally seen as fundamentally incompatible with most protein coding genes or engineered response elements, including my own.

Thankfully, prior groups have also sidestepped this problem by designing RNAPII-driven gRNA cassettes with modified 5' and 3' moieties to remove the mRNA m7G-cap and poly(A) tail, respectively. To test designs based on this principle, I first deployed to Jurkat T cells a construct coding for a CRISPRa artificial reporter system (**Fig 5.2a, b**). In this model, my system codes for a constitutive (MND-driven) CRISPRa transgene, a variable gRNA cassette, and contains a CRISPRa synthetic target gene encoding a blue fluorescent protein (mTagBFP2). When provided a competent (i.e. native U6) targeting gRNA, this design was able to achieve marked overexpression of the synthetic (mTagBFP2) reporter (**Fig 5.2b, e**). I then modified this reference construct by replacing the U6 promoter with the RNAPII-class strong T cell promoter, MND. As expected, this design had much lower levels of mTagBFP2 induction (**Fig 5.2c**). I then attempted to spur gRNA cleavage by installing pre-microRNA (miRNA) sequences (both synthetic LacZ versions and native) bracketing the gRNA or position towards one of its termini; these sequences were expected to generate secondary structures ripe for Drosha processing, a natural mechanism for endogenous pre-miRNA maturation (**Fig 5.2d *top***).[274] Tested concurrently was the inclusion of an unusual 3' RNA processing element, u1snRNA "3'box." Studies have indicated that this element specifically truncates snRNAs and gRNA generated from RNAPII promoters, removing *in cis* transcripts' poly(A) tails.[275–277] Generally I found that the inclusion of the pre-miRNA sequences appeared to impede downstream CRISPRa function, rather than enhance it; although this may tendency may have been lessened with increasing *in*

cis pre-miRNA copies. In contrast, exchanging the 3' SV40 poly(A) signal sequence with the 3'box appeared to improve downstream CRISPRa activity (**Fig 5.2c**).

I iterated on this modest success and chose to also steer the model system towards a more realistic implementation. Here, I developed CRISPRa-targeting vectors aiming for overexpression of CCR2, deployed with an optimized RFP CRISPRa reporter detailed in **Chapter 2** (**Fig 5.2f**). I again examined candidates with 3' box gRNA designs. In addition, I tested the inclusion of flanking or terminal tRNA, or ribozyme sequences (**Fig 5.2d *middle***). tRNAs naturally form structures that are susceptible to RNase P cleavage, making them ideal substrates for positioning at gRNA 5' and 3' ends.[278] Somewhat inconveniently, tRNAs also possess intrinsic RNAPIII promoter activity, so I choose to profile chimeric tRNAs with this feature greatly reduced.[279] Lastly, I also examined ribozymes, an ancient class of RNA enzymes with self-cleaving activity.[280] I selected two species of ribozyme derived from either the plant-based Hammerhead (HH)[281] or the Hepatic Delta virus (HDV)[282] known to effectively liberate RNAPII-encoded gRNAs (**Fig 5.2d *bottom***).[117,283,284] When tested in the new model system, surprisingly, I observed nearly imperceptible levels of CCR2 overexpression using any construct other than the parental U6-gRNA vector (**Fig 5.2*g left***). When examined extremely closely, I did discern that perhaps the accumulation of flanking tRNAs or ribozyme might offset any apparent inefficiencies brought about by their inclusion (**Fig5.2*g right***). Regardless, given the marked underperformance of the secondary vector system, coupled high probability that it likely offered a more predictive CRISPRa performance simulation, I chose to halt attempts to enable RNAPII-driven gRNA production.

However, before abandoning gRNA modification entirely, I conceived of a competing strategy that did not depend upon RNAPIII activity to achieve gRNA transcriptional regulation. Here, rather than seeking to modify the gRNA cassette directly, I considered slightly altering the U6 RNAPIII promoter by installing DNA-binding sites for a class of transcriptional regulators. The Tet repressor (TetR) is an extremely well-documented bacterial protein used to regulate genes in mammalian cellular systems in response to Doxycycline (Dox), a tetracycline analog. Originally discovered as binding to tet operator (tetO) sites and thereby regulating the tet operon,[285] TetR has since been re-designed for many purposes and functions – which I will expound upon later. Here, I followed prior study designs and inserted two tetO sequences upstream of the U6 promoter TSS (**Fig 5.3a, b**).[286–288] As reported by other labs, this modification caused a relatively large drop in CRISPRa target expression (i.e. CCR2 gMFI) (**Fig 5.3c**).[289] This reduction appeared consistently regardless of the presence of either TetR variant ("V10"/"V16").[290] Given the non-trivial drop in potency even in the absence of Dox, I chose to also abandon this approach.

5.3.2 | Druggable transcriptional CRISPRa regulation

While prior efforts to use transcriptional control devices to modulate gRNA expression proved largely unfruitful, given the ubiquity of TetR-based designs,[291–293] I took a second look at this system, now as a potential regulator of the dCas9- and PPH-encoding CRISPRa transgene. The two most common Tet implementations are the Tet-On and Tet-Off systems, both of which share two core components: the (1) Tet Response Element (TRE) and (2) a modified TetR. The TRE is a series of tetO concatamers situated adjacent to a minimal promoter; meanwhile, the

modified TetR includes a fusion to VP16, constituting a site-specific Dox-repressible Tet transactivator (tTA).[294,295] Together, these components make up the Tet-Off system. To reverse this logic, alternate forms of TetR have also been engineered to confer Dox-inducibility, which when tethered again to VP16, constitute the Tet reverse-transactivator (rtTA) – the effector protein in the Tet-On system.[195]

To mimic the architecture of the intended CRISPRa-CAR dual-promoter system, I established a potent parent reporter construct with an upstream RFP-tagged CRISPRa transgene and a secondary constitutive promoter encoding TurboGFP to enable simultaneous monitoring of both bicistronic coding cassettes. Along with a CCR2-targeting gRNA cassette, this "CRISPRa-Max" vector was used as a reference construct for this particular study and then for many subsequent experiments detailed later in this chapter (**Fig 5.4a**). I then engineered modified forms of this vector bearing a tTA and TRE-driven CRISPRa transgene; given the success of divergent Tet-based designs,[296] I also cloned divergent Tet-Off and divergent CRISPRa-Max reference constructs (**Fig 5.4a**). When transiently deployed to Jurkat T cells in antibiotic-(Dox or tetracycline) free culture media, both Tet-Off designs evidenced very high transgene levels – actually in excess of CRISPRa-Max (**Fig 5.4b, c**). Interestingly, despite higher transgene levels, both Tet-Off and CRISPRa-Max systems yielded equivalent levels of CCR2 gMFI, suggesting that the CCR2 locus was saturated in either condition, or perhaps that gRNA was limiting. When treated with Dox simultaneous with transfection, as expected, cells bearing Tet-Off constructs saw markedly lower levels of CCR2 gMFI, RFP gMFI, and RFP positivity – with all three parameters approaching baseline parental (untransfected) cell levels (**Fig 5.4c**). Of note, while both divergent and unidirectional designs evidenced similar profiles of CRISPRa transgene and

target upregulation, the expression pattern of the CAR placeholder gene (TurboGFP) within unidirectional and divergent Tet-Off systems was markedly different in the absence of Dox supplementation. Specifically, the divergent Tet-Off design ("CRISPRa-TetOff.div") exhibited very high levels of TurboGFP expression, consistently proportional to dCas9-mScarlet expression; in contrast the unidirectional Tet-Off design ("CRISPRa-TetOff") maintained low but observable levels of TurboGFP regardless of Dox level (**Fig 5.4d**). In the divergent format, I believe that this apparent promoter 'cross-talk' can be adequately explained by proximity of the TRE and opposing EF1α-HTLV promoter – with the VP16 supplying transcriptional boosting to both; this effect may be magnified through the inadvertent triggering of a positive feedback loop whereby increased EF1α-HTLV transcription generates additional tTA, which goes onto to bind to the proximal TRE and repeats the cycle again. Also of interest is the relatively diminished TurboGFP observed using the unidirectional Tet-On or Dox-treated Tet-Off forms relative to either CRISPRa-Max variant. This may be explained by more prominent transcriptional interference, driven by the unusually high expression levels of the CRISPRa transgene that then bleeds through into the 5' region of the EF1α-HTLV or its CDS (and thereby lowering TurboGFP output). Alternatively, this diminished TurboGFP could represent rapid, episomal transgene silencing[297,298] spreading from the nearby Tet-regulated CRISPRa transgene

Given the extensive challenges with CRISPRa transgene silencing observed in primary T cells, along with isolated reports of TRE gene silencing,[299,300] I choose to move forward with unidirectional Tet-Off designs for future implementation. This Tet-Off system design was ultimately trialed in primary CAR T cells with data reported earlier (**Fig 3.5c**). As detailed there, efforts to generate viable, functional $^{\text{Tet-Off}}$CRISPRa-CAR T cells was largely impeded by

presumptive CRISPRa transgene silencing that had either quietly occurred during early manufacturing or rapidly upon Dox withdrawal. Interestingly, Dox-treated $^{Tet\text{-}Off}$CRISPRa-CAR T cells bore cell yields approaching (tTA-*null*) ^{TRE3G}CRISPRa-CAR T cells or CRISPRa-CAR.v1; in contrast, yields of untreated $^{Tet\text{-}Off}$CRISPRa-CAR T cells were exceptionally low. While I did not follow up this observation with additional de-silencing attempts, this result is consistent with transgene silencing that had spread across transgenes; this appears to have occurred despite the intentional selection of designs largely insensitive to apparent promoter 'crosstalk' in Jurkat T cells (**Fig 5.4d**).

5.3.3 | Druggable post-translational CRISPRa regulation

Until now, I had limited my investigation to transcriptional control devices, mostly to avoid the associated gene delivery costs with increasing DNA footprint and risking further transgene silencing. However, given failed previous attempts, I now chose to expand the exploration into reported regulatory devices known to post-translationally affect protein activity and/or stability. When I began this exploration, I had a slight preference for a druggable-OFF system, so that I could restrict CRISPRa expression or activity throughout manufacturing and then relieve this inhibition just prior to landscape initiation. This was an attractive option, as this implementation would permit me to (1) avoid the complication of potentially undefined drug artifacts on selection landscapes, while also (2) mitigating any potential CRISPRa-driven toxicity. At this point in time, I had not yet obtained the data reported in **Chapter 3** that suggested, against my expectations, that CRISPRa was not imposing gross toxicity within primary T cells (**Fig 3.5b**).

One attractive, recently profiled CRISPR-compatible druggable-OFF switch is the small molecule-assisted shut-off (SMASh) system.[301] SMASh is a design based on the Hepatitis C virus (HCV) nonstructural protein 3 (NS3) protease.[302] SMASh also possesses a NS3 cleavage site and HCV peptide sequences that act as a functional degron. Under basal conditions the NS3 protease engages in rapid and efficient *in cis* proteolysis of its proximal cleavage site, resulting in release of the tethered degron domain. Importantly, NS3 protease is potently inhibited by multiple HCV inhibitors (simeprevir, danoprevir/ grazoprevir, asunaprevir and ciluprevir), some of which are available clinically and have even been tested on primary human CAR T cells.[303,304] When fusion proteins bearing SMASh tags are treated with an NS3 inhibitor, asunaprevir (ASV), the impaired proteolytic activity permits functional degron activity, culminating in efficient protein destruction. Prior reports demonstrated that Cas9-SMASh fusion systems treated with ASV rapidly degrade with a resulting loss of endonuclease activity. To my knowledge, no group had previously tested this specific system with dCas9, although upon further review, dCas9 implementations with other NS3-based systems were later found.[305,306] To test this design in my hands, I modified the CRISPRa-Max parent vector by tethering SMASh sequences to dCas9-CTD ("SMASh.1"), PPH-CTD ("SMASh.2"), or PPH-NTD ("SMASh.3") (**Fig 5.5a**). Following the now standard Jurkat transient assay, I observed that all three candidates achieved near-equivalent levels of CCR2 overexpression in the absence of drug treatment as assessed by gMFI (**Fig 5.5b, c, d**) – with SMASh.3 having only modestly reduced levels. In response to dose escalation with ASV, I saw stepwise decreases in CCR2 overexpression across all SMASh variants. While dCas9-SMASh CCR2 loss decelerated with increasing ASV dose (in line with observed mScarlet-dCas9 levels), both PPH-SMASh variants saw stepwise reductions that approached baseline CCR2

expression (<5%) in Jurkat parental cells. Between the two PPH-SMASh variants, SMASh.2 evidenced a slightly higher CCR2 ceiling in the absence of inhibitor, while requiring greater amounts of ASV to achieve the same CCR2 reduction. I chose to advance the SMASh.2 design on the basis of higher max potency, but also considered SMASh.3 to be a well-performing candidate, worthy of potential further development at a later date.

While in this development space, I also chose to profile CRISPRa post-translational druggable-ON candidate designs. My lab had already possessed experience employing a tamoxifen-sensitive DNA-binding domain derived from the estrogen receptor alpha mutant (ERT2 or ER-LBD).[307,308] In addition, multiple groups had previously examined this device as a potential regulator of Cas9 or CRISPR effector enzymatic activity.[309–312] ERT2 has been used to confer tamoxifen dependency upon a variety of multiprotein systems, and its mechanism of action remains controversial, but may involve a form of cellular sequestration that is thereafter relieved by tamoxifen (4-OHT).[313–315] As with the prior SMASh implementation, I examined the impact of ER-LBD tethering both to dCas9 and PPH. For dCas9 implementation, in addition to testing a direct CTD ER-LBD tether ("ER.1"), I also closely aligned with a prior study indicating a suitable dCas9 internal site amenable to the insertion of a large ER-LBD polypeptide.[310] As this study did not appear to employ ERT2 but the native ER-LBD, I created constructs of both varieties ("ER.4" through "ER.7") (**Fig 5.6a**). For PPH implementation, I chose to install ER-LBD (1) as a tethered CTD ("ER.3"), (2) as an internal protein linking PCP and p65 ("ER.2"), or (3) as a tethered NTD ("ER.8"). Of note, the ER.8 candidate was retrieved from a publication that used an ER-LBD of slightly reduced overall size compared to ERT2 and with several amino acid substitutions; the authors referred to it explicitly as a "degradation domain".[316] In my hands, I

noted that all four internal dCas9 implementations fared poorly – with greatly diminished CCR2 expression even in the presence of inducer, 4-OHT (**Fig 5.6b, c, d**). I am uncertain if this discrepancy is due to a potential failed implementation on my part or perhaps is the result of higher-order sterics specific to CRISPRa (PPH) or the modified dCas9 (+mScarlet). The dCas9-CTD ER-LBD fusion performed, exhibiting higher mScarlet-dCas9 levels and some measure of induction with 4-OHT addition; however, the degree of stringency and impact on CCR2 expression were negligible (**Fig 5.6c**). In contrast, and as with the SMASh variants, the highest CRISPRa potency and greatest drug stringency were achieved through ER-LBD fusions to PPH, with ER.2 performing best by both metrics (**Fig 5.6c, d**). I find it notable that PPH is consistently more amenable to additional protein fusions, and that bringing it under some form of druggable regulation appears to result in the most sizeable shift in CRISPRa activity. This leads me to suspect that PPH may generally function as the limiting reagent in most experiments reported previously. In closing, I chose to also advance ER.2 as a druggable ON switch in CRISPRa-CAR T cells.

5.3.4 | CAR-inducible CRISPRa regulation

Up until this point in this chapter, I have only outlined attempts to design druggable control switches. Also of interest as outlined in the background section, are cell-autologous circuits. In addition to prior development with ERT2 technology, my lab had also previously engineered a potent inducible synthetic promoter ("iSynPro"), shown to be rapidly and specifically engaged following T cell activation.[200] iSynPro is composed of a productive tiling of transcription factor binding motifs generated via golden gate assembly ("S1-61"), followed by a minimal IL-2

promoter (IL-2mp). Implemented within CAR T cells, iSynPro can synchronize transgene expression to CAR ligation. To test performance, I engineered two iSynPro-CRISPRa variants. The first candidate merely replaced the CRISPRa-Max MND promoter with iSynPro directly ("CRISPRa-Auto"), while the second candidate iterated on this design by also relocating PPH to the downstream EF1α-HTLV promoter ("CRISPRa-Auto.2"). Given my suspicions that PPH may be acting as a limiting reagent in prior studies, I hoped that pairing this species with its own promoter might improve potency and/or regulatability. I transiently delivered these constructs to Jurkat T cells with or without the addition of phorbol myristate acetate (PMA) and Ionomycin (Iono) – a cocktail of powerful T cell activator. I was pleased to see that absent activation, both iSynPro-regulated CRISPRa variants exhibited high stringency, with only minimal mScarlet-dCas9 leak or CCR2 upregulation relative to baseline (**Fig 5.7c, e**). In contrast, transfected Jurkat T cells supplied with PMA/Iono saw high levels of mScarlet-dCas9 induction and subsequent robust CCR2 overexpression (**Fig 5.7c, e**). To my surprise, both "CRISPRa-Auto.2" and its reference construct "CRISPRa-Max.2" evidenced lower levels of both mScarlet-dCas9 and CCR2 overexpression relative to their all-in-one CRISPRa polycistron equivalents. This might suggest that the PPH CDS provides some form of stability to the long-form CRISPRa cassette that paradoxically improves, rather than impedes expression. I also noticed in my experimental system that PMA/Iono-stimulated or any iSynPro-containing cells had far greater expression levels of TurboGFP (**Fig 5.7d**). My experiment was not designed to elucidate the possible causes for these phenomena, although it is well known that T cell activation can induce large changes in transcription, translation, and protein activity[317–323] that may account for these results. However, because of this I also provided readouts that gated on total live cells rather than

those that were also TurboGFP^{+} (**Fig 5.7c**). Examined this way, it was clear that both iSynPro-regulated constructs provided tight regulation without loss of potency relative to CRISPRa-Max; although, the full polycistron versions (Max.1 and Auto.1) were still consistently stronger expressers. I thus decided to advance the CRISPRa-Auto.1 design into primary CAR T cells.

5.3.5 | CAR T cell CRISPRa regulation

Finally, I was prepared to incorporate the panel of well-performing CRISPRa regulators (i.e. Druggable-OFF, SMASh.2; Druggable-ON, ER.2; CAR-inducible, CRISPRa-Auto.v1) into CAR-compatible vectors and profile drug and cell-autologous CRISPRa regulation patterns in primary T cells (**Fig 5.8a**). In **Chapter 3**, I reported on an attempt to profile an iSynPro-like CRISPRa-CAR implementation that included S1-61 sandwiched between divergent EF1α-HTLV promoter pair, intended to act as a putative, activation-sensitive enhancer element. Now I devised similar construct designs that replaced in its entirety the CRISPRa-facing EF1α-HTLV with bona fide iSynPro (S1-61 + IL-2mp); in addition, these designs kept the selectable marker, DHFR^{FS}, within the anti-CD19 CAR (CD19CAR) cassette to relieve CRISPRa selection and permit iSynPro-directed transgene fluctuations (**Fig 5.8b**). To generate CAR T cells, I performed EP-TICLE as described in **chapter 3** using 1:1 CD4/CD8 T cell admixtures as starting cell input. To test CRISPRa induction, I then intercepted cultures between Day 17 and Day 19 of manufacturing and co-incubated these expanding cells with CD19CAR targets (Raji) for 48 hours. When examined via flow cytometry, I observed CRISPRa induction of variable magnitude (5 - 65%), with the cells containing an intronized CRISPRa transgene ("iSynPro-CRISPRa-CAR.v1.5i") reaching consistently higher levels of mScarlet-dCas9 positivity, but also exhibiting a greater degree of basal-state leak compared

to the non-intronized form ("iSynPro-CRISPRa-CAR.v1.5") (**Fig 5.8c, d**). Perhaps most disappointingly, gRNA-equipped iSynPro-CRISPRa-CAR.v1.5i cells appeared to generally engage in similar levels of target gene overexpression (EGFR), with or without the addition of Raji targets (19% → 27%) (**Fig 5.8d**). While I cannot rule out the possibility that assay timeline may not be optimized to capture maximum induction or most stringent basal activity, I nevertheless felt that this design was likely in need of substantial improvement if it were to offer substantive value as a cell-autonomous GoF screening tool.

I also tested implementations of my druggable CRISPRa designs within CAR T cells. Here I built on CRISPRa-CAR construct derivatives that contained the durable divergent EF1α-HTLV promoter pair. Pilot experiments revealed that derivatives of this design with modified PPH domains exhibited extremely poor mScarlet-dCas9 expression (***data not shown***) with ER.2 being slightly more tolerated relative to SMASh.2. Presuming that the inclusion of additional CDSs had reignited severe transgene silencing despite employing my silencing-resistant divergent EF1α-HTLV intervention, I pivoted. Now focusing only on ER.2, I transferred this design to the CRISPRa-CAR.v2i$_{gRNA}$ vector, generating "CRISPRa[ON]-CAR.v2i$_{gRNA}$" (**Fig 5.9a**). As with iSynPro-CRISPRa-CAR.v1.5i cells, I intercepted T cells on EP-TICLE Day 17: splitting cells into several specific daughter cultures +/- Raji targets and +/- ER.2 inducer (4-OHT). Here, in the absence of 4-OHT, I observed incredibly stringent regulation of target gene induction with EGFR registering at baseline levels (**Fig 5.9b**). When supplied 4-OHT, EGFR modestly rose (to 18%), which increased significantly when the cells were also co-incubated with Raji cells (to 62%). Notably, there was no evidence of leaky CRISPRa activity with Raji co-cultured CRISPRa[ON]-CAR.v2$_{gRNA}$ T cells withheld 4-OHT; this was despite observing a notable increase in mScarlet-dCas9 gMFI

following Raji addition (**Fig 5.9b**). Overall, these results suggest that CRISPRa[ON]-CAR.v2i$_{gRNA}$ T cells may possess potency on par with unregulated CRISPRa-CAR.v2i$_{gRNA}$ equivalents, while also exhibiting very high dependence on 4-OHT for requisite CRISPRa activity. To substantiate this finding, I suggest that future experiments should increase donor number and translate this system to combination EP-TICLE and distal gRNA-LV transduction manufacturing process.

5.4 | Discussion

5.4.1 | CRISPRa[ON]-CAR: ready for longitudinal testing

My preliminary studies featuring the CAR-adapted ER.2 design (CRISPRa[ON]-CAR.v2i) in primary T cells suggest that this system likely exhibits ideal behavior as a GoF screen master regulator. Namely, these cells evidence undetectable leakiness, high induction, and high maximum potency. Future studies will aim to replicate this finding across multiple T cell donors, translated to the EP-TICLE/LV-transduction manufacturing pipeline. Ultimately, establishing control over when CRISPRa becomes functionally active will expand the breadth of available selective landscapes by permitting the focused interrogation of conditioned cell states (e.g. exhaustion reversal, de-differentiation). Additionally, although not tested in these experiments, I expect the ER-LBD design to permit truly toggleable functional control. In this way, I can imagine also executing screens that seek to identify genetic modulators with the capacity to drive long-term behavior through short-term activity alone. Lastly, a druggable-ON system would allow a new form of simplified reference for studies, as experimental samples can be directly compared to undrugged cultures from the same lot of manufactured cells.

5.4.2 | CRISPRa[AUTO]-CAR: not quite there yet

Unlike CRISPRa[ON]-CAR T cells, CRISPRa[AUTO]-CAR T cells evidenced sporadic leakiness, sub-par CRISPRa expression, and low CRISPRa target induction with tumor co-culture. The exact cause of these results is not presently clear. Stacked up against my expectations however, several of these outcomes do not surprise. Firstly, a certain level of baseline leakiness is to be expected, especially as one refines the coding sequence to maximize reporter fidelity. I also anticipate transgene intronization, as observed with the constitutive EF1α-HTLV promoter, to enable a higher magnitude of transgene induction and perhaps be more resistant to long-term silencing. Indeed, I do see evidence of non-trivial transgene induction concurrent with Raji co-culture. Most discordant with expectations and perhaps most disappointing, I observed very little evidence of CRISPRa target induction as a function of Raji co-culture (ON:OFF $\bar{x}$ = 2.0; SD = 1.3). In these studies and within my larger research lab, iSynPro has shown sequence-dependent behavior: at times exhibiting (1) unusually high levels of leakiness, (2) usually low levels of induction, or (3) usually poor maximum expression levels. I have observed biological variation both between cells sourced from separate donors, as well as between culture wells originating from the same source, but manufactured independently. These differences may be partially driven by the stochastic nature of both transgene transposition and subsequent silencing. I note that as with Tet-based designs, transgene systems that rely on periodic transcription may be especially susceptible to transgene silencing.[299,300,324,325] Lastly, I acknowledge that I have not carefully profiled CRISPRa-mediated EGFR decay kinetics, and it is possible that observed EGFR expression attributed to iSynPro CRISPRa “leak” is in fact residual holdover from early T cell activation following CAR-restricted cell expansion. Pivoting from

early-acting *in cis* gRNA to late-acting *trans* gRNA-LV delivery would offer a suitable means to isolate this potential confounder, while druggable CRISPRa[ON] system could function as an ideal tool for modeling CRISPRa target decay kinetics.

One notable difference between iSynPro-CRISPRa-CAR.v1.5 and CRISPRa[ON]-CAR.v2i (other than the mere control device) is the positioning of $DHFR^{FS}$. Of course, to permit iSynPro cycling, I was obliged to avoid selection of enforced CRISPRa; however, selection on an intronized cassette not only imposes a demand of robust transgene expression but also of appropriate intron processing. With the tested iSynPro designs, I can imagine the many permutations of possible intron processing errors made available through the introduction of 11 human introns. Furthermore, intron processing fidelity and preferencing vary considerably across human promoters[326] and as a function of T cell activation.[327] These biological realities may hold clues for why despite observing modest increases in measurable mScarlet fluorescence, concordant increases in expression of the chosen target gene (EGFR), were not seen.

5.4.3 | Alternative CRISPRa regulatory designs

Given the behavior exhibited to date, I confess that I do not see a clear way forward engineering iSynPro-mediated CRISPRa[Auto]-CAR designs. I can conceive of alterations that might mollify transgene silencing (e.g. promoter engineering) or improve intron processing (e.g. iterative RACE and optimization rounds); however, I expect that these two forces may work against one another or ultimately alter the benchmarked transcriptional behavior of my team's generalized inducible transcription system. A more economical approach may be to re-screen

additional iSynPro variants to select candidates exhibiting ideal profiles of antigen-inducible CRISPRa activity. Alternatively, given the successful preliminary translation of a Druggable-ON switch operating post-translationally, an analogous design implementation may be more practical for my needs. Notably, a recent study demonstrated the use of a CAR-dependent (TEV) protease system capable of cleaving and releasing a membrane-tethered dCas9-VPR.[328] This specific design could be easily adapted to my construct design, by affixing a membrane anchor and TEV substrate to dCas9 or PPH, and then tested for feasibility. More broadly, use of protease-based logic circuitry has increased in recent years, including other derivatives of NS3.[329] These systems are often devised with the long-term aim of achieving layered orthogonal or multimodal control. These discrete experiments profile components of what could ultimately summate to a complex CRISPRa system fed inputs as directed by experimenter and cell milieu. In the broader academic field, I anticipate the imminent arrival and implementation of future CRISPR-based tools in primary T cells, perhaps bolstered by my findings presented here.

5.5 | Materials and Methods

5.5.1 | Immortalized cell culture

Experiments utilizing Jurkat T cells were carried out as described in **Chapter 2**. Where indicated, inducer/repressor compounds were added immediately following transfection. Raji cells were maintained as described in **Chapter 3**. Flow cytometry antibodies are indicated in **table 2.5.6**. General reagents for experiments are indicated in **table 2.5.7**, **3.5.X**, and **4.5.4**.

5.5.2 | Primary T cell experiments

CD4/CD8 T cell admixtures were generated via EP-TICLE as described in **Chapter 3**. CRISPRa target gene (EGFR) overexpression was enabled by the inclusion of a donor plasmid *in cis* gRNA cassette. Cells generated utilizing iSynPro sequences ("CRISPRa[AUTO]") were specifically gated on $CD8^+$ live singlets subsets during flow cytometric analyses; $CD8^+$ T cells have evidenced lower levels of basal iSynPro leakiness relative to CD4s. In contrast, experiments featuring the ER.2 design ("CRISPRa[ON]") were gated on $CD4^+$ or $CD8^+$ live singlets during analysis.

5.5.3 | Table: Sequence origins

DNA CDS	Source	PMID
CTS2	Ferry et al, 2017	28256578
8xCTS2p	Ferry et al, 2017	28256578
AdMLP	Ferry et al, 2017	28256578
SV40p(A)	Ferry et al, 2017	28256578
mTagBFP2	Subach et al 2011	22174863
miRLacZ	BLOCK-iT™ Invitrogen	*NA*
miR23a	Xie et al, 2017	28724960
miR27a	Xie et al, 2017	28724960
mIR24-2	Xie et al, 2017	28724960
3'U1snRNA	Shechner et al, 2015	26030444
tRNAgly	Knapp et al, 2019	30940799
ΔC55GtRNApro	Knapp et al, 2019	30940799
HHribozyme	Gao et al 2014	24373158
HDVribozyme	Gao et al 2014	24373158
TetO	Aramaki et al, 1995	8869638
TetR.v10	Das et al, 2015	26030444
TetR.v16	Das et al, 2015	26030444
tTA	Baron et al, 1997	9207017
SMASh	Wu et al, 2020	32000033
ER	Oakes et al 2016	27136077
ERT2	Indra et al, 1999	10536138
ER.DD	Miyazaki et al, 2012	22332638
iSynPro / S1-61	Wei et al, 2020	*NA*

5.5.4 | Table: Reagents

Reagent or Equipment	Vendor	Product No.
eBioscience Cell Stimulation Cocktail (500x)	Invitrogen	00-4970-03
Asunaprevir	Sigma	ADV465749194-25MG
(Z)-4-Hydroxytamoxifen	Sigma	H7904-25MG

5.6 | Acknowledgements

The author thanks Marlena Urvater, Natalie Murren, and Pittra Jaengprajak – three undergraduate students attending the University of Washington – for their assistance with molecular cloning, Jurkat T cell nucleofection, and primary EP-TICLE culture maintenance. Ian Blumenthal assisted with ER-LBD sample staining for flow cytometry.

Also enabling this work, were useful suggestions and feedback provided by other members of the Jensen lab including James Rosser, Jacob Appelbaum, and Jeremy Bjelejac. Michael Jensen supervised the project and provided funding.

All studies were conceived of by Benjamin Curtis.

5.7 | Figures

Figure 5.1

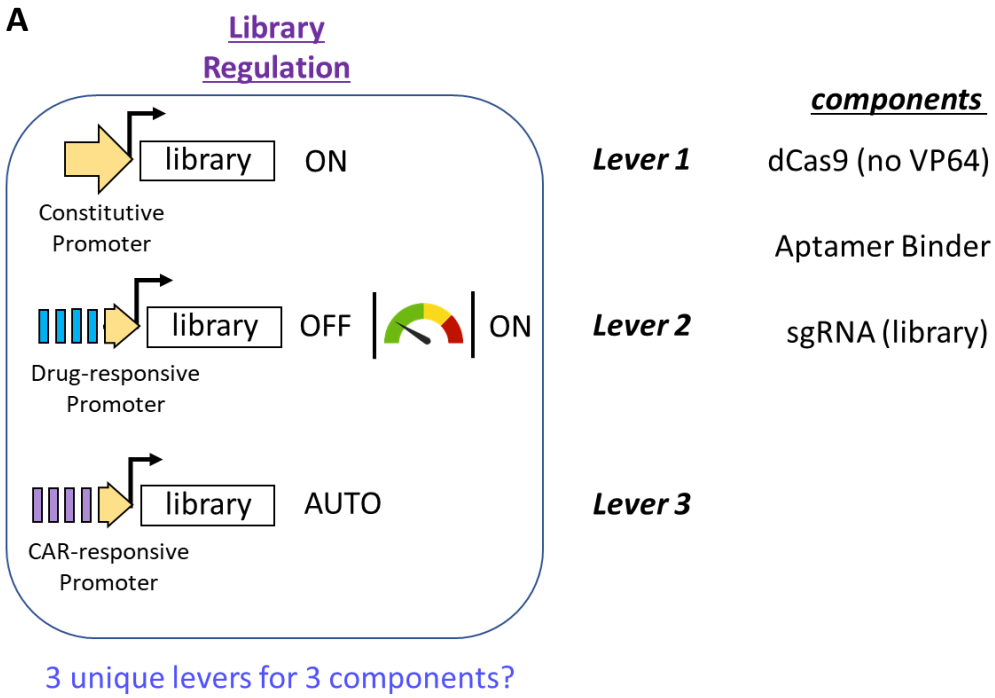

Figure 5.1: Illustration of multiple forms of potential CRISPRa transcriptional regulation and potential design implications. (**A**) Graphic depicting identified transcriptional regulatory schemas versus available discrete CRISPRa component. (**B**) Expected impact to CRISPRa kinetics as a function of regulated component chosen.

Figure 5.2

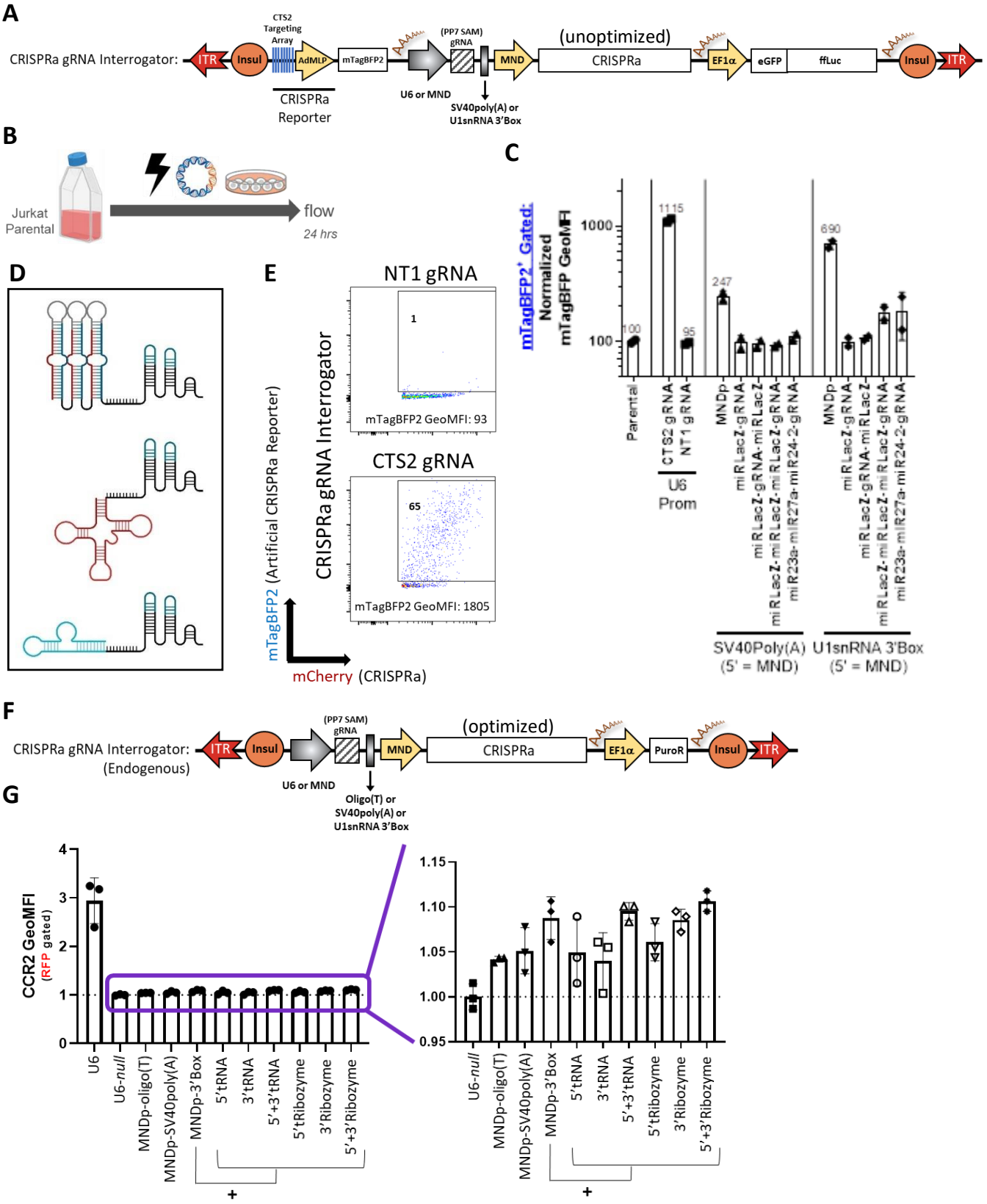
A
CRISPRa gRNA Interrogator:
ITR
Insul
CTS2 Targeting Array
AdMLP
mTagBFP2
(PP7 SAM) gRNA
MND
(unoptimized)
CRISPRa
EF1α
eGFP
ffLuc
Insul
ITR
CRISPRa Reporter
U6 or MND
SV40poly(A) or U1snRNA 3'Box
B
Jurkat Parental
flow
24 hrs
C
mTagBFP2+ Gated: Normalized mTagBFP GeoMFI
1000
100
100
1115
95
247
690
Parental
CTS2 gRNA
NT1 gRNA
U6 Prom
MNDp
miRLacZ-gRNA
miRLacZ-gRNA-miRLacZ
miRLacZ-miRLacZ-gRNA
miR23a-miR27a-miR24-2-gRNA
SV40Poly(A) (5' = MND)
U1snRNA 3'Box (5' = MND)
D
E
NT1 gRNA
1
mTagBFP2 GeoMFI: 93
CTS2 gRNA
65
mTagBFP2 GeoMFI: 1805
CRISPRa gRNA Interrogator
mTagBFP2 (Artificial CRISPRa Reporter)
mCherry (CRISPRa)
F
CRISPRa gRNA Interrogator: (Endogenous)
ITR
Insul
(PP7 SAM) gRNA
MND
(optimized)
CRISPRa
EF1α
PuroR
Insul
ITR
U6 or MND
Oligo(T) or SV40poly(A) or U1snRNA 3'Box
G
CCR2 GeoMFI (RFP gated)
4
3
2
1
0
1.15
1.10
1.05
1.00
0.95
U6
U6-null
MNDp-oligo(T)
MNDp-SV40poly(A)
MNDp-3'Box
5'tRNA
3'tRNA
5'+3'tRNA
5'tRibozyme
3'Ribozyme
5'+3'Ribozyme
+

Figure 5.2: Evaluation of modified gRNA expression cassettes to permit robust RNAPII expression and downstream CRISPRa target activation. (**A**) Graphic of "CRISPRa gRNA Interrogator," a CRISPR artificial reporter vector, deployed in (C) and (E). (**B**) Experimental schema depicting transient transfection (EP) followed by overnight recovery in media. (**C**) Quantified, normalized geometric mean fluorescent intensities from flow analysis of all cultures. (**D**) Graphics of select modified gRNA designs with 5' premIR, tRNA, and ribozyme respectively (*top to bottom*). (**E**) Representative flow cytometry plots of CRISPRa gRNA Interrogator cells with benchmark U6 promoter and on-target (CTS2) or non-targeting (NT1) gRNAs. (**F**) Graphic of "Endogenous CRISPRa gRNA Interrogator," a CRISPR endogenous gene reporter vector, deployed in (G). (**G**) Quantified, normalized geometric mean fluorescent intensities from flow analysis of all cultures. CRISPRa gRNA Interrogator samples are gated on live, mTagBFP2+ singlets (C). Endogenous CRISPRa Interrogator samples are gated on live, RFP (CRISPRa transgene)$^{+}$ singlets only (G). Parent cells are gated on live singles only (C).

Figure 5.3

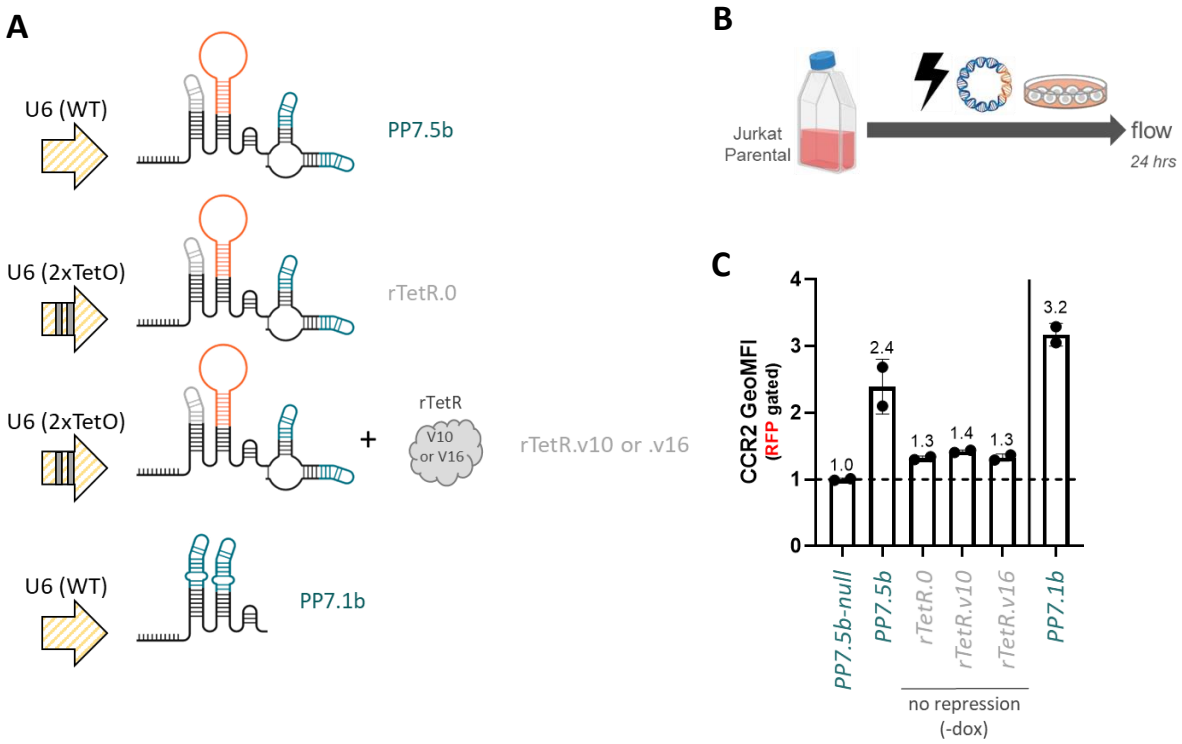
A
U6 (WT)
PP7.5b
U6 (2xTetO)
rTetR.0
U6 (2xTetO)
rTetR
V10
or V16
rTetR.v10 or .v16
U6 (WT)
PP7.1b
B
Jurkat
Parental
flow
24 hrs
C
CCR2 GeoMFI
(RFP gated)
0
1
2
3
4
1.0
2.4
1.3
1.4
1.3
3.2
PP7.5b-null
PP7.5b
rTetR.0
rTetR.v10
rTetR.v16
PP7.1b
no repression
(-dox)

Figure 5.3: Evaluation of TetR-gRNA(TetO) variants as CRISPRa druggable off-switch in Jurkat T cells. (**A**) Curated graphics of gRNA(TetO) +/- TetR variants and CRISPRa control (omitting CRISPRa transgene). (**B**) Experimental schema depicting transient transfection (EP) followed by overnight recovery in media +/- repressor, Dox. (**C**) quantified, normalized geometric mean fluorescent intensities from flow analysis of all cultures. All experimental samples are gated on live, RFP (CRISPRa transgene)$^{+}$ singlets only.

Figure 5.4

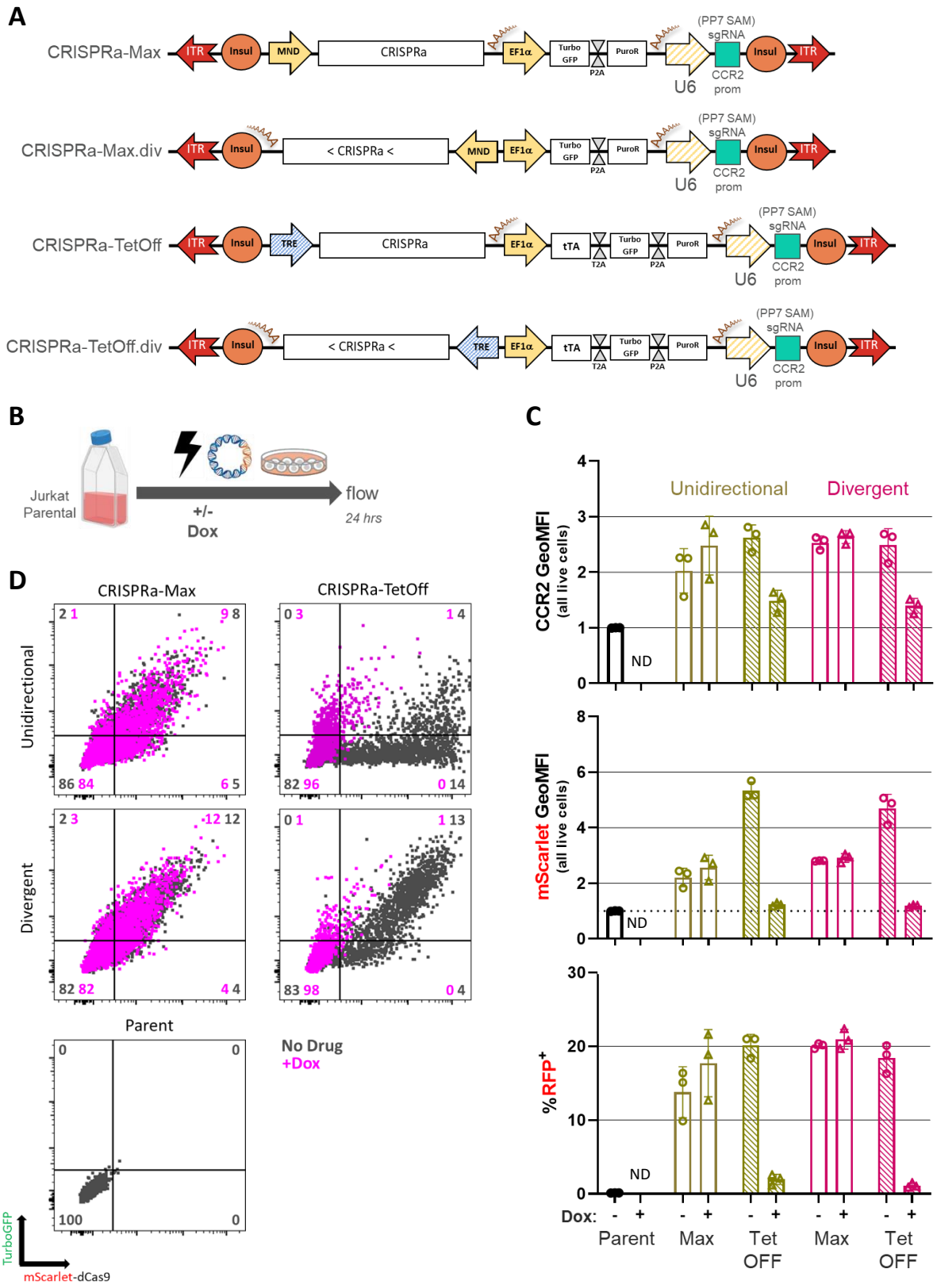
A
CRISPRa-Max
CRISPRa-Max.div
CRISPRa-TetOff
CRISPRa-TetOff.div
ITR
Insul
MND
TRE
CRISPRa
< CRISPRa <
EF1α
tTA
T2A
Turbo GFP
P2A
PuroR
(PP7 SAM) sgRNA
U6
CCR2 prom
B
Jurkat Parental
+/- Dox
flow
24 hrs
C
Unidirectional
Divergent
CCR2 GeoMFI (all live cells)
mScarlet GeoMFI (all live cells)
%RFP+
ND
Dox: - + - + - + - + - +
Parent
Max
Tet OFF
Max
Tet OFF
D
CRISPRa-Max
CRISPRa-TetOff
Unidirectional
Divergent
Parent
No Drug
+Dox
TurboGFP
mScarlet-dCas9

Figure 5.4: Evaluation of TetOff variants as CRISPRa druggable off-switch in Jurkat T cells. (**A**) Graphics of CRISPRa-Max vector and TetOff variants in both unidirectional and divergent configurations. (**B**) Experimental schema depicting transient transfection (EP) followed by overnight recovery in media +/- repressor, Dox. (**D**) Representative histograms and (**C**) quantified, normalized gMFI from flow analysis of all cultures. All experimental samples are gated on live singlets only. Portions of this data and graphics are duplicated in **Figure 3.5**.

Figure 5.5

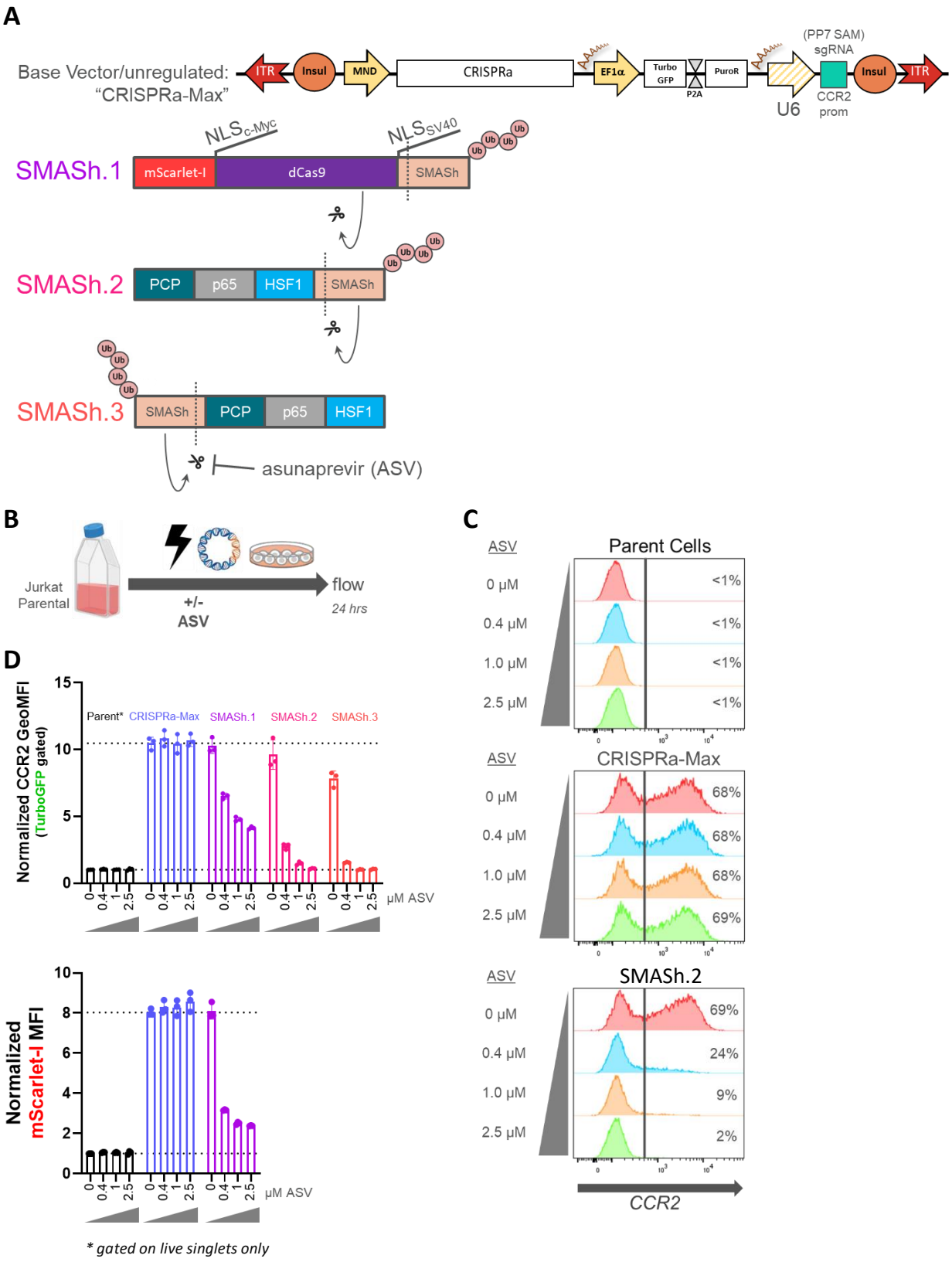

** gated on live singlets only*

Figure 5.5: Evaluation of SMASh variants as CRISPRa druggable off-switch in Jurkat T cells. (**A**) Graphics of CRISPRa-Max vector and subsequent genetic modification to the CRISPRa coding cassette. (**B**) Experimental schema depicting transient transfection (EP) followed by overnight recovery in media +/- repressor, asunaprevir (ASV). (**C**) Curated histograms and (**D**) quantified, normalized geometric mean fluorescent intensities from flow analysis of SMASh.2 cultures and relevant reference cultures. Experimental samples are gated on live, TurboGFP^{+} singlets, whereas parent cells are only gated on live singlets.

Figure 5.6

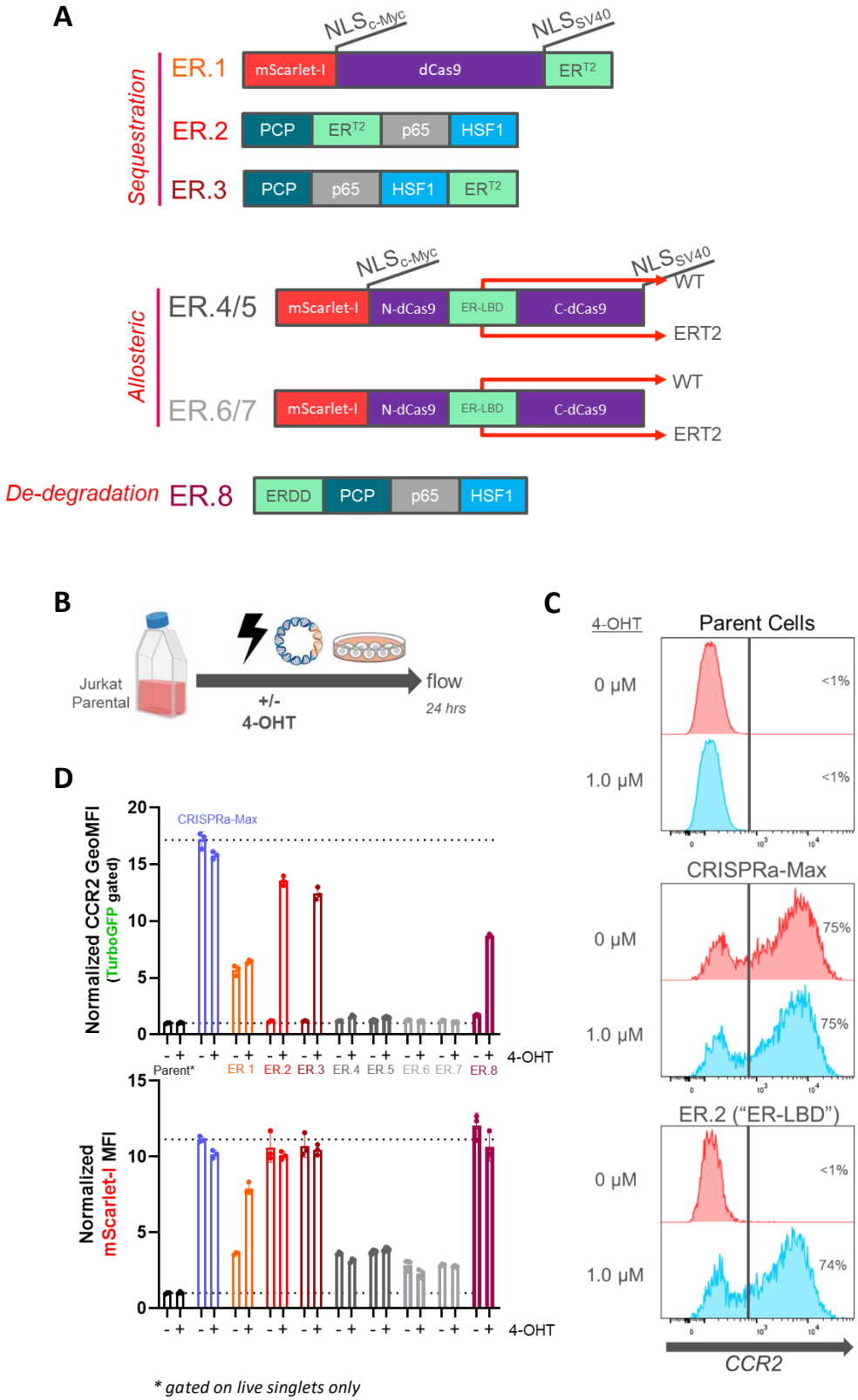
A
NLSc-Myc
NLSSV40
Sequestration
ER.1
mScarlet-I
dCas9
ERT2
ER.2
PCP
ERT2
p65
HSF1
ER.3
PCP
p65
HSF1
ERT2
Allosteric
ER.4/5
mScarlet-I
N-dCas9
ER-LBD
C-dCas9
WT
ERT2
ER.6/7
mScarlet-I
N-dCas9
ER-LBD
C-dCas9
WT
ERT2
De-degradation
ER.8
ERDD
PCP
p65
HSF1
B
Jurkat Parental
+/- 4-OHT
flow
24 hrs
C
4-OHT
Parent Cells
0 μM
<1%
1.0 μM
<1%
CRISPRa-Max
0 μM
75%
1.0 μM
75%
ER.2 ("ER-LBD")
0 μM
<1%
1.0 μM
74%
CCR2
D
Normalized CCR2 GeoMFI (TurboGFP gated)
CRISPRa-Max
Parent*
ER.1
ER.2
ER.3
ER.4
ER.5
ER.6
ER.7
ER.8
4-OHT
Normalized mScarlet-I MFI
4-OHT
* gated on live singlets only

Figure 5.6: Evaluation of ER-LBD variants as CRISPRa druggable on-switch in Jurkat T cells. (**A**) Graphics of CRISPRa-Max modifications, sorting into three suggested categories by reported mechanism of action. (**B**) Experimental schema depicting transient transfection (EP) followed by overnight recovery in media +/- inducer, tamoxifen (4-OHT). (**C**) Curated histograms and (**D**) quantified, normalized geometric mean fluorescent intensities from flow analysis of ER.2 cultures and relevant reference cultures. Experimental samples are gated on live, TurboGFP^{+} singlets, whereas parent cells are only gated on live singlets.

Figure 5.7

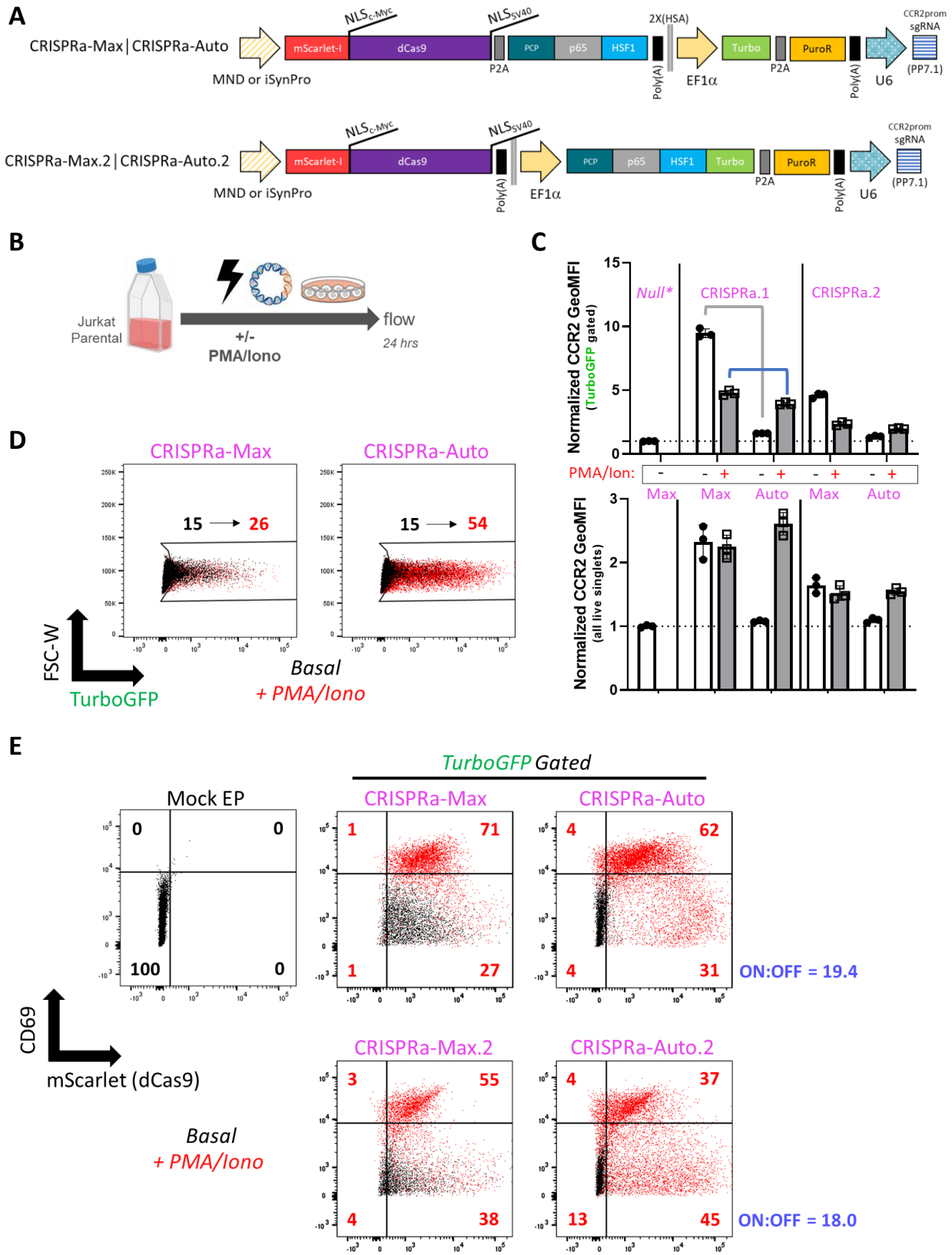
A
CRISPRa-Max | CRISPRa-Auto
MND or iSynPro
mScarlet-I
dCas9
PCP
p65
HSF1
P2A
2X(HSA)
Poly(A)
EF1α
Turbo
PuroR
U6
CCR2prom
sgRNA
(PP7.1)
CRISPRa-Max.2 | CRISPRa-Auto.2
B
Jurkat
Parental
+/-
PMA/Iono
flow
24 hrs
C
Normalized CCR2 GeoMFI
(TurboGFP gated)
Null*
CRISPRa.1
CRISPRa.2
PMA/Ion:
Max
Auto
Normalized CCR2 GeoMFI
(all live singlets)
D
CRISPRa-Max
CRISPRa-Auto
15 → 26
15 → 54
FSC-W
TurboGFP
Basal
+ PMA/Iono
E
TurboGFP Gated
Mock EP
CRISPRa-Max
CRISPRa-Auto
0
0
100
0
1
71
1
27
4
62
4
31
ON:OFF = 19.4
CD69
mScarlet (dCas9)
CRISPRa-Max.2
CRISPRa-Auto.2
3
55
4
38
4
37
13
45
ON:OFF = 18.0

Figure 5.7: Evaluation of a T cell - autologous CRISPRa switch in Jurkat T cells. A) Graphics of CRISPRa-Max (constitutive, ON) and CRISPRa-Auto (T cell autologous induction) variants, with alternate configuration of PPH. (**B**) Experimental schema depicting transient transfection (EP) followed by overnight recovery in media +/- T cell activation cocktail, phorbol myristate acetate and ionomycin (PMA/Iono). (**C**) Quantified, normalized geometric mean fluorescent intensities from flow analysis of CRISPR-Auto variants and references cultures with or without stimulation. (**D**) Flow plots reporting downstream transfection reporter, TurboGFP. (**E**) Flow plots reporting mScarlet and CD69 induction, as function of +/- PMA/Iono. Experimental samples are gated on live, TurboGFP^{+} singlets (upper C, D) as well as bulk live singlets only (C lower), whereas parent cells are only gated on live singlets throughout.

Figure 5.8

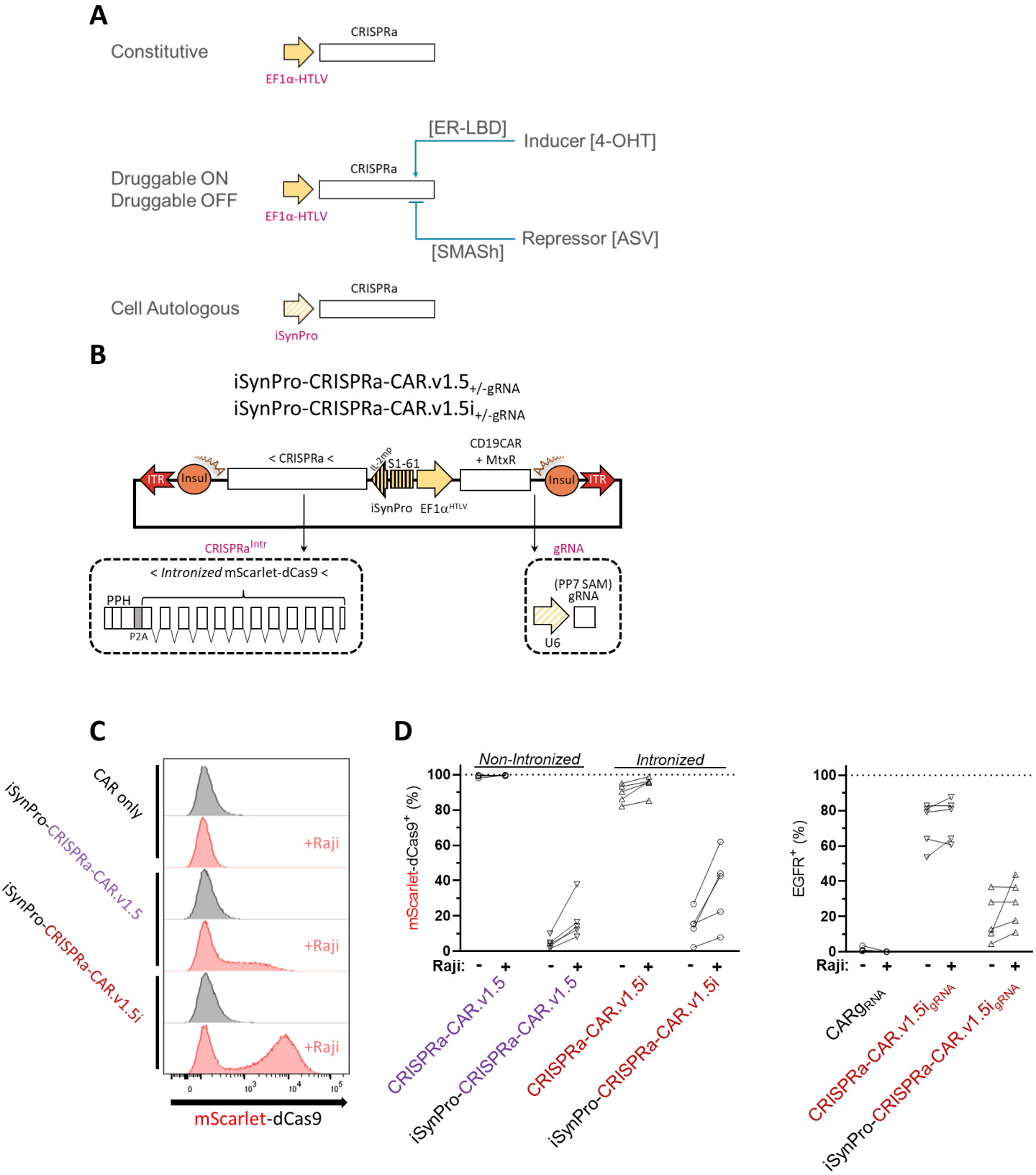
A
Constitutive
CRISPRa
EF1α-HTLV
Druggable ON
Druggable OFF
[ER-LBD]
Inducer [4-OHT]
CRISPRa
EF1α-HTLV
Repressor [ASV]
[SMASh]
Cell Autologous
CRISPRa
iSynPro
B
iSynPro-CRISPRa-CAR.v1.5+/-gRNA
iSynPro-CRISPRa-CAR.v1.5i+/-gRNA
< CRISPRa <
IL2rnp
S1-61
CD19CAR
+ MtxR
ITR
Insul
iSynPro
EF1α HTLV
CRISPRa Intr
< Intronized mScarlet-dCas9 <
PPH
P2A
gRNA
(PP7 SAM)
gRNA
U6
C
CAR only
+Raji
+Raji
+Raji
iSynPro-CRISPRa-CAR.v1.5
iSynPro-CRISPRa-CAR.v1.5i
mScarlet-dCas9
D
Non-Intronized
Intronized
mScarlet-dCas9+ (%)
Raji:
CRISPRa-CAR.v1.5
iSynPro-CRISPRa-CAR.v1.5
CRISPRa-CAR.v1.5i
iSynPro-CRISPRa-CAR.v1.5i
EGFR+ (%)
CARgRNA
CRISPRa-CAR.v1.5igRNA
iSynPro-CRISPRa-CAR.v1.5igRNA

Figure 5.8: Evaluation of a CAR-inducible CRISPRa in CAR T cells manufactured via EP-TICLE. (**A**) Graphical concept of multimodal CRISPRa control systems for use in primary CAR T cells. (**B**) Abridged donor plasmid maps of CRISPRa[AUTO]-CAR.v1.5 variants. (**C**) Flow cytometry mScarlet-Cas9 expression histogram of EP-TICLE $CD8^+$ T cells as a function of donor plasmid and Raji co-culture. (**D**) Quantification of mScarlet-dCas9 (*left*) and EGFR (*right*) EP-TICLE cell positivity as a function of donor plasmid and Raji co-culture status. Histograms in (C) and reported percentages in (D) are based on prior gating on $CD8^+$ live singlets. All experiments depicted here used 1:1 mixtures of $CD8^+$ and $CD4^+$ T cells as EP-TICLE input. Quantified data in (D) is compiled from cells generated from 4 - 5 human donors.

Figure 5.9

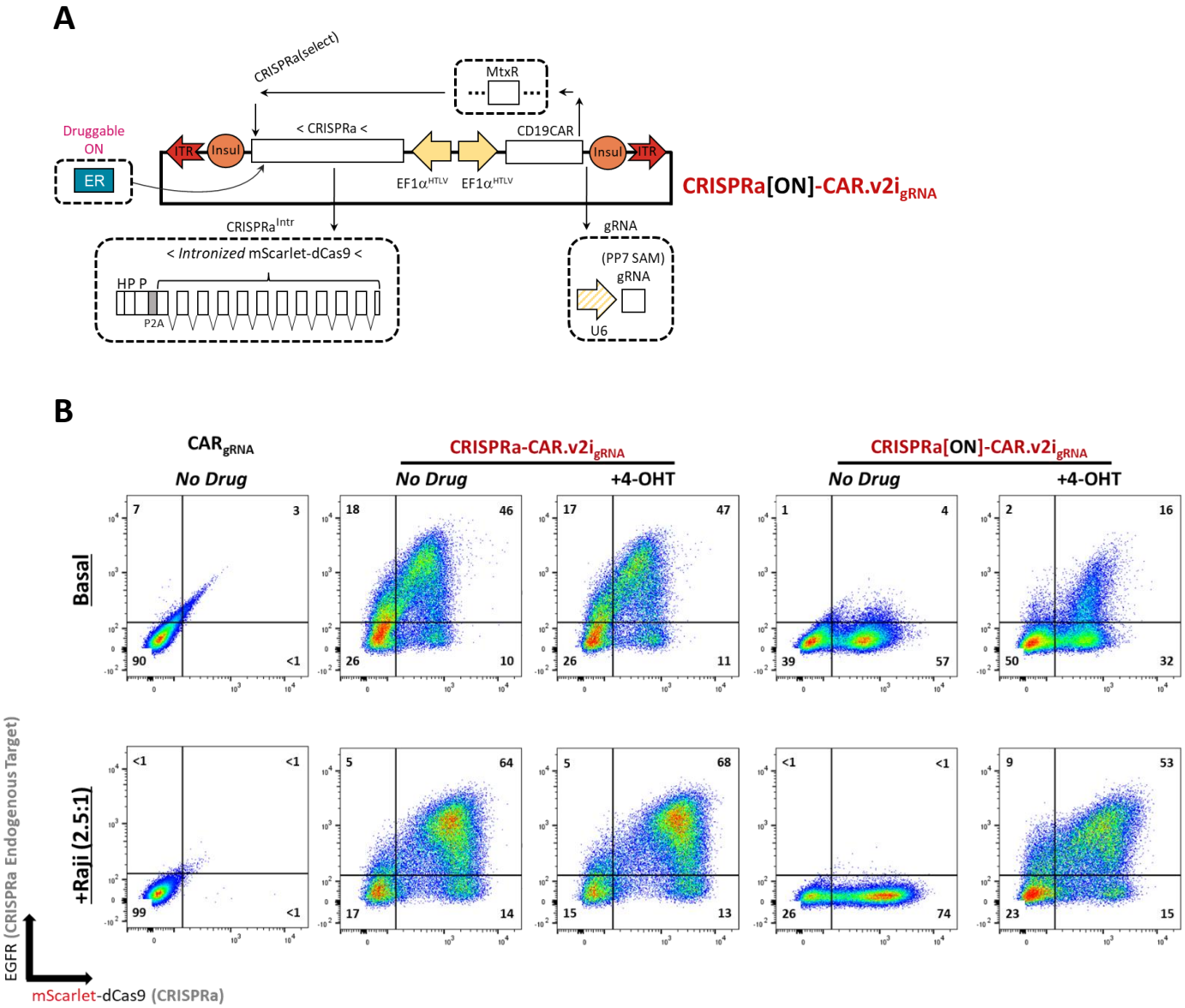
A
CRISPRa(select)
MtxR
Druggable
ON
ER
< CRISPRa <
CD19CAR
ITR
Insul
EF1α^HTLV
EF1α^HTLV
Insul
ITR
CRISPRa[ON]-CAR.v2i_gRNA
CRISPRa^Intr
< Intronized mScarlet-dCas9 <
HP P
P2A
gRNA
(PP7 SAM)
gRNA
U6
B
CAR_gRNA
CRISPRa-CAR.v2i_gRNA
CRISPRa[ON]-CAR.v2i_gRNA
No Drug
No Drug
+4-OHT
No Drug
+4-OHT
Basal
+Raji (2.5:1)
7
3
90
<1
18
46
26
10
17
47
26
11
1
4
39
57
2
16
50
32
<1
<1
99
<1
5
64
17
14
5
68
15
13
<1
<1
26
74
9
53
23
15
EGFR (CRISPRa Endogenous Target)
mScarlet-dCas9 (CRISPRa)

Figure 5.9: Evaluation of a drug-inducible CRISPRa in CAR T cells manufactured via EP-TICLE. (**A**) Abridged donor plasmid map of CRISPRa[ON]-CAR.v2i. (**B**) Bivariate mScarlet-Cas9 and EGFR expression of EP-TICLE T cells as a function of donor plasmid, 4-OHT, and Raji co-culture. Plots in (B) are based on prior gating on $CD4^+$ or $CD8^+$ live singlets. The experiment depicted here used 1:1 mixtures of $CD8^+$ and $CD4^+$ T cells from a single human donor as EP-TICLE input.

Chapter 6 | Future Directions and Concluding Remarks

In this work, I outlined studies to build and ultimately execute a genome-wide gain-of-function screen in CAR T cells. To realize that goal, I first optimized CRISPRa components in a T cell line. Like prior reports, I struggled to significantly increase gene overexpression beyond what was offered by conventional designs,[118] despite pursuing a variety of divergent strategies. Nevertheless, my experiments identified an improved CRISPRa reporter (tethered mScarlet) and component features (PCP, pure PP7 gRNA, c-Myc NLS) that increased successful identification of CRISPRa-competent cells and modestly bolstered overall activity (see **Chapter 2**).

In primary T cells, I successfully implemented a novel manufacturing method combining sequential transposon and lentiviral gene delivery, coupled with CAR-restricted expansion. This approach could generate >10^9 CRISPRa-CAR T cells – well above the cell requirements (10^7 - 10^8) needed for genome-scale screening. While literature review failed to enumerate estimates of documented primary CRISPRa or CRISPRa-CAR T cell yields, I nevertheless assess that established processes fall far short of cell requirements and/or activity levels. This conclusion is drawn from (1) prior reports of poor CRISPRa transgene delivery, (2) the dearth of published large-scale CRISPRa screening experiments and (3) the overabundance of reviews highlighting the utility of CRISPRa for next-generation T cell therapy development.[330–332] To overcome abbreviated CRISPRa activity, I pinpointed CRISPRa transgene silencing as a significant contributor, and my results further suggest that this phenomenon may occur across multiple gene delivery methods. By exchanging promoter species and orientation, I identified an emergent, silencing-resistant divergent dual promoter (EF1α-HTLV)$_2$ that enabled sustained,

durable CRISPRa activity across multiple T cell phenotypes and timescales of interest. Such performance will be necessary when deploying these cells to selection landscapes of considerable duration (e.g. serial tumor challenge) or transitioning to *in vivo* models. Notably, my studies also document the first known implementation of intronization to Cas9/dCas9 coding cassettes, delivered to primary human T cells (see **Chapter 3**).

This manufacturing and screening system was then demonstrated at genome-scale, producing $gRNA^{+}$ CRISPRa-CAR T cells that were assessed for homeostatic persistence and cytokine-free survival, via a pooled survival-based readout. Upon analysis, the screen successfully nominated pro-persistence genes with documented (MYC, IRF4, STATA, STATB, IL7R) or unidentified (GSE1, SERPINB9, DYM) roles in T cell proliferation. Likewise, my platform identified endogenous genes capable of enhancing cytokine-free survival (CSF2RB, STAT6, TNFRSF1A, TNFRSF1B), and aligned with a prior report of a mutated form of CSF2RB driving cytokine-independent growth in a patient case of T-ALL.[242] While genes identified through this screen await subsequent validation experiments, the list of preliminary hits serves to confirm known biology, and this greatly increases confidence in the predictive power of this novel system (see **Chapter 4**).

To broaden the use of the screening platform, I also profiled CRISPRa-CAR design adaptations that early results suggest may confer stringent druggability to the CRISPRa system using the FDA-approved inducer, 4-Hydroxytamoxifen (4-OHT). This system will further expand the scope of possible GoF screens by instituting global control of (1) timing, (2) periodicity, or (3) dosage. My drug-based system also provides the opportunity for time-matched inert reference pools derived from the same parent cultures; such a control is ideal for animal-based studies, with

most murine cell recovery procedures being terminal, and yielding cell quantities unsuitable for extensive sorting (see **Chapter 5**).

These processes and tools make possible many forms of GoF pooled screening in therapeutic T cells. In particular, generating pure populations of dCas9^{high} cells will obviate the need for sample-depleting sorting procedures where survival is a sufficient phenotype. Additionally, my gRNA designs for high content screening may eventually be coupled with more high-throughput single cell screening methods, to identity molecular phenotypes *in silico*, *post hoc* (see **Chapter 5**). I also expect that these manufacturing methods may form the basis of other CRISPR-based screening approaches, such as CRISPRi or dCas9-derivatives directed at the epigenome. Alternatively, I envision that these methods could enable multiplexed modulation readouts (CRISPRi x CRISPRa), or genome-scale CRISPR screening layered onto existing cell therapy designs for more tailored product development.

I anticipate future studies to examine dCas9 intron processing fidelity, and likely to nominate improved designs that maximize expression/durability of full-length dCas9 while minimizing DNA footprint. I also anticipate that future codon-optimization algorithms will emerge that more effectively curtail sequence-specific transgene silencing. Alternatively, I hypothesize that the targeted integration of CRISPRa-CAR coding cassettes into the loci of housekeeping genes is likely to be an effective, alternative means to overcome gene silencing.[333] Indeed, this is a worthwhile direction for future work permitted that inefficiencies in homology-directed repair can be overcome or sidestepped.

Further, while reports of Cas9 immunogenicity likely prohibit immediate direct clinical implementation of this system as a *bone fide* standalone CAR T cell therapy, I can conceive of *ex vivo* or *in vivo* cellular therapies that one day may operate using the sustained expression of a dCas9 derivative. Indeed, there are several pharmaceutical companies that exist today with this explicit product development aim.

In any eventuality, pooled screening methods will likely form a prominent component of drug discovery efforts for informing subsequent product development. Outside of CRISPR-based screening, the CAR-restricted expansion and distal lentiviral transduction methods outlined here suggest that T cell expansion and gene delivery potential remains untapped using conventional manufacturing methods. These are critical parameters for scale-up in pooled formats. I anticipate and hope that derivatives of the manufacturing and platform outlined here will ultimately quicken the pace of therapy advancement, and lead to more effective, durable treatments and hopefully cancer cures. I look forward to that time and am excited to watch the story unfold.

References

1. Siegel, R. L., Miller, K. D., Fuchs, H. E. & Jemal, A. Cancer statistics, 2022. *CA. Cancer J. Clin.* **72**, 7–33 (2022).
2. Maguire, F. B. *et al.* Evaluation of Cancer Deaths Attributable to Tobacco in California, 2014-2019. *JAMA Netw. Open* **5**, e2246651 (2022).
3. Miller, K. D. *et al.* Cancer treatment and survivorship statistics, 2022. *CA. Cancer J. Clin.* **72**, 409–436 (2022).
4. Henry, D. H. *et al.* Symptoms and treatment burden associated with cancer treatment: results from a cross-sectional national survey in the U.S. *Support. Care Cancer* **16**, 791–801 (2008).
5. Boffa, D. J. *et al.* Survival After Cancer Treatment at Top-Ranked US Cancer Hospitals vs Affiliates of Top-Ranked Cancer Hospitals. *JAMA Netw. Open* **3**, e203942 (2020).
6. National Academies of Sciences, E. Diagnosing and treating adult cancers and associated impairments. (2021).
7. Coley, W. B. II. Contribution to the Knowledge of Sarcoma. *Ann. Surg.* **14**, 199–220 (1891).
8. Burnet, M. Cancer—A Biological Approach. *Br. Med. J.* **1**, 779–786 (1957).
9. Ding, Z. *et al.* Personalized neoantigen pulsed dendritic cell vaccine for advanced lung cancer. *Signal Transduct. Target. Ther.* **6**, 1–12 (2021).
10. Seery, T. E. *et al. Overall survival in patients with metastatic or locally advanced pancreatic cancer following chemoradiation with novel combination of aldoxorubicin, N-803 IL-15 superagonist, and PDL1-NK cell therapy.* (American Society of Clinical Oncology, 2023).
11. Disis, M. L. (Nora) *et al.* Safety and Outcomes of a Plasmid DNA Vaccine Encoding the ERBB2 Intracellular Domain in Patients With Advanced-Stage ERBB2-Positive Breast Cancer: A Phase 1 Nonrandomized Clinical Trial. *JAMA Oncol.* **9**, 71–78 (2023).

12. Makkouk, A. & Weiner, G. Cancer Immunotherapy and Breaking Immune Tolerance-New Approaches to an Old Challenge. *Cancer Res.* **75**, 5–10 (2015).

13. Rosenberg, S. A. & Dudley, M. E. Cancer regression in patients with metastatic melanoma after the transfer of autologous antitumor lymphocytes. *Proc. Natl. Acad. Sci.* **101**, 14639–14645 (2004).

14. Overwijk, W. W. *et al.* Tumor Regression and Autoimmunity after Reversal of a Functionally Tolerant State of Self-reactive CD8+ T Cells. *J. Exp. Med.* **198**, 569–580 (2003).

15. Morgan, R. A. *et al.* Cancer Regression in Patients After Transfer of Genetically Engineered Lymphocytes. *Science* **314**, 126–129 (2006).

16. Slatkin, M. Linkage disequilibrium—understanding the evolutionary past and mapping the medical future. *Nat. Rev. Genet.* **9**, 477–485 (2008).

17. Brocker, T. Chimeric Fv-ζ or Fv-ε receptors are not sufficient to induce activation or cytokine production in peripheral T cells. *Blood* **96**, 1999–2001 (2000).

18. FDA, U. FDA approval brings first gene therapy to the United States. *CAR T-Cell Ther. Approv. Treat Certain Child. Young Adults B-Cell Acute Lymphoblastic Leuk. FDA USA* (2017).

19. Prasad, V. Tisagenlecleucel—the first approved CAR-T-cell therapy: implications for payers and policy makers. *Nat. Rev. Clin. Oncol.* **15**, 11–12 (2018).

20. Institute, N. C. *CAR T Cells: Engineering Patients' Immune Cells to Treat Their Cancers*. (2022).

21. Kamdar, M. *et al.* Lisocabtagene maraleucel (liso-cel), a CD19-directed chimeric antigen receptor (CAR) T cell therapy, versus standard of care (SOC) with salvage chemotherapy (CT) followed by autologous stem cell transplantation (ASCT) as second-line (2L) treatment in patients (Pts) with relapsed or refractory (R/R) large B-cell lymphoma (LBCL): results from the randomized phase 3 transform study. *Blood* **138**, 91 (2021).

22. Westin, J. & Sehn, L. H. CAR T cells as a second-line therapy for large B-cell lymphoma: a paradigm shift? *Blood J. Am. Soc. Hematol.* **139**, 2737–2746 (2022).

23. Yip, A. & Webster, R. M. The market for chimeric antigen receptor T cell therapies. *Nat Rev Drug Discov* **17**, 161–162 (2018).

24. Nam, S., Smith, J. & Yang, G. Driving the next wave of innovation in CAR T-cell therapies. *McKinsey Co.* (2019).

25. Young, C. M., Quinn, C. & Trusheim, M. R. Durable cell and gene therapy potential patient and financial impact: US projections of product approvals, patients treated, and product revenues. *Drug Discov. Today* **27**, 17–30 (2022).

26. Maude, S. L. *et al.* Chimeric antigen receptor T cells for sustained remissions in leukemia. *N. Engl. J. Med.* **371**, 1507–1517 (2014).

27. Gardner, R. A. *et al.* Intent-to-treat leukemia remission by CD19 CAR T cells of defined formulation and dose in children and young adults. *Blood* **129**, 3322–3331 (2017).

28. Singh, N., Frey, N. V., Grupp, S. A. & Maude, S. L. CAR T cell therapy in acute lymphoblastic leukemia and potential for chronic lymphocytic leukemia. *Curr. Treat. Options Oncol.* **17**, 28 (2016).

29. Melenhorst, J. J. *et al.* Decade-long leukaemia remissions with persistence of CD4+ CAR T cells. *Nature* **602**, 503–509 (2022).

30. Zhang, C. *et al.* Phase I Escalating-Dose Trial of CAR-T Therapy Targeting CEA+ Metastatic Colorectal Cancers. *Mol. Ther.* **25**, 1248–1258 (2017).

31. Reinhard, K. *et al.* An RNA vaccine drives expansion and efficacy of claudin-CAR-T cells against solid tumors. *Science* **367**, 446–453 (2020).

32. Feng, Z. *et al.* Potent suppression of neuroendocrine tumors and gastrointestinal cancers by CDH17CAR T cells without toxicity to normal tissues. *Nat. Cancer* **3**, 581–594 (2022).

33. Morgan, R. A. *et al.* Case Report of a Serious Adverse Event Following the Administration of T Cells Transduced With a Chimeric Antigen Receptor Recognizing ERBB2. *Mol. Ther.* **18**, 843–851 (2010).

34. Moon, E. K. *et al.* Multifactorial T-cell hypofunction that is reversible can limit the efficacy of chimeric antigen receptor–transduced human T cells in solid tumors. *Clin. Cancer Res.* **20**, 4262–4273 (2014).

35. Park, J. H., Geyer, M. B. & Brentjens, R. J. CD19-targeted CAR T-cell therapeutics for hematologic malignancies: interpreting clinical outcomes to date. *Blood J. Am. Soc. Hematol.* **127**, 3312–3320 (2016).

36. Haas, A. R. *et al.* Phase I Study of Lentiviral-Transduced Chimeric Antigen Receptor-Modified T Cells Recognizing Mesothelin in Advanced Solid Cancers. *Mol. Ther.* **27**, 1919–1929 (2019).

37. Lin, Y. *et al.* Phase I clinical trial of PD-1 knockout anti-MUC1 CAR-T cells in the treatment of patients with non-small cell lung cancer. *Ann. Oncol.* **30**, xi12 (2019).

38. Singh, N., Perazzelli, J., Grupp, S. A. & Barrett, D. M. Early memory phenotypes drive T cell proliferation in patients with pediatric malignancies. *Sci. Transl. Med.* **8**, 320ra3-320ra3 (2016).

39. Krenciute, G., Balyasnikova, I., Dotti, G. & Gottschalk, S. 76. Transgenic Expression of IL15 Improves Antiglioma Activity of IL13Rα2-CAR T Cells. *Mol. Ther.* **24**, S33 (2016).

40. Orlando, E. J. *et al.* Genetic mechanisms of target antigen loss in CAR19 therapy of acute lymphoblastic leukemia. *Nat. Med.* **24**, 1504–1506 (2018).

41. Schuster, S. J. *et al.* Global Pivotal Phase 2 trial of the CD19-targeted therapy CTL019 in adult patients with relapsed or refractory (R/R) diffuse large B-cell lymphoma (DLBCL)—an interim analysis. *Hematol. Oncol.* **35**, 27–27 (2017).

42. Mirzaei, H. R., Rodriguez, A., Shepphird, J., Brown, C. E. & Badie, B. Chimeric antigen receptors T cell therapy in solid tumor: challenges and clinical applications. *Front. Immunol.* **8**, 1850 (2017).

43. Knochelmann, H. M. *et al.* CAR T cells in solid tumors: blueprints for building effective therapies. *Front. Immunol.* **9**, 1740 (2018).

44. Oda, S. K. *et al.* A CD200R-CD28 fusion protein appropriates an inhibitory signal to enhance T-cell function and therapy of murine leukemia. *Blood J. Am. Soc. Hematol.* **130**, 2410–2419 (2017).

45. Kloss, C. C. *et al.* Dominant-negative TGF-β receptor enhances PSMA-targeted human CAR T cell proliferation and augments prostate cancer eradication. *Mol. Ther.* **26**, 1855–1866 (2018).

46. Lynn, R. C. *et al.* c-Jun overexpression in CAR T cells induces exhaustion resistance. *Nature* **576**, 293–300 (2019).

47. Batra, S. A. *et al.* Glypican-3–Specific CAR T Cells Coexpressing IL15 and IL21 Have Superior Expansion and Antitumor Activity against Hepatocellular CarcinomaIL15 and IL21 Armored GPC3-CAR T Cells against Liver Cancer. *Cancer Immunol. Res.* **8**, 309–320 (2020).

48. Cimons, J., Kohler, M. E., Yarnell, M. & Fry, T. J. Overexpression of Rorγt in CAR T Cells Improves Persistence and Reduces Exhaustion. *Blood* **138**, 2801 (2021).

49. Wherry, E. J. T cell exhaustion. *Nat. Immunol.* **12**, 492–499 (2011).

50. Chow, A., Perica, K., Klebanoff, C. A. & Wolchok, J. D. Clinical implications of T cell exhaustion for cancer immunotherapy. *Nat. Rev. Clin. Oncol.* **19**, 775–790 (2022).

51. Belk, J. A., Daniel, B. & Satpathy, A. T. Epigenetic regulation of T cell exhaustion. *Nat. Immunol.* **23**, 848–860 (2022).

52. Delgoffe, G. M. *et al.* The role of exhaustion in CAR T cell therapy. *Cancer Cell* **39**, 885–888 (2021).

53. Anderson, A. C., Joller, N. & Kuchroo, V. K. Lag-3, Tim-3, and TIGIT: co-inhibitory receptors with specialized functions in immune regulation. *Immunity* **44**, 989–1004 (2016).

54. Sasidharan Nair, V. *et al.* DNA methylation and repressive H3K9 and H3K27 trimethylation in the promoter regions of PD-1, CTLA-4, TIM-3, LAG-3, TIGIT, and PD-L1 genes in human primary breast cancer. *Clin. Epigenetics* **10**, 1–12 (2018).

55. Lee, Y.-H. *et al.* PD-1 and TIGIT downregulation distinctly affect the effector and early memory phenotypes of CD19-targeting CAR T cells. *Mol. Ther.* **30**, 579–592 (2022).

56. McKinney, E. F., Lee, J. C., Jayne, D. R., Lyons, P. A. & Smith, K. G. T-cell exhaustion, co-stimulation and clinical outcome in autoimmunity and infection. *Nature* **523**, 612–616 (2015).

57. Young, A., Quandt, Z. & Bluestone, J. A. The balancing act between cancer immunity and autoimmunity in response to immunotherapy. *Cancer Immunol. Res.* **6**, 1445–1452 (2018).

58. Weber, E. W. *et al.* Transient rest restores functionality in exhausted CAR-T cells through epigenetic remodeling. *Science* **372**, eaba1786 (2021).

59. Zebley, C. C. & Youngblood, B. CAR T cells need a pitstop to win the race. *Cancer Cell* **39**, 756–758 (2021).

60. Gu, X., He, D., Li, C., Wang, H. & Yang, G. Development of inducible CD19-CAR T cells with a Tet-on system for controlled activity and enhanced clinical safety. *Int. J. Mol. Sci.* **19**, 3455 (2018).

61. Viaud, S. *et al.* Switchable control over in vivo CAR T expansion, B cell depletion, and induction of memory. *Proc. Natl. Acad. Sci.* **115**, E10898–E10906 (2018).

62. Juillerat, A. *et al.* Modulation of chimeric antigen receptor surface expression by a small molecule switch. *BMC Biotechnol.* **19**, 1–9 (2019).

63. Leung, W.-H. *et al.* Sensitive and adaptable pharmacological control of CAR T cells through extracellular receptor dimerization. *JCI Insight* **4**, (2019).

64. Richman, S. A. *et al.* Ligand-induced degradation of a CAR permits reversible remote control of CAR T cell activity in vitro and in vivo. *Mol. Ther.* **28**, 1600–1613 (2020).

65. Li, H. *et al.* Overcome trastuzumab resistance of breast cancer using anti-HER2 chimeric antigen receptor T cells and PD1 blockade. *Am. J. Cancer Res.* **10**, 688 (2020).

66. Agarwal, S. *et al.* Disruption of cell-intrinsic checkpoint regulator CTLA-4 in CD19 directed CAR T cells provides clinical efficacy in CLL patients. *Cancer Res.* **82**, 5571–5571 (2022).

67. Hargadon, K. M., Johnson, C. E. & Williams, C. J. Immune checkpoint blockade therapy for cancer: an overview of FDA-approved immune checkpoint inhibitors. *Int. Immunopharmacol.* **62**, 29–39 (2018).

68. Lozano, A. X. *et al.* T cell characteristics associated with toxicity to immune checkpoint blockade in patients with melanoma. *Nat. Med.* **28**, 353–362 (2022).

69. Liu, H. *et al.* CD19-specific CAR T Cells that Express a PD-1/CD28 Chimeric Switch-Receptor are Effective in Patients with PD-L1–positive B-Cell LymphomaA Novel CD19 CAR T Therapy for B-Cell Lymphoma. *Clin. Cancer Res.* **27**, 473–484 (2021).

70. Zhao, S. *et al.* Switch receptor T3/28 improves long-term persistence and antitumor efficacy of CAR-T cells. *J. Immunother. Cancer* **9**, (2021).

71. Oda, S. K. *et al.* A Fas-4-1BB fusion protein converts a death to a pro-survival signal and enhances T cell therapy. *J. Exp. Med.* **217**, e20191166 (2020).

72. Anderson, K. G. *et al.* Engineering adoptive T cell therapy to co-opt Fas ligand-mediated death signaling in ovarian cancer enhances therapeutic efficacy. *J. Immunother. Cancer* **10**, (2022).

73. Qin, L. *et al.* Co-expression of a PD-L1-specific chimeric switch receptor augments the efficacy and persistence of CAR T cells via the CD70-CD27 axis. *Nat. Commun.* **13**, 6051 (2022).

74. Gerlach, C. *et al.* Heterogeneous Differentiation Patterns of Individual CD8+ T Cells. *Science* **340**, 635–639 (2013).

75. Saravia, J., Chapman, N. M. & Chi, H. Helper T cell differentiation. *Cell. Mol. Immunol.* **16**, 634–643 (2019).

76. Garcia-Perez, L. *et al.* Functional definition of a transcription factor hierarchy regulating T cell lineage commitment. *Sci. Adv.* **6**, eaaw7313 (2020).

77. Jensen, M. C. & Riddell, S. R. Design and implementation of adoptive therapy with chimeric antigen receptor-modified T cells. *Immunol. Rev.* **257**, 127–144 (2014).

78. Wang, X. *et al.* Phase 1 studies of central memory–derived CD19 CAR T–cell therapy following autologous HSCT in patients with B-cell NHL. *Blood J. Am. Soc. Hematol.* **127**, 2980–2990 (2016).

79. Fraietta, J. A. *et al.* Determinants of response and resistance to CD19 chimeric antigen receptor (CAR) T cell therapy of chronic lymphocytic leukemia. *Nat. Med.* **24**, 563–571 (2018).

80. Kotani, H. *et al.* Aged CAR T cells exhibit enhanced cytotoxicity and effector function but shorter persistence and less memory-like phenotypes. *Blood* **132**, 2047 (2018).

81. Biasco, L. *et al.* Clonal expansion of T memory stem cells determines early anti-leukemic responses and long-term CAR T cell persistence in patients. *Nat. Cancer* **2**, 629–642 (2021).

82. Arcangeli, S. *et al.* CAR T cell manufacturing from naive/stem memory T lymphocytes enhances antitumor responses while curtailing cytokine release syndrome. *J. Clin. Invest.* **132**, (2022).

83. Li, L. *et al.* Transgenic expression of IL-7 regulates CAR-T cell metabolism and enhances in vivo persistence against tumor cells. *Sci. Rep.* **12**, 12506 (2022).

84. Kiesgen, S., Messinger, J. C., Chintala, N. K., Tano, Z. & Adusumilli, P. S. Comparative analysis of assays to measure CAR T cell–mediated cytotoxicity. *Nat. Protoc.* **16**, 1331–1342 (2021).

85. Ye, L. *et al.* A genome-scale gain-of-function CRISPR screen in CD8 T cells identifies proline metabolism as a means to enhance CAR-T therapy. *Cell Metab.* **34**, 595-614.e14 (2022).

86. Schmidt, R. *et al.* CRISPR activation and interference screens decode stimulation responses in primary human T cells. *Science* **375**, eabj4008 (2022).

87. Goodman, D. B. *et al.* Pooled screening of CAR T cells identifies diverse immune signaling domains for next-generation immunotherapies. *Sci. Transl. Med.* **14**, eabm1463 (2022).

88. Atkins, R. M., Menges, M. A., Bauer, A., Turner, J. G. & Locke, F. L. Metabolically Flexible CAR T Cells (mfCAR-T), with Constitutive Expression of PGC-1α Resistant to Post Translational Modifications, Exhibit Superior Survival and Function in Vitro. *Blood* **136**, 30 (2020).

89. Kondo, T. *et al.* The NOTCH–FOXM1 Axis Plays a Key Role in Mitochondrial Biogenesis in the Induction of Human Stem Cell Memory–like CAR-T Cells. *Cancer Res.* **80**, 471–483 (2020).

90. Veliça, P. *et al.* Modified Hypoxia-Inducible Factor Expression in CD8+ T Cells Increases Antitumor Efficacy. *Cancer Immunol. Res.* **9**, 401–414 (2021).

91. Juillerat, A. *et al.* An oxygen sensitive self-decision making engineered CAR T-cell. *Sci. Rep.* **7**, 39833 (2017).

92. Kosti, P. *et al.* Hypoxia-sensing CAR T cells provide safety and efficacy in treating solid tumors. *Cell Rep. Med.* **2**, 100227 (2021).

93. Castellanos-Rueda, R. *et al.* speedingCARs: accelerating the engineering of CAR T cells by signaling domain shuffling and single-cell sequencing. *Nat. Commun.* **13**, 6555 (2022).

94. Roth, T. L. *et al.* Pooled Knockin Targeting for Genome Engineering of Cellular Immunotherapies. *Cell* **181**, 728-744.e21 (2020).

95. Legut, M. *et al.* A genome-scale screen for synthetic drivers of T cell proliferation. *Nature* **603**, 728–735 (2022).

96. Krehenwinkel, H. *et al.* Estimating and mitigating amplification bias in qualitative and quantitative arthropod metabarcoding. *Sci. Rep.* **7**, 17668 (2017).

97. Shifrut, E. *et al.* Genome-wide CRISPR Screens in Primary Human T Cells Reveal Key Regulators of Immune Function. *Cell* **175**, 1958-1971.e15 (2018).

98. Carnevale, J. *et al.* RASA2 ablation in T cells boosts antigen sensitivity and long-term function. *Nature* **609**, 174–182 (2022).

99. Gilbert, L. A. *et al.* Genome-scale CRISPR-mediated control of gene repression and activation. *Cell* **159**, 647–661 (2014).

100. Hilton, I. B. *et al.* Epigenome editing by a CRISPR-Cas9-based acetyltransferase activates genes from promoters and enhancers. *Nat. Biotechnol.* **33**, 510–517 (2015).

101. La Russa, M. F. & Qi, L. S. The New State of the Art: Cas9 for Gene Activation and Repression. *Mol. Cell. Biol.* **35**, 3800–3809 (2015).

102. Jinek, M. *et al.* A Programmable Dual-RNA–Guided DNA Endonuclease in Adaptive Bacterial Immunity. *Science* **337**, 816–821 (2012).

103. Qi, L. S. *et al.* Repurposing CRISPR as an RNA-guided platform for sequence-specific control of gene expression. *Cell* **152**, 1173–1183 (2013).

104. Mali, P. *et al.* CAS9 transcriptional activators for target specificity screening and paired nickases for cooperative genome engineering. *Nat. Biotechnol.* **31**, 833–838 (2013).

105. Wong, N., Liu, W. & Wang, X. WU-CRISPR: characteristics of functional guide RNAs for the CRISPR/Cas9 system. *Genome Biol.* **16**, 1–8 (2015).

106. Radzisheuskaya, A., Shlyueva, D., Müller, I. & Helin, K. Optimizing sgRNA position markedly improves the efficiency of CRISPR/dCas9-mediated transcriptional repression. *Nucleic Acids Res.* **44**, e141–e141 (2016).

107. Dong, C., Fontana, J., Patel, A., Carothers, J. M. & Zalatan, J. G. Synthetic CRISPR-Cas gene activators for transcriptional reprogramming in bacteria. *Nat. Commun.* **9**, 2489 (2018).

108. Fontana, J. *et al.* Effective CRISPRa-mediated control of gene expression in bacteria must overcome strict target site requirements. *Nat. Commun.* **11**, 1618 (2020).

109. Hsu, P. D. *et al.* DNA targeting specificity of RNA-guided Cas9 nucleases. *Nat. Biotechnol.* **31**, 827–832 (2013).

110. Veres, A. *et al.* Low incidence of off-target mutations in individual CRISPR-Cas9 and TALEN targeted human stem cell clones detected by whole-genome sequencing. *Cell Stem Cell* **15**, 27–30 (2014).

111. Hartenian, E. & Doench, J. G. Genetic screens and functional genomics using CRISPR/Cas9 technology. *FEBS J.* **282**, 1383–1393 (2015).

112. Doench, J. G. *et al.* Optimized sgRNA design to maximize activity and minimize off-target effects of CRISPR-Cas9. *Nat. Biotechnol.* **34**, 184–191 (2016).

113. Hirao, I., Spingola, M., Peabody, D. & Ellington, A. D. The limits of specificity: an experimental analysis with RNA aptamers to MS2 coat protein variants. *Mol. Divers.* **4**, 75–89 (1998).

114. Li, Z. *et al.* A potent Cas9-derived gene activator for plant and mammalian cells. *Nat. Plants* **3**, 930–936 (2017).

115. Konermann, S. *et al.* Genome-scale transcriptional activation by an engineered CRISPR-Cas9 complex. *Nature* **517**, 583–588 (2015).

116. Chavez, A. *et al.* Highly efficient Cas9-mediated transcriptional programming. *Nat. Methods* **12**, 326–328 (2015).

117. Zalatan, J. G. *et al.* Engineering Complex Synthetic Transcriptional Programs with CRISPR RNA Scaffolds. *Cell* **160**, 339–350 (2015).

118. Chavez, A. *et al.* Comparison of Cas9 activators in multiple species. *Nat. Methods* **13**, 563–567 (2016).

119. Klanschnig, M., Cserjan-Puschmann, M., Striedner, G. & Grabherr, R. CRISPRactivation-SMS, a message for PAM sequence independent gene up-regulation in Escherichia coli. *Nucleic Acids Res.* **50**, 10772–10784 (2022).

120. Ottina, E. *et al.* DNA-binding of the Tet-transactivator curtails antigen-induced lymphocyte activation in mice. *Nat. Commun.* **8**, 1–12 (2017).

121. Jia, Y. *et al.* Next-generation CRISPR/Cas9 transcriptional activation in Drosophila using flySAM. *Proc. Natl. Acad. Sci.* **115**, 4719–4724 (2018).

122. Cho, S. *et al.* High-level dCas9 expression induces abnormal cell morphology in Escherichia coli. *ACS Synth. Biol.* **7**, 1085–1094 (2018).

123. Cui, L. *et al.* A CRISPRi screen in E. coli reveals sequence-specific toxicity of dCas9. *Nat. Commun.* **9**, 1912 (2018).

124. Tang, F. *et al.* mRNA-Seq whole-transcriptome analysis of a single cell. *Nat. Methods* **6**, 377–382 (2009).

125. Mimitou, E. P. *et al.* Multiplexed detection of proteins, transcriptomes, clonotypes and CRISPR perturbations in single cells. *Nat. Methods* **16**, 409–412 (2019).

126. Gao, S. *et al.* Single-cell RNA sequencing coupled to TCR profiling of large granular lymphocyte leukemia T cells. *Nat. Commun.* **13**, 1982 (2022).

127. Stoeckius, M. *et al.* Simultaneous epitope and transcriptome measurement in single cells. *Nat. Methods* **14**, 865–868 (2017).

128. Adamson, B. *et al.* A Multiplexed Single-Cell CRISPR Screening Platform Enables Systematic Dissection of the Unfolded Protein Response. *Cell* **167**, 1867-1882.e21 (2016).

129. Replogle, J. M. *et al.* Combinatorial single-cell CRISPR screens by direct guide RNA capture and targeted sequencing. *Nat. Biotechnol.* **38**, 954–961 (2020).

130. Choo, X. Y. *et al.* Evaluating Capture Sequence Performance for Single-Cell CRISPR Activation Experiments. *ACS Synth. Biol.* **10**, 640–645 (2021).

131. Song, Q. *et al.* Direct-seq: programmed gRNA scaffold for streamlined scRNA-seq in CRISPR screen. *Genome Biol.* **21**, 136 (2020).

132. Datlinger, P. *et al.* Pooled CRISPR screening with single-cell transcriptome readout. *Nat. Methods* **14**, 297–301 (2017).

133. Schwenk, H.-U. & Schneider, U. Cell cycle dependency of a T-cell marker on lymphoblasts. *Blut Z. Für Gesamte Blutforsch.* **31**, 299–306 (1975).

134. Schneider, U., Schwenk, H.-U. & Bornkamm, G. Characterization of EBV-genome negative “null” and “T” cell lines derived from children with acute lymphoblastic leukemia and leukemic transformed non-Hodgkin lymphoma. *Int. J. Cancer* **19**, 621–626 (1977).

135. Fidanza, A. *et al.* An all-in-one UniSam vector system for efficient gene activation. *Sci. Rep.* **7**, 6394 (2017).

136. Challita, P. M. *et al.* Multiple modifications in cis elements of the long terminal repeat of retroviral vectors lead to increased expression and decreased DNA methylation in embryonic carcinoma cells. *J. Virol.* **69**, 748–755 (1995).

137. Vara, J. A., Portela, A., Ortìn, J. & Jimènez, A. Expression in mammalian cells of a gene from Streptomyces alboniger conferring puromycin resistance. *Nucleic Acids Res.* **14**, 4617–4624 (1986).

138. Jonnalagadda, M. *et al.* Engineering Human T Cells for Resistance to Methotrexate and Mycophenolate Mofetil as an In Vivo Cell Selection Strategy. *PLOS ONE* **8**, e65519 (2013).

139. Gerby, B. *et al.* Optimized gene transfer into human primary leukemic T cell with NOD-SCID/leukemia-initiating cell activity. *Leukemia* **24**, 646–649 (2010).

140. Stavrou, E. F. *et al.* The β-globin Replicator greatly enhances the potential of S/MAR based episomal vectors for gene transfer into human haematopoietic progenitor cells. *Sci. Rep.* **7**, 1–15 (2017).

141. Monjezi, R. *et al.* Enhanced CAR T-cell engineering using non-viral Sleeping Beauty transposition from minicircle vectors. *Leukemia* **31**, 186–194 (2017).

142. Rad SM, A. H., Poudel, A., Tan, G. M. Y. & McLellan, A. D. Promoter choice: Who should drive the CAR in T cells? *PLoS One* **15**, e0232915 (2020).

143. Ho, J.-Y. *et al.* Promoter usage regulating the surface density of CAR molecules may modulate the kinetics of CAR-T cells in vivo. *Mol. Ther.-Methods Clin. Dev.* **21**, 237–246 (2021).

144. Emery, D. W. The Use of Chromatin Insulators to Improve the Expression and Safety of Integrating Gene Transfer Vectors. *Hum. Gene Ther.* **22**, 761–774 (2011).

145. Mossine, V. V., Waters, J. K., Hannink, M. & Mawhinney, T. P. piggyBac Transposon plus Insulators Overcome Epigenetic Silencing to Provide for Stable Signaling Pathway Reporter Cell Lines. *PLoS ONE* **8**, e85494 (2013).

146. MoyrOn-QuirOz, J. E., Partida-Sánchez, S., Donís-Hernández, R., Sandoval-Montes, C. & Santos-Argumedo, L. Expression and Function of CD22, a B-cell Restricted Molecule*. *Scand. J. Immunol.* **55**, 343–351 (2002).

147. Sallusto, F. *et al.* Switch in chemokine receptor expression upon TCR stimulation reveals novel homing potential for recently activated T cells. *Eur. J. Immunol.* **29**, 2037–2045 (1999).

148. Rabin, R. L. *et al.* Chemokine receptor responses on T cells are achieved through regulation of both receptor expression and signaling. *J. Immunol. Baltim. Md 1950* **162**, 3840–3850 (1999).

149. Gao, S. Y., Jack, M. M. & O'Neill, C. Towards Optimising the Production of and Expression from Polycistronic Vectors in Embryonic Stem Cells. *PLOS ONE* **7**, e48668 (2012).

150. Liu, Z. *et al.* Systematic comparison of 2A peptides for cloning multi-genes in a polycistronic vector. *Sci. Rep.* **7**, 2193 (2017).

151. Martella, A. *et al.* Systematic Evaluation of CRISPRa and CRISPRi Modalities Enables Development of a Multiplexed, Orthogonal Gene Activation and Repression System. *ACS Synth. Biol.* **8**, 1998–2006 (2019).

152. Bajar, B. T. *et al.* Improving brightness and photostability of green and red fluorescent proteins for live cell imaging and FRET reporting. *Sci. Rep.* **6**, 20889 (2016).

153. Bindels, D. S. *et al.* mScarlet: a bright monomeric red fluorescent protein for cellular imaging. *Nat. Methods* **14**, 53–56 (2017).

154. Sanson, K. R. *et al.* Optimized libraries for CRISPR-Cas9 genetic screens with multiple modalities. *Nat. Commun.* **9**, 1–15 (2018).

155. Goodale, A. B. An Interrogation of ORF Versus CRISPRa Pooled-Screening Technologies Used to Define Cancer Drug-Resistance Landscapes. (2020).

156. Cong, L. *et al.* Multiplex genome engineering using CRISPR/Cas systems. *Science* **339**, 819–823 (2013).

157. Mali, P. *et al.* RNA-guided human genome engineering via Cas9. *Science* **339**, 823–826 (2013).

158. Shen, B. *et al.* Generation of gene-modified mice via Cas9/RNA-mediated gene targeting. *Cell Res.* **23**, 720–723 (2013).

159. Kalderon, D., Roberts, B. L., Richardson, W. D. & Smith, A. E. A short amino acid sequence able to specify nuclear location. *Cell* **39**, 499–509 (1984).

160. Dang, C. V. & Lee, Wm. Identification of the human c-myc protein nuclear translocation signal. *Mol. Cell. Biol.* **8**, 4048–4054 (1988).

161. Ray, M., Tang, R., Jiang, Z. & Rotello, V. M. Quantitative tracking of protein trafficking to the nucleus using cytosolic protein delivery by nanoparticle-stabilized nanocapsules. *Bioconjug. Chem.* **26**, 1004–1007 (2015).

162. Backstrom, J. R., Sheng, J., Wang, M. C., Bernardo-Colón, A. & Rex, T. S. Optimization of S. aureus dCas9 and CRISPRi elements for a single adeno-associated virus that targets an endogenous gene. *Mol. Ther.-Methods Clin. Dev.* **19**, 139–148 (2020).

163. Gier, R. A. *et al.* High-performance CRISPR-Cas12a genome editing for combinatorial genetic screening. *Nat. Commun.* **11**, 3455 (2020).

164. Lim, F. & Peabody, D. S. RNA recognition site of PP7 coat protein. *Nucleic Acids Res.* **30**, 4138–4144 (2002).

165. Zhu, S. *et al.* Guide RNAs with embedded barcodes boost CRISPR-pooled screens. *Genome Biol.* **20**, 20 (2019).

166. Yang, X.-D., Tajkhorshid, E. & Chen, L.-F. Functional interplay between acetylation and methylation of the RelA subunit of NF-κB. *Mol. Cell. Biol.* **30**, 2170–2180 (2010).

167. He, Z., Zhao, J., Zhang, J., Jung, J. U. & Feng, P. NF-κB Activation Coordinated by IKKβ and IKKε Enables Latent Infection of Kaposi's Sarcoma-Associated Herpesvirus. *J. Virol.* **88**, 444–455 (2014).

168. Jensen, M. C., OOI, T. & Wei, J. Chimeric transcription factor variants with augmented sensitivity to drug ligand induction of transgene expression in mammalian cells. (2018).

169. Gemmill, D., D'souza, S., Meier-Stephenson, V. & Patel, T. R. Current approaches for RNA-labelling to identify RNA-binding proteins. *Biochem. Cell Biol. Biochim. Biol. Cell.* **98**, 31–41 (2020).

170. Niewoehner, O., Jinek, M. & Doudna, J. A. Evolution of CRISPR RNA recognition and processing by Cas6 endonucleases. *Nucleic Acids Res.* **42**, 1341–1353 (2014).

171. Haurwitz, R. E., Jinek, M., Wiedenheft, B., Zhou, K. & Doudna, J. A. Sequence- and Structure-Specific RNA Processing by a CRISPR Endonuclease. *Science* **329**, 1355–1358 (2010).

172. Sajwan, S. & Mannervik, M. Gene activation by dCas9-CBP and the SAM system differ in target preference. *Sci. Rep.* **9**, 18104 (2019).

173. Omachi, K. & Miner, J. H. Comparative analysis of dCas9-VP64 variants and multiplexed guide RNAs mediating CRISPR activation. *PLoS ONE* **17**, e0270008 (2022).

174. Dominguez, A. A. *et al.* CRISPR-Mediated Synergistic Epigenetic and Transcriptional Control. *CRISPR J.* **5**, 264–275 (2022).

175. Zhou, H. *et al.* In vivo simultaneous transcriptional activation of multiple genes in the brain using CRISPR-dCas9-activator transgenic mice. *Nat. Neurosci.* **21**, 440–446 (2018).

176. Harbury, P. B., Zhang, T., Kim, P. S. & Alber, T. A switch between two-, three-, and four-stranded coiled coils in GCN4 leucine zipper mutants. *Science* **262**, 1401–1407 (1993).

177. Gurnon, D. G., Whitaker, J. A. & Oakley, M. G. Design and Characterization of a Homodimeric Antiparallel Coiled Coil. *J. Am. Chem. Soc.* **125**, 7518–7519 (2003).

178. Deng, Y. *et al.* Antiparallel Four-Stranded Coiled Coil Specified by a 3-3-1 Hydrophobic Heptad Repeat. *Structure* **14**, 247–255 (2006).

179. Boyle, A. L. *et al.* Squaring the Circle in Peptide Assembly: From Fibers to Discrete Nanostructures by de Novo Design. *J Am Chem Soc* (2012).

180. Correnti, C. E. *et al.* Engineering and functionalization of large circular tandem repeat protein nanoparticles. *Nat. Struct. Mol. Biol.* **27**, 342–350 (2020).

181. Heidersbach, A. J., Dorighi, K. M., Gomez, J. A., Jacobi, A. M. & Haley, B. A versatile, high-efficiency platform for CRISPR-based gene activation. *Nat. Commun.* **14**, 902 (2023).

182. Nishimasu, H. *et al.* Crystal Structure of Cas9 in Complex with Guide RNA and Target DNA. *Cell* **156**, 935–949 (2014).

183. Tanenbaum, M. E., Gilbert, L. A., Qi, L. S., Weissman, J. S. & Vale, R. D. A protein-tagging system for signal amplification in gene expression and fluorescence imaging. *Cell* **159**, 635–646 (2014).

184. Liu, X. S. *et al.* Editing DNA methylation in the mammalian genome. *Cell* **167**, 233-247. e17 (2016).

185. Cano-Rodriguez, D. *et al.* Writing of H3K4Me3 overcomes epigenetic silencing in a sustained but context-dependent manner. *Nat. Commun.* **7**, 12284 (2016).

186. Kumar, M., Keller, B., Makalou, N. & Sutton, R. E. Systematic determination of the packaging limit of lentiviral vectors. *Hum. Gene Ther.* **12**, 1893–1905 (2001).

187. Wu, Z., Yang, H. & Colosi, P. Effect of genome size on AAV vector packaging. *Mol. Ther.* **18**, 80–86 (2010).

188. Wang, X. *et al.* A transgene-encoded cell surface polypeptide for selection, in vivo tracking, and ablation of engineered cells. *Blood* **118**, 1255–1263 (2011).

189. Troyanovsky, B., Bitko, V., Pastukh, V., Fouty, B. & Solodushko, V. The functionality of minimal piggyBac transposons in mammalian cells. *Mol. Ther.-Nucleic Acids* **5**, e369 (2016).

190. Ptáčková, P. *et al.* A new approach to CAR T-cell gene engineering and cultivation using piggyBac transposon in the presence of IL-4, IL-7 and IL-21. *Cytotherapy* **20**, 507–520 (2018).

191. Štach, M. *et al.* Inducible secretion of IL-21 augments anti-tumor activity of piggyBac-manufactured chimeric antigen receptor T cells. *Cytotherapy* **22**, 744–754 (2020).

192. Seczynska, M., Bloor, S., Cuesta, S. M. & Lehner, P. J. Genome surveillance by HUSH-mediated silencing of intronless mobile elements. *Nature* **601**, 440–445 (2022).

193. Moore, T. V. *et al.* HDAC inhibition prevents transgene expression downregulation and loss-of-function in T cell-receptor-transduced T cells. *Mol. Ther. - Oncolytics* **20**, 352–363 (2021).

194. Ewen-Campen, B. *et al.* Optimized strategy for in vivo Cas9-activation in Drosophila. *Proc. Natl. Acad. Sci.* **114**, 9409–9414 (2017).

195. Gossen, M. *et al.* Transcriptional activation by tetracyclines in mammalian cells. *Science* **268**, 1766–1769 (1995).

196. Jensen, T. I. *et al.* Targeted regulation of transcription in primary cells using CRISPRa and CRISPRi. *Genome Res.* **31**, 2120–2130 (2021).

197. Grützner, R. *et al.* High-efficiency genome editing in plants mediated by a Cas9 gene containing multiple introns. *Plant Commun.* **2**, 100135 (2021).

198. Pan, W., Liu, X., Li, D. & Zhang, H. Establishment of an Efficient Genome Editing System in Lettuce Without Sacrificing Specificity. *Front. Plant Sci.* 1985 (2022).

199. Rudina, S. S. & Smolke, C. D. A novel chromatin-opening element for stable long-term transgene expression. *bioRxiv* 626713 (2019).

200. Wei, J. & Jensen, M. C. Generating mammalian t cell activation inducible synthetic promoters (syn+ pro) to improve t cell therapy. (2020).

201. Naldini, L. *et al.* In Vivo Gene Delivery and Stable Transduction of Nondividing Cells by a Lentiviral Vector. *Science* **272**, 263–267 (1996).

202. Cavalieri, S. *et al.* Human T lymphocytes transduced by lentiviral vectors in the absence of TCR activation maintain an intact immune competence. *Blood* **102**, 497–505 (2003).

203. Ghassemi, S. *et al.* Rapid manufacturing of non-activated potent CAR T cells. *Nat. Biomed. Eng.* **6**, 118–128 (2022).

204. Bernadin, O. *et al.* Baboon envelope LVs efficiently transduced human adult, fetal, and progenitor T cells and corrected SCID-X1 T-cell deficiency. *Blood Adv.* **3**, 461–475 (2019).

205. Brocker, T. Chimeric Fv-ζ or Fv-ε receptors are not sufficient to induce activation or cytokine production in peripheral T cells. *Blood* **96**, 1999–2001 (2000).

206. Flugel, C. L. *et al.* Overcoming on-target, off-tumour toxicity of CAR T cell therapy for solid tumours. *Nat. Rev. Clin. Oncol.* **20**, 49–62 (2023).

207. Lepoivre, C. *et al.* Divergent transcription is associated with promoters of transcriptional regulators. *BMC Genomics* **14**, 914 (2013).

208. Wooten, M., Takushi, B., Ahmad, K. & Henikoff, S. Aclarubicin stimulates RNA polymerase II elongation at closely spaced divergent promoters. *BioRxiv Prepr. Serv. Biol.* 2023.01.09.523323 (2023) doi:10.1101/2023.01.09.523323.

209. Cabrera, A. *et al.* The sound of silence: Transgene silencing in mammalian cell engineering. *Cell Syst.* **13**, 950–973 (2022).

210. Finkelshtein, D., Werman, A., Novick, D., Barak, S. & Rubinstein, M. LDL receptor and its family members serve as the cellular receptors for vesicular stomatitis virus. *Proc. Natl. Acad. Sci.* **110**, 7306–7311 (2013).

211. Amirache, F. *et al.* Mystery solved: VSV-G-LVs do not allow efficient gene transfer into unstimulated T cells, B cells, and HSCs because they lack the LDL receptor. *Blood* **123**, 1422–1424 (2014).

212. Simhadri, V. L. *et al.* Prevalence of pre-existing antibodies to CRISPR-associated nuclease Cas9 in the USA population. *Mol. Ther.-Methods Clin. Dev.* **10**, 105–112 (2018).

213. Charlesworth, C. T. *et al.* Identification of preexisting adaptive immunity to Cas9 proteins in humans. *Nat. Med.* **25**, 249–254 (2019).

214. Wagner, D. L. *et al.* High prevalence of Streptococcus pyogenes Cas9-reactive T cells within the adult human population. *Nat. Med.* **25**, 242–248 (2019).

215. Wagner, D. L., Peter, L. & Schmueck-Henneresse, M. Cas9-directed immune tolerance in humans—a model to evaluate regulatory T cells in gene therapy? *Gene Ther.* **28**, 549–559 (2021).

216. Ferdosi, S. R. *et al.* Multifunctional CRISPR-Cas9 with engineered immunosilenced human T cell epitopes. *Nat. Commun.* **10**, 1–10 (2019).

217. Micklethwaite, K. P. *et al.* Investigation of product-derived lymphoma following infusion of piggyBac-modified CD19 chimeric antigen receptor T cells. *Blood* **138**, 1391–1405 (2021).

218. Jaeger, D., Baier, T. & Lauersen, K. J. Intronserter, an advanced online tool for design of intron containing transgenes. *Algal Res.* **42**, 101588 (2019).

219. Richmond, T. Prediction of intron splice sites. *Genome Biol.* **1**, reports223 (2000).

220. Kittle, J. D., Simons, R. W., Lee, J. & Kleckner, N. Insertion sequence IS10 anti-sense pairing initiates by an interaction between the 5’ end of the target RNA and a loop in the anti-sense RNA. *J. Mol. Biol.* **210**, 561–572 (1989).

221. Saitoh, N. *et al.* Structural and functional conservation at the boundaries of the chicken beta-globin domain. *EMBO J.* **19**, 2315–2322 (2000).

222. Appleman, L. J., Berezovskaya, A., Grass, I. & Boussiotis, V. A. CD28 Costimulation Mediates T Cell Expansion Via IL-2-Independent and IL-2-Dependent Regulation of Cell Cycle Progression1. *J. Immunol.* **164**, 144–151 (2000).

223. Tan, J. T. *et al.* IL-7 is critical for homeostatic proliferation and survival of naïve T cells. *Proc. Natl. Acad. Sci.* **98**, 8732–8737 (2001).

224. Lodolce, J. P. *et al.* IL-15 Receptor Maintains Lymphoid Homeostasis by Supporting Lymphocyte Homing and Proliferation. *Immunity* **9**, 669–676 (1998).

225. Vella, A., Teague, T. K., Ihle, J., Kappler, J. & Marrack, P. Interleukin 4 (IL-4) or IL-7 Prevents the Death of Resting T Cells: Stat6 Is Probably Not Required for the Effect of IL-4. *J. Exp. Med.* **186**, 325–330 (1997).

226. Jiang, Y., Li, Y. & Zhu, B. T-cell exhaustion in the tumor microenvironment. *Cell Death Dis.* **6**, e1792–e1792 (2015).

227. Bell, M. & Gottschalk, S. Engineered Cytokine Signaling to Improve CAR T Cell Effector Function. *Front. Immunol.* **12**, (2021).

228. Li, W. *et al.* Quality control, modeling, and visualization of CRISPR screens with MAGeCK-VISPR. *Genome Biol.* **16**, 281 (2015).

229. Wang, B. *et al.* Integrative analysis of pooled CRISPR genetic screens using MAGeCKFlute. *Nat. Protoc.* **14**, 756–780 (2019).

230. Odagiu, L. *et al.* Early programming of CD8+ T cell response by the orphan nuclear receptor NR4A3. *Proc. Natl. Acad. Sci. U. S. A.* **117**, 24392–24402 (2020).

231. Morcinek, J. C., Weisser, C., Geissinger, E., Schartl, M. & Wellbrock, C. Activation of STAT5 triggers proliferation and contributes to anti-apoptotic signalling mediated by the oncogenic Xmrk kinase. *Oncogene* **21**, 1668–1678 (2002).

232. Wu, Y., Deng, Z., Tang, Y., Zhang, S. & Zhang, Y.-Q. Over-expressing Akt in T cells to resist tumor immunosuppression and increase anti-tumor activity. *BMC Cancer* **15**, 603 (2015).

233. Ribeiro, D. *et al.* STAT5 is essential for IL-7–mediated viability, growth, and proliferation of T-cell acute lymphoblastic leukemia cells. *Blood Adv.* **2**, 2199–2213 (2018).

234. Ding, Z.-C. *et al.* Persistent STAT5 activation reprograms the epigenetic landscape in CD4+ T cells to drive polyfunctionality and antitumor immunity. *Sci. Immunol.* **5**, eaba5962 (2020).

235. Zhou, J. *et al.* The ubiquitin ligase MDM2 sustains STAT5 stability to control T cell-mediated antitumor immunity. *Nat. Immunol.* **22**, 460–470 (2021).

236. Silva, A. *et al.* Overexpression of wild-type IL-7Rα promotes T-cell acute lymphoblastic leukemia/lymphoma. *Blood* **138**, 1040–1052 (2021).

237. Inoue, K. *et al.* Aberrant Overexpression of the Wilms Tumor Gene (WT1) in Human Leukemia. *Blood* **89**, 1405–1412 (1997).

238. Atwal, G. S. *et al.* Haplotype structure and selection of the MDM2 oncogene in humans. *Proc. Natl. Acad. Sci.* **104**, 4524–4529 (2007).

239. Wang, R. *et al.* The Transcription Factor Myc Controls Metabolic Reprogramming upon T Lymphocyte Activation. *Immunity* **35**, 871–882 (2011).

240. Nath, S. & Mukherjee, P. Muc1: a multifaceted oncoprotein with a key role in cancer progression. *Trends Mol. Med.* **20**, 332–342 (2014).

241. Bird, C. H. *et al.* The granzyme B-Serpinb9 axis controls the fate of lymphocytes after lysosomal stress. *Cell Death Differ.* **21**, 876–887 (2014).

242. Watanabe-Smith, K. *et al.* Discovery and functional characterization of a germline, CSF2RB-activating mutation in leukemia. *Leukemia* **30**, 1950–1953 (2016).

243. Zhu, J., Guo, L., Watson, C. J., Hu-Li, J. & Paul, W. E. Stat6 is necessary and sufficient for IL-4's role in Th2 differentiation and cell expansion. *J. Immunol. Baltim. Md 1950* **166**, 7276–7281 (2001).

244. Arroyo-Olarte, R. D. *et al.* STAT6 controls the stability and suppressive function of regulatory T cells. *Eur. J. Immunol.* **53**, 2250128 (2023).

245. Wen, X. *et al.* Large-scale temporal gene expression mapping of central nervous system development. *Proc. Natl. Acad. Sci.* **95**, 334–339 (1998).

246. Strober, B. J. *et al.* Dynamic genetic regulation of gene expression during cellular differentiation. *Science* **364**, 1287–1290 (2019).

247. Grün, D. Revealing dynamics of gene expression variability in cell state space. *Nat. Methods* **17**, 45–49 (2020).

248. Işıldak, U., Somel, M., Thornton, J. M. & Dönertaş, H. M. Temporal changes in the gene expression heterogeneity during brain development and aging. *Sci. Rep.* **10**, 4080 (2020).

249. Teague, T. K. *et al.* Activation changes the spectrum but not the diversity of genes expressed by T cells. *Proc. Natl. Acad. Sci.* **96**, 12691–12696 (1999).

250. Sousa, I. G. *et al.* Gene expression profile of human T cells following a single stimulation of peripheral blood mononuclear cells with anti-CD3 antibodies. *BMC Genomics* **20**, 593 (2019).

251. Szabo, P. A. *et al.* Single-cell transcriptomics of human T cells reveals tissue and activation signatures in health and disease. *Nat. Commun.* **10**, 4706 (2019).

252. Salerno, F., Turner, M. & Wolkers, M. C. Dynamic post-transcriptional events governing CD8+ T cell homeostasis and effector function. *Trends Immunol.* **41**, 240–254 (2020).

253. Qin, J. Y. *et al.* Systematic Comparison of Constitutive Promoters and the Doxycycline-Inducible Promoter. *PLOS ONE* **5**, e10611 (2010).

254. Borch Jensen, M. & Marblestone, A. In vivo Pooled Screening: A Scalable Tool to Study the Complexity of Aging and Age-Related Disease. *Front. Aging* **2**, (2021).

255. Schedl, A. *et al.* Influence of PAX6 Gene Dosage on Development: Overexpression Causes Severe Eye Abnormalities. *Cell* **86**, 71–82 (1996).

256. Wozniak, G. G. & Strahl, B. D. Catalysis-dependent stabilization of Bre1 fine-tunes histone H2B ubiquitylation to regulate gene transcription. *Genes Dev.* **28**, 1647–1652 (2014).

257. Rice, A. M. & McLysaght, A. Dosage sensitivity is a major determinant of human copy number variant pathogenicity. *Nat. Commun.* **8**, 14366 (2017).

258. Rieker, C. *et al.* Apolipoprotein E4 Expression Causes Gain of Toxic Function in Isogenic Human Induced Pluripotent Stem Cell-Derived Endothelial Cells. *Arterioscler. Thromb. Vasc. Biol.* **39**, e195–e207 (2019).

259. Van Alstyne, M. *et al.* Gain of toxic function by long-term AAV9-mediated SMN overexpression in the sensorimotor circuit. *Nat. Neurosci.* **24**, 930–940 (2021).

260. Landolin, J. M. *et al.* Sequence features that drive human promoter function and tissue specificity. *Genome Res.* **20**, 890 (2010).

261. Einarsson, H. *et al.* Promoter sequence and architecture determine expression variability and confer robustness to genetic variants. *eLife* **11**, e80943 (2022).

262. Mondragón, L. *et al.* GAPDH Overexpression in the T Cell Lineage Promotes Angioimmunoblastic T Cell Lymphoma through an NF-κB-Dependent Mechanism. *Cancer Cell* **36**, 268-287.e10 (2019).

263. Oliveira, M. L. *et al.* Mutant IL7R collaborates with MYC to induce T-cell acute lymphoblastic leukemia. *Leukemia* **36**, 1533–1540 (2022).

264. Zhang, L. *et al.* Improving Adoptive T Cell Therapy by Targeting and Controlling IL-12 Expression to the Tumor Environment. *Mol. Ther.* **19**, 751–759 (2011).

265. Hu, B. *et al.* Augmentation of Antitumor Immunity by Human and Mouse CAR T Cells Secreting IL-18. *Cell Rep.* **20**, 3025–3033 (2017).

266. Greenshpan, Y. *et al.* Synthetic promoters to induce immune-effectors into the tumor microenvironment. *Commun. Biol.* **4**, 1–11 (2021).

267. Sharabi, O. *et al.* High throughput screen for the improvement of inducible promoters for tumor microenvironment cues. *Sci. Rep.* **12**, 7169 (2022).

268. Uchibori, R. *et al.* Functional Analysis of an Inducible Promoter Driven by Activation Signals from a Chimeric Antigen Receptor. *Mol. Ther. - Oncolytics* **12**, 16–25 (2019).

269. Guo, T., Ma, D. & Lu, T. K. Sense-and-Respond Payload Delivery Using a Novel Antigen-Inducible Promoter Improves Suboptimal CAR-T Activation. *ACS Synth. Biol.* **11**, 1440–1453 (2022).

270. Arimbasseri, A. G., Rijal, K. & Maraia, R. J. Comparative overview of RNA polymerase II and III transcription cycles, with focus on RNA polymerase III termination and reinitiation. *Transcription* **5**, e27369 (2013).

271. Slobodin, B. *et al.* Transcription Impacts the Efficiency of mRNA Translation via Co-transcriptional N6-adenosine Methylation. *Cell* **169**, 326-337.e12 (2017).

272. Kunkel, G. R. & Pederson, T. Transcription of a human U6 small nuclear RNA gene in vivo withstands deletion of intragenic sequences but not of an upstream TATATA box. *Nucleic Acids Res.* **17**, 7371–7379 (1989).

273. Baer, M., Nilsen, T. W., Costigan, C. & Altman, S. Structure and transcription of a human gene for H1 RNA, the RNA component of human RNase P. *Nucleic Acids Res.* **18**, 97–103 (1990).

274. Xie, C. *et al.* SgRNA Expression of CRIPSR-Cas9 System Based on MiRNA Polycistrons as a Versatile Tool to Manipulate Multiple and Tissue-Specific Genome Editing. *Sci. Rep.* **7**, 5795 (2017).

275. Uguen, P. & Murphy, S. The 3’ ends of human pre-snRNAs are produced by RNA polymerase II CTD-dependent RNA processing. *EMBO J.* **22**, 4544–4554 (2003).

276. Uguen, P. & Murphy, S. 3’-Box-dependent processing of human pre-U1 snRNA requires a combination of RNA and protein co-factors. *Nucleic Acids Res.* **32**, 2987–2994 (2004).

277. Shechner, D. M., Hacisüleyman, E., Younger, S. T. & Rinn, J. L. CRISPR Display: A modular method for locus-specific targeting of long noncoding RNAs and synthetic RNA devices in vivo. *Nat. Methods* **12**, 664–670 (2015).

278. Altman, S. The road to RNase P. *Nat. Struct. Biol.* **7**, 827–828 (2000).

279. Knapp, D. J. H. F. *et al.* Decoupling tRNA promoter and processing activities enables specific Pol-II Cas9 guide RNA expression. *Nat. Commun.* **10**, 1490 (2019).

280. Kruger, K. *et al.* Self-splicing RNA: autoexcision and autocyclization of the ribosomal RNA intervening sequence of Tetrahymena. *Cell* **31**, 147–157 (1982).

281. Forster, A. C. & Symons, R. H. Self-cleavage of plus and minus RNAs of a virusoid and a structural model for the active sites. *Cell* **49**, 211–220 (1987).

282. Ferré-D'Amaré, A. R., Zhou, K. & Doudna, J. A. Crystal structure of a hepatitis delta virus ribozyme. *Nature* **395**, 567–574 (1998).

283. Gao, Y. & Zhao, Y. Self-processing of ribozyme-flanked RNAs into guide RNAs in vitro and in vivo for CRISPR-mediated genome editing. *J. Integr. Plant Biol.* **56**, 343–349 (2014).

284. He, Y. *et al.* Self-cleaving ribozymes enable the production of guide RNAs from unlimited choices of promoters for CRISPR/Cas9 mediated genome editing. *J. Genet. Genomics Yi Chuan Xue Bao* **44**, 469–472 (2017).

285. Aramaki, H., Yagi, N. & Suzuki, M. Residues important for the function of a multihelical DNA binding domain in the new transcription factor family of Cam and Tet repressors. *Protein Eng. Des. Sel.* **8**, 1259–1266 (1995).

286. Lin, X. *et al.* Development of a tightly regulated U6 promoter for shRNA expression. *FEBS Lett.* **577**, 376–380 (2004).

287. Henriksen, J. R. *et al.* Comparison of RNAi efficiency mediated by tetracycline-responsive H1 and U6 promoter variants in mammalian cell lines. *Nucleic Acids Res.* **35**, e67 (2007).

288. Kelkar, A. *et al.* Doxycycline-Dependent Self-Inactivation of CRISPR-Cas9 to Temporally Regulate On- and Off-Target Editing. *Mol. Ther.* **28**, 29–41 (2020).

289. Sun, N. *et al.* Development of drug-inducible CRISPR-Cas9 systems for large-scale functional screening. *BMC Genomics* **20**, 225 (2019).

290. Das, A. T., Tenenbaum, L. & Berkhout, B. Tet-On Systems For Doxycycline-inducible Gene Expression. *Curr. Gene Ther.* **16**, 156–167 (2016).

291. Dow, L. E. *et al.* Inducible in vivo genome editing with CRISPR-Cas9. *Nat. Biotechnol.* **33**, 390–394 (2015).

292. Rico, E., Jeacock, L., Kovářová, J. & Horn, D. Inducible high-efficiency CRISPR-Cas9-targeted gene editing and precision base editing in African trypanosomes. *Sci. Rep.* **8**, 7960 (2018).

293. Lundin, A. *et al.* Development of an ObLiGaRe Doxycycline Inducible Cas9 system for pre-clinical cancer drug discovery. *Nat. Commun.* **11**, 4903 (2020).

294. Gossen, M. & Bujard, H. Tight control of gene expression in mammalian cells by tetracycline-responsive promoters. *Proc. Natl. Acad. Sci.* **89**, 5547–5551 (1992).

295. Baron, U., Gossen, M. & Bujard, H. Tetracycline-controlled transcription in eukaryotes: novel transactivators with graded transactivation potential. *Nucleic Acids Res.* **25**, 2723–2729 (1997).

296. Kang, K. *et al.* An improved Tet-on system in microRNA overexpression and CRISPR/Cas9-mediated gene editing. *J. Anim. Sci. Biotechnol.* **10**, 43 (2019).

297. Chen, Z. Y., He, C. Y., Meuse, L. & Kay, M. A. Silencing of episomal transgene expression by plasmid bacterial DNA elements in vivo. *Gene Ther.* **11**, 856–864 (2004).

298. Chen, Z.-Y., Riu, E., He, C.-Y., Xu, H. & Kay, M. A. Silencing of Episomal Transgene Expression in Liver by Plasmid Bacterial Backbone DNA Is Independent of CpG Methylation. *Mol. Ther.* **16**, 548–556 (2008).

299. Zhu, P. *et al.* Silencing and Un-silencing of Tetracycline-Controlled Genes in Neurons. *PLoS ONE* **2**, e533 (2007).

300. Yu, Y., Lowy, M. M. & Elble, R. C. Tet-On lentiviral transductants lose inducibility when silenced for extended intervals in mammary epithelial cells. *Metab. Eng. Commun.* **3**, 64–67 (2016).

301. Wu, Y., Yang, L., Chang, T., Kandeel, F. & Yee, J.-K. A small molecule-controlled Cas9 repressible system. *Mol. Ther.-Nucleic Acids* **19**, 922–932 (2020).

302. Chung, H. K. *et al.* Tunable and reversible drug control of protein production via a self-excising degron. *Nat. Chem. Biol.* **11**, 713–720 (2015).

303. Sahillioglu, A. C., Toebes, M., Apriamashvili, G., Gomez, R. & Schumacher, T. N. CRASH-IT Switch Enables Reversible and Dose-Dependent Control of TCR and CAR T-cell Function. *Cancer Immunol. Res.* **9**, 999–1007 (2021).

304. Labanieh, L. *et al.* Enhanced safety and efficacy of protease-regulated CAR-T cell receptors. *Cell* **185**, 1745-1763.e22 (2022).

305. Tague, E. P., Dotson, H. L., Tunney, S. N., Sloas, D. C. & Ngo, J. T. Chemogenetic control of gene expression and cell signaling with antiviral drugs. *Nat. Methods* **15**, 519–522 (2018).

306. Oakes, B. L. *et al.* CRISPR-Cas9 Circular Permutants as Programmable Scaffolds for Genome Modification. *Cell* **176**, 254-267.e16 (2019).

307. Indra, A. K. *et al.* Temporally-controlled site-specific mutagenesis in the basal layer of the epidermis: comparison of the recombinase activity of the tamoxifen-inducible Cre-ERT and Cre-ERT2 recombinases. *Nucleic Acids Res.* **27**, 4324–4327 (1999).

308. US Patent Application for CHIMERIC TRANSCRIPTION FACTOR VARIANTS WITH AUGMENTED SENSITIVITY TO DRUG LIGAND INDUCTION OF TRANSGENE EXPRESSION IN MAMMALIAN CELLS Patent Application (Application #20220411805 issued December 29, 2022) - Justia Patents Search. https://patents.justia.com/patent/20220411805.

309. Liu, K. I. *et al.* A chemical-inducible CRISPR–Cas9 system for rapid control of genome editing. *Nat. Chem. Biol.* **12**, 980–987 (2016).

310. Oakes, B. L. *et al.* Profiling of engineering hotspots identifies an allosteric CRISPR-Cas9 switch. *Nat. Biotechnol.* **34**, 646–651 (2016).

311. Lu, J. *et al.* Multimode drug inducible CRISPR/Cas9 devices for transcriptional activation and genome editing. *Nucleic Acids Res.* **46**, e25 (2018).

312. Dominguez-Monedero, A. & Davies, J. A. Tamoxifen- and Mifepristone-Inducible Versions of CRISPR Effectors, Cas9 and Cpf1. *ACS Synth. Biol.* **7**, 2160–2169 (2018).

313. Fliss, A. E., Benzeno, S., Rao, J. & Caplan, A. J. Control of estrogen receptor ligand binding by Hsp90. *J. Steroid Biochem. Mol. Biol.* **72**, 223–230 (2000).

314. Kocanova, S., Mazaheri, M., Caze-Subra, S. & Bystricky, K. Ligands specify estrogen receptor alpha nuclear localization and degradation. *BMC Cell Biol.* **11**, 98 (2010).

315. Miyazaki, Y., Imoto, H., Chen, L. & Wandless, T. J. Destabilizing Domains Derived from the Human Estrogen Receptor. *J. Am. Chem. Soc.* **134**, 3942–3945 (2012).

316. Maji, B. *et al.* Multidimensional chemical control of CRISPR–Cas9. *Nat. Chem. Biol.* **13**, 9–11 (2017).

317. Welsh, G. I., Miyamoto, S., Price, N. T., Safer, B. & Proud, C. G. T-cell Activation Leads to Rapid Stimulation of Translation Initiation Factor eIF2B and Inactivation of Glycogen Synthase Kinase-3 (∗). *J. Biol. Chem.* **271**, 11410–11413 (1996).

318. Marrack, P. *et al.* Genomic-scale analysis of gene expression in resting and activated T cells. *Curr. Opin. Immunol.* **12**, 206–209 (2000).

319. Ellisen, L. W. *et al.* Cascades of transcriptional induction during human lymphocyte activation. *Eur. J. Cell Biol.* **80**, 321–328 (2001).

320. Feske, S., Giltnane, J., Dolmetsch, R., Staudt, L. M. & Rao, A. Gene regulation mediated by calcium signals in T lymphocytes. *Nat. Immunol.* **2**, 316–324 (2001).

321. Raghavan, A. *et al.* Genome-wide analysis of mRNA decay in resting and activated primary human T lymphocytes. *Nucleic Acids Res.* **30**, 5529–5538 (2002).

322. Adachi, K. & Davis, M. M. T-cell receptor ligation induces distinct signaling pathways in naïve vs. antigen-experienced T cells. *Proc. Natl. Acad. Sci.* **108**, 1549–1554 (2011).

323. Ricciardi, S. *et al.* The translational machinery of human CD4+ T cells is poised for activation and controls the switch from quiescence to metabolic remodeling. *Cell Metab.* **28**, 895-906. e5 (2018).

324. Calero-Nieto, F. J., Bert, A. G. & Cockerill, P. N. Transcription-dependent silencing of inducible convergent transgenes in transgenic mice. *Epigenetics Chromatin* **3**, 3 (2010).

325. DiAndreth, B., Wauford, N., Hu, E., Palacios, S. & Weiss, R. PERSIST platform provides programmable RNA regulation using CRISPR endoRNases. *Nat. Commun.* **13**, 2582 (2022).

326. Cramer, P., Pesce, C. G., Baralle, F. E. & Kornblihtt, A. R. Functional association between promoter structure and transcript alternative splicing. *Proc. Natl. Acad. Sci.* **94**, 11456–11460 (1997).

327. Ip, J. Y. *et al.* Global analysis of alternative splicing during T-cell activation. *RNA* **13**, 563–572 (2007).

328. Yang, Z. *et al.* Nanoscale, antigen encounter-dependent, IL-12 delivery by CAR T cells plus PD-L1 blockade for cancer treatment. *J. Transl. Med.* **21**, 158 (2023).

329. Foight, G. W. *et al.* Multi-input chemical control of protein dimerization for programming graded cellular responses. *Nat. Biotechnol.* **37**, 1209–1216 (2019).

330. Buquicchio, F. A. & Satpathy, A. T. Interrogating immune cells and cancer with CRISPR-Cas9. *Trends Immunol.* **42**, 432–446 (2021).

331. Dong, M. B., Tang, K., Zhou, X., Zhou, J. J. & Chen, S. Tumor immunology CRISPR screening: present, past, and future. *Trends Cancer* **8**, 210–225 (2022).

332. Alvanou, M. *et al.* Empowering the Potential of CAR-T Cell Immunotherapies by Epigenetic Reprogramming. *Cancers* **15**, 1935 (2023).

333. Chavez, M., Rane, D. A., Chen, X. & Qi, L. S. Stable expression of large transgenes via the knock-in of an integrase-deficient lentivirus. *Nat. Biomed. Eng.* **7**, 661–671 (2023).